

NDOR Sponsoring Agency Contract No. DPU-STWD (94)

DESIGN AND EVALUATION OF AN ENERGY- ABSORBING, REUSABLE ROADSIDE/MEDIAN BARRIER

Submitted by

Jennifer D. Schmidt, Ph.D., P.E.
Research Assistant Professor

Scott K. Rosenbaugh, M.S.C.E., E.I.T.
Research Associate Engineer

Ronald K. Faller, Ph.D., P.E.,
Research Associate Professor
MwRSF Director

Robert W. Bielenberg, M.S.M.E., E.I.T.
Research Associate Engineer

John D. Reid, Ph.D.
Professor

Jim C. Holloway, M.S.C.E., E.I.T.
Test Site Manager

Karla A. Lechtenberg, M.S.M.E., E.I.T.
Research Associate Engineer

Justine E. Kohtz
Undergraduate Research Assistant

MIDWEST ROADSIDE SAFETY FACILITY

Nebraska Transportation Center
University of Nebraska-Lincoln
130 Whittier Research Center
2200 Vine Street
Lincoln, Nebraska 68583-0853
(402) 472-0965

Submitted to

NEBRASKA DEPARTMENT OF ROADS

1500 Nebraska Highway 2
Lincoln, Nebraska 68502

FEDERAL HIGHWAY ADMINISTRATION

Nebraska Division
100 Centennial Mall North Room 220
Lincoln, Nebraska 68508

MwRSF Research Report No. TRP-03-317-15

July 29, 2015

TECHNICAL REPORT DOCUMENTATION PAGE

1. Report No. TRP-03-317-15	2.	3. Recipient's Accession No.	
4. Title and Subtitle Design and Evaluation of an Energy-Absorbing, Reusable Roadside/Median Barrier		5. Report Date July 29, 2015	
		6.	
7. Author(s) Schmidt, J.D., Rosenbaugh, S.K., Faller, R.K., Bielenberg, R.W., Reid, J.D., Lechtenberg, K.A., Holloway, J.C., and Kohtz, J. E.		8. Performing Organization Report No. TRP-03-317-15	
9. Performing Organization Name and Address Midwest Roadside Safety Facility (MwRSF) Nebraska Transportation Center University of Nebraska-Lincoln 130 Whittier Research Center 2200 Vine Street Lincoln, Nebraska 68583-0853		10. Project/Task/Work Unit No.	
		11. Contract © or Grant (G) No. NDOR DPU-STWD (94)	
12. Sponsoring Organization Name and Address Nebraska Department of Roads 1500 Nebraska Highway 2 Lincoln, Nebraska 68502 Federal Highway Administration Nebraska Division 100 Centennial Mall North Room 220 Lincoln, Nebraska 68508		13. Type of Report and Period Covered Final Report: 2010 – 2015	
		14. Sponsoring Agency Code	
15. Supplementary Notes Prepared in cooperation with U.S. Department of Transportation, Federal Highway Administration.			
16. Abstract (Limit: 200 words) Further design and evaluation was conducted on an energy-absorbing, restorable and reusable roadside/median barrier, designated the RESTORE barrier. A series of dynamic component tests were conducted on 11 ⁵ / ₈ -in. (295-mm) tall x 10-in. (254-mm) wide x 15 ³ / ₄ -in. (400-mm) long rubber posts to characterize their energy-absorption properties. A hybrid precast concrete beam and steel tube rail was optimized to meet the design criteria for the new system. Several concrete beam splices were evaluated using LS-DYNA to add continuity to the concrete beam segments. A 240-ft (73-m) barrier model was created, and the barrier performance was evaluated with TL-4 impacts with the 1100C, 2270P, and 10000S vehicle models. The 1100C and 2270P vehicle models were successfully captured and redirected, while the 10000S single-unit truck demonstrated likelihood to be contained by the barrier and began to redirect. The occupant risk values for the passenger vehicle impacts were up to 28 percent lower than what occurred in a comparable simulated impact into a rigid concrete barrier. The full-scale system was installed, and the stability of the system was evaluated. The final design is recommended for full-scale crash testing according to the MASH TL-4 criteria.			
17. Document Analysis/Descriptors Highway Safety, Crash Test, Roadside Appurtenances, MASH, LS-DYNA, Computer Simulation, Elastomers, Rubber Posts, Energy-Absorbing Barrier, and TL-4		18. Availability Statement No restrictions. Document available from: National Technical Information Services, Springfield, Virginia 22161	
19. Security Class (this report) Unclassified	20. Security Class (this page) Unclassified	21. No. of Pages 155	22. Price

DISCLAIMER STATEMENT

This report was completed with funding from the Federal Highway Administration, U.S. Department of Transportation. The contents of this report reflect the views and opinions of the authors who are responsible for the facts and the accuracy of the data presented herein. The contents do not necessarily reflect the official views or policies of Nebraska Department of Roads nor the Federal Highway Administration, U.S. Department of Transportation. This report does not constitute a standard, specification, regulation, product endorsement, or an endorsement of manufacturers.

UNCERTAINTY OF MEASUREMENT STATEMENT

The Midwest Roadside Safety Facility (MwRSF) has determined the uncertainty of measurements for several parameters involved in standard full-scale crash testing and non-standard testing of roadside safety features. Information regarding the uncertainty of measurements for critical parameters is available upon request by the sponsor and the Federal Highway Administration. Test nos. SF10-1 through SF10-2, SFD-1 through SFD-5, and SF10P-1 through SF10P-2 were non-certified component tests conducted for research and development purposes only and are outside the scope of the MwRSF's A2LA Accreditation.

ACKNOWLEDGEMENTS

The authors wish to acknowledge several sources that made a contribution to this project: (1) the Federal Highway Administration and the Nebraska Department of Roads for sponsoring this project; (2) the Holland Computing Center at the University of Nebraska for providing the computing resources; and (3) MwRSF personnel for constructing the systems and conducting the component tests.

Acknowledgement is also given to the following individuals who made a contribution to the completion of this research project.

Midwest Roadside Safety Facility

C.S. Stolle, Ph.D., Research Assistant Professor
A.T. Russell, B.S.B.A., Shop Manager
K.L. Krenk, B.S.M.A., Maintenance Mechanic
S.M. Tighe, Laboratory Mechanic
D.S. Charroin, Laboratory Mechanic
Undergraduate and Graduate Research Assistants

Nebraska Department of Roads

Phil TenHulzen, P.E., Design Standards Engineer
Jim Knott, P.E., State Roadway Design Engineer
Jodi Gibson, Research Coordinator

Federal Highway Administration

John Perry, P.E., Nebraska Division Office
Danny Briggs, Nebraska Division Office

TABLE OF CONTENTS

TECHNICAL REPORT DOCUMENTATION PAGE	i
DISCLAIMER STATEMENT	ii
UNCERTAINTY OF MEASUREMENT STATEMENT	ii
ACKNOWLEDGEMENTS	iii
TABLE OF CONTENTS	iv
LIST OF FIGURES	vi
LIST OF TABLES	ix
1 INTRODUCTION	1
1.1 Background	1
1.2 Objective	6
1.3 Scope	6
2 COMPONENT TESTING CONDITIONS	7
2.1 Purpose	7
2.2 Scope	7
2.3 Equipment and Instrumentation	27
2.3.1 Bogie Vehicle	27
2.3.2 Accelerometers	28
2.3.3 Retroreflective Optic Speed Trap	30
2.3.4 Digital Photography	30
2.4 Data Processing	31
3 POST TESTING RESULTS AND DISCUSSION	32
3.1 Results	32
3.1.1 11 ⁵ / ₈ -in. (295-mm) Tall Rubber Post Tests	33
3.1.1 11 ⁵ / ₈ -in. (295-mm) Tall Rubber Post Tests with Steel Pipe	34
3.2 Discussion	43
4 SYSTEM DESIGN AND ANALYSIS	47
4.1 Introduction	47
4.2 Post Design	47
4.3 Rail Design	50
4.4 Concrete Rail Splices	52
4.5 Final System Design	62
5 COMPUTER SIMULATION	81
5.1 Baseline Simulations with Rigid Concrete Barriers	81
5.2 RESTORE Barrier Model	82
5.2.1 1100C Dodge Neon	85
5.2.2 2270P Chevrolet Silverado	89

5.2.1 10000S Single-Unit Truck 93

5.3 Simulation Summary 95

6 INSTALLATION AND STABILITY EVALUATION 97

6.1 Additional Steel Pipe in Post 99

6.2 Development and Installation of Steel Skids 101

6.3 Simulations with Skids 104

7 SUMMARY, CONCLUSIONS, AND RECOMMENDATIONS 111

8 REFERENCES 137

9 APPENDICES 139

Appendix A. Material Specifications 140

Appendix B. Bogie Test Results 142

Appendix C. Simulation Issues 154

LIST OF FIGURES

Figure 1. Initial Barrier Concept [1]	2
Figure 2. Post Schematic.....	4
Figure 3. 11 $\frac{5}{8}$ -in. (295-mm) Tall Shear Fender.....	7
Figure 4. Bogie Test Setup, All Tests	8
Figure 5. Bogie Testing Matrix and Setup – Test Nos. SF10-1 and SF10-2, Sheet 1 of 6.....	9
Figure 6. Bogie Testing Matrix and Setup – Test Nos. SF10-1 and SF10-2, Sheet 2 of 6.....	10
Figure 7. Bogie Testing Matrix and Setup – Test Nos. SF10-1 and SF10-2, Sheet 3 of 6.....	11
Figure 8. Bogie Testing Matrix and Setup – Test Nos. SF10-1 and SF10-2, Sheet 4 of 6.....	12
Figure 9. Bogie Testing Matrix and Setup – Test Nos. SF10-1 and SF10-2, Sheet 5 of 6.....	13
Figure 10. Bogie Testing Matrix and Setup – Test Nos. SF10-1 and SF10-2, Sheet 6 of 6.....	14
Figure 11. Bogie Testing Matrix and Setup – Test Nos. SFD-1 through SFD-5, Sheet 1 of 6	15
Figure 12. Bogie Testing Matrix and Setup – Test Nos. SFD-1 through SFD-5, Sheet 2 of 6	16
Figure 13. Bogie Testing Matrix and Setup – Test Nos. SFD-1 through SFD-5, Sheet 3 of 6	17
Figure 14. Bogie Testing Matrix and Setup – Test Nos. SFD-1 through SFD-5, Sheet 4 of 6	18
Figure 15. Bogie Testing Matrix and Setup – Test Nos. SFD-1 through SFD-5, Sheet 5 of 6	19
Figure 16. Bogie Testing Matrix and Setup – Test Nos. SFD-1 through SFD-5, Sheet 6 of 6	20
Figure 17. Bogie Testing Matrix and Setup – Test Nos. SF10P-1 and SF10P-2, Sheet 1 of 6	21
Figure 18. Bogie Testing Matrix and Setup – Test Nos. SF10P-1 and SF10P-2, Sheet 2 of 6	22
Figure 19. Bogie Testing Matrix and Setup – Test Nos. SF10P-1 and SF10P-2, Sheet 3 of 6	23
Figure 20. Bogie Testing Matrix and Setup – Test Nos. SF10P-1 and SF10P-2, Sheet 4 of 6	24
Figure 21. Bogie Testing Matrix and Setup – Test Nos. SF10P-1 and SF10P-2, Sheet 5 of 6	25
Figure 22. Bogie Testing Matrix and Setup – Test Nos. SF10P-1 and SF10P-2, Sheet 6 of 6	26
Figure 23. Rigid-Frame Bogie on Guidance Track	28
Figure 24. Energy and Force vs. Deflection, Test No. SF10-1	35
Figure 25. Time-Sequential Photographs, Test No. SF10-1	36
Figure 26. Time-Sequential Photographs, Test No. SFD-	37
Figure 27. Force vs. Deflection Comparison, All Bogie Tests Without Steel Pipe.....	38
Figure 28. Energy vs. Deflection Comparison, All Bogie Tests Without Steel Pipe	39
Figure 29. Time-Sequential Photographs, Test No. SF10P-1	40
Figure 30. Force vs. Deflection Comparison, All Bogie Tests Without Steel Pipe.....	41
Figure 31. Energy vs. Deflection Comparison, All Bogie Tests Without Steel Pipe	42
*taken from film analysis.....	44
Figure 32. Force vs. Deflection Comparison, Pipe vs. No Pipe Bogie Tests	45
Figure 33. Energy vs. Deflection Comparison, Pipe vs. No Pipe Bogie Tests	46
Figure 34. Static Energy vs. Deflection, 11 $\frac{5}{8}$ -in. (295-mm) and 16-in. (406-mm) Tall Posts [8].....	48
Figure 35. Dynamic Energy vs. Deflection, 11 $\frac{5}{8}$ -in. (295-mm) and 16-in. (406-mm) Tall Posts	49
Figure 36. Optimized Rail Cross Section	51
Figure 37. Splice Plates Concept	54
Figure 38. Splice Tubes Concept	55
Figure 39. X-Connection Concept	56
Figure 40. ACJ Concept.....	57
Figure 41. 160-ft Barrier Model for Exploring Concrete Beam Splices.....	58
Figure 42. Dynamic Deflection of Concrete Beam Splices	62

Figure 43. Preliminary Barrier Design, System Layout	64
Figure 44. Preliminary Barrier Design, Barrier Assembly	65
Figure 45. Preliminary Barrier Design, Post and Tubing Details	66
Figure 46. Preliminary Barrier Design, Splice Details	67
Figure 47. Preliminary Barrier Design, Concrete Rail Geometry	68
Figure 48. Preliminary Barrier Design, Concrete Rail and Rebar Assembly	69
Figure 49. Preliminary Barrier Design, Rebar Assembly Details.....	70
Figure 50. Preliminary Barrier Design, Rebar Assembly Details.....	71
Figure 51. Preliminary Barrier Design, Rebar Assembly Details.....	72
Figure 52. Preliminary Barrier Design, Bill of Bars	73
Figure 53. Preliminary Barrier Design, Rail Assembly	74
Figure 54. Preliminary Barrier Design, End Tubing Assembly.....	75
Figure 55. Preliminary Barrier Design, Steel Rail Components.....	76
Figure 56. Preliminary Barrier Design, Adjustable Continuity Joint Details	77
Figure 57. Preliminary Barrier Design, Shear Fender Details	78
Figure 58. Preliminary Barrier Design, Fasteners	79
Figure 59. Preliminary Barrier Design, Bill of Materials	80
Figure 60. Simulation Part Numbers	83
Figure 61. RESTORE Barrier Simulation with MASH Test Designation 4-10 Impact (1100C)	87
Figure 62. Simulated Lateral Acceleration – MASH Test Designation 4-10	88
Figure 63. RESTORE Barrier Simulation with MASH Test Designation 4-11 (2270P) Impact	91
Figure 64. Simulated Lateral Acceleration – MASH Test Designation 4-11	92
Figure 65. RESTORE Barrier Simulation with MASH Test Designation 4-12 (10000S) Impact	94
Figure 66. ACJ Variable Gap Width.....	98
Figure 67. Barrier Stability with Steel Pipe Inserts	100
Figure 68. Barrier Deflection with Steel Pipe Inserts	100
Figure 69. Steel Support Skids.....	101
Figure 70. Barrier Stability with Two Support Skids with Shims	103
Figure 71. Maximum Barrier Deflection with Two Support Skids with Shims	103
Figure 72. Skid Model	104
Figure 73. RESTORE Barrier Simulation with Test Designation 4-10 Impacts	106
Figure 74. RESTORE Barrier Simulation with Test Designation 4-11 Impacts	107
Figure 75. Dynamic Barrier Deflection with and without Skids	108
Figure 76. RESTORE Barrier Simulation with Test Designation 4-12 Impacts	110
Figure 77. Recommended Barrier Design for Full-Scale Crash Testing, System Layout	114
Figure 78. Recommended Barrier Design for Full-Scale Crash Testing, Barrier Assembly.....	115
Figure 79. Recommended Barrier Design for Full-Scale Crash Testing, Post and Tubing Details	116
Figure 80. Recommended Barrier Design for Full-Scale Crash Testing, Splice Details.....	117
Figure 81. Recommended Barrier Design for Full-Scale Crash Testing, Instrumentation.....	118
Figure 82. Recommended Barrier Design for Full-Scale Crash Testing, Concrete Rail Geometry.....	119
Figure 83. Recommended Barrier Design for Full-Scale Crash Testing, Concrete Rail Details	120

Figure 84. Recommended Barrier Design for Full-Scale Crash Testing, Concrete Rail Details	121
Figure 85. Recommended Barrier Design for Full-Scale Crash Testing, Concrete Rail Details	122
Figure 86. Recommended Barrier Design for Full-Scale Crash Testing, Concrete Rail Details	123
Figure 87. Recommended Barrier Design for Full-Scale Crash Testing, Concrete Rail Details	124
Figure 88. Recommended Barrier Design for Full-Scale Crash Testing, Bill of Bars	125
Figure 89. Recommended Barrier Design for Full-Scale Crash Testing, Skid Details	126
Figure 90. Recommended Barrier Design for Full-Scale Crash Testing, Skid Assembly Details	127
Figure 91. Recommended Barrier Design for Full-Scale Crash Testing, Skid Component Details	128
Figure 92. Recommended Barrier Design for Full-Scale Crash Testing, Skid Top Plate Detail	129
Figure 93. Recommended Barrier Design for Full-Scale Crash Testing, Steel Rail Assembly.....	130
Figure 94. Recommended Barrier Design for Full-Scale Crash Testing, Steel End Tubing Assembly.....	131
Figure 95. Recommended Barrier Design for Full-Scale Crash Testing, Steel Rail Components	132
Figure 96. Recommended Barrier Design for Full-Scale Crash Testing, Adjustable Continuity Joint Details	133
Figure 97. Recommended Barrier Design for Full-Scale Crash Testing, Rubber Post Details ...	134
Figure 98. Recommended Barrier Design for Full-Scale Crash Testing, Fastener Details	135
Figure 99. Recommended Barrier Design for Full-Scale Crash Testing, Bill of Materials.....	136
Figure A-1. Rubber Post Certificate of Conformance	141
Figure B-1. Test No. SF10-1 Results (DTS).....	143
Figure B-2. Test No. SF10-1 Results (EDR-3).....	144
Figure B-3. Test No. SF10-2 Results (DTS).....	145
Figure B-4. Test No. SF10-2 Results (EDR-3).....	146
Figure B-5. Test No. SFD-1 Results (SLICE-2).....	147
Figure B-6. Test No. SFD-2 Results (SLICE-2).....	148
Figure B-7. Test No. SFD-3 Results (SLICE-2).....	149
Figure B-8. Test No. SFD-4 Results (SLICE-2).....	150
Figure B-9. Test No. SFD-5 Results (SLICE-2).....	151
Figure B-10. Test No. SF10P-1 Results (SLICE-2)	152
Figure B-11. Test No. SF10P-2 Results (SLICE-2)	153

LIST OF TABLES

Table 1. Video Cameras and Locations in Dynamic Component Tests	30
Table 2. Dynamic Testing Results, All Tests without Steel Pipe	33
Table 3. Dynamic Testing Results, All Tests with Steel Pipe	35
Table 4. Dynamic Testing Results, All Component Tests.....	44
Table 5. Dynamic Test Comparisons, 11 ⁵ / ₈ -in. (295-mm) and 16-in. (406-mm) Tall Posts.....	49
Table 6. Barrier Model Parts, Elements, and Materials	84
Table 7. Simulation Occupant Risk Data – MASH Test Designation 4-10.....	88
Table 8. Simulation Parallel and Exit Conditions – MASH Test Designation 4-10.....	88
Table 9. Simulation Occupant Risk Data – MASH Test Designation 4-11.....	92
Table 10. Simulation Parallel and Exit Condition – MASH Test Designation 4-11	92
Table 11. Skid Model Parts, Elements, and Materials.....	105
Table 12. Simulation Parallel and Exit Conditions – MASH Test Designation 4-10.....	108
Table 13. Simulation Parallel and Exit Conditions – MASH Test Designation 4-11.....	109

1 INTRODUCTION

1.1 Background

Concrete barriers are successful at containing and redirecting large-trucks during impact events. However, passenger vehicle impacts into rigid concrete barriers can result in high impact forces, which can lead to severe and fatal injuries to the occupants due to the large vehicle accelerations. Therefore, a restorable, energy-absorbing longitudinal barrier concept was developed by Schmidt, et al. [1-2] that would reduce the lateral acceleration imparted to passenger vehicle occupants, while still redirecting large-trucks.

There were several design criteria for the barrier. First, the barrier was to pass the Association of American State Highway and Transportation Officials (AASHTO) *Manual for Assessing Safety Hardware* (MASH) Test Level 4 (TL-4) crash testing criteria [3]. The TL-4 crash tests for a longitudinal barrier include test no. 4-10 with a 2,425-lb (1,100-kg) small car (designated 1100C) impacting at 62 mph (100 km/h) and 25 degrees, test no. 4-11 with a 5,000-lb (2,268-kg) pickup truck (designated 2270P) impacting at 62 mph (100 km/h) and 25 degrees, and test no. 4-12 with a 22,046-lb (10,000-kg) single-unit truck (designated 10000S) impacting at 56 mph (90 km/h) and 15 degrees. Also, a 30 percent decrease in the lateral acceleration on passenger vehicles was desired with impacts into the new barrier as compared to similar impacts with rigid concrete barriers. A comparison of previous testing as well as computer simulations helped to determine that 7 to 10 in. (178 to 254 mm) of barrier deflection should achieve the desired acceleration reductions for the 2270P impact event. The barrier width needs to be less than or equal to 36 in. (914 mm) to accommodate current urban median widths. The initial fabrication and installation cost needs to be competitive with current concrete barriers. Maintenance costs for the new barrier system should be virtually zero under typical impact conditions. The system should be restorable and reusable, with no damage during passenger

vehicle impacts. A minimal amount of damage is permissible with single-unit truck impact events.

The initial concept had discrete elastomer posts with a segmented concrete rail on top of the posts, as shown in Figure 1 [1]. The posts were 16 in. (406 mm) tall x 22 in. (559 mm) wide x 14 in. (356 mm) long, spaced at 10 ft (3.0 m). The concrete beam was 20 in. (508 mm) tall x 22 in. (559 mm) wide and was spliced at post locations. A material model of the rubber posts was developed for use in LS-DYNA finite element analysis by Schmidt, et al. [1]. A model of the barrier concept was created in LS-DYNA, and simulations of 1100C, 2270P, and 10000S vehicle models impacting the barrier were conducted. The initial simulation results indicated that the barrier had the potential to satisfy the design criteria.

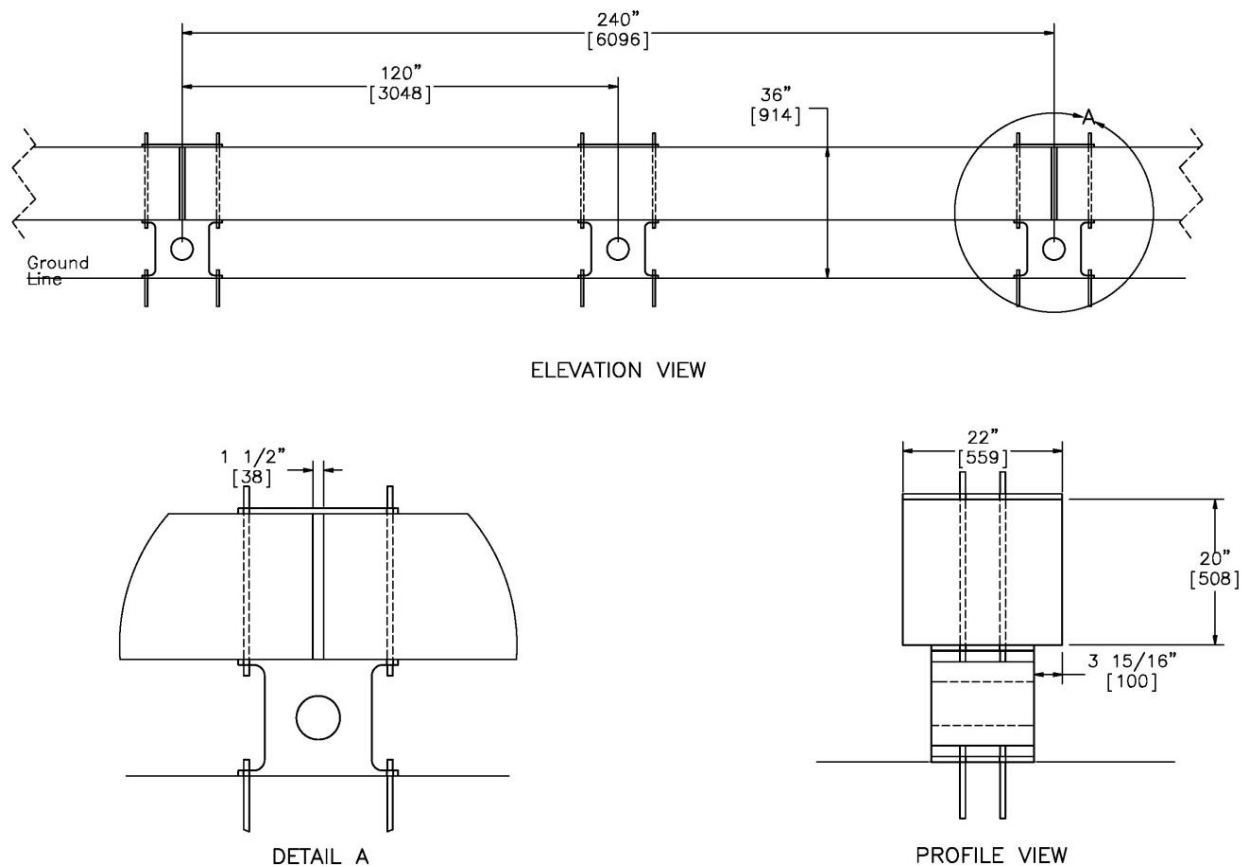


Figure 1. Initial Barrier Concept [1]

Several aspects of the barrier design discussed in Schmidt, et al. [1] warranted further investigation:

- 1) reduced height of the barrier due to the beam weight;
- 2) effect of the end constraints on the barrier system;
- 3) transitions and upstream and downstream termination;
- 4) effect of temperature on the rubber posts; and
- 5) the MASH TL-4 performance of the barrier including impacts with a 2,425-lb (1,100-kg) small car, 5,000-lb (2,268-kg) pickup truck, and 22,046-lb (10,000-kg) single-unit truck.

The reduced height of the barrier due to beam weight and the effect of temperature on the rubber posts were further evaluated by Schmidt, et al. [2]. When a 5,000 lb (2,268-kg) static load was applied to the 16-in. (406-mm) tall x 14-in. (356-mm) wide x 22-in. (559-mm) long posts, the vertical deflections at 16°F (-9°C), 67°F (19°C), and 130°F (54°C) were 1.4 in. (36 mm), 1.4 in. (36 mm), and 1.5 in. (38 mm), respectively. Therefore, the temperature of the rubber within the extremes found on American highways did not significantly affect the vertical deflection of the barrier. However, at warmer temperatures, the posts could not support the applied static load, and the load wanted to tip to one side. Stability of the barrier system was a concern if the weight was not evenly distributed on the posts.

It was previously established that a maximum 22-in. (559-mm) lower rail height would be necessary to capture the 1100C small car [1]. However, a large portion of the 1100C vehicle could still penetrate underneath the rail at this height, posing a concern for the car to snag on the posts, which could lead to excessive vehicle decelerations and/or occupant compartment deformation. Even with the 16-in. (406-mm) tall posts and equivalent lower rail height, the researchers believed that the tires and bumper of small cars could potentially snag on the posts. The Nebraska open concrete bridge rail had a 13-in. (330-mm) high clear opening below the rail

with discrete posts spaced every 8 ft (2.4 m) [4-6]. Since the RESTORE barrier will deflect and possibly expose a greater portion of the posts and allow the small car to snag on the posts, the height to the bottom of the rail was changed to $11\frac{5}{8}$ in. (295 mm). This height was selected from readily available parts, as shown in Figure 2. The posts were $11\frac{5}{8}$ in. (295 mm) tall x 10 in. (254 mm) wide x $15\frac{3}{4}$ in. (400 mm) long, with four vertical holes to accommodate $\frac{3}{4}$ -in. (19-mm) diameter bolts. A 4-in. (102-mm) diameter hole extended through the center of the post.

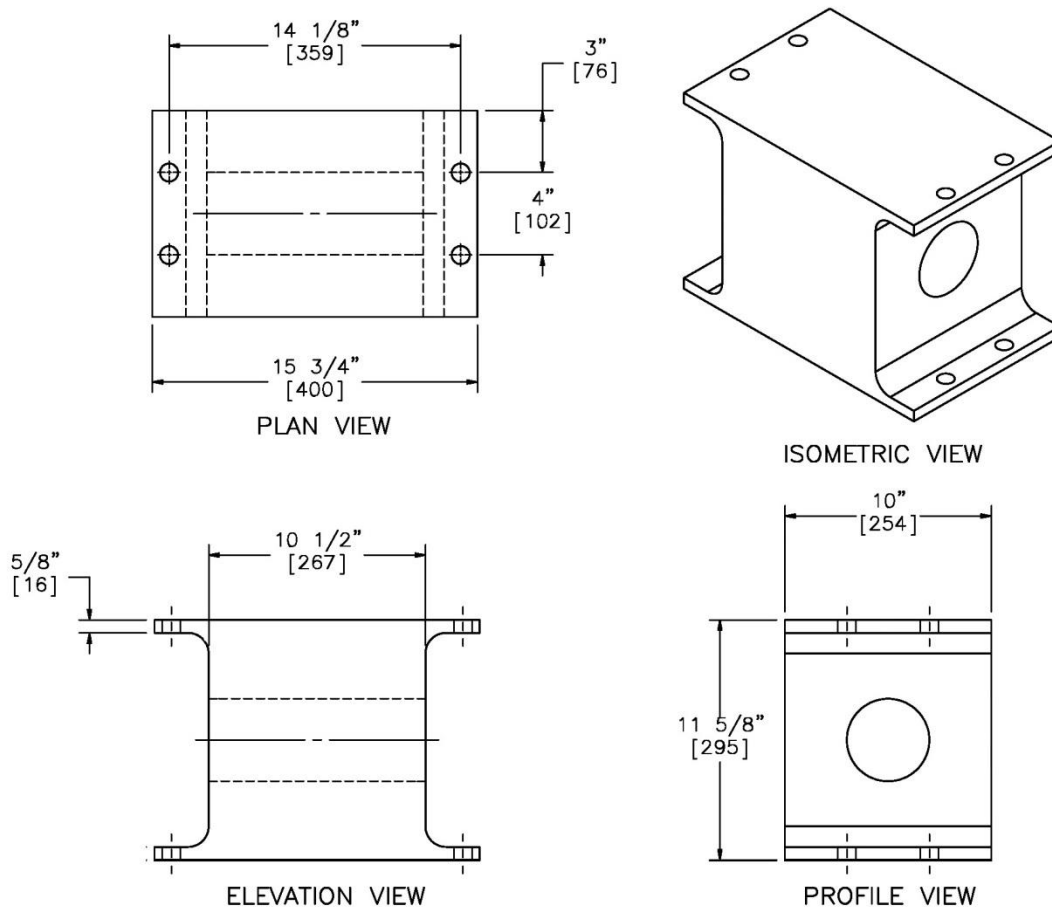


Figure 2. Post Schematic

Six static tests were conducted on smaller posts measuring $11\frac{5}{8}$ in. (295 mm) tall x 10 in. (254 mm) wide x $15\frac{3}{4}$ in. (400 mm) long [2]. Three to four posts were spaced at 4-ft (1.2-m) to 7-ft (2.1-m) intervals, and a 16-ft (4.9-m) long uniform weight concrete beam was gradually

lowered onto the posts. The deflection and stability of the system was recorded incrementally. Four posts spaced at 5-ft (1.5-m) increments were stable and supported over 7,000 lb (3,175 kg) on level terrain and supported over 3,500 lb (1,588 kg) when placed on a 14 percent slope. Three posts spaced at 7-ft (2.1-m) increments were stable and supported 6,500 lb (2,948 kg).

Based on the system performance, the targeted weight for a new rail was approximately 320 lb/ft (476 kg/m) when the 11⁵/₈-in. (295-mm) tall rubber posts were spaced at 5 ft (1.5 m), with a maximum 8 percent superelevated road [2]. A maximum of ½ in. (13 mm) vertical deflection from the static weight of a beam is anticipated for a hot temperature condition. The spacing of the 11⁵/₈-in. (295-mm) tall rubber posts may be increased up to 7 ft (2.1 m) if further evaluation shows favorable results.

A bogie test was conducted on a 28-ft (8.5-m) long prototype rubber post and timber rail beam system to determine the deflection and energy absorption of the barrier system [2]. Four 11⁵/₈-in. (295-mm) tall rubber posts were spaced at 96 in. (2,438 mm) on center. The center of gravity of the bogie was about 6 in. (152 mm) higher than the impact height on the timber rail. Therefore, the barrier was loaded eccentrically, and the posts rotated more than deforming in shear. The timber rail rotated backward and completely fractured near the bogie's maximum displacement of 35 in. (889 mm). The bogie's kinetic energy was absorbed by the barrier primarily through the deflection of the rubber posts and bending and fracture of the timber rail. When compared to the total energy absorbed by the barrier, approximately 76 percent was absorbed by the four posts. If an optimal rail and splice were designed to distribute the impact load to multiple posts, then this barrier concept had the potential to reduce lateral accelerations by 30 percent during passenger vehicle impact events, as compared to similar impact events into a rigid concrete barrier. The posts absorb more energy per unit deflection when deforming in

shear rather than rotating [2], so optimizing the barrier to deform in shear would also increase energy absorption.

1.2 Objective

After the initial development of the barrier concept, further design and analysis was needed before evaluation of the system with a full-scale crash test program. Therefore, the objective of this study was to finalize the design of the new energy-absorbing, restorable and reusable barrier system, designated as the RESTORE barrier.

1.3 Scope

The research objectives were accomplished through several tasks. First, dynamic component tests were conducted on the 11 $\frac{5}{8}$ -in. (295-mm) tall rubber posts to characterize the energy-absorption properties of the posts during repeated impacts and to determine the post spacing. The rail geometry was optimized to reduce the weight to the targeted weight of 320 lb/ft (476 kg/m). A finite element analysis model was constructed with the new post and rail geometry to analyze various splices between the concrete beams. The performance of the final barrier model was evaluated with TL-4 impacts with the 1100C, 2270P, and 10000S vehicle models. The system was fabricated and installed, and final design recommendations were made.

2 COMPONENT TESTING CONDITIONS

2.1 Purpose

Dynamic bogie tests were conducted on 11 $\frac{5}{8}$ -in. (295-mm) tall rubber shear fenders manufactured by Morse Rubber, as shown in Figure 3, to determine their energy vs. deflection properties and evaluate their use as posts. Two tests (SF10-1 and SF10-2) were conducted to get the initial behavior of the posts. An additional five tests (SFD-1 through SFD-5) were conducted as repeatability tests to determine if the properties change with repeated impacts. Two more tests (SF10P-1 and SF10P-2) were conducted with a steel pipe inserted in the lengthwise hole in the post to determine if the steel pipe influenced the shear behavior of the post.



Figure 3. 11 $\frac{5}{8}$ -in. (295-mm) Tall Shear Fender

2.2 Scope

A total of nine dynamic bogie tests were conducted on an E46496 shear fender with dimensions of 11 $\frac{5}{8}$ in. (295 mm) tall x 10 in. (254 mm) wide x 15 $\frac{3}{4}$ in. (400 mm) long with a 4-in. (102-mm) diameter hole lengthwise through the shear fender. The bogie tests were conducted with the post loaded longitudinally, which is parallel to the length of the hole. The target impact conditions for tests SF10-1, SF10-2, SF10P-1, and SF10P-2 were a speed of 5 mph (8 km/h) and

an angle of 0 degrees, while the target impact conditions for tests SFD-1 through SFD-5 were a speed of 8 mph (13 km/h) and an angle of 0 degrees. The impact height for all dynamic bogie tests was 13 $\frac{3}{8}$ in. (340 mm) above the groundline. A steel-frame structure was bolted to the top of the post to transfer a shear load to the post and prevent direct contact between the bogie and the post. The bottom of the post was attached to the ground with $\frac{3}{4}$ -in. (19-mm) diameter threaded rods embedded 8 in. (203 mm) into the concrete tarmac and anchored with a minimum bond strength of 1,300 psi (8.96 MPa). A test setup photograph is shown in Figure 4. The test matrices and test setup are shown in Figures 5 through 10 for test nos. SF10-1 and SF10-2, Figures 11 through 16 for test nos. SFD-1 through SFD-5, and Figures 17 through 22 for test nos. SF10P-1 and SF10P-2. A certificate of conformity for the posts is shown in Appendix A.



Figure 4. Bogie Test Setup, All Tests

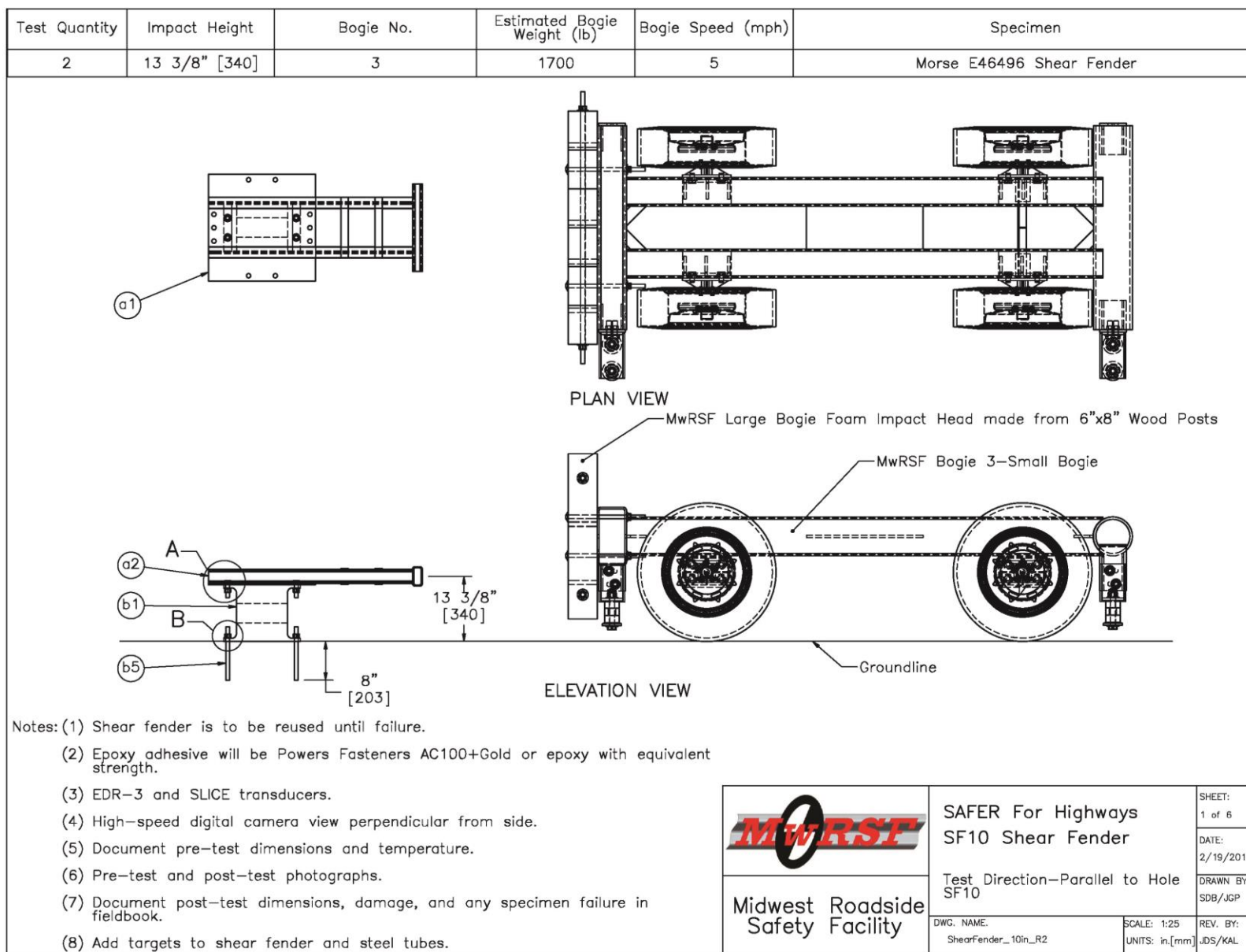


Figure 5. Bogie Testing Matrix and Setup – Test Nos. SF10-1 and SF10-2, Sheet 1 of 6

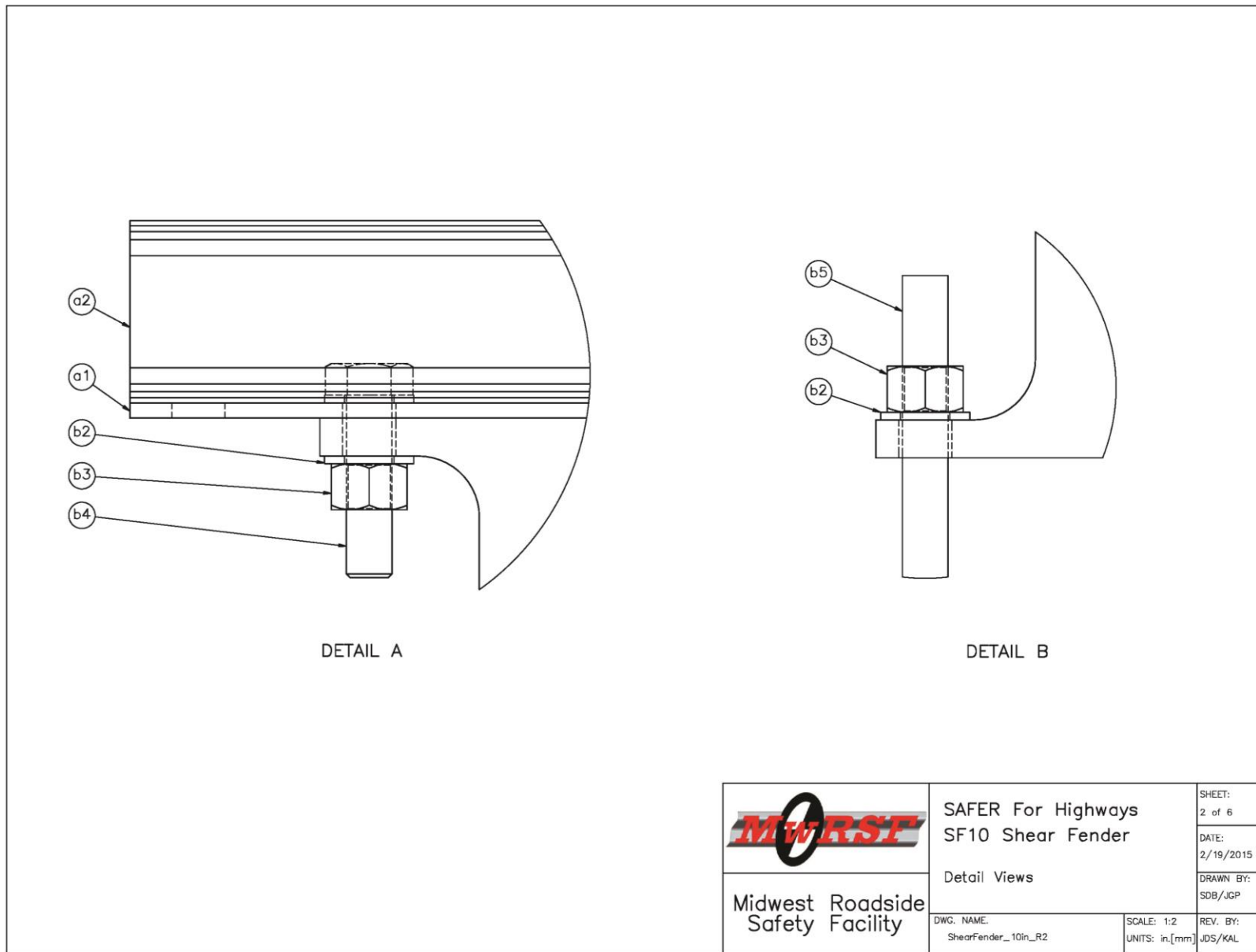


Figure 6. Bogie Testing Matrix and Setup – Test Nos. SF10-1 and SF10-2, Sheet 2 of 6

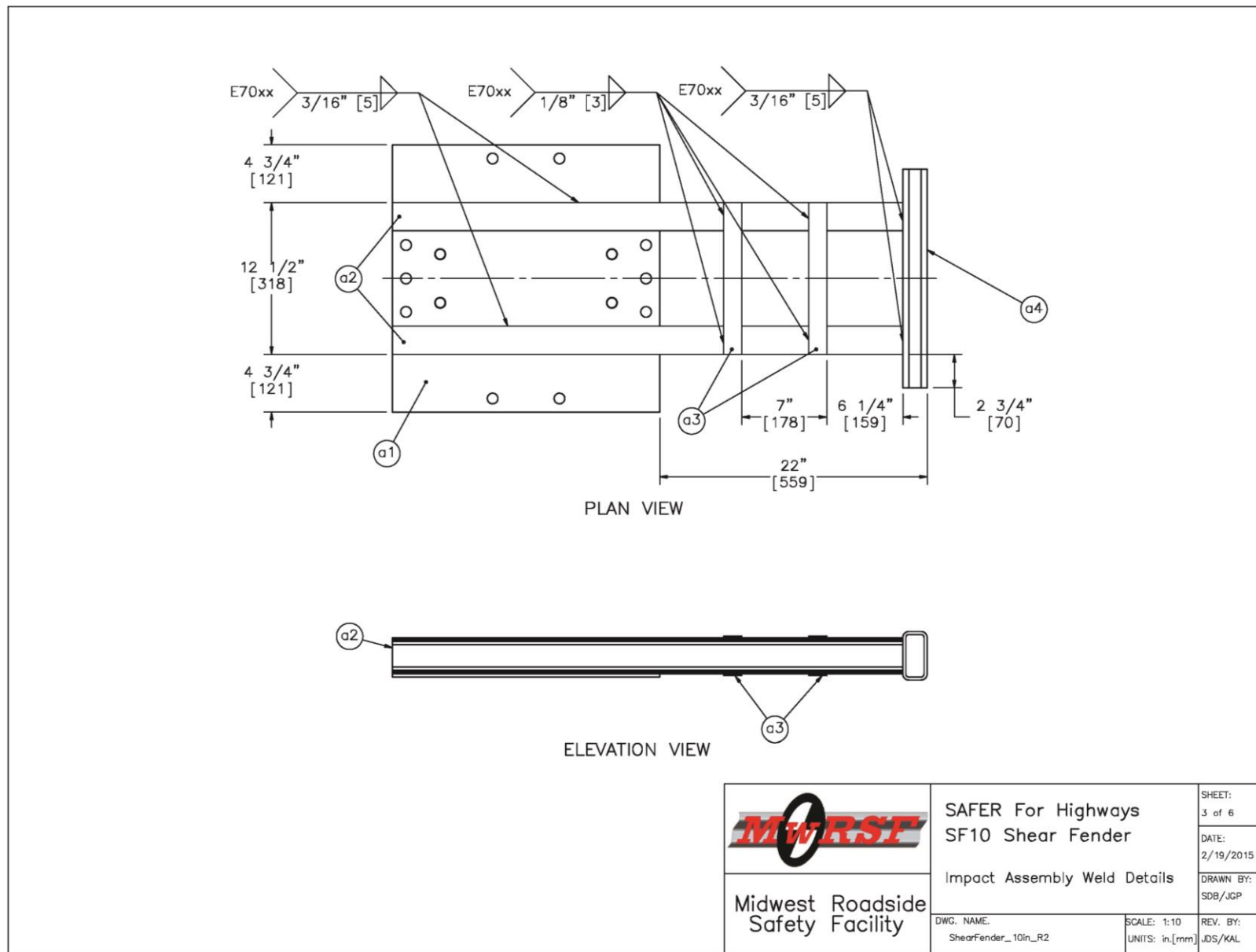


Figure 7. Bogie Testing Matrix and Setup – Test Nos. SF10-1 and SF10-2, Sheet 3 of 6

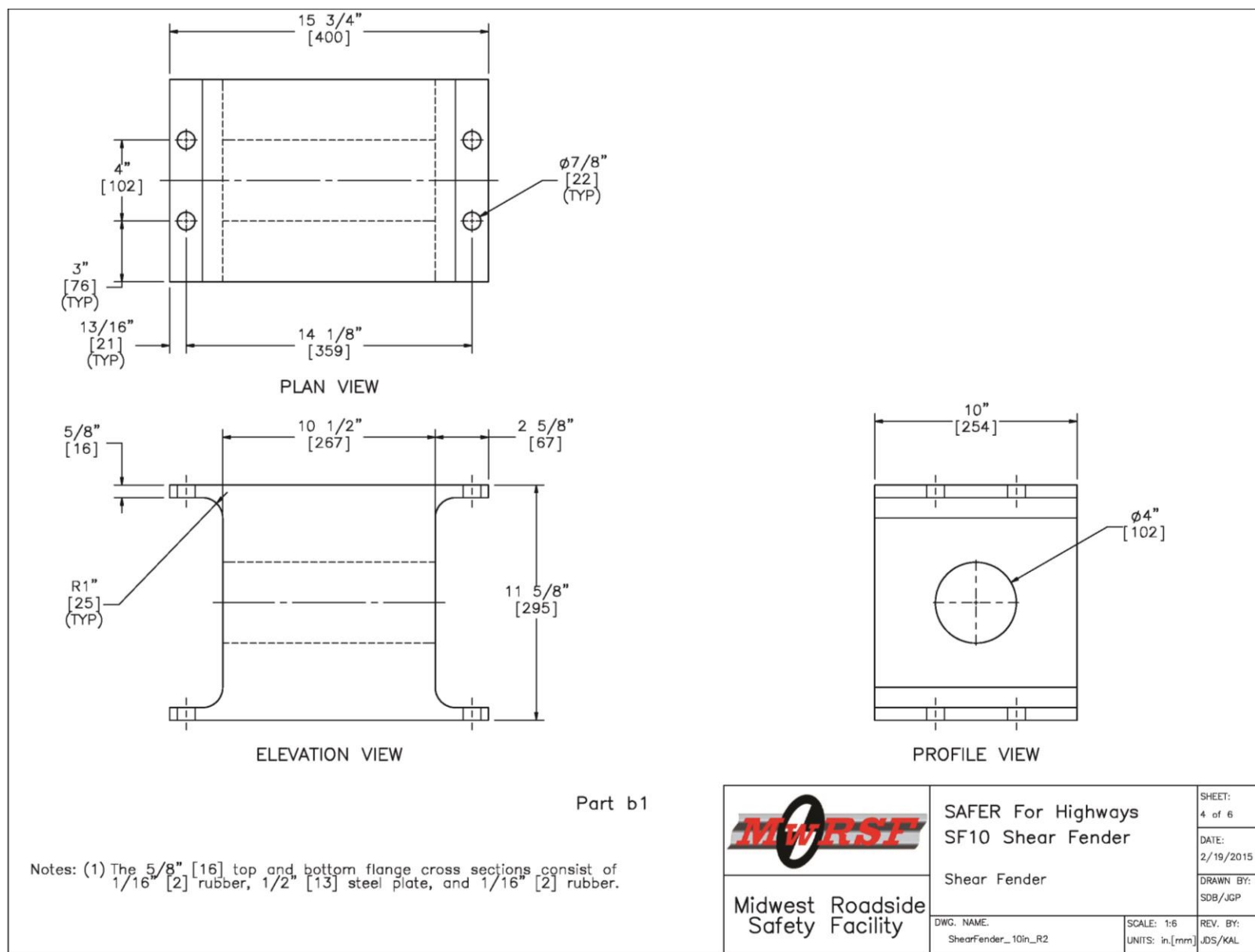


Figure 8. Bogie Testing Matrix and Setup – Test Nos. SF10-1 and SF10-2, Sheet 4 of 6

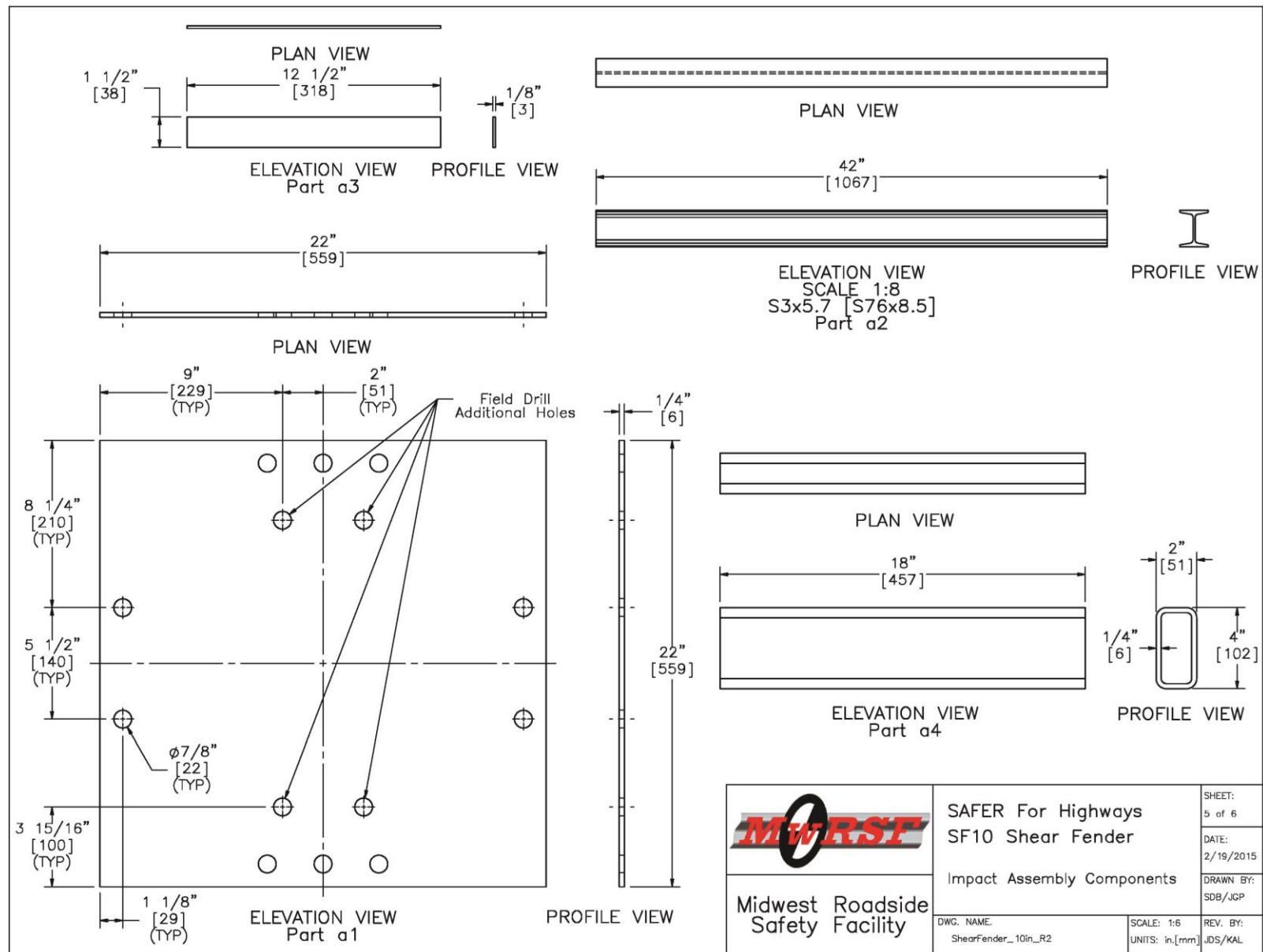


Figure 9. Bogie Testing Matrix and Setup – Test Nos. SF10-1 and SF10-2, Sheet 5 of 6

Item No.	QTY.	Description	Material Specification
a1	1	22"x22"x1/4" [559x559x6] Steel Mounting Plate	ASTM A36
a2	2	42" [1067] Long S3x5.7 [S76x8.5] Steel Beam	ASTM A36/A992
a3	4	12 1/2" [318] Long 1/8"x1 1/2" [3x38] Strap	ASTM A36
a4	1	18" [457] Long 4"x2"x1/4" [102x51x6] Rectangular Tube	ASTM A500 Grade B
b1	1	Morse E46496 Shear Fender	ASTM D2000
b2	12	3/4" [19] Dia. Flat Washer	ASTM F436
b3	8	Dia. 3/4" [19] – 10 UNC Heavy Hex Nut	ASTM A563
b4	4	Dia. 3/4" [19] x 2" [51] Long – 10 UNC Heavy Hex Bolt	ASTM A325
b5	4	Dia. 3/4" [19] x 11" [279] Long – 10 UNC Threaded Rod	ASTM A193 type B7
b6	–	Powers Fasteners AC100+Gold Epoxy or Epoxy with equivalent strength	Minimum Bond Strength = 1300 psi

 Midwest Roadside Safety Facility	SAFER For Highways SF10 Shear Fender	SHEET: 6 of 6
	Bill of Materials	DATE: 2/19/2015
DWG. NAME: ShearFender_10in_R2	SCALE: 1:16 UNITS: in.[mm]	DRAWN BY: SDB/JGP
		REV. BY: JDS/KAL

Figure 10. Bogie Testing Matrix and Setup – Test Nos. SF10-1 and SF10-2, Sheet 6 of 6

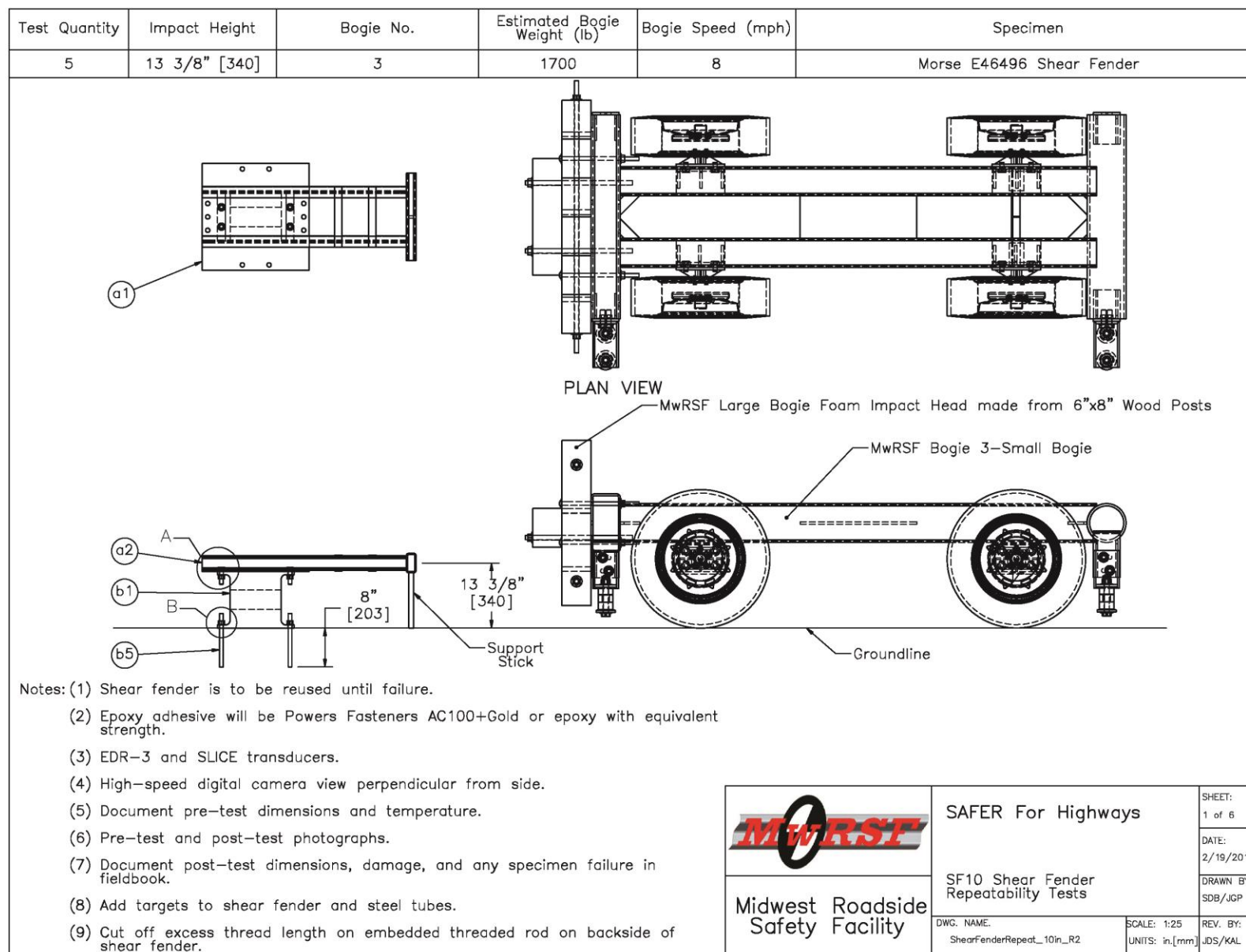


Figure 11. Bogie Testing Matrix and Setup – Test Nos. SFD-1 through SFD-5, Sheet 1 of 6

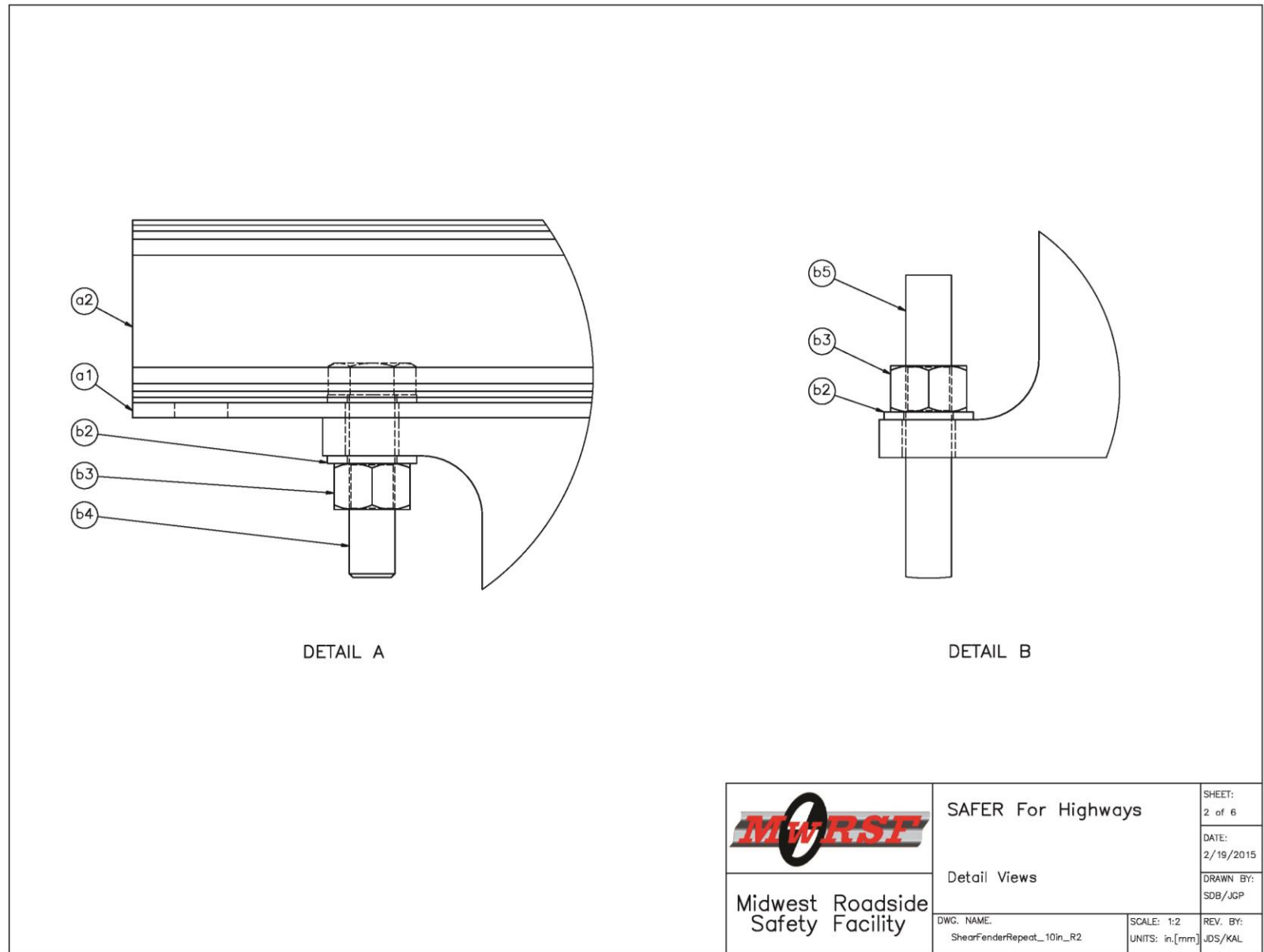


Figure 12. Bogie Testing Matrix and Setup – Test Nos. SFD-1 through SFD-5, Sheet 2 of 6

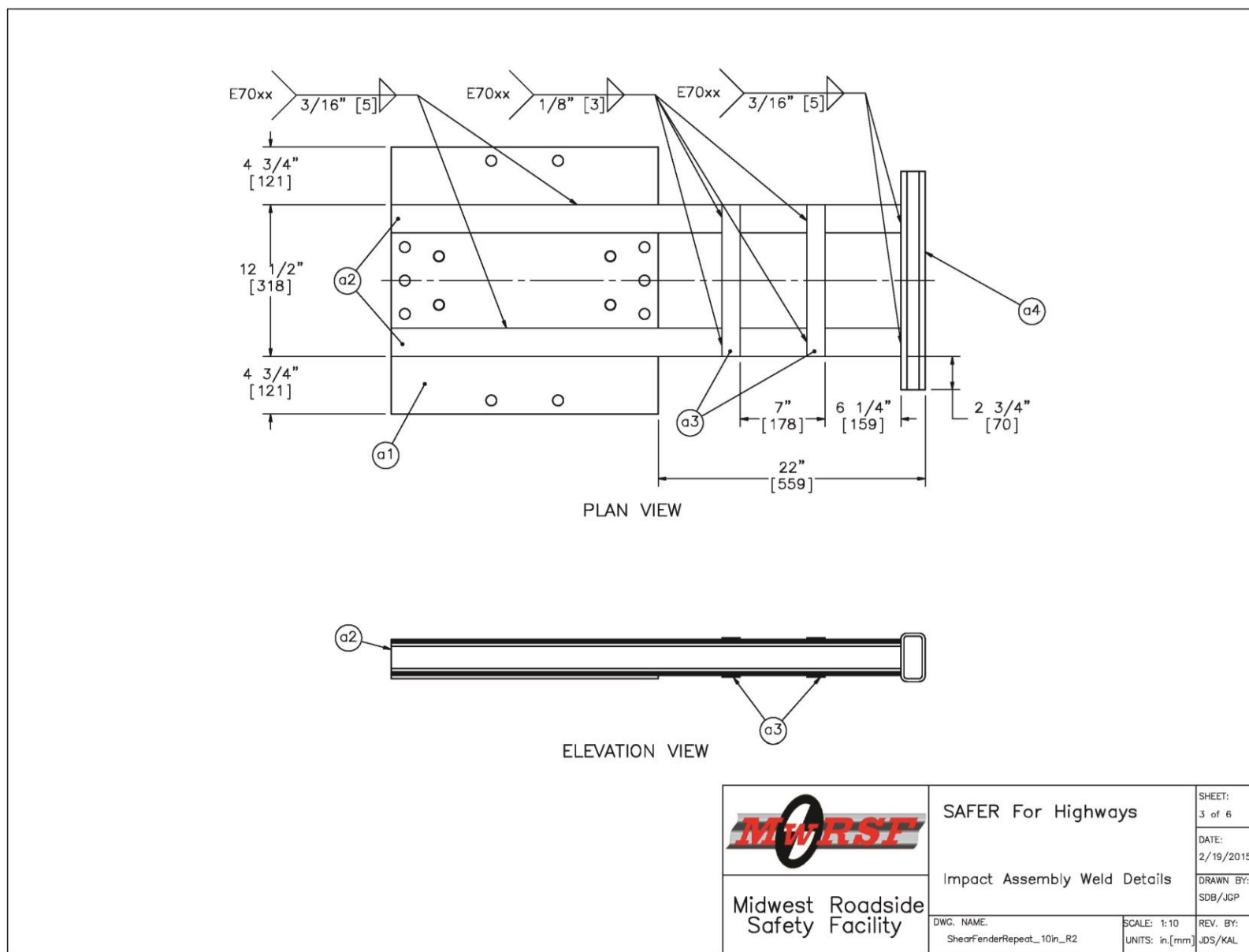


Figure 13. Bogie Testing Matrix and Setup – Test Nos. SFD-1 through SFD-5, Sheet 3 of 6

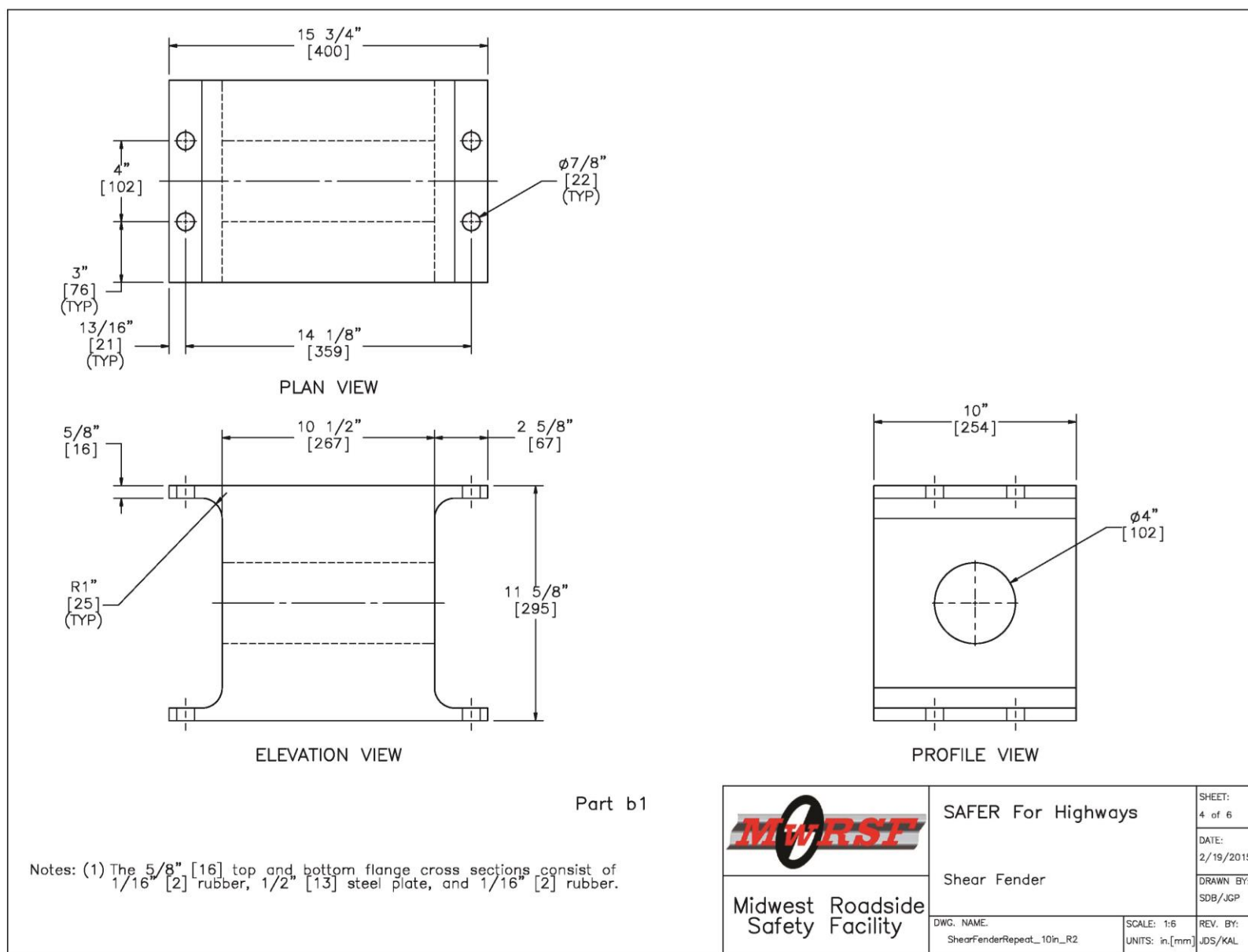


Figure 14. Bogie Testing Matrix and Setup – Test Nos. SFD-1 through SFD-5, Sheet 4 of 6

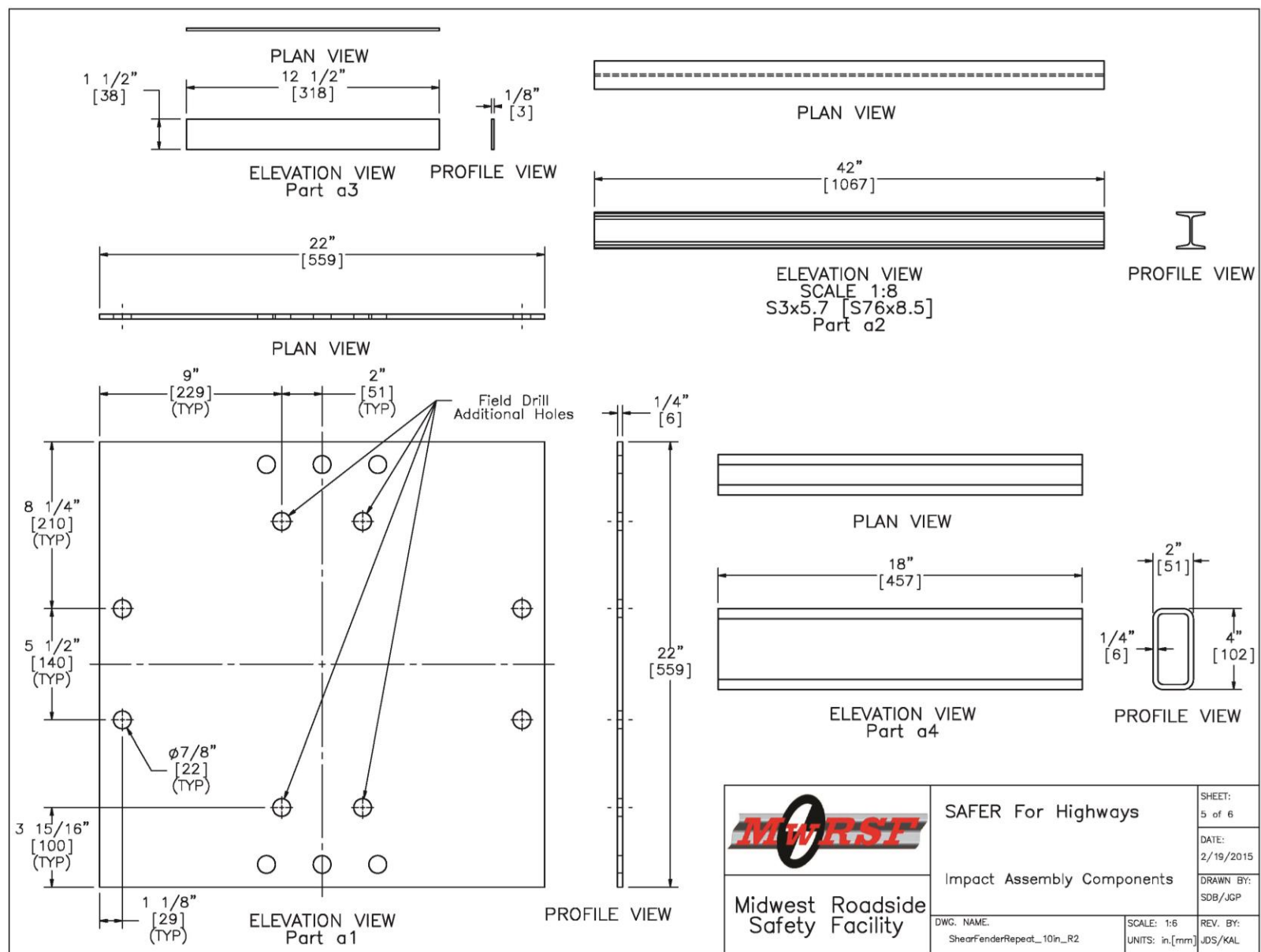


Figure 15. Bogie Testing Matrix and Setup – Test Nos. SFD-1 through SFD-5, Sheet 5 of 6


Item No.	QTY.	Description	Material Specification
a1	1	22"x22"x1/4" [559x559x6] Steel Mounting Plate	ASTM A36
a2	2	42" [1067] Long S3x5.7 [S76x8.5] Steel Beam	ASTM A36/A992
a3	4	12 1/2" [318] Long 1/8"x1 1/2" [3x38] Strap	ASTM A36
a4	1	18" [457] Long 4"x2"x1/4" [102x51x6] Rectangular Tube	ASTM A500 Grade B
b1	1	Morse E46496 Shear Fender	ASTM D2000
b2	12	3/4" [19] Dia. Flat Washer	ASTM F436
b3	8	Dia. 3/4" [19] – 10 UNC Heavy Hex Nut	ASTM A563
b4	4	Dia. 3/4" [19] x 2" [51] Long – 10 UNC Heavy Hex Bolt	ASTM A325
b5	4	Dia. 3/4" [19] x 11" [279] Long – 10 UNC Threaded Rod	ASTM A193 type B7
b6	–	Powers Fasteners AC100+Gold Epoxy or Epoxy with equivalent strength	Minimum Bond Strength = 1300 psi
<div>  <div> <div>SAFER For Highways</div> <div>Bill of Materials</div> <div> <div>DWG. NAME: ShearFenderRepeat_10in_R2</div> <div>SCALE: 1:16 UNITS: in,[mm]</div> <div>REV. BY: JDS/KAL</div> </div> </div> <div> <div>SHEET: 6 of 6</div> <div>DATE: 2/19/2015</div> <div>DRAWN BY: SDB/JGP</div> </div> </div>			

Figure 16. Bogie Testing Matrix and Setup – Test Nos. SFD-1 through SFD-5, Sheet 6 of 6

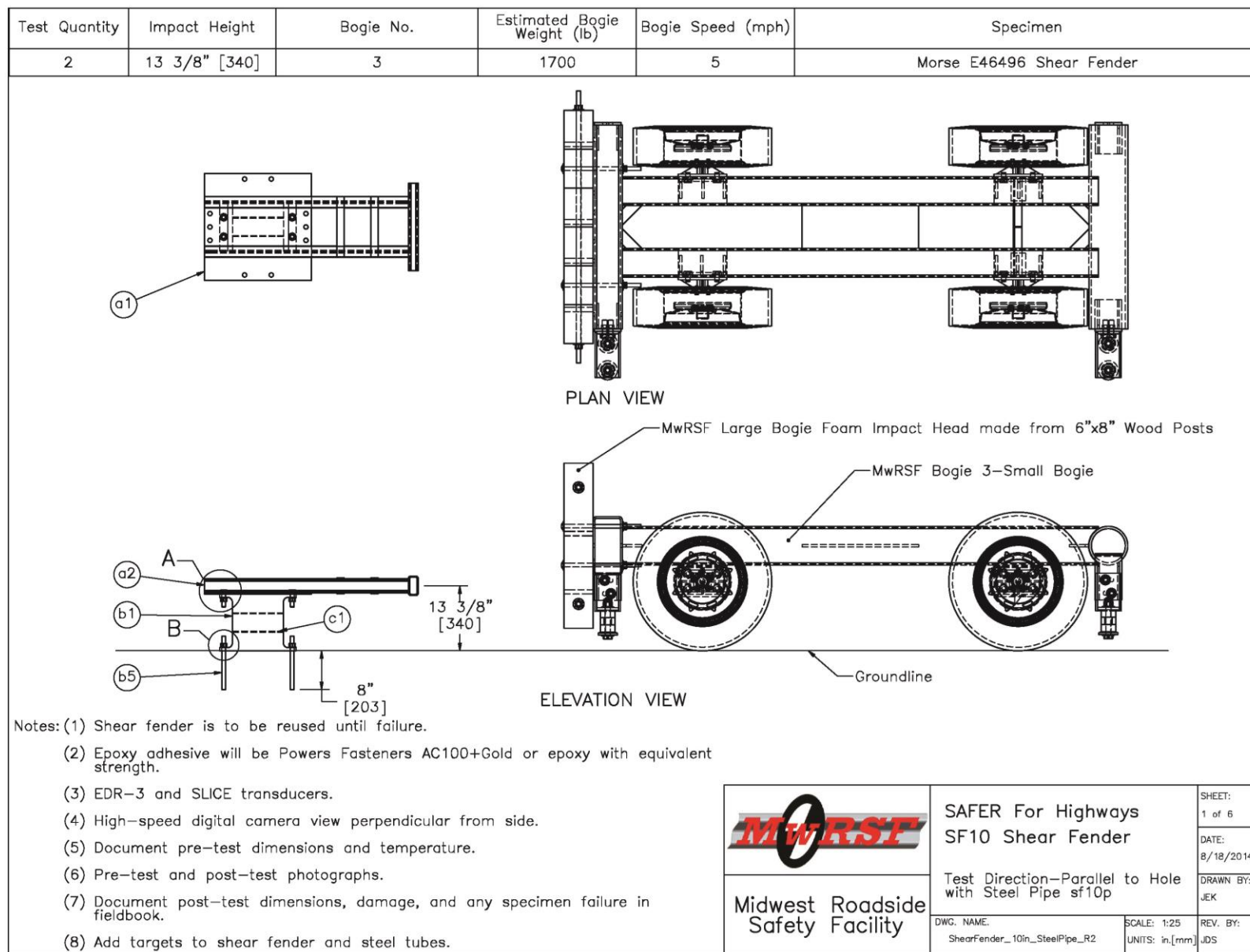


Figure 17. Bogie Testing Matrix and Setup – Test Nos. SF10P-1 and SF10P-2, Sheet 1 of 6

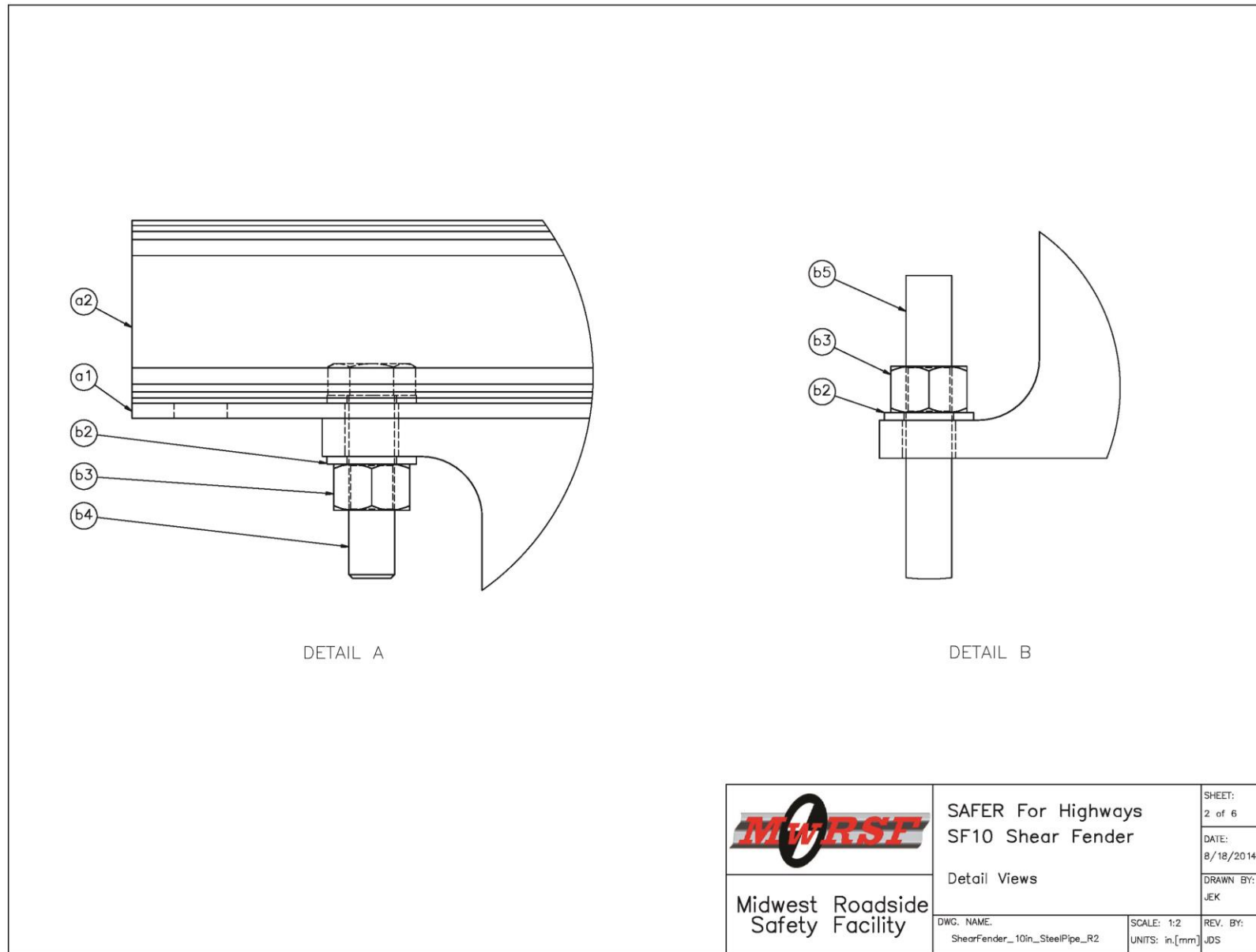


Figure 18. Bogie Testing Matrix and Setup – Test Nos. SF10P-1 and SF10P-2, Sheet 2 of 6

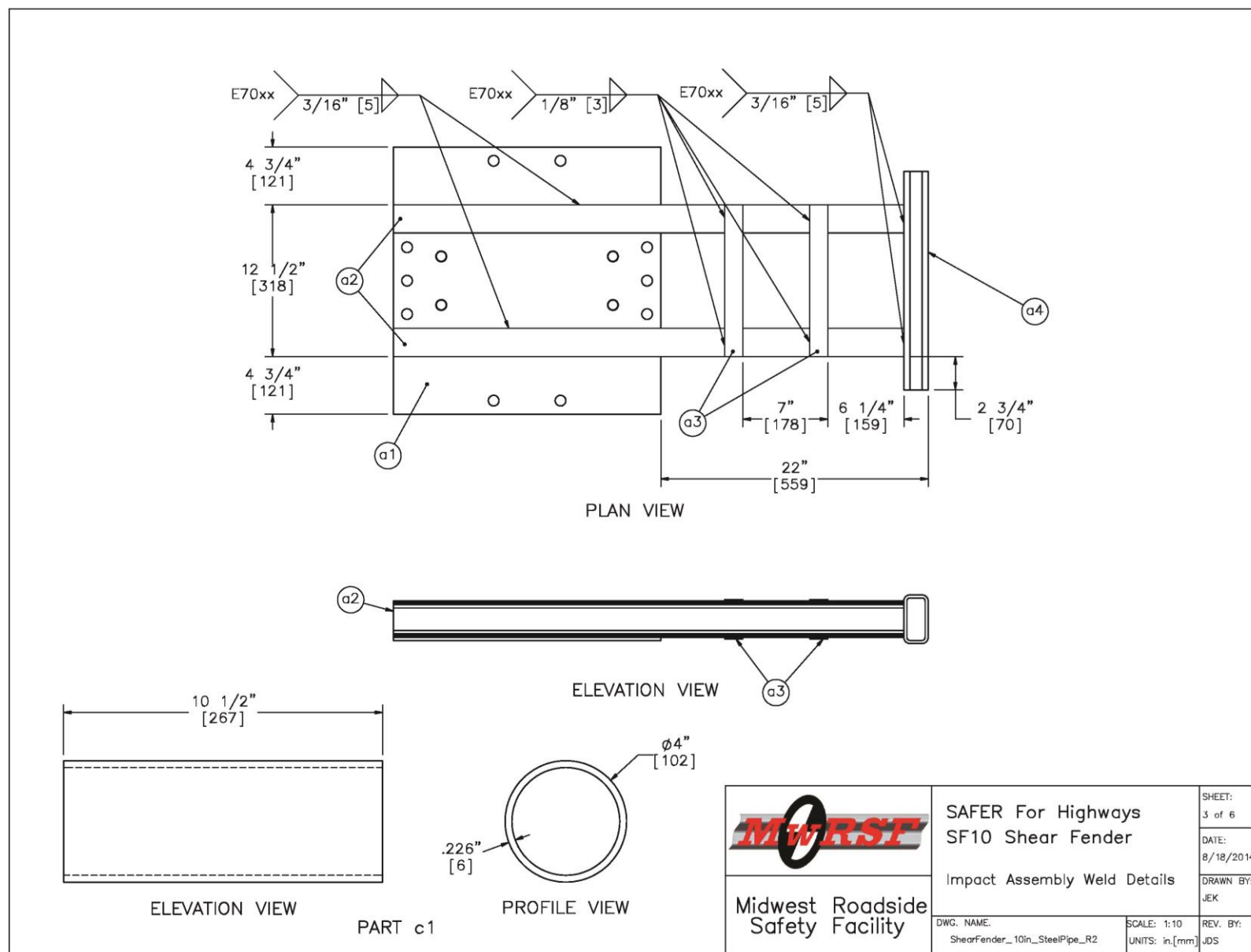


Figure 19. Bogie Testing Matrix and Setup – Test Nos. SF10P-1 and SF10P-2, Sheet 3 of 6

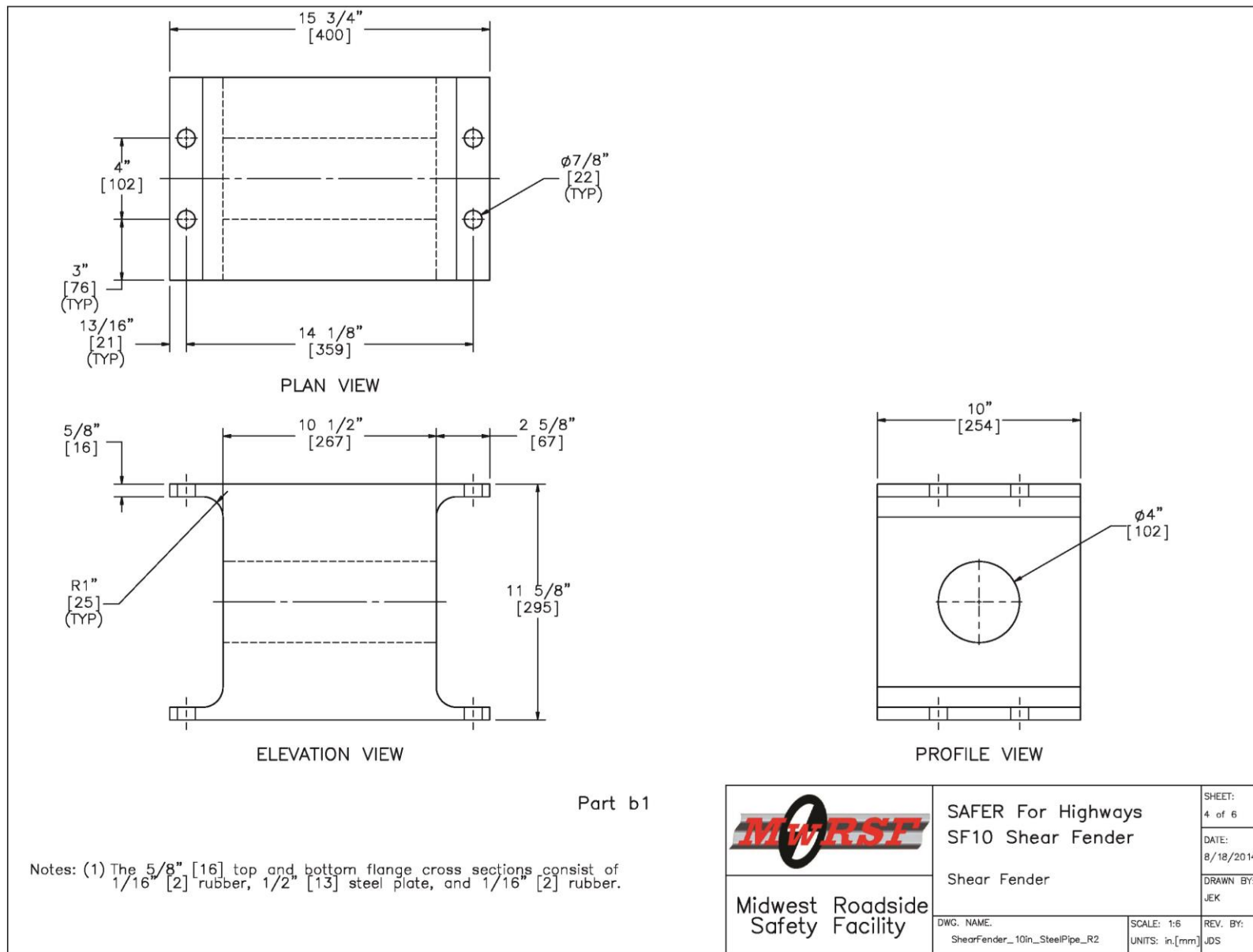


Figure 20. Bogie Testing Matrix and Setup – Test Nos. SF10P-1 and SF10P-2, Sheet 4 of 6

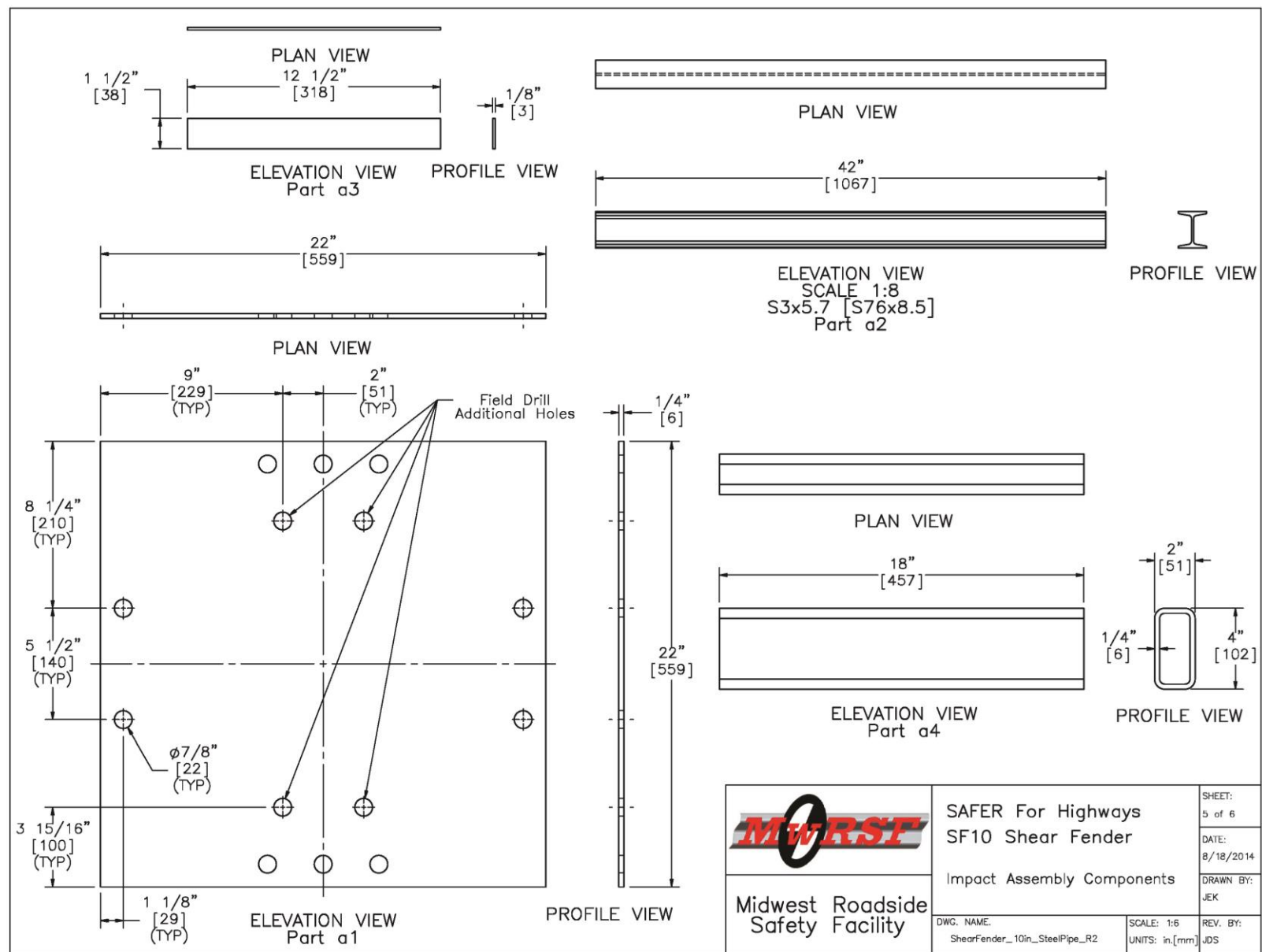


Figure 21. Bogie Testing Matrix and Setup – Test Nos. SF10P-1 and SF10P-2, Sheet 5 of 6

Figure 22. Bogie Testing Matrix and Setup – Test Nos. SF10P-1 and SF10P-2, Sheet 6 of 6

2.3 Equipment and Instrumentation

All dynamic tests were conducted at the MwRSF Proving Grounds in Lincoln, Nebraska. Equipment and instrumentation utilized to collect and record data during the dynamic bogie tests included a bogie vehicle, accelerometers, optical speed system, high-speed and standard-speed digital video, and still cameras.

2.3.1 Bogie Vehicle

A rigid-frame bogie was used to impact the posts. A variable-height, detachable impact head was used in the testing. The bogie head was constructed of six 6-in. (152-mm) wide x 8-in. (203-mm) deep x 34-in. (864-mm) tall timbers covered with plywood. An additional 6-in. (152-mm) x 8-in. (203-mm) timber beam was attached horizontally to the impact head, so that the steel frame attached to the top of the post would impact just under the additional timber beam and not slide up the face of the impact head. The bogie with the impact head is shown in Figure 23. The weight of the bogie with the addition of the mountable impact head and accelerometers was 1,854 lb (841 kg) in test nos. SF10-1 and SF10-2 and 1,886 lb (85 kg) in test nos. SFD-1 through SFD-5, SF10P-1, and SF10P-2.

A steel-pipe guidance track was used to guide the bogie vehicle for the tests, as shown in Figure 23. A pickup truck with a reverse cable tow system was used to propel the bogie to the target impact speed. When the bogie approached the end of the guidance system, it was released from the tow cable, allowing it to be free-rolling when it impacted the post. A remote braking system was installed on the bogie, allowing it to be brought safely to rest after the test.



Figure 23. Rigid-Frame Bogie on Guidance Track

2.3.2 Accelerometers

Three environmental shock and vibration sensor/recorder systems were used to measure the accelerations in the longitudinal, lateral, and vertical directions. However, only the longitudinal acceleration was processed and reported. All of the accelerometers were mounted near the center of gravity of the bogie vehicle.

The first system, the SLICE-2 unit, was a modular data acquisition system manufactured by Diversified Technical Systems, Inc. (DTS) of Seal Beach, California. The acceleration

sensors were mounted inside the body of a custom-built SLICE 6DX event data recorder and recorded data at 10,000 Hz to the onboard microprocessor. The SLICE 6DX was configured with 7 GB of non-volatile flash memory, a range of ± 500 g's, a sample rate of 10,000 Hz, and a 1,650 Hz (CFC 1000) anti-aliasing filter. The "SLICEWare" computer software program and a customized Microsoft Excel worksheet were used to analyze and plot the accelerometer data. The SLICE-2 was used in test nos. SFD-1 through SFD-5, SF10P-1, and SF10P-2.

The second accelerometer system, the DTS unit, was a two-arm piezoresistive accelerometer system manufactured by Endevco of San Juan Capistrano, California. Three accelerometers were used to measure each of the longitudinal, lateral, and vertical accelerations independently at a sample rate of 10,000 Hz. The accelerometers were configured and controlled using a system developed and manufactured by DTS. More specifically, data was collected using a DTS Sensor Input Module (SIM), Model TDAS3-SIM-16M. The SIM was configured with 16 MB SRAM and 8 sensor input channels with 250 kB SRAM/channel. The SIM was mounted on a TDAS3-R4 module rack. The module rack was configured with isolated power/event/communications, 10BaseT Ethernet and RS232 communication, and an internal backup battery. Both the SIM and module rack were crashworthy. The "DTS TDAS Control" computer software program and a customized Microsoft Excel worksheet were used to analyze and plot the accelerometer data. The DTS was used in test nos. SF10-1 and SF10-2.

The third system, Model EDR-3, was a triaxial piezoresistive accelerometer system manufactured by Instrumented Sensor Technology, Inc. (IST) of Okemos, Michigan. The EDR-3 was configured with 256 kB of RAM, a range of ± 200 g's, a sample rate of 3,200 Hz, and a 1,120 Hz low-pass filter. The "DynaMax 1 (DM-1)" computer software program and a customized Microsoft Excel worksheet were used to analyze and plot the accelerometer data. The EDR-3 was used in test nos. SF10-1 and SF10-2.

2.3.3 Retroreflective Optic Speed Trap

A retroreflective optic speed trap was used to determine the speed of the bogie vehicle before impact. Three retroreflective targets, spaced at approximately 18-in. (457-mm) intervals, were applied to the side of the vehicle. When the emitted beam of light was reflected by the targets and returned to the Emitter/Receiver, a signal was sent to the data acquisition computer, recording at 10,000 Hz, as well as the external LED box activating the LED flashes. The speed was then calculated using the spacing between the retroreflective targets and the time between the signals. LED lights and high-speed digital video analysis are only used as a backup in the event that vehicle speeds cannot be determined from the electronic data.

2.3.4 Digital Photography

AOS S-VIT high-speed digital video cameras, Go Pro Hero 3 digital video cameras, and JVC digital cameras were used to document each test. The cameras used in each test and their locations are shown in Table 1.

Table 1. Video Cameras and Locations in Dynamic Component Tests

Test No.	Digital Video Cameras	
	Description	Location
SF10-1 and SF10-2	AOS S-VIT	Lateral – Left Side of Bogie
	JVC	Lateral –Right Side of Bogie
	Go Pro	Oblique Downstream
SFD-1	AOS S-VIT	Lateral – Left Side of Bogie
	Go Pro	Lateral – Left Side of Bogie
SFD-2 through SFD-5	AOS S-VIT	Lateral – Left Side of Bogie
	Go Pro	Lateral – Left Side of Bogie
	Go Pro	Lateral – Left Side of Bogie
SF10P-1	AOS S-VIT	Lateral – Left Side of Bogie
	Go Pro	Lateral – Left Side of Bogie
SF10P-2	AOS S-VIT	Lateral – Left Side of Bogie
	Go Pro	Lateral – Left Side of Bogie
	Go Pro	Downstream

The AOS S-VIT high-speed cameras had a frame rate of 500 frames per second, the Go Pro video cameras had a frame rate of 120 frames per second, and the JVC digital video cameras had a frame rate of 29.97 frames per second. A Nikon D50 digital still camera was also used to document pre- and post-test conditions for all tests.

2.4 Data Processing

The electronic accelerometer data obtained in dynamic testing was filtered using the SAE Class 60 Butterworth filter conforming to the SAE J211/1 specifications [7]. The pertinent acceleration signal was extracted from the bulk of the data signals. The processed acceleration data was then multiplied by the mass of the bogie to get the impact force using Newton's Second Law. Next, the acceleration trace was integrated to find the change in velocity versus time. Initial velocity of the bogie, calculated from the optical speed system, was then used to determine the bogie velocity, and the calculated velocity trace was integrated to find the bogie's displacement. The bogie's displacement is also the deflection of the post in most cases. Due to the fact that the rubber posts rebounded during some tests and the bogie continued moving forward, the displacement from the acceleration trace may not accurately portray the deflection of the energy absorber.

3 POST TESTING RESULTS AND DISCUSSION

3.1 Results

The information desired from the bogie tests was the force versus deflection behavior of the post. This data was then used to find total energy (the area under the force vs. deflection curve) dissipated during each test.

Although the acceleration data was applied to the impact location, the data came from the center of gravity of the bogie. Since the bogie head was not perfectly rigid and sustained vibrations, error was added to the data. The bogie may have also rotated during the impact event, thus causing differences in accelerations between the bogie center of mass and the bogie impact head. Since filtering procedures were applied to the data to smooth out vibrations, and the rotations of the bogie during the tests were minor, these issues were deemed minor, and the data was still valid.

Significant pitch angles did develop late in some tests as the bogie overrode the post. However, these motions occurred after the primary deflection of the post. One useful aspect of using accelerometer data was that it included influences of the post inertia on the reaction force. This influence was important, as the mass of the post would affect barrier performance as well as test results.

The accelerometer data for each test was processed in order to obtain acceleration, velocity, and deflection curves, as well as force vs. deflection and energy vs. deflection curves. Although the individual transducers produced similar results, the values described herein were calculated from the DTS or SLICE-2 data curves in order to provide common basis for comparing results from multiple tests. Test results for all transducers are provided in Appendix A.

3.1.1 11⁵/₈-in. (295-mm) Tall Rubber Post Tests

A total of seven dynamic bogie tests were conducted on the 11⁵/₈-in. (295-mm) tall posts with a targeted angle of 0 degrees and a speed of 5 mph (8 km/h) for test nos. SF10-1 and SF10-2 and 8 mph (12.9 km/h) for test nos. SFD-1 through SFD-5. Test nos. SF10-1 and SF10-2 were conducted on the same post on the same day. Test nos. SFD-1 through SFD-5 were conducted on the same post on the same day. Upon post-test examination, none of the shear fenders were damaged and had no permanent set. The impact conditions and results of these tests are summarized in Table 2.

Table 2. Dynamic Testing Results, All Tests without Steel Pipe

Test No.	Bogie Weight lb (kg)	Surface Temp. °F (°C)	Impact Velocity mph (km/h)	Max. Deflection in. (mm)	Peak Force kips (kN)
SF10-1	1,854 (841)	89 (32)	6.3 (10.1)	8.4 (213)	17.1 (76.1)
SF10-2	1,854 (841)	94 (34)	8.0 (12.9)	11.7 (297)	18.4 (81.8)
SFD-1	1,886 (855)	96 (36)	11.1 (17.8)	17.8 (452)	24.8 (110.3)
SFD-2	1,886 (855)	92 (33)	8.2 (13.2)	11.8 (300)	25.2 (112.1)
SFD-3	1,886 (855)	94 (34)	8.6 (13.9)	13.5 (343)	19.3 (85.9)
SFD-4	1,886 (855)	93 (34)	8.4 (13.5)	13.5 (343)*	15.4 (68.5)
SFD-5	1,886 (855)	92 (33)	8.6 (13.9)	14.2 (361)	19.2 (85.4)

Test No.	Energy at Deflection k-in. (kJ)				Total Energy k-in. (kJ)
	4 in. (102 mm)	6 in. (152 mm)	8 in. (203 mm)	10 in. (254 mm)	
SF10-1	11.0 (1.2)	18.2 (2.1)	27.4 (3.1)	NA	29.4 (3.3)
SF10-2	11.9 (1.3)	17.4 (2.0)	26.2 (3.0)	36.9 (4.2)	47.4 (5.4)
SFD-1	13.0 (1.5)	23.1 (2.6)	27.7 (3.1)	37.6 (4.2)	93.0 (10.5)
SFD-2	17.9 (2.0)	22.8 (2.6)	31.6 (3.6)	41.1 (4.6)	51.0 (5.8)
SFD-3	12.6 (1.4)	19.5 (2.2)	27.2 (3.1)	36.1 (4.1)	56.1 (6.3)
SFD-4	9.1 (1.0)	15.7 (1.8)	23.2 (2.6)	30.8 (3.5)	52.9 (6.0)
SFD-5	10.2 (1.2)	17.0 (1.9)	23.9 (2.7)	32.3 (3.6)	56.3 (6.4)

*taken from film analysis

Force vs. deflection and energy vs. deflection curves for test no. SF10-1 were created from the DTS accelerometer data and are shown in Figure 24. The bogie deflected the post in

shear until it reached a maximum deflection, and then the upper steel impact assembly began rotating upward which the bogie to pitch slightly as it rebounded. Sequential photographs are shown in Figure 25. The bogie and post behavior were very similar in all seven of the post tests, except test no. SFD-4. Therefore, force vs. deflection and energy vs. deflection curves and sequential photographs are not shown independently for each test.

In test no. SFD-4, the bogie was bouncing prior to the impact. As a result, the structure was impacted higher on the bogie head than the other tests. Due to the high impact, post rotation and front-end lift of the bogie increased. The largest displacement recorded by the accelerometer was 15.1 in. (384 mm) and occurred at the end of the event when the bogie lost contact with the impact structure. However, the maximum deflection that the post obtained was approximately 13.5 in. (343 mm) at approximately 0.150 seconds, as determined from high-speed film analysis. Sequential photographs of test no. SFD-4 are shown in Figure 26.

Force vs. deflection and energy vs. deflection curves for all tests on the 11 $\frac{5}{8}$ -in. (295-mm) tall posts without the steel pipe are shown in Figures 27 and 28, respectively. The energy vs. deflection curves were all within a narrow band for all of the tests, and the energy per unit deflection was very consistent after the initial inertial spike.

3.1.1 11 $\frac{5}{8}$ -in. (295-mm) Tall Rubber Post Tests with Steel Pipe

Two dynamic bogie tests were conducted on the 11 $\frac{5}{8}$ -in. (295-mm) tall posts with a targeted speed of 8 mph (12.9 km/h). Test nos. SF10P-1 and SF10P-2 were conducted on the same post on the same day. Upon examination, the post was not damaged and had no permanent set. However, the steel pipe moved in the hole as the post was loaded, so it was not flush with the post face after impact.

Table 3. Dynamic Testing Results, All Tests with Steel Pipe

Test No.	Bogie Weight lb (kg)	Surface Temp. °F (°C)	Impact Velocity mph (km/h)	Max. Deflection in. (mm)	Peak Force kips (kN)
SF10P-1	1,886 (855)	86 (30)	6.6 (10.6)	9.9 (251)	13.8 (61.4)
SF10P-2	1,886 (855)	88 (31)	9.5 (15.3)	14.6 (371)	21.2 (94.3)

Test No.	Energy at Deflection k-in. (kJ)				Total Energy k-in. (kJ)
	4 in. (102 mm)	6 in. (152 mm)	8 in. (203 mm)	10 in. (254 mm)	
SF10P-1	9.4 (1.1)	15.4 (1.7)	23.4 (2.6)	NA	32.5 (3.7)
SF10P-2	12.4 (1.4)	20.8 (2.4)	28.5 (3.2)	38.5 (4.3)	68.2 (7.7)

Similar to the component tests with no steel pipe inserted in the posts, the bogie deflects the post in shear until it reaches a maximum deflection, and then the upper steel impact assembly begins rotating upward and causes the bogie to pitch slightly as it is pushed backward. Sequential photographs from test no. SF10P-1 are shown in Figure 29. Results are not shown for each test independently, since they were very similar.

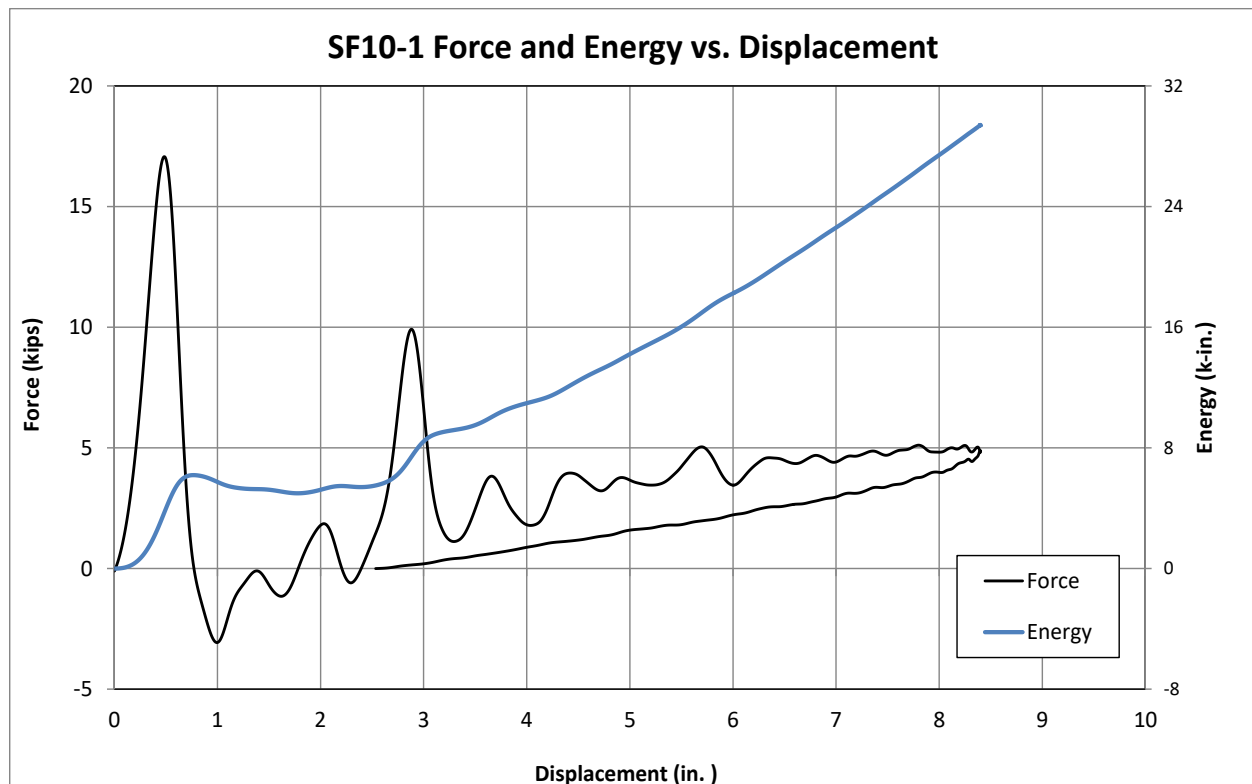


Figure 24. Energy and Force vs. Deflection, Test No. SF10-1



IMPACT



0.322 sec



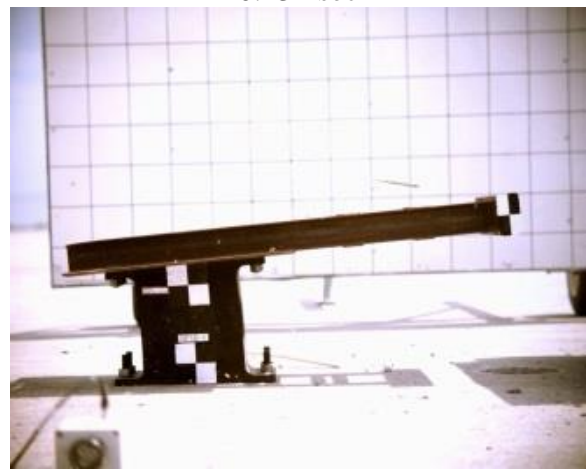
0.066 sec



0.432 sec



0.176 sec



0.584 sec

Figure 25. Time-Sequential Photographs, Test No. SF10-1



IMPACT



0.442 sec



0.120 sec



0.620 sec



0.212 sec



0.962 sec

Figure 26. Time-Sequential Photographs, Test No. SFD-4

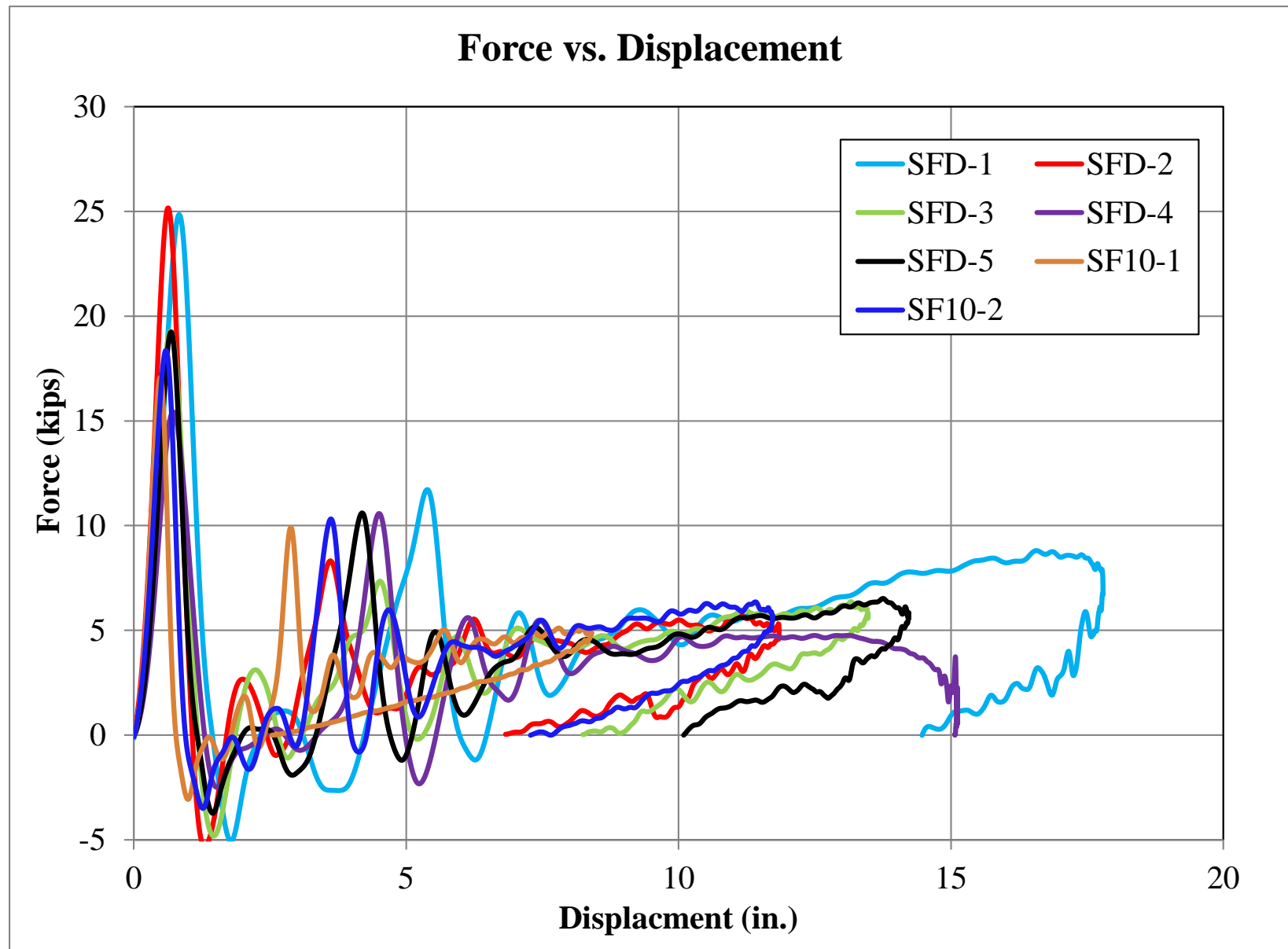


Figure 27. Force vs. Deflection Comparison, All Bogie Tests Without Steel Pipe

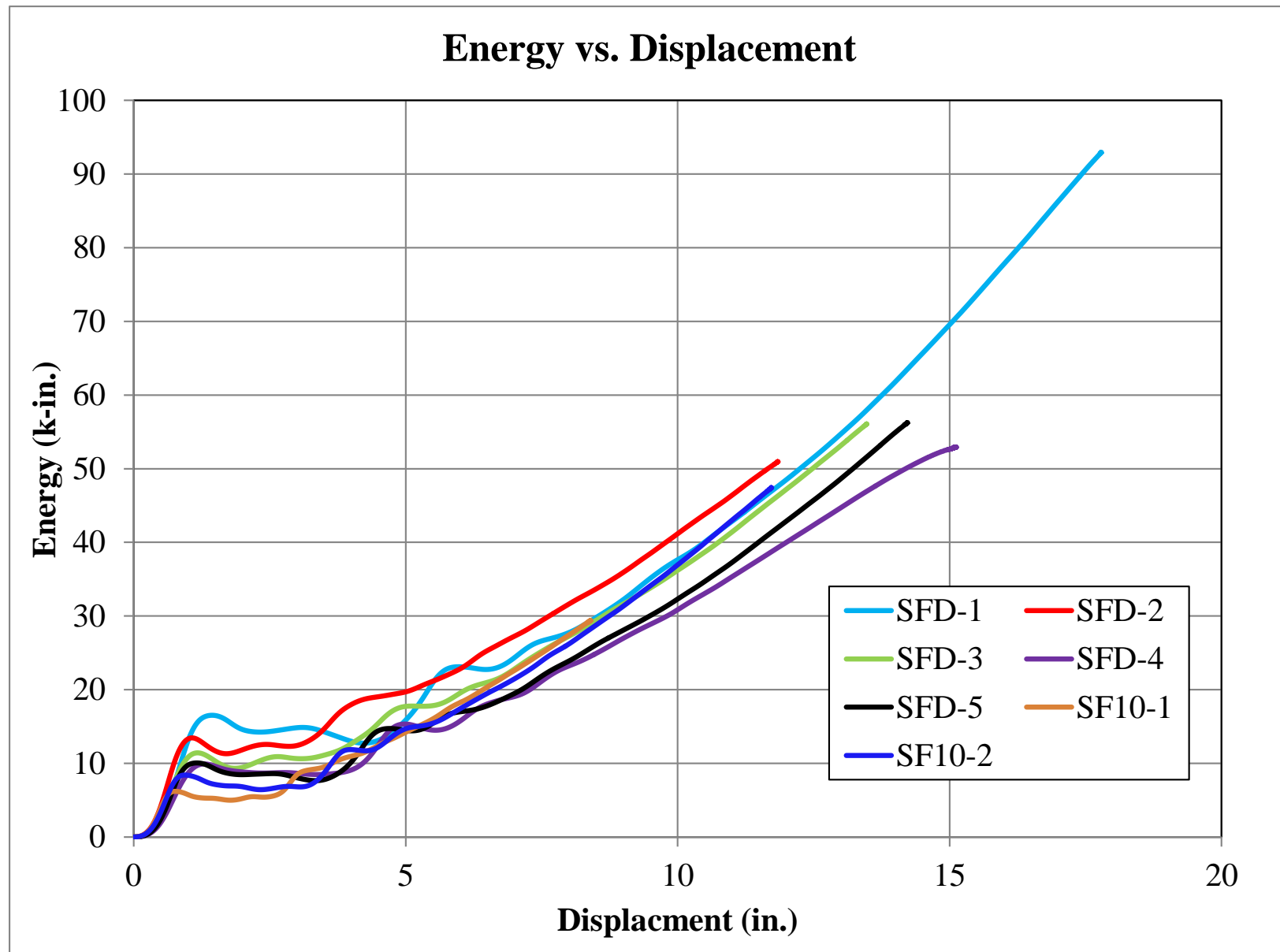


Figure 28. Energy vs. Deflection Comparison, All Bogie Tests Without Steel Pipe



IMPACT



0.418 sec



0.170 sec



0.590 sec



0.286 sec



0.752 sec

Figure 29. Time-Sequential Photographs, Test No. SF10P-1

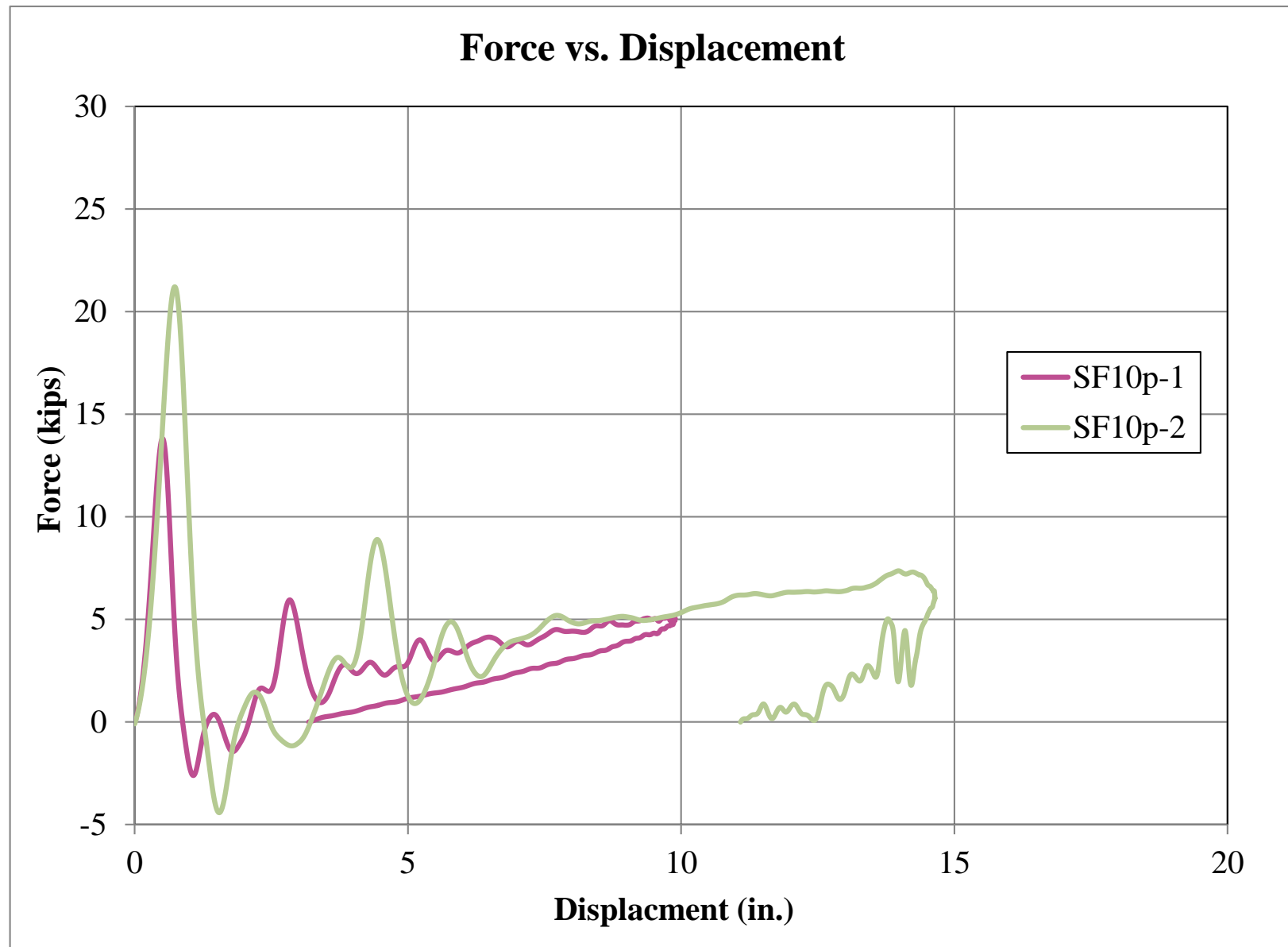


Figure 30. Force vs. Deflection Comparison, All Bogie Tests Without Steel Pipe

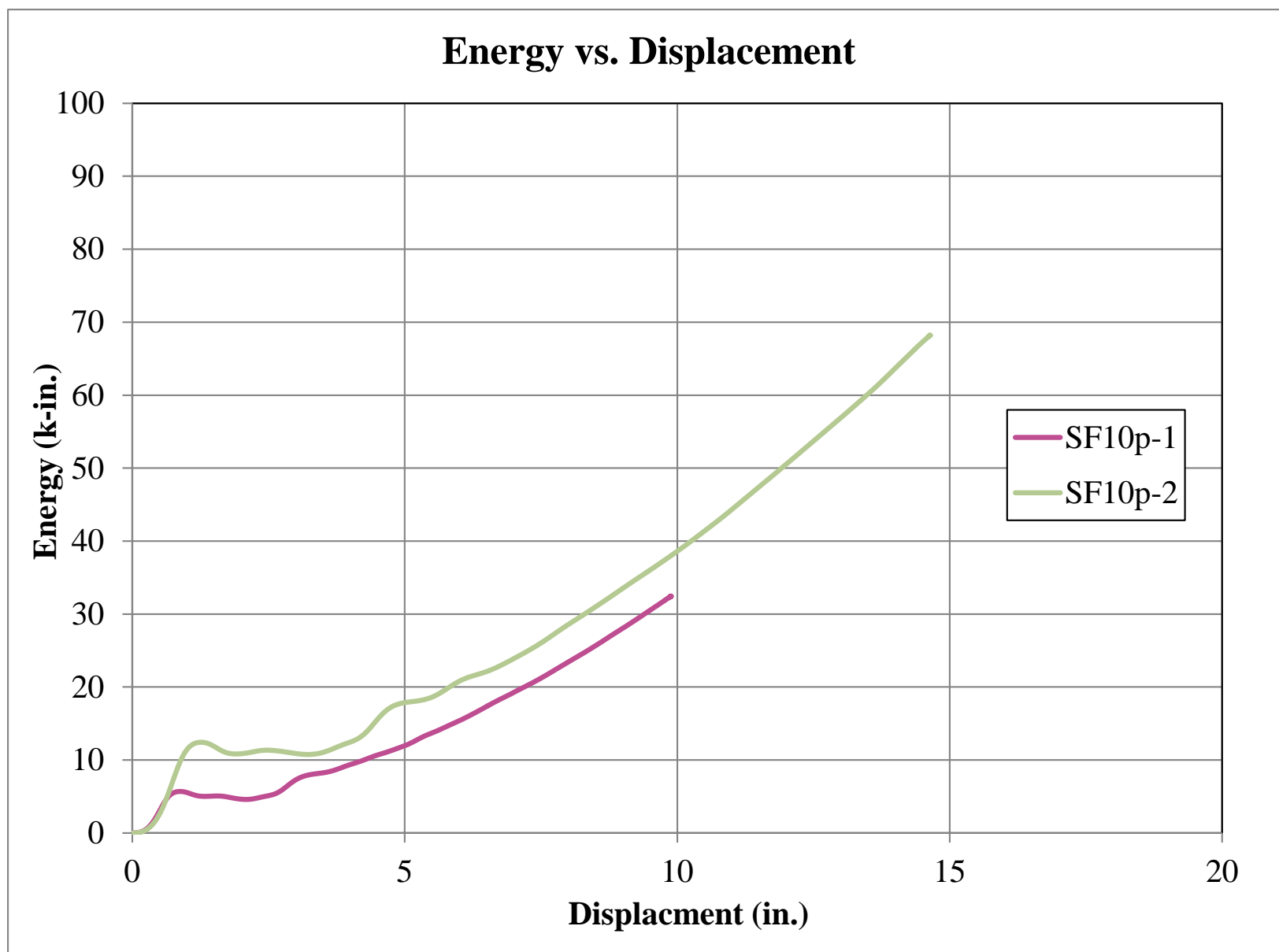


Figure 31. Energy vs. Deflection Comparison, All Bogie Tests Without Steel Pipe

3.2 Discussion

The results from the bogie testing matrix are summarized in Table 4. When examining the SFD-1 through SFD-5 test series, the energy absorbed at each deflection overall tended to decrease with repetitive impacts. However, this was not always the case. The differences seen in energy absorbed may be contributed to slight changes in how the bogie interacted with the post and if the post deformed in shear or rotated more. The energy absorbed may also degrade slightly with each impact after being subjected to an extreme deflection, similar to the 17.8 in. (452 mm) that occurred in test no. SFD-1. However, the posts are not expected to be loaded above 10 in. (254 mm) of deflection for impact events up to 62 mph (100 km/h) and 25 degrees for passenger vehicles, so they may only experience more extreme deflections during rare larger truck impact events. So, the posts should maintain adequate energy absorption for repeated impact events.

Also, test no. SFD-4 had much more noticeable post rotation than observed in other bogie tests. This test also had overall lower energy absorption per unit deflection. Therefore, it is optimal that the posts deform in shear, rather than rotating, to provide the maximum energy absorbed and lower passenger accelerations.

The surface temperature of the posts did not vary enough to determine if temperature affected the energy absorption. The force vs. deflection and energy vs. deflection plots for comparing posts with and without the steel pipes are shown in Figures 32 and 33, respectively. The steel pipe had no apparent effects on the energy absorption behavior of the post, and the pipes were difficult to keep in place when loaded and unloaded.

Table 4. Dynamic Testing Results, All Component Tests

Test No.	Bogie Weight lb (kg)	Surface Temp. °F (°C)	Impact Velocity mph (km/h)	Max. Deflection in. (mm)	Peak Force kips (kN)
SF10-1	1,854 (841)	89 (32)	6.3 (10.1)	8.4 (213)	17.1 (76.1)
SF10-2	1,854 (841)	94 (34)	8.0 (12.9)	11.7 (297)	18.4 (81.8)
SFD-1	1,886 (855)	96 (36)	11.1 (17.8)	17.8 (452)	24.8 (110.3)
SFD-2	1,886 (855)	92 (33)	8.2 (13.2)	11.8 (300)	25.2 (112.1)
SFD-3	1,886 (855)	94 (34)	8.6 (13.9)	13.5 (343)	19.3 (85.9)
SFD-4	1,886 (855)	93 (34)	8.4 (13.5)	13.5 (343)*	15.4 (68.5)
SFD-5	1,886 (855)	92 (33)	8.6 (13.9)	14.2 (361)	19.2 (85.4)
SF10P-1	1,886 (855)	86 (30)	6.6 (10.6)	9.9 (251)	13.8 (61.4)
SF10P-2	1,886 (855)	88 (31)	9.5 (15.3)	14.6 (371)	21.2 (94.3)

Test No.	Energy at Deflection k-in. (kJ)				Total Energy k-in. (kJ)
	4 in. (102 mm)	6 in. (152 mm)	8 in. (203 mm)	10 in. (254 mm)	
SF10-1	11.0 (1.2)	18.2 (2.1)	27.4 (3.1)	NA	29.4 (3.3)
SF10-2	11.9 (1.3)	17.4 (2.0)	26.2 (3.0)	36.9 (4.2)	47.4 (5.4)
SFD-1	13.0 (1.5)	23.1 (2.6)	27.7 (3.1)	37.6 (4.2)	93.0 (10.5)
SFD-2	17.9 (2.0)	22.8 (2.6)	31.6 (3.6)	41.1 (4.6)	51.0 (5.8)
SFD-3	12.6 (1.4)	19.5 (2.2)	27.2 (3.1)	36.1 (4.1)	56.1 (6.3)
SFD-4	9.1 (1.0)	15.7 (1.8)	23.2 (2.6)	30.8 (3.5)	52.9 (6.0)
SFD-5	10.2 (1.2)	17.0 (1.9)	23.9 (2.7)	32.3 (3.6)	56.3 (6.4)
SF10P-1	9.4 (1.1)	15.4 (1.7)	23.4 (2.6)	NA	32.5 (3.7)
SF10P-2	12.4 (1.4)	20.8 (2.4)	28.5 (3.2)	38.5 (4.3)	68.2 (7.7)

*taken from film analysis

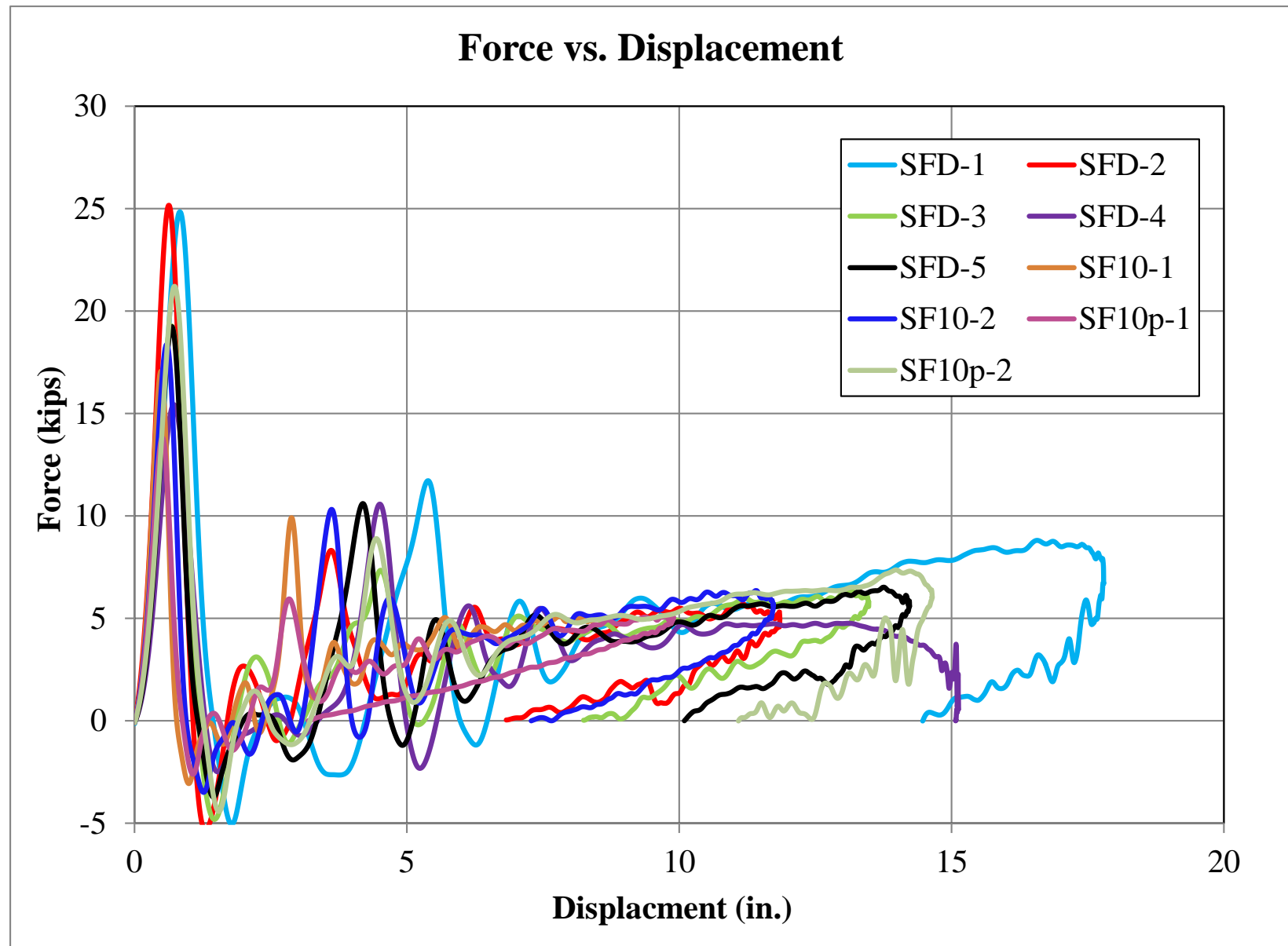


Figure 32. Force vs. Deflection Comparison, Pipe vs. No Pipe Bogie Tests

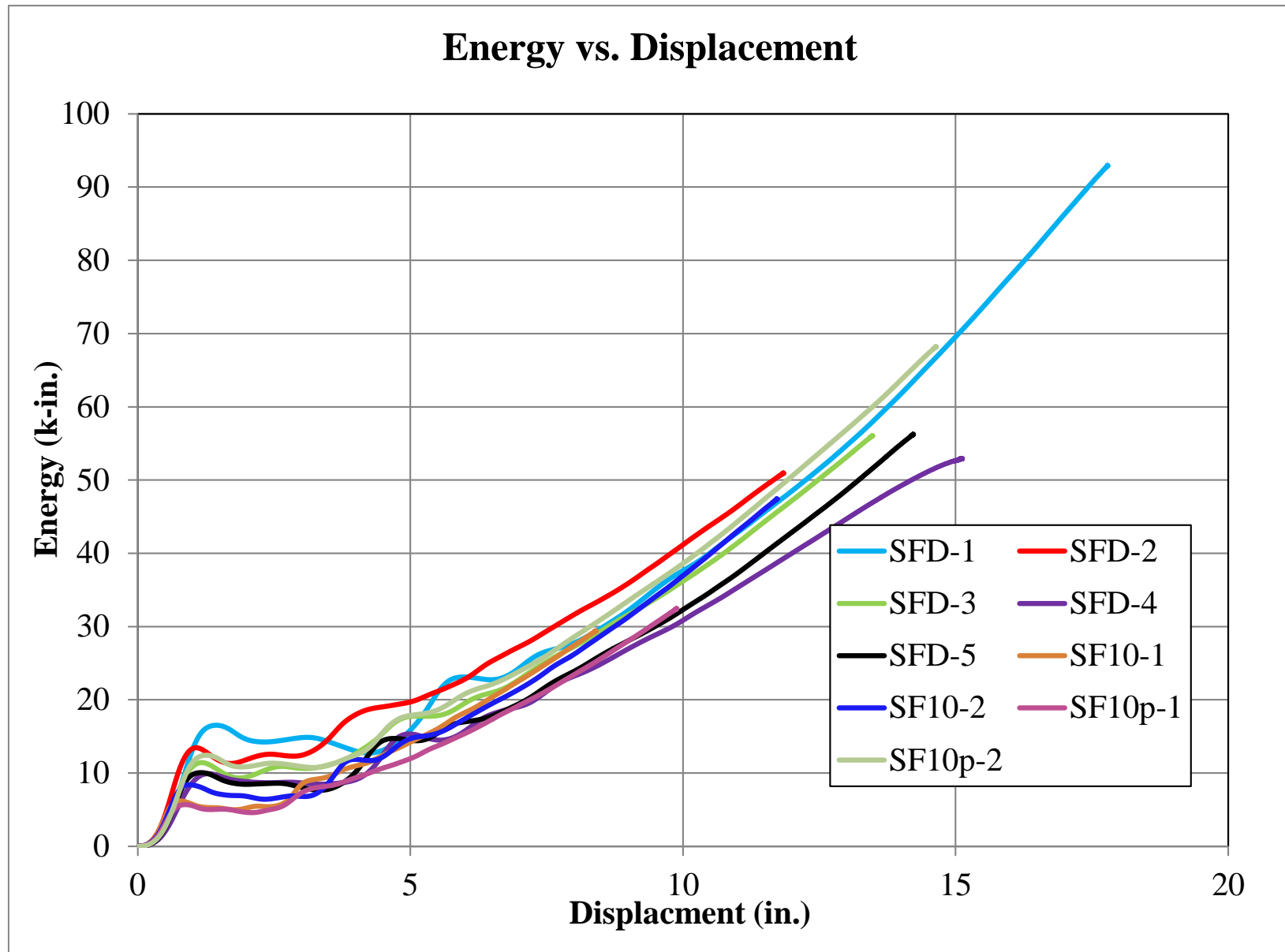


Figure 33. Energy vs. Deflection Comparison, Pipe vs. No Pipe Bogie Tests

4 SYSTEM DESIGN AND ANALYSIS

4.1 Introduction

Previously, the rail in the system was comprised of 20-ft (6.1-m) long concrete segments with a lower height of 16 in. (406 mm) above ground and an upper height of 36 in. (914 mm) above ground, as shown previously in Figure 1. Bolts connected upper splice plates, the concrete segments, and the posts at each concrete joint. Due to the new post geometry and stability concerns, the post spacing, the rail geometry and splices needed to be redesigned. During the rail design, several rounds of static load testing of the posts were conducted, as detailed in Schmidt, et al. [2], to determine the rail weight which could be supported by the rubber posts. The optimal weight for the rail was determined to be under approximately 320 lb/ft (476 kg/m) with 11 $\frac{5}{8}$ -in. (295-mm) tall posts spaced at 5 ft (1.5 m). The precast concrete segment length of 20 ft (6.1 m) was maintained for ease of constructability.

4.2 Post Design

According to the static energy vs. deflection curves provided by Morse Rubber, as shown in Figure 34 [8], the 16-in. (406-mm) tall posts absorbed approximately twice as much energy per unit deflection as the 11 $\frac{5}{8}$ -in. (295-mm) tall posts for small deflections. However, at larger deflections, the difference in energy dissipated was not as significant.

From the dynamic bogie tests that were conducted on the 11 $\frac{5}{8}$ -in. (295-mm) and 16-in. (406-mm) tall posts, three had similar impact severities. In test no. HSF14-3, a 16-in. (406-mm) tall post was impacted by a bogie weighing 1,818 lb (825 kg) and traveling at a velocity of 9.1 mph (14.6 km/h) [2]. In test nos. SFD-3 and SFD-5, 11 $\frac{5}{8}$ -in. (295-mm) tall posts were impacted by a bogie weighing 1,886 lb (855 kg) and traveling at a velocity of 8.6 mph (13.8 km/h). As shown in Table 5, the energy absorbed by the 16-in. (406-mm) tall posts varied from 1.5 to 1.9

times greater than 11 $\frac{5}{8}$ -in. (295-mm) tall posts at 4 in. (102 mm), 6 in. (152 mm), 8 in. (203 mm), and 10 in. (254 mm) of deflection. The dynamic energy vs. deflection plot over the entire event is also shown in Figure 35. Since the energy absorbed by the smaller post was almost half as much as the larger post, the post spacing was decreased to 5 ft (1.5 m) so that the system with the smaller posts would absorb approximately the same energy as the system with larger posts at 10-ft (3.0-m) spacing.

The previous design included a post at each concrete beam splice, which was to provide continuity to the barrier system at the splices. The smaller, narrower posts only had a 4-in. (102-mm) spacing between the bolt holes that attached the posts to the concrete, which would not allow for a bolt to be placed through the concrete beam and still have adequate clear cover at the ends of the concrete rails. Therefore, the post locations were moved away from the concrete beam splices.

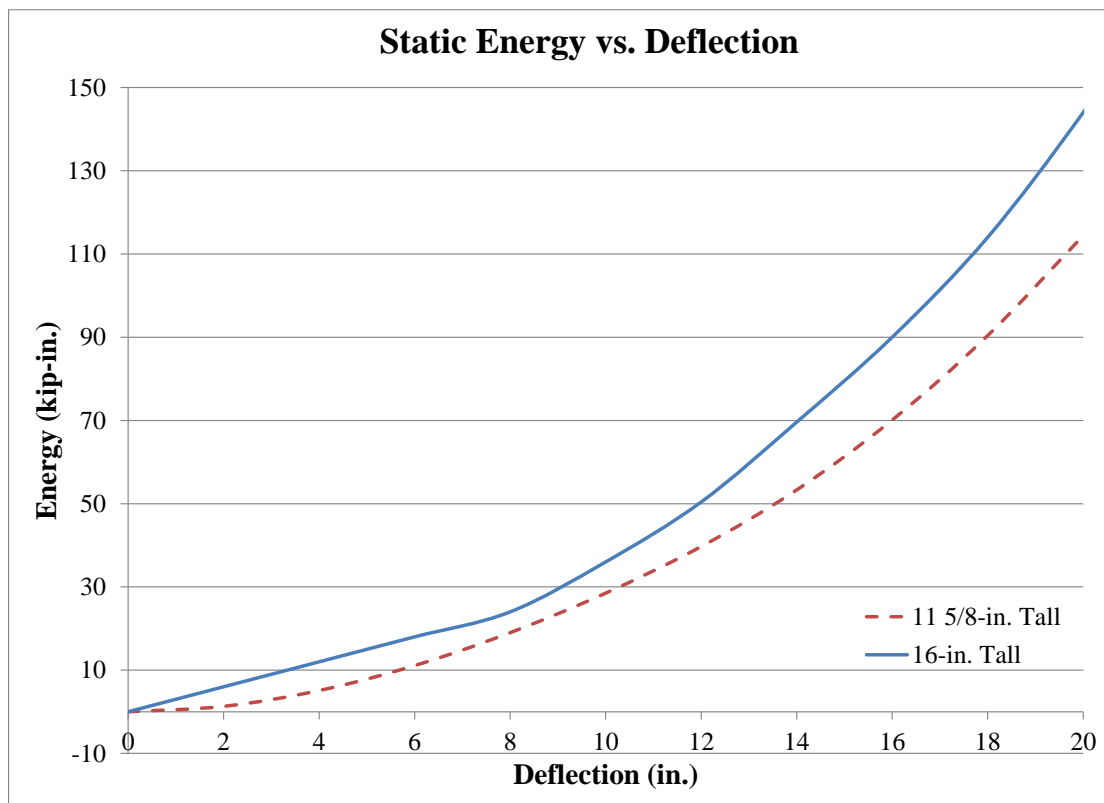
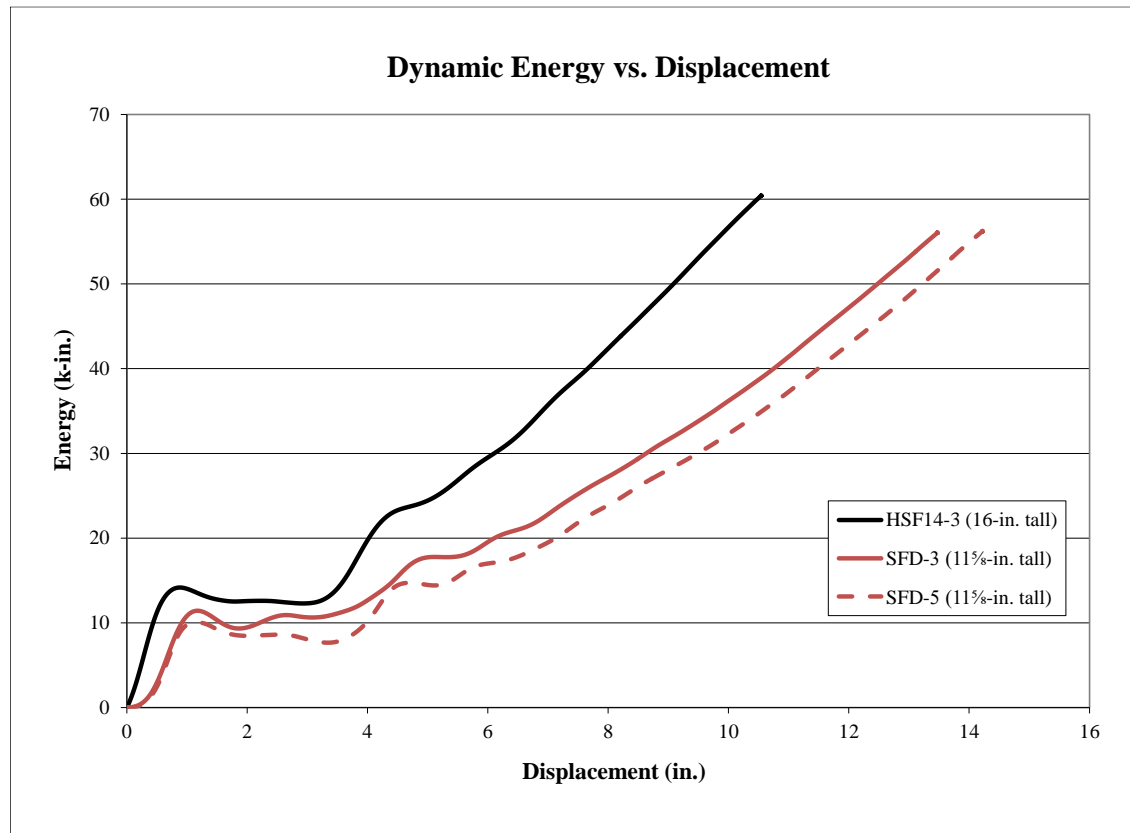


Figure 34. Static Energy vs. Deflection, 11 $\frac{5}{8}$ -in. (295-mm) and 16-in. (406-mm) Tall Posts [8]

Table 5. Dynamic Test Comparisons, 11⁵/₈-in. (295-mm) and 16-in. (406-mm) Tall Posts

Test No.	Post Height x Width in. (mm)	Velocity mph (km/h)	Max Deflection in. (mm)	Peak Force kip (kN)	Energy at Deflection kip-in. (kJ)				Total Energy kip-in.
					4 in. (102 mm)	6 in. (152 mm)	8 in. (203 mm)	10 in. (254 mm)	
HSF14-3	16x14 (406x356)	9.1 (5.7)	10.5 (267)	26.5 (117.9)	19.8 (2.2)	29.5 (3.3)	42.4 (4.8)	56.7 (6.4)	60.5 (6.8)
SFD-3	11 ⁵ / ₈ x10 (295x254)	8.6 (13.9)	13.5 (343)	19.3 (85.9)	12.7 (1.4)	19.6 (2.2)	27.3 (3.1)	36.2 (4.1)	56.1 (6.3)
SFD-5	11 ⁵ / ₈ x10 (295x254)	8.6 (13.9)	14.2 (361)	19.2 (85.4)	10.2 (1.2)	17.0 (1.9)	23.9 (2.7)	32.3 (3.6)	56.3 (6.4)

Figure 35. Dynamic Energy vs. Deflection, 11⁵/₈-in. (295-mm) and 16-in. (406-mm) Tall Posts

4.3 Rail Design

Previously, the reinforcement was designed for a 20-ft (6.1-m) long continuous beam with a 75-kip (334-kN) point load, which produced a maximum moment of 2,250 k-in. (255 kN-m) in the beam [1]. Yield-line analysis was used to determine if the beam capacity was adequate with the new post capacities. At 10 in. (254 mm) of deflection, each post would have an average force of approximately 2.6 kips (11.6 kN) and moment of 30 k-in. (3.4 kN-m). From yield-line with a post capacity of 30 kip-in. (3.4 kN-m) every 5 ft (1.5 m) and a beam capacity of 2,250 kip-in. (255 kN-m), the barrier should withstand a factored impact load of 76 kips (338 kN) for the 2270P pickup truck and 90 kips (400 kN) for the 10000S single-unit truck. Since the original design goal was to resist a 75-kip (334-kN) impact with the single-unit truck, designing the moment capacity of the beam to be 2,250 kip-in. (255 kN-m) was conservative but still reasonable.

Several design configurations were considered so that the rail weight was under 320 lb/ft (476 kg/m). First, the barrier width was established based on the bolt spacing pattern on the posts. The desire to enclose the post bolts inside the rebar cage led to concrete rail being a minimum of 21½ in. (546 mm) wide. The minimum top rail height of 36 in. (914 mm) was previously established to successfully capture a MASH TL-4 single-unit truck, and the lower rail height of 11⅝ in. (295 mm) was determined by the post height. Based on these minimum width and heights, a solid concrete rail would be approximately 1.7 times larger than the targeted weight of the beam. Therefore, other rail configurations were explored to reduce the weight of the rail but still provide adequate capacity.

One configuration included reducing the height of the concrete section and adding a top steel tube to provide the necessary height for single-unit truck capture, as shown in Figure 36.

Based on several previous TL-3 rigid barrier crash tests, the height to the top of the concrete beam should be approximately 29 to 30 in. (737 to 762 mm) above the ground to capture the 2270P pickup truck. Approximately ½ in. (13 mm) of settlement was estimated due to a 320-lb/ft (476-kg/m) static dead load of the rail [2], so the height of the concrete beam needed to be approximately 18½ in. (470 mm) tall. Vertical deflection may occur during a single-unit truck impact from the box leaning on the rail, as noted in previous simulations [1], so the overall height was targeted at approximately 38½ in. (978 mm) to allow for settling due to self-weight and some of the vertical deflection that may occur from box lean and the barrier translating and/or rotating.

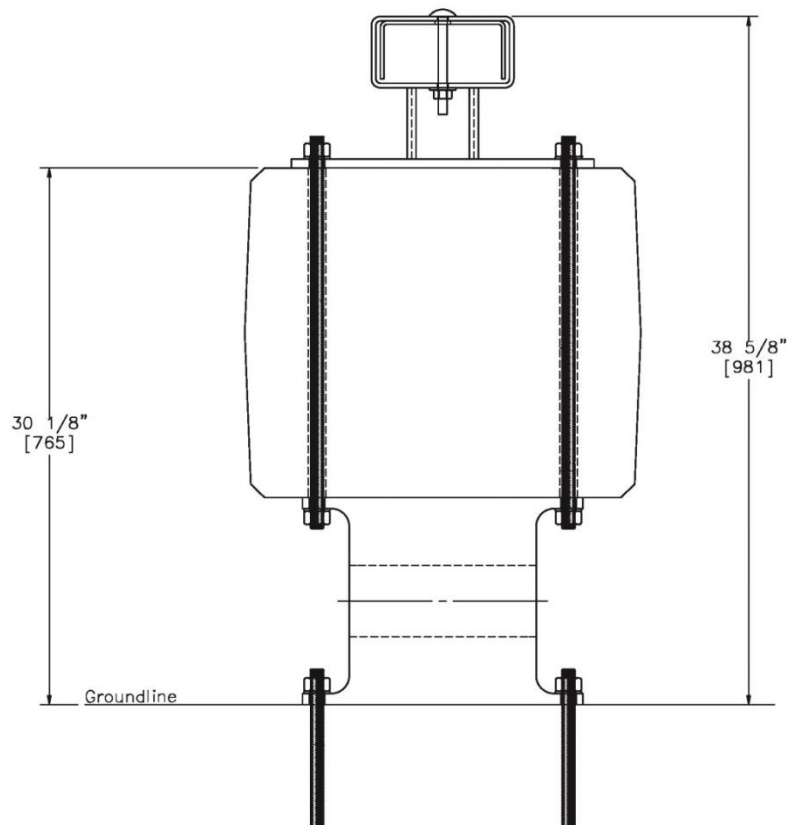


Figure 36. Optimized Rail Cross Section

Vertical holes in the interior sections of the concrete were utilized to reduce weight. However, they had to be small enough and selectively placed to maintain capacity of the section.

Therefore, lightweight concrete with a density of 110 lb/ft³ (1,762 kg/m³) and a minimum compressive strength of 5 ksi (34.5 MPa) was selected to reduce the weight of the beam. The approximate weight of the beam with this configuration was 318 lb/ft (473 kg/m).

One of the original design criteria was that a minimal amount of damage was permissible during single-unit truck impact events. The steel tubes will likely experience some permanent damage during single-unit truck impact events, but they will be easily replaceable as long as the concrete and connecting bolts are not damaged.

4.4 Concrete Rail Splices

The concrete rail splice was designed to meet several criteria: provide continuity to concrete rail; have a capacity greater than the rail; accommodate construction tolerances; have smooth front and back faces for aesthetics as well as to reduce snag potential; and not interfere with concrete rail reinforcement. Several splices were considered, including: splice plates on the top and bottom faces (Figure 37); splice tubes at the center of the top and bottom faces (Figure 38); a cross-bolted connection (X-connection) through the front and back faces which was originally developed at the Texas A&M Transportation Institute (TTI) as a connection between temporary concrete barriers (Figure 39) [9]; and a wedge-shaped connection through the front and back faces, now denoted as the Adjustable Continuity Joint (ACJ) (Figure 40).

Splice plates, attached to the top and bottom faces of the concrete beams, would add continuity across the joint. Thus, all joint hardware is away from the front and back impact faces of the barrier, as shown in Figure 37. The initial concept had ½-in. (13-mm) thick steel plates with six (three in each beam) ¾-in. (19-mm) diameter vertical bolts through each plate and the concrete section. The splice plates would need slots for the bolts to allow for construction tolerances as well as allow installation for on roadways with vertical and horizontal curvature.

Splice tubes at the center of the top and bottom faces allows for a larger steel section than the plates to transfer impact loads across the joint, and all joint hardware is away from the front and back impact faces of the barrier, as shown in Figure 38. The initial concept had approximately 3-in. x 7-in. x ½-in. (76-mm x 178-mm x 13-mm) steel tubes with a gap between the tubes and concrete. Six (three in each beam) ¾-in. (19-mm) diameter vertical bolts attached the end of each tube through the concrete section. The bolt holes in the splice tubes would need to be slotted to allow for construction tolerances as well as allow for installation on roadways with vertical and horizontal curvature.

The X-connection utilized two 1¼-in. (32-mm) diameter bolts attached diagonally through the front and back faces of the beams at the ends, as shown in Figure 39. This connection has exposed hardware on the front and back faces, but a cover plate could be implemented to create a continuous surface to reduce vehicle snag as well as provide improved aesthetics. The holes in the concrete beam would be oversized to allow construction tolerances as well as allow for installation on roadways with vertical and horizontal curvature.

The ACJ connection utilized two 6-in. x 6-in. x ½-in. (152-mm x 152-mm x 13-mm) steel angles attached vertically to the front and back faces of the concrete beams at the ends, as shown in Figure 40. A total of eight 1-in. (25-mm) diameter bolts attached the steel angles to the concrete beams at each joint. The ends of the concrete beams were chamfered and an interior void was created so that the ends of the bolts were contained within the concrete section. This connection has exposed hardware on the front and back faces, but a cover plate could be implemented to create a smooth surface to reduce vehicle snag as well as provide improved aesthetics. Slots in the angles allow the ACJ to slide inward or outward to accommodate larger or small gaps between adjacent beam ends, respectively.

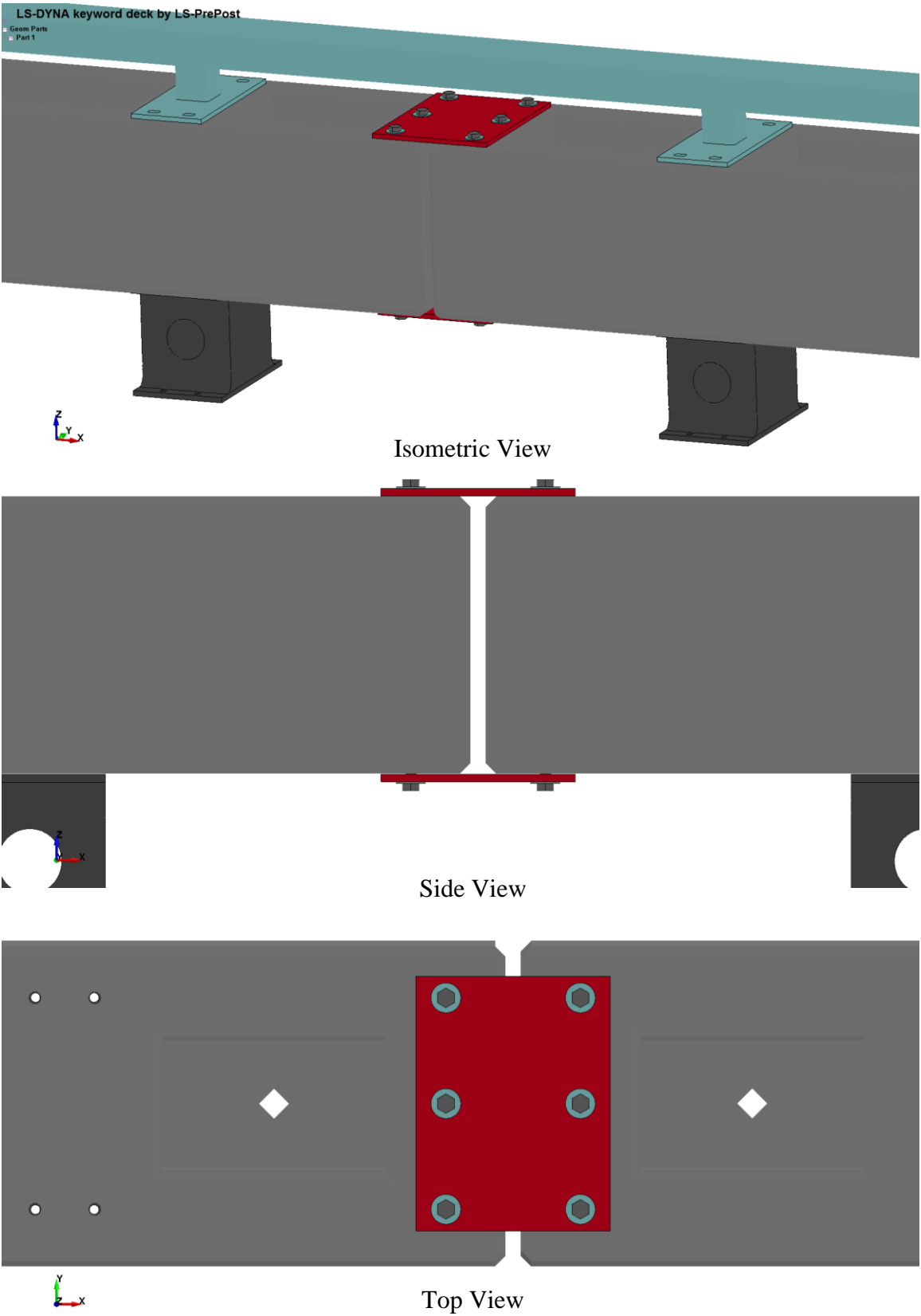


Figure 37. Splice Plates Concept

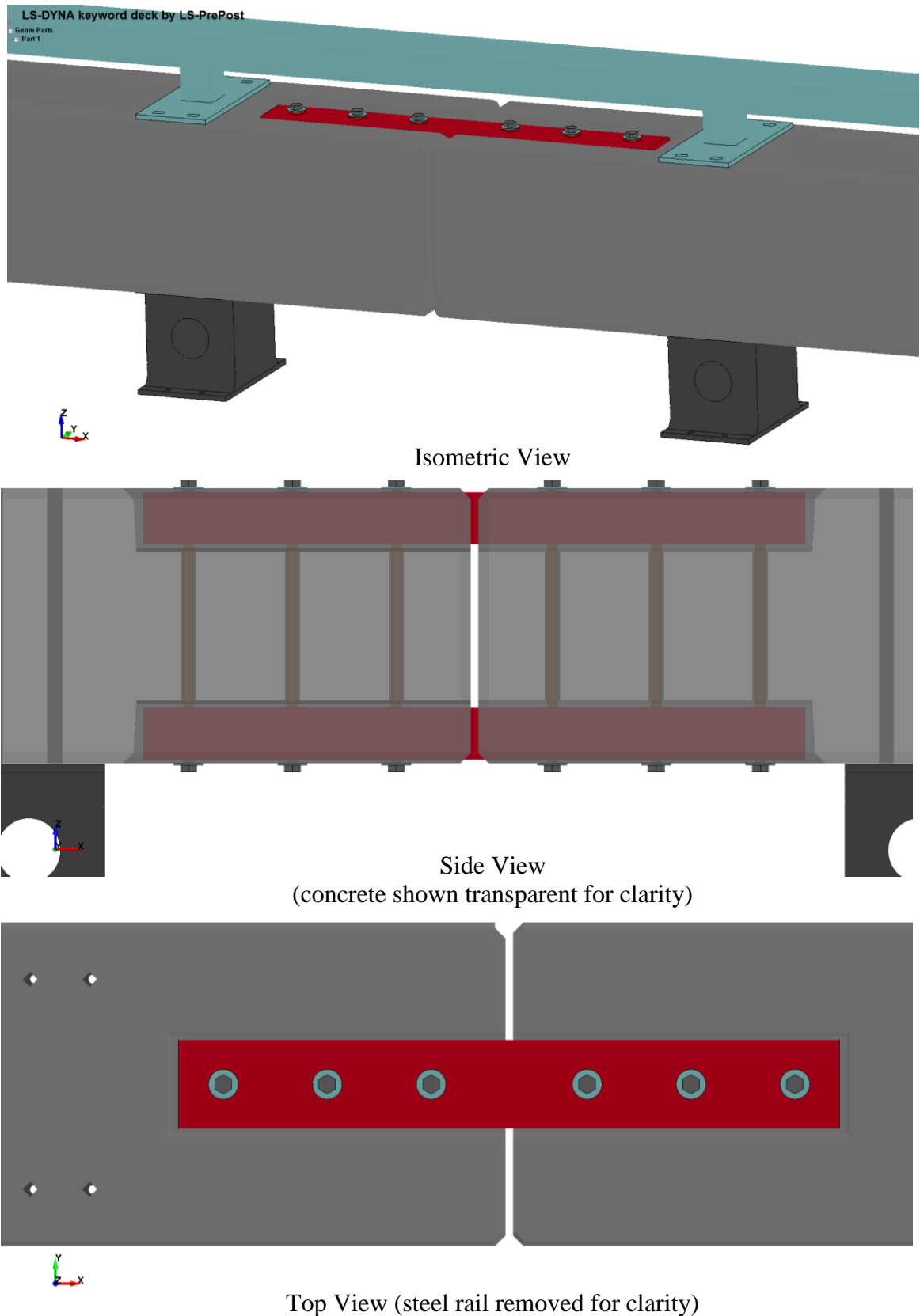


Figure 38. Splice Tubes Concept

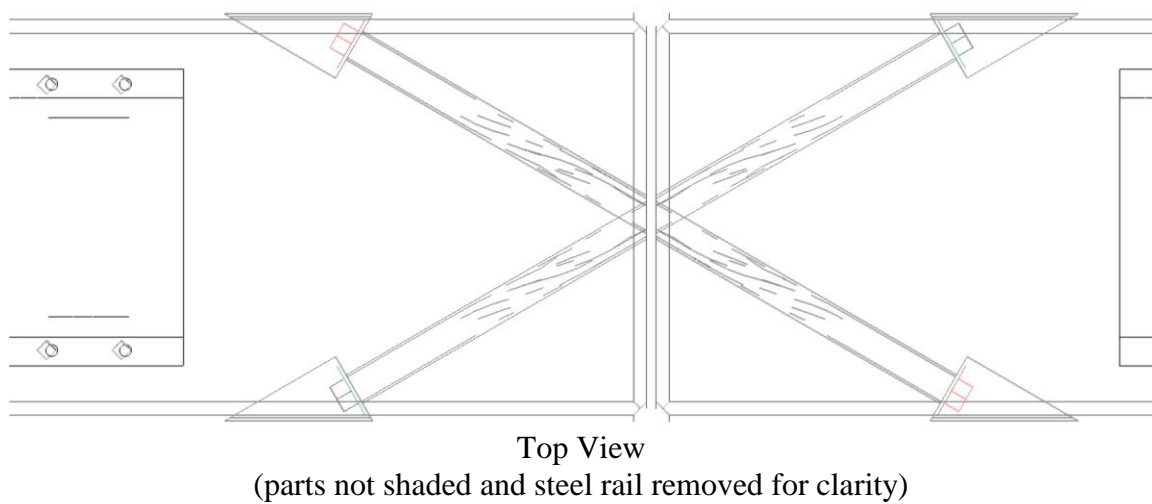
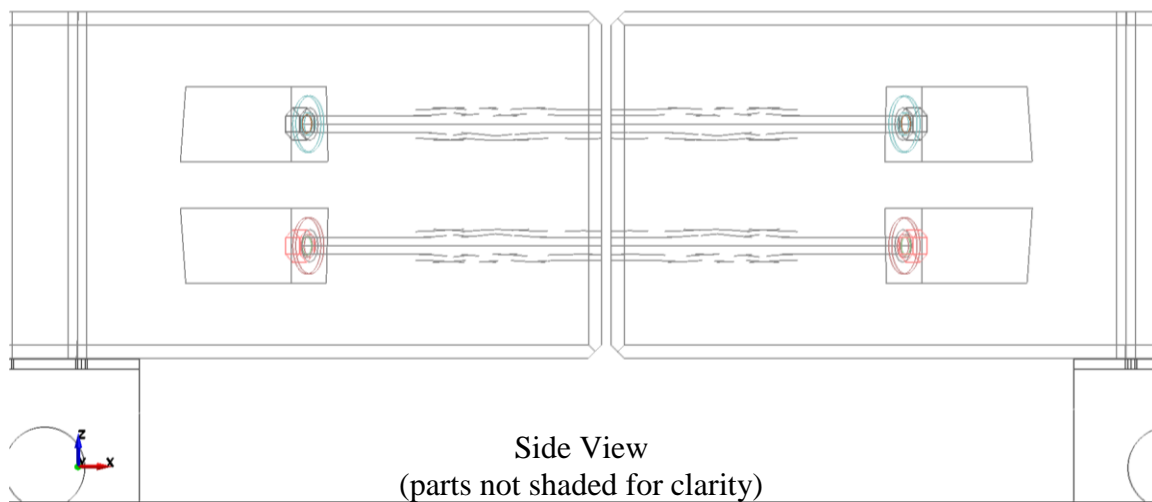
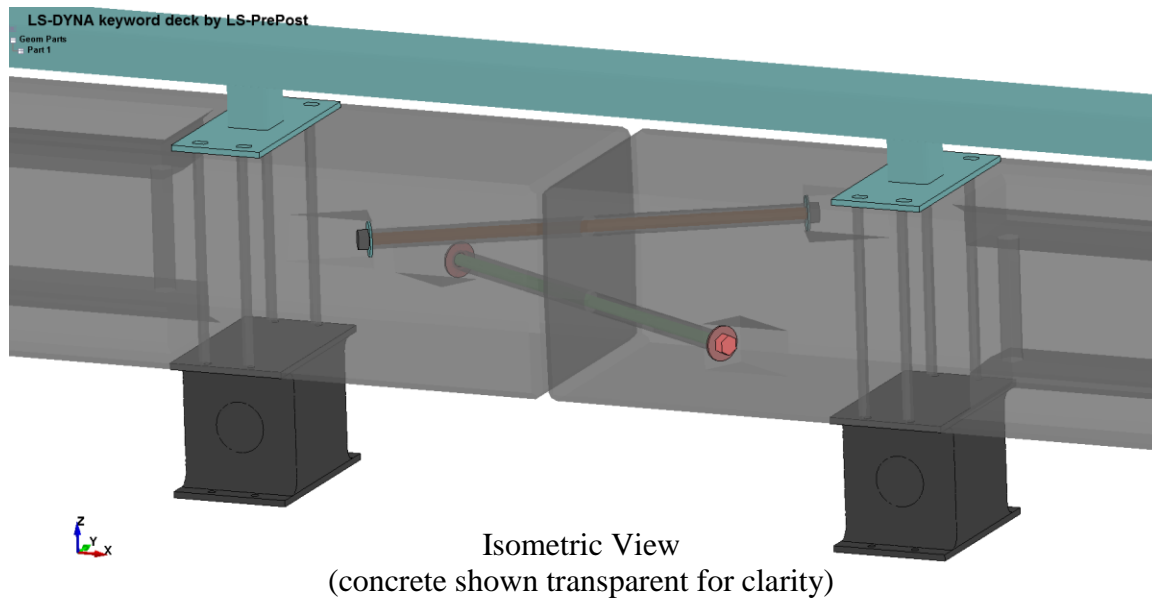


Figure 39. X-Connection Concept

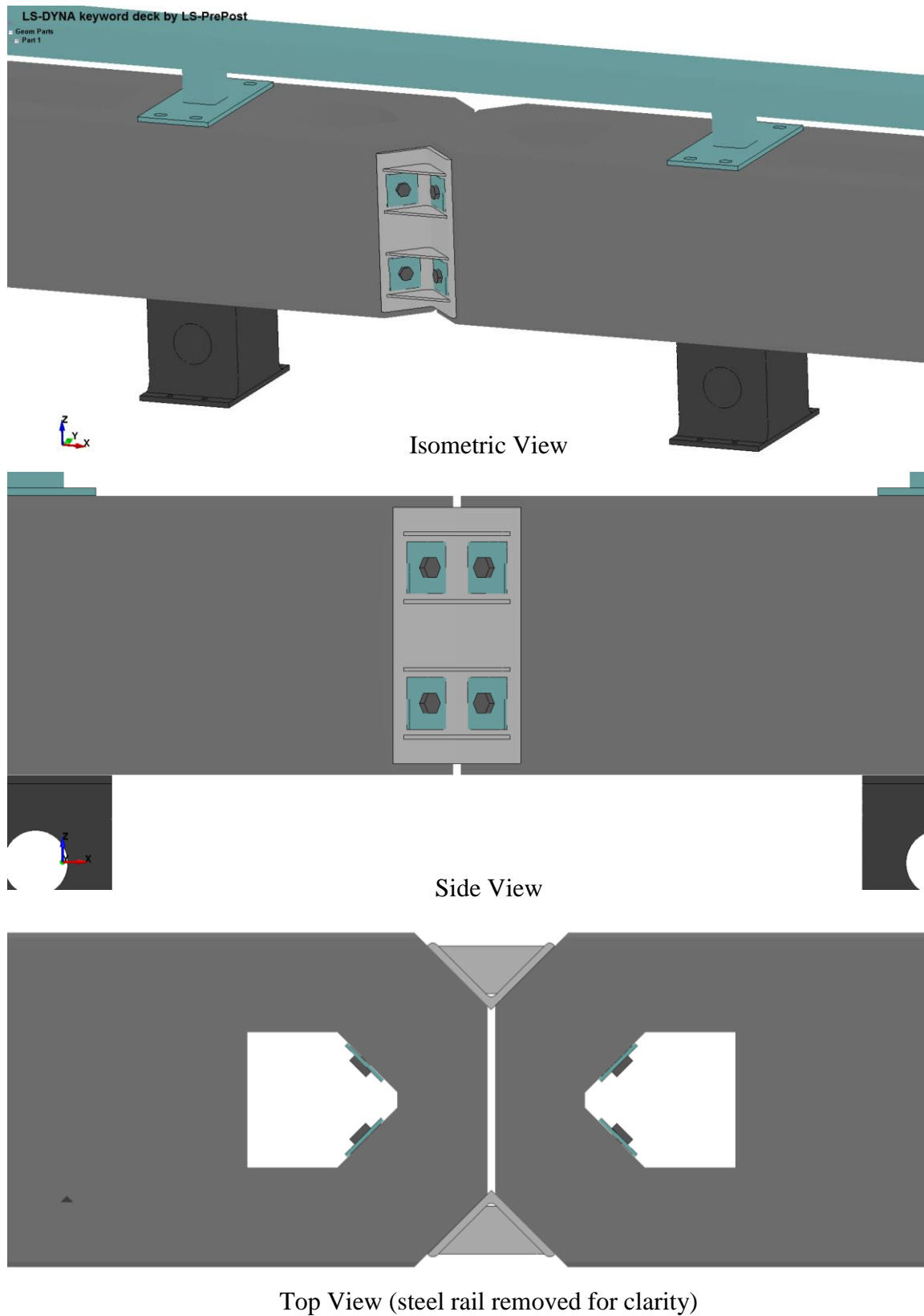


Figure 40. ACJ Concept

The four splice concepts were simulated with MASH test designation 4-11 impacts. A 160-ft (48.8-m) barrier model was adapted from previous work [1] and is shown in Figure 41.

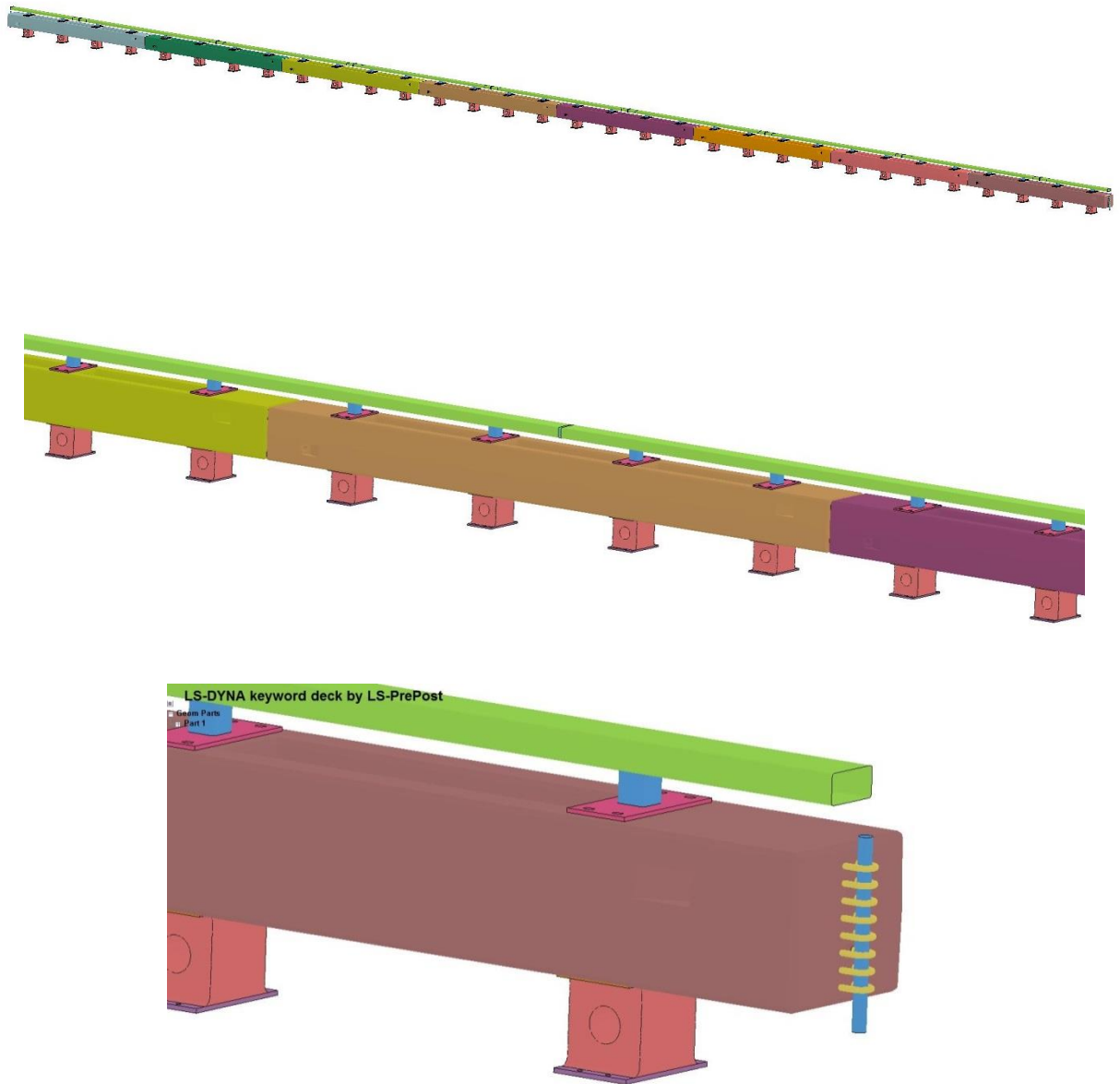


Figure 41. 160-ft Barrier Model for Exploring Concrete Beam Splices

The major features of the barrier model were:

- 1) 38 $\frac{5}{8}$ -in. (981-mm) height before applying gravity;
- 2) 11 $\frac{5}{8}$ -in. (295-mm) tall rubber posts spaced at 5 ft (1.5 m) on center;

- 3) 20-ft (6.1-m) long rigid concrete beams;
- 4) 8½-in. (216-mm) tall steel tube assembly with splices; and
- 5) pinned connection on the upstream and downstream ends that allowed free vertical displacement and rotation around the vertical direction, minimal longitudinal displacement and rotations around the longitudinal and lateral directions, and no lateral displacement.

The 2270P Silverado pickup truck model impacted the RESTORE barrier at a speed of 62 mph (27.8 m/s) and an angle of 25 degrees approximately 64 in. (1,626 mm) upstream from the splice between barrier nos. 4 and 5.

Several configurations were explored with top and bottom splice plate concept. The bolt holes in the splice plate were initially slotted to allow some construction tolerance. However, this allowed for greater joint deflection than desired, and the joint did not provide enough moment continuity to the system. Additional configurations of vertical bolts with slots in the splice plates were analyzed, but they still did not provide the desired continuity. The final configuration which provided the lowest system deflections utilized six ¾-in. (19-mm) vertical bolts with no slots in the top and bottom plates. This configuration allowed for no construction tolerance, and the maximum deflection was 11.5 in. (292 mm) which occurred during tailslap. It should be noted that the 2270P pickup truck model is believed to exaggerate the tailslap event. No permanent damage appeared to occur in the splice plates. Since the concrete beams were modeled as rigid parts, possible damage to the concrete could not be assessed. In the final model, the vertical bolts were modeled as rigid parts. However, during previous models when the bolts were deformable parts, the stresses were close to the yield strength throughout the impact event.

The slice tubes concept was evaluated with 3-in. x 7-in. x ½-in. (76-mm x 178-mm x 13-mm) steel tubes. However, the gap between tube and the cavity in the concrete beam and the effects of slots in the tubes at each bolt location were varied. The slotted splice tubes had similar

problems to the splice plates in that the slots allowed greater joint deflection than desired. However, when the tubes fit tight in the cavity in the concrete beam, the joint deflection could be minimized, but the stresses in the tubes near impact were greater than the yield strength. The final configuration had 1½-in. (38-mm) long slots in the splice tubes at each of the six ¾-in. (19-mm) diameter vertical bolt locations. This configuration allowed for some construction tolerances, and the maximum deflection was 12.2 in. (310 mm) which occurred during tailslap.

The cross-bolted connection utilized two 1¼-in. (32-mm) diameter bolts attached diagonally through the front and back faces of the end of each beam. The holes in the concrete beams were oversized by ½ in. (13 mm). This configuration created larger than desired deflections. Larger 1½-in. (38-mm) diameter bolts were also modeled with larger oversized holes in the concrete beam, but the system deflections were not significantly affected. Due to the oversized holes in the concrete beam and the 1-in. (25-mm) gap between adjacent concrete beams, the ends of the beams could still rotate easily, and system deflections were directly related to those two factors. Therefore, ½-in. (13-mm) steel shims were added in between adjacent concrete beams. System deflections were significantly reduced with the shims. During actual installations, shims would only be necessary and would be sized in the field if the gap between adjacent barrier segments was greater than ½ in. (13 mm). The final configuration utilized two 1¼-in. (32-mm) diameter bolts attached diagonally through the front and back faces of the end of each beam. This configuration allowed the beams to act continuous across the joints. No permanent damage occurred at the joint, although the stresses in the bolts were near yield strength and the concrete beams were modeled using rigid parts. This configuration allowed for some construction tolerance if shims are sized according to the actual gap size, and the maximum deflection was 9.1 in. (231 mm) during tailslap.

Several configurations of the ACJ connection were also evaluated. The initial concept utilized 5-in. x 5-in. x ½-in. (127-mm x 127-mm x 13-mm) steel angles attached vertically to the front and back faces of the concrete beams with a total of twelve ⅞-in. (22-mm) diameter bolts (three per each chamfered beam corner) at each joint. Slots also allow up to 1 in. (25 mm) of construction tolerance. With this configuration, the system deflections were higher than desired. It was desired that only two bolts were utilized per each chamfered beam corner to make installation easier. Therefore, the final configuration utilized two 6-in. x 6-in. x ½-in. (152-mm x 152-mm x 13-mm) steel angles attached vertically to the front and back faces of the concrete beams with a total of eight 1-in. (25-mm) diameter bolts at each joint. The slots were also decreased to accommodate ½ in. (13 mm) of construction tolerance. This configuration allowed the beams to act continuous across the joints. No permanent damage occurred at the joint, although the stresses in the bolts were near yield strength, and the concrete beams were modeled using rigid parts. The maximum deflection was 10.4 in. (264 mm) during tailslap.

The maximum dynamic deflection that occurred at the splice nearest impact for the final configuration of each splice concept is shown in Figure 42. The cross-bolted connection and the ACJ provided the lowest deflections that were in the desired range of approximately 8 to 10 in. (203 to 254 mm).

The cross-bolted connection provided the lowest deflection, so the concrete beam was designed incorporating this splice concept. However, the cross-bolted connection required 1¾-in. (44-mm) diameter bolts for adequate strength and large bolt holes in the concrete for construction tolerances, which did not allow room for adequate internal steel reinforcement and also created voids on the front and back faces of the rail that would likely require a cover.

The second design pursued was with the Adjustable Continuity Joint concept. The ACJ accommodated construction tolerances and allowed the concrete rail segments to act

continuously. Open hardware existed on the face of the rail. However, a cover plate could be designed to cover the exposed hardware. The bolts were designed to not interfere with internal reinforcement.

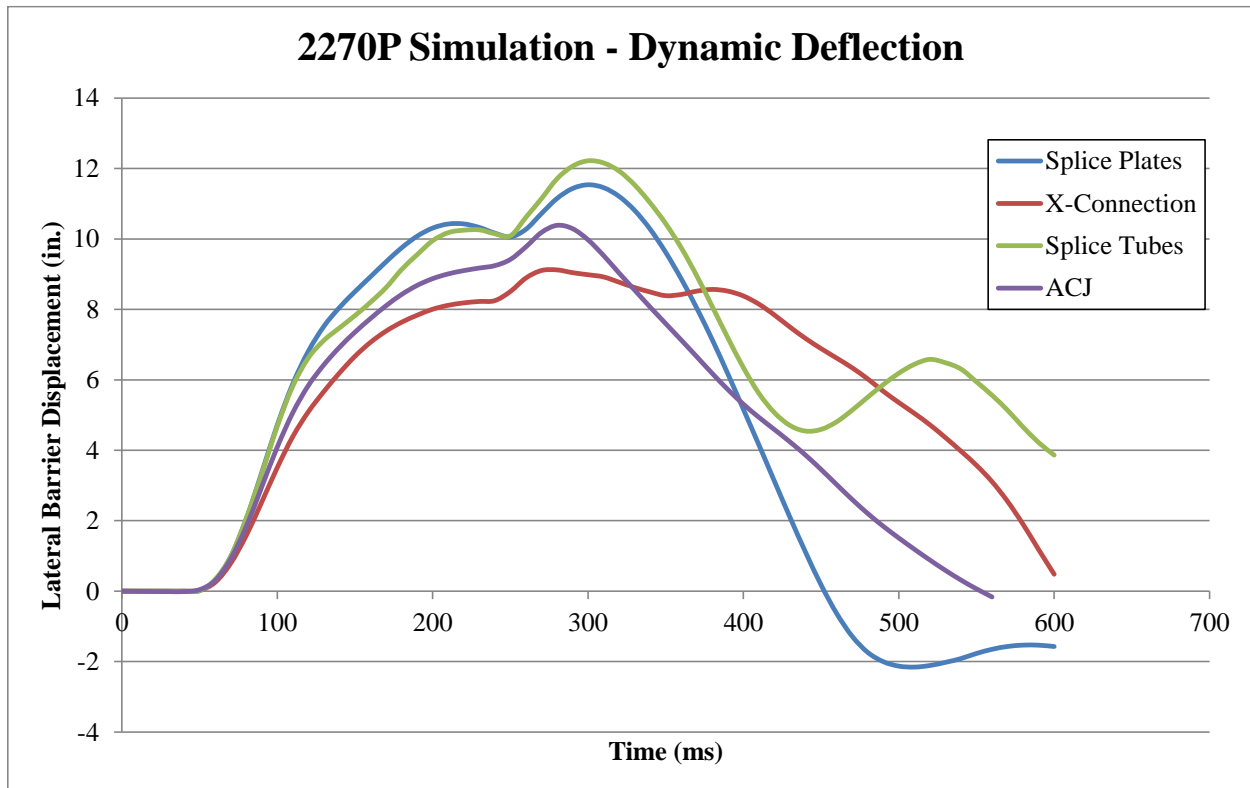


Figure 42. Dynamic Deflection of Concrete Beam Splices

4.5 Final System Design

The complete preliminary system design is shown in Figures 43 through 59. The nominal concrete beam dimensions were 21½ in. (546 mm) wide x 18½ in. (470 mm) tall x 19 ft - 11½ in. (6.1 m) long. The longitudinal and transverse reinforcement in the concrete beams were No. 6 and No. 4 steel, respectively. Nine 6⅝-in. (168-mm) diameter vertical holes reduced the weight of each concrete beam. Two pentagon-shaped holes occurred at each end of the concrete beam, further reduced the weight of the beam, and allowed for the ACJ connection in the interior of the beam. The ends of the beams were chamfered 4½ in. (114-mm) to accommodate the ACJ

connection on the exterior of the beam. The ACJ was comprised of two 6-in. x 6-in. x ½-in. (152-mm x 152-mm x 13-mm) steel angles attached vertically to the front and back faces of the concrete beams with a total of eight 1-in. (25-mm) diameter bolts at each joint. A nominal ½-in. (13-mm) gap occurred between adjacent concrete beams, and the splice can accommodate +/- ¼ in. (6.4 mm) of tolerance.

The rubber posts were 11⁵/₈ in. (295 mm) tall x 10 in. (254 mm) wide x 15³/₄ in. (400 mm) long, with four vertical holes to accommodate ¾-in. (19-mm) diameter bolts. The bases of the rubber posts were attached to the foundation with ¾-in. (19-mm) threaded rods and a chemical epoxy adhesive. The upper tube assembly was comprised of 4-in. x 8-in. x ¼ in. (102-mm x 203-mm x 6.4-mm) steel tube supported by 4-in. x 4-in. x ¼-in. (102-mm x 102-mm x ¼-in.) steel tube posts on steel base plates every 5 ft (1.5 m). The steel tubes were spliced every 20 ft (6.1 m) with bent steel plate. Vertical bolts connected the base plates, the concrete beam, and the rubber posts.

The final weight of the concrete and steel rail combined was estimated to be 318 lb/ft (473 kg/m) excluding bolts, nuts, and washers. The nominal flexural strength of the concrete beam was 2,602 kip-in. (294 kN-m). The nominal flexural strength of the concrete beam in the vertical direction was 2,098 kip-in. (237 kN-m). The nominal shear strength of the concrete section at its weakest point (at the circular vertical hole) is 66 kips (294 kN).

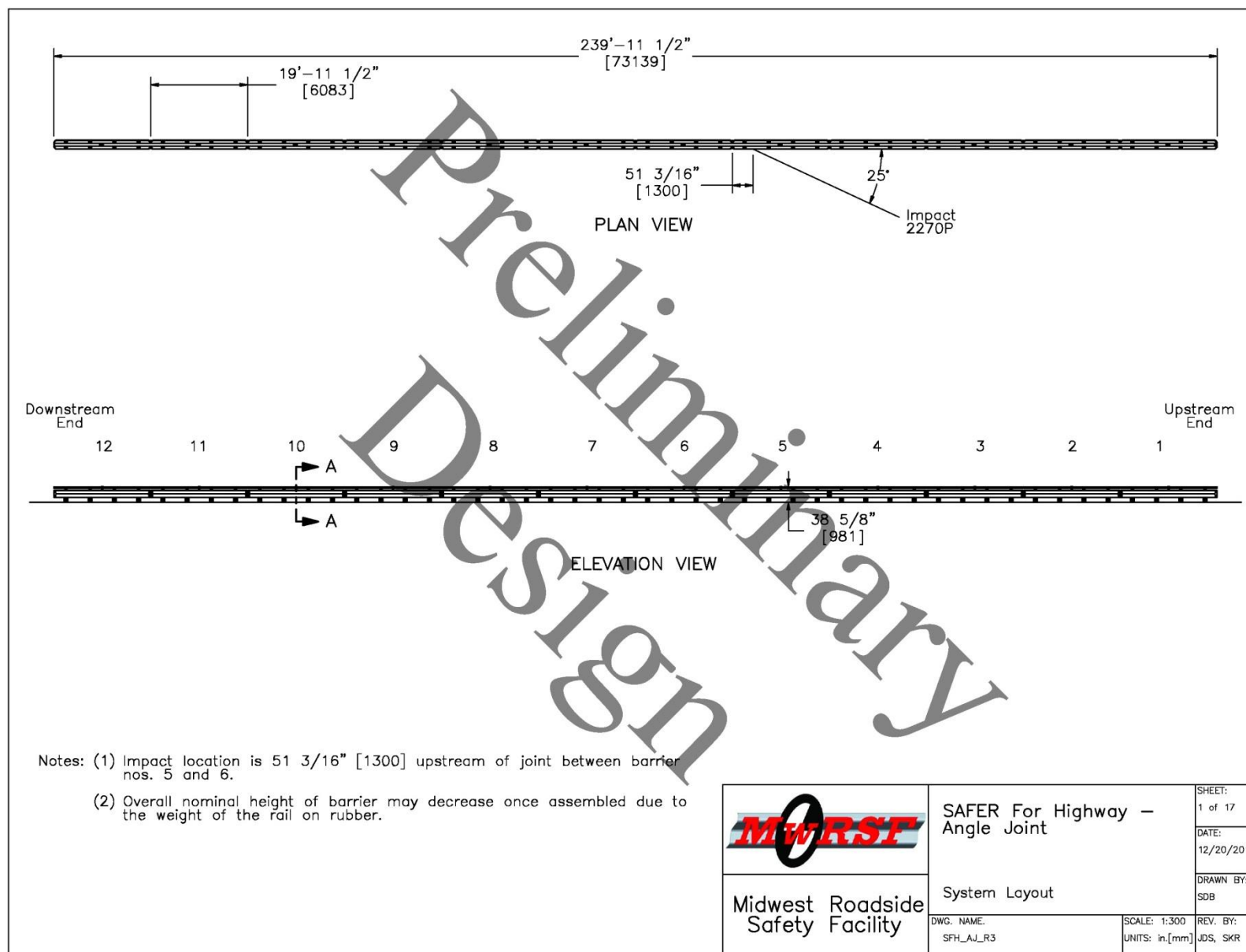


Figure 43. Preliminary Barrier Design, System Layout

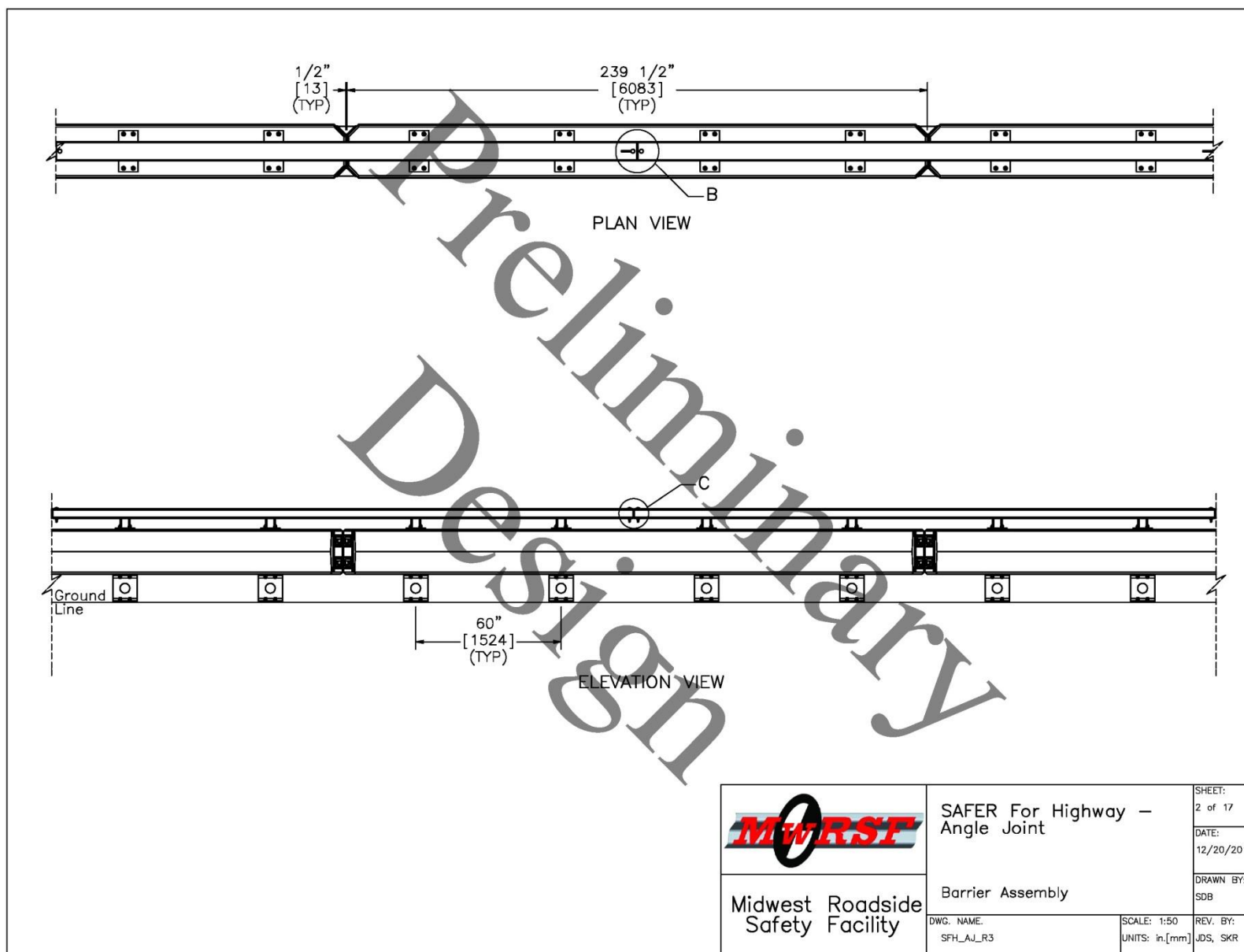


Figure 44. Preliminary Barrier Design, Barrier Assembly

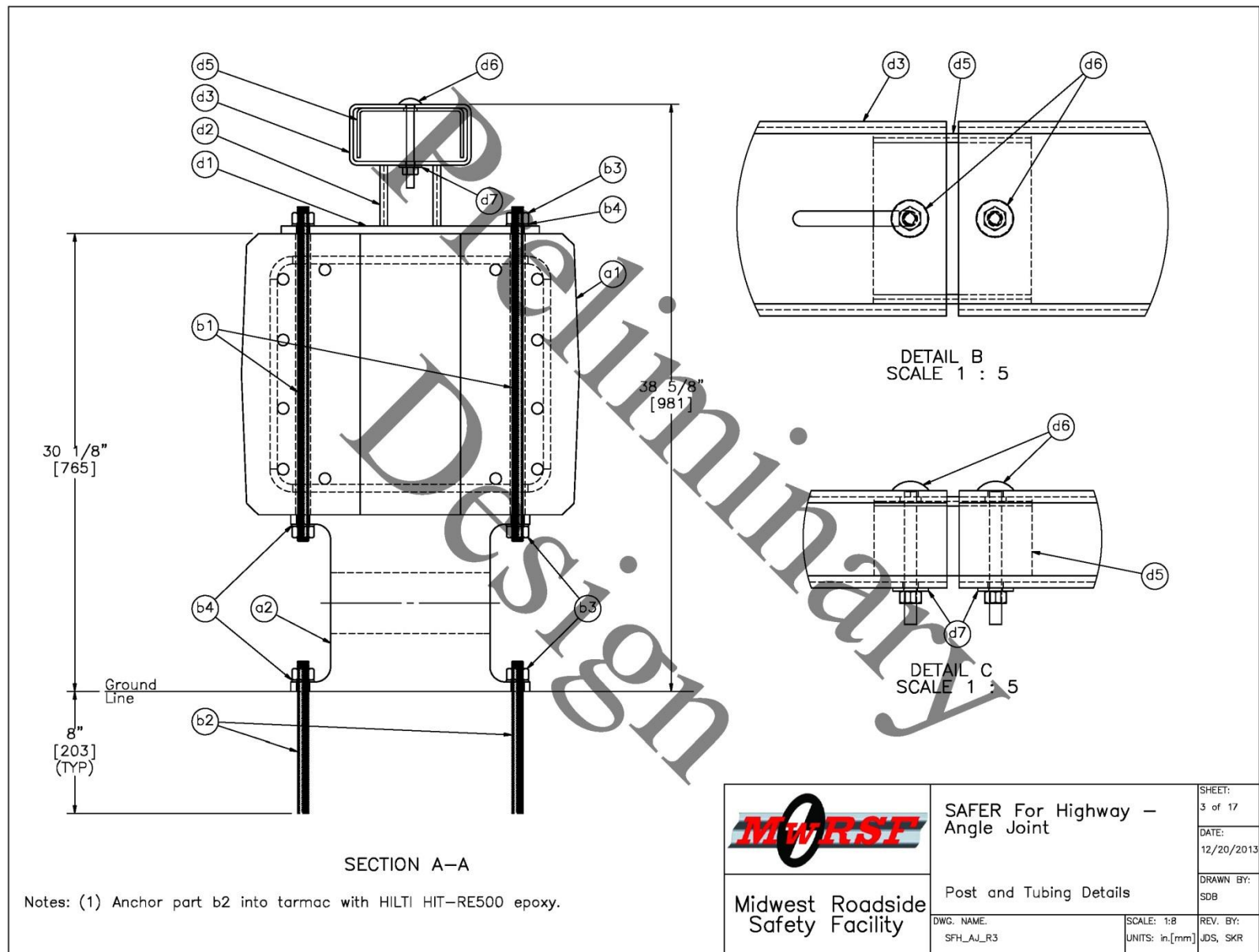


Figure 45. Preliminary Barrier Design, Post and Tubing Details

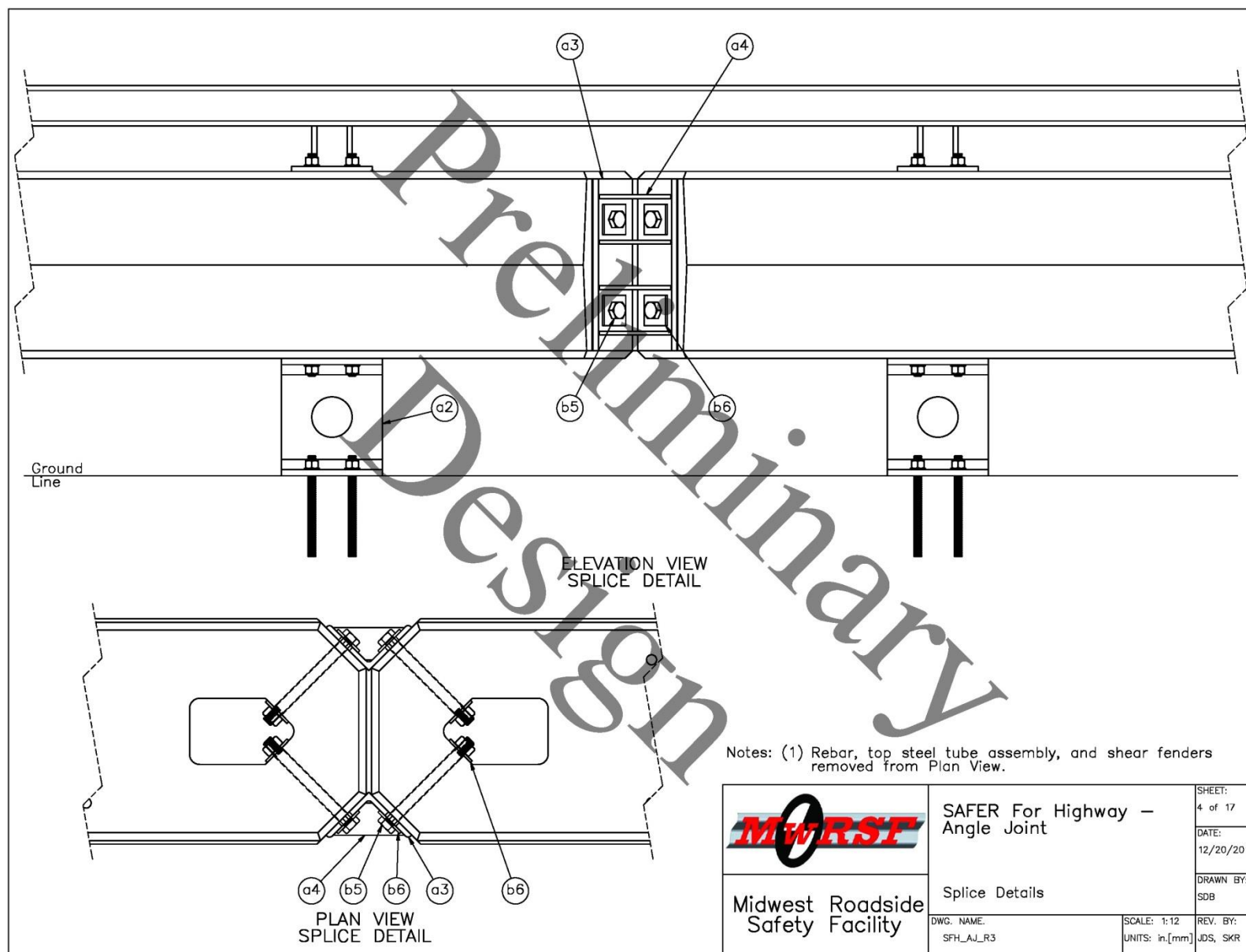


Figure 46. Preliminary Barrier Design, Splice Details

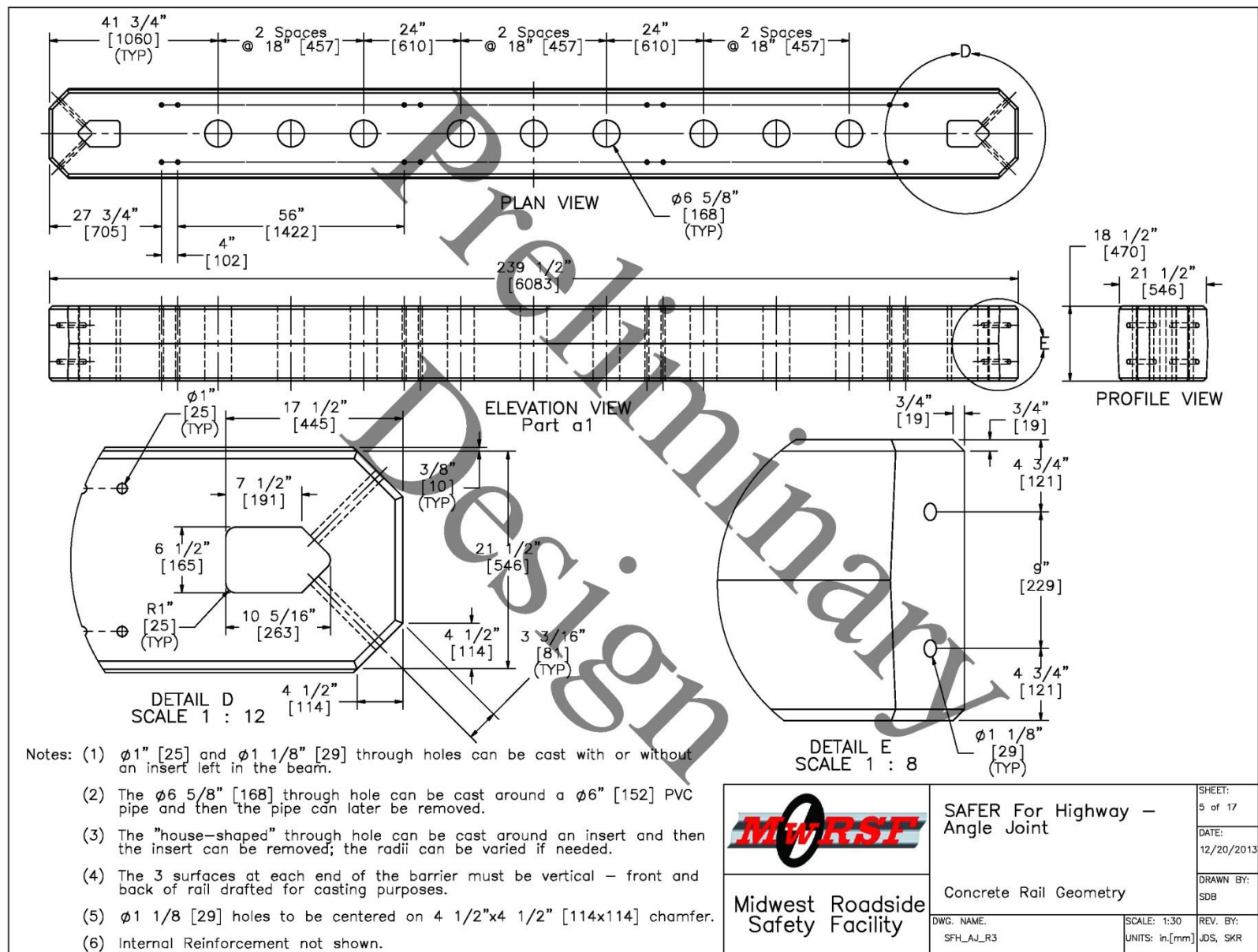


Figure 47. Preliminary Barrier Design, Concrete Rail Geometry

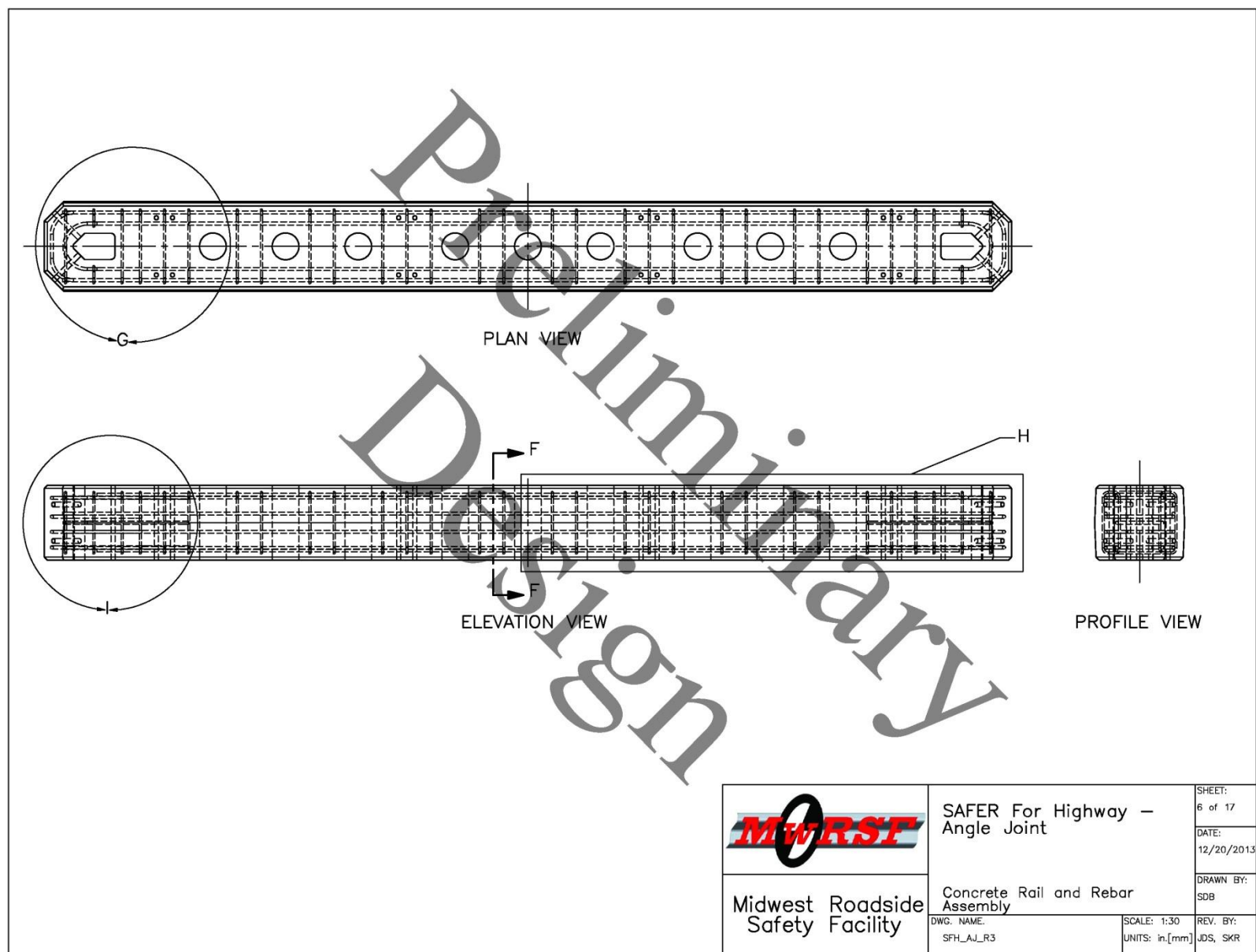


Figure 48. Preliminary Barrier Design, Concrete Rail and Rebar Assembly

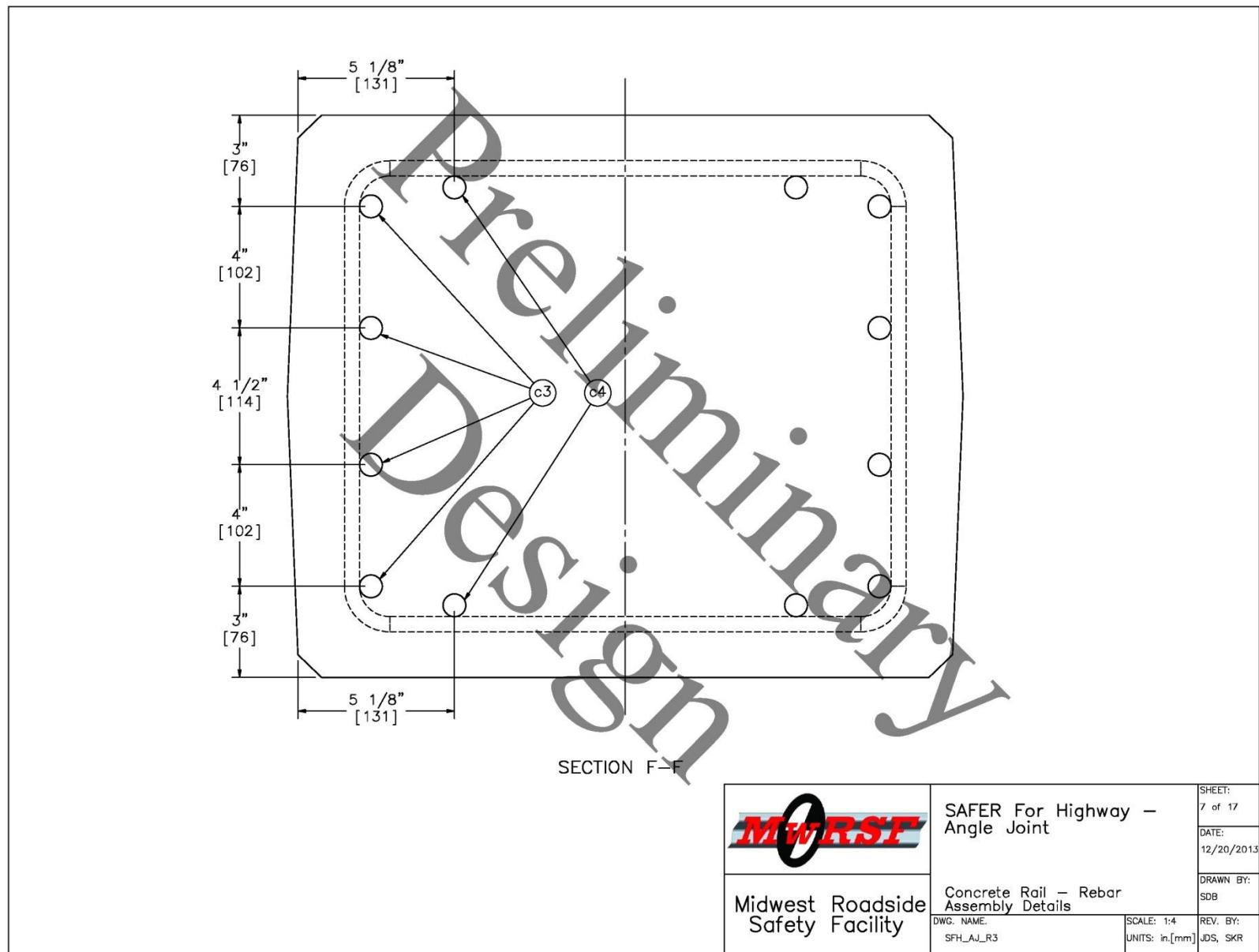


Figure 49. Preliminary Barrier Design, Rebar Assembly Details

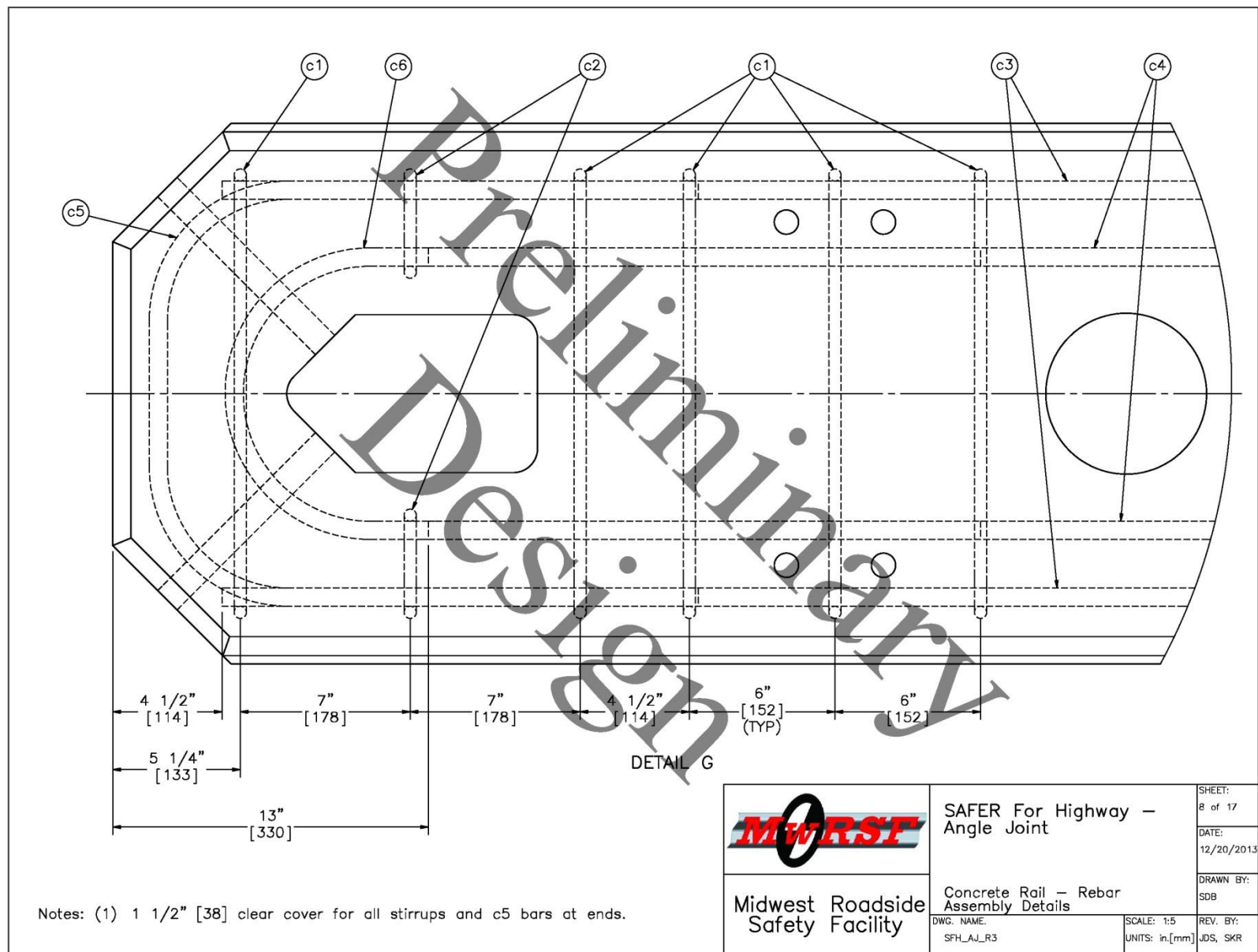


Figure 50. Preliminary Barrier Design, Rebar Assembly Details

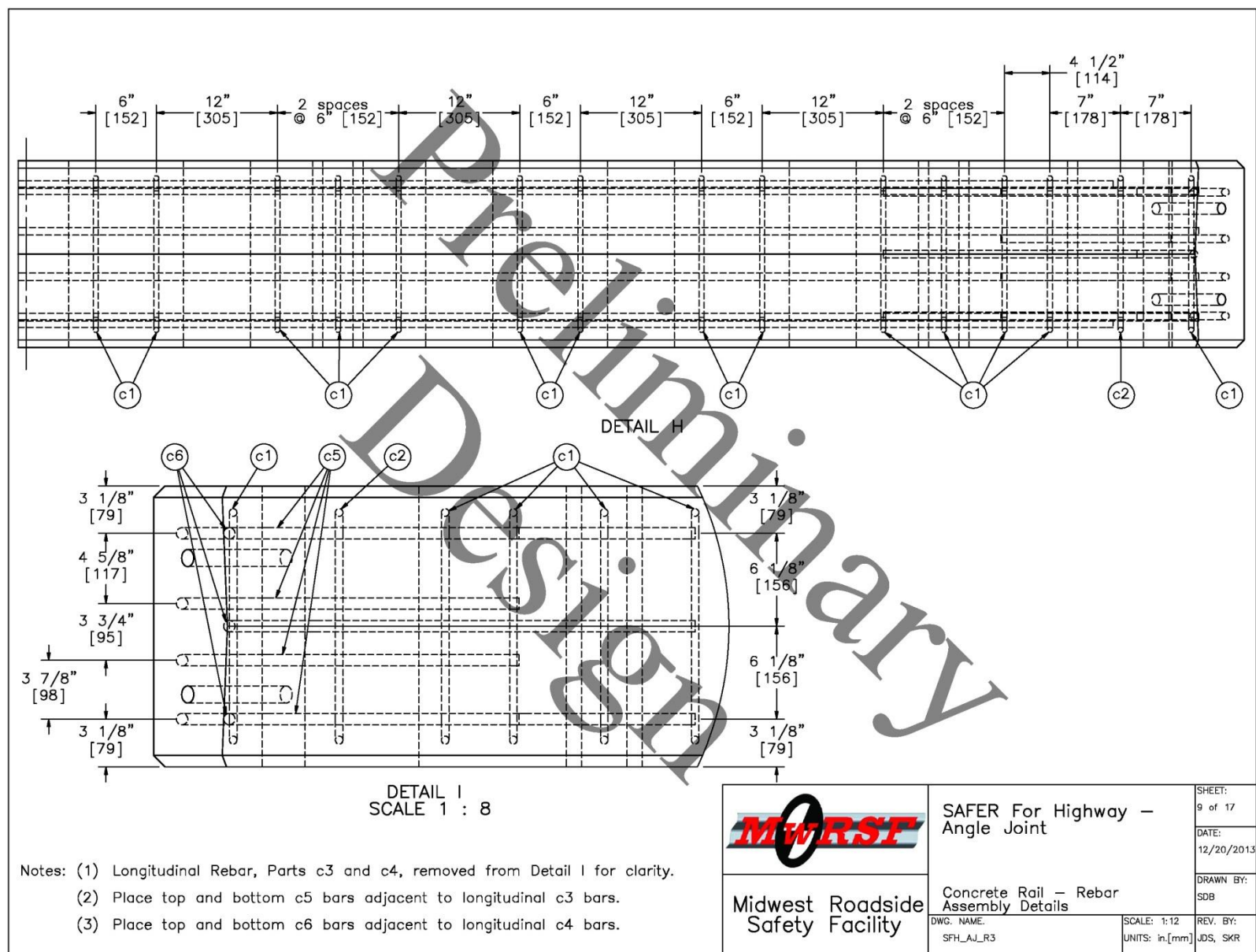


Figure 51. Preliminary Barrier Design, Rebar Assembly Details

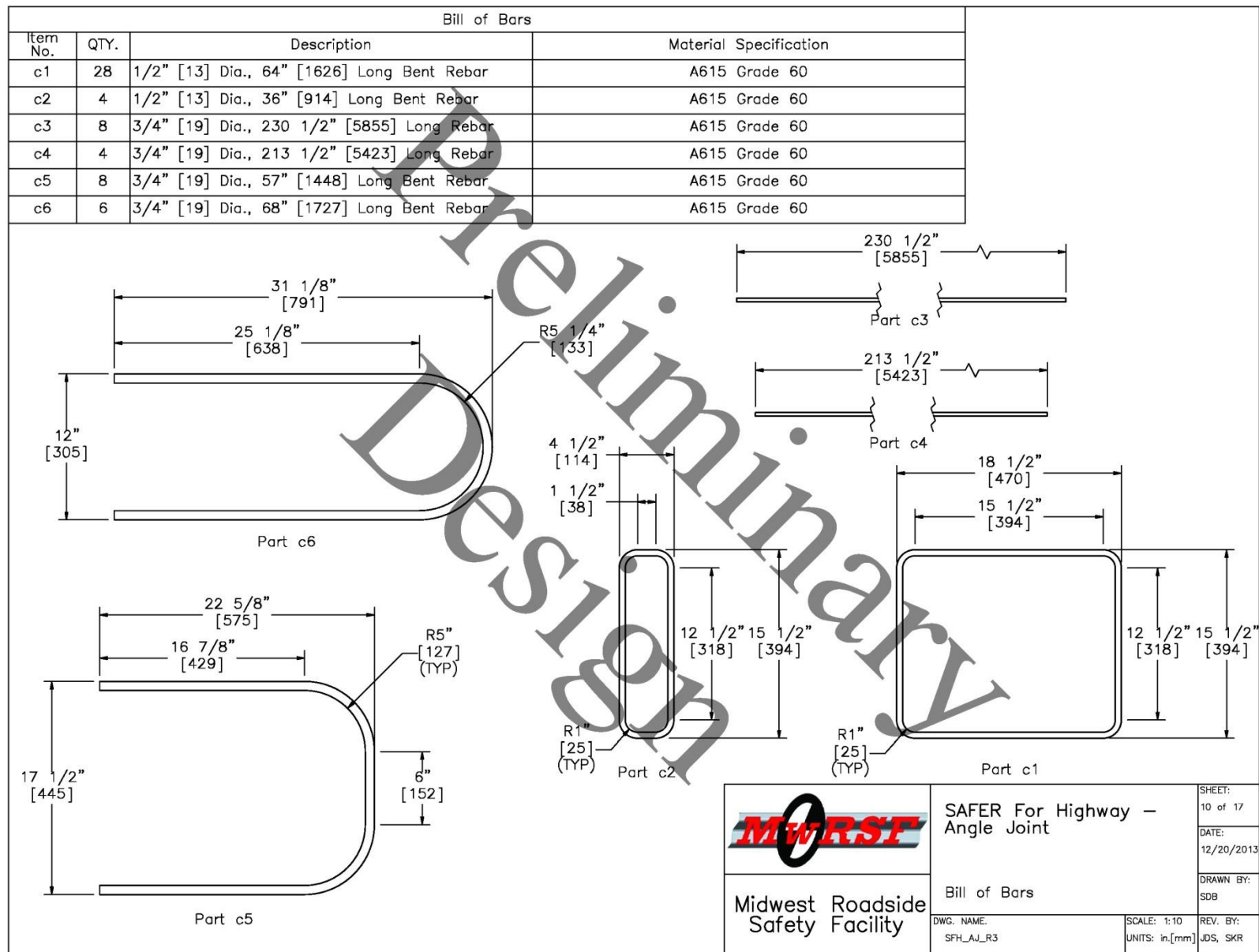


Figure 52. Preliminary Barrier Design, Bill of Bars

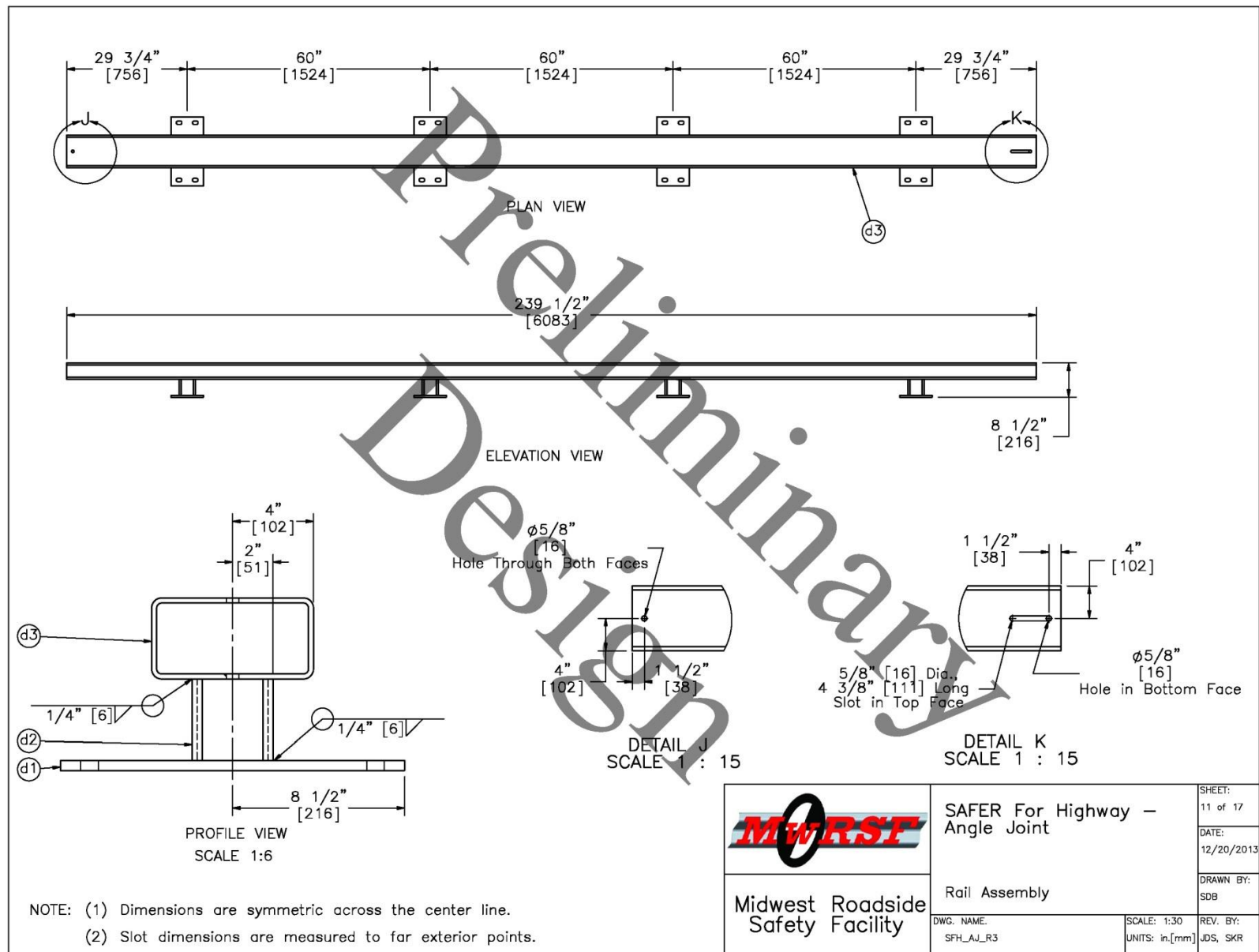


Figure 53. Preliminary Barrier Design, Rail Assembly

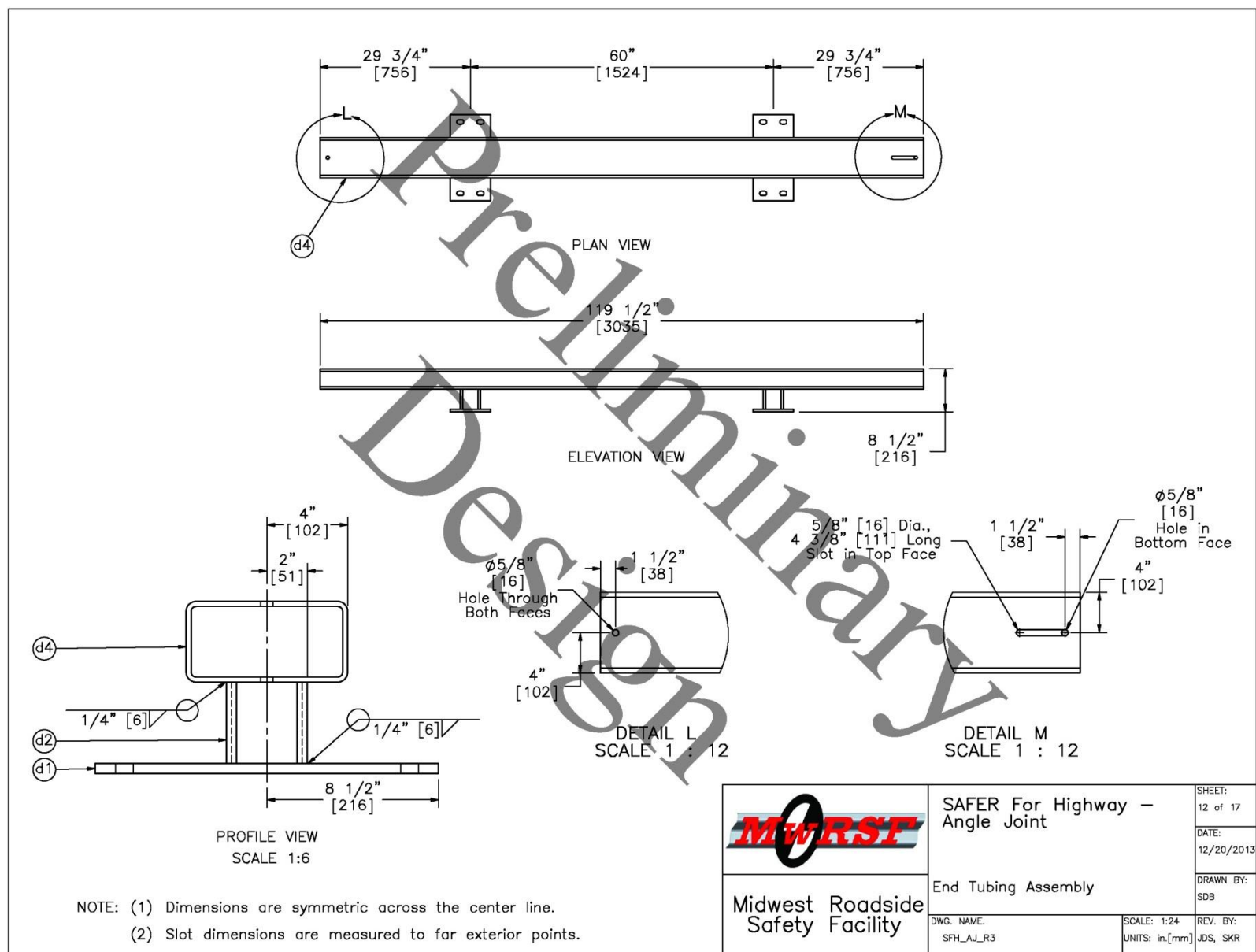


Figure 54. Preliminary Barrier Design, End Tubing Assembly

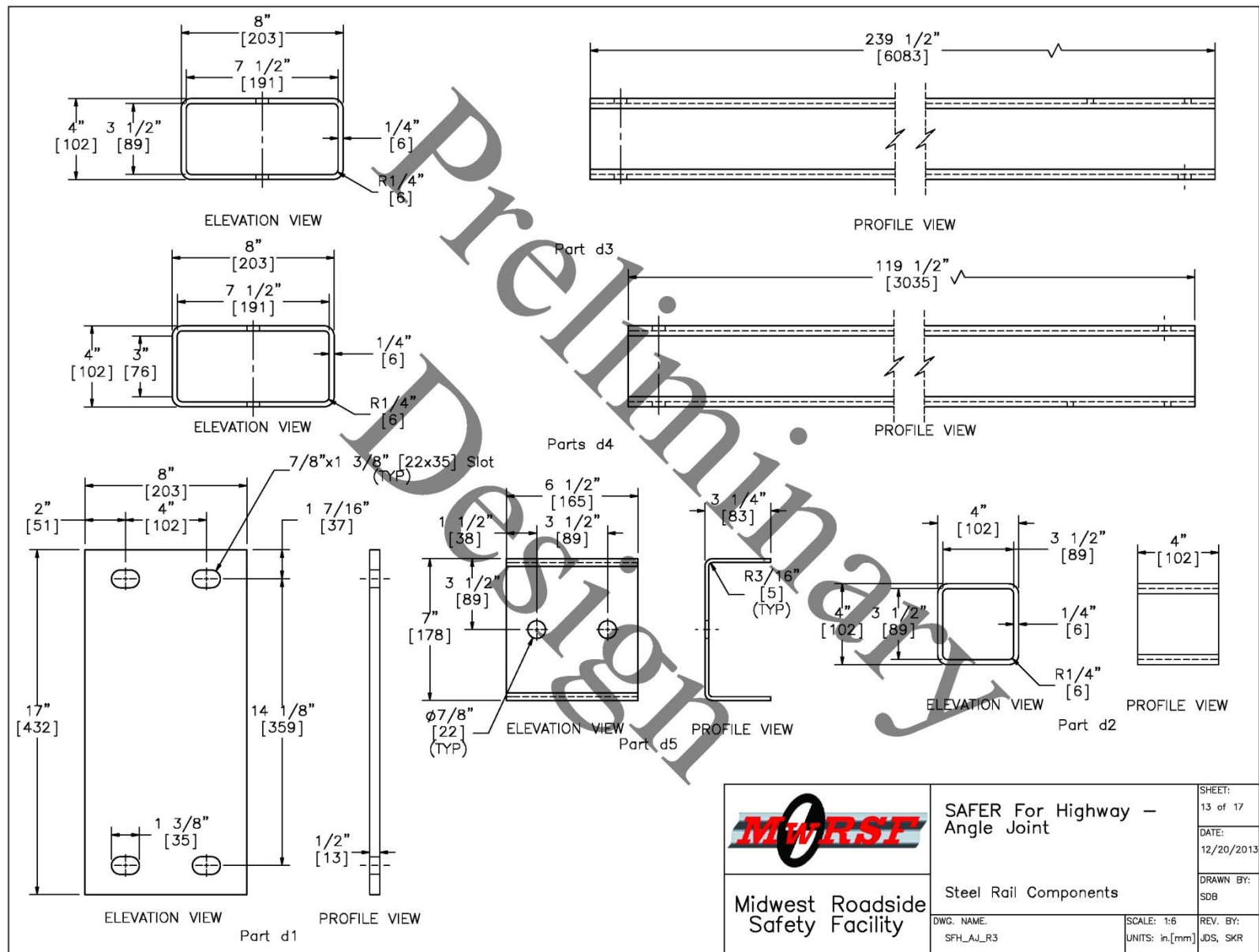


Figure 55. Preliminary Barrier Design, Steel Rail Components

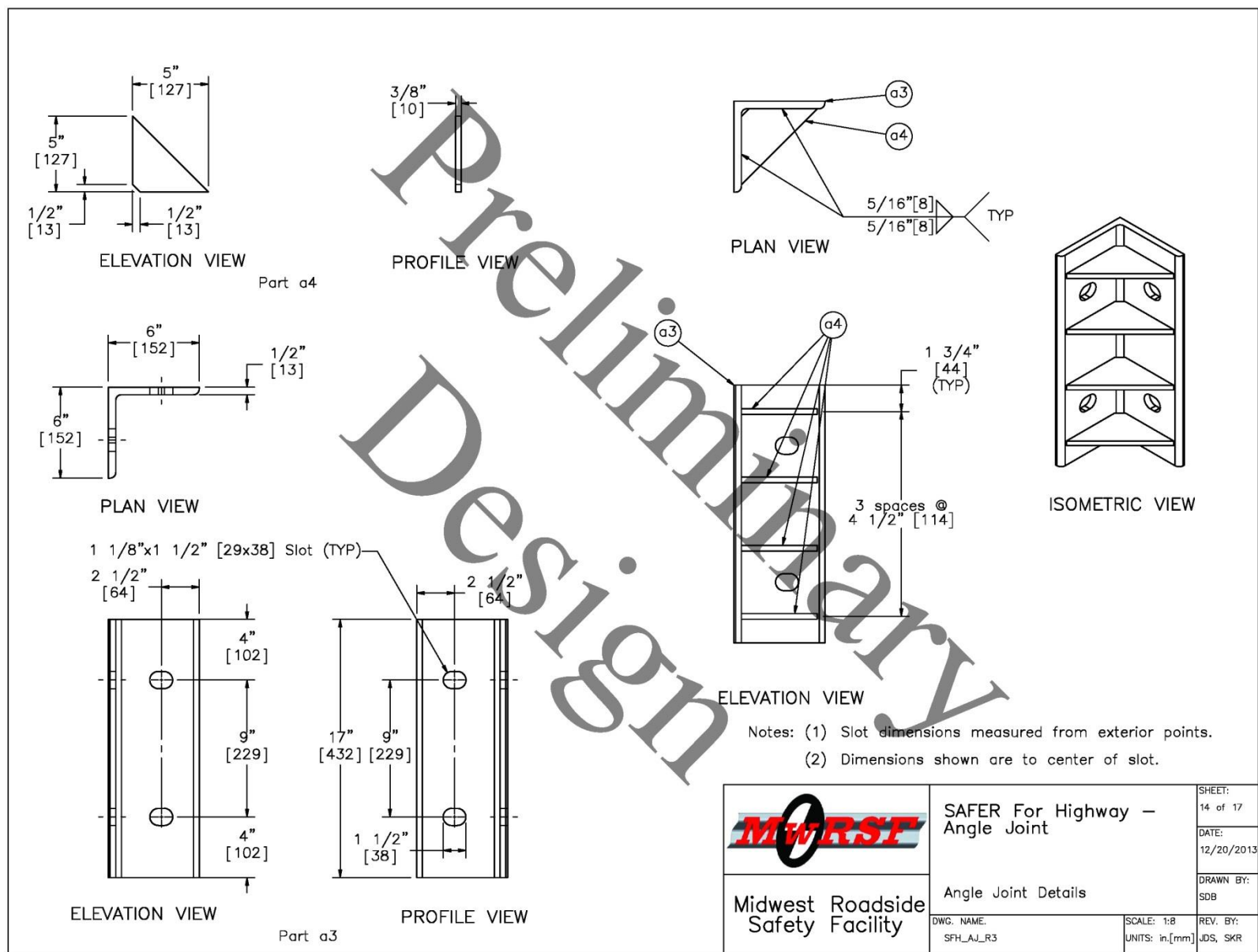


Figure 56. Preliminary Barrier Design, Adjustable Continuity Joint Details

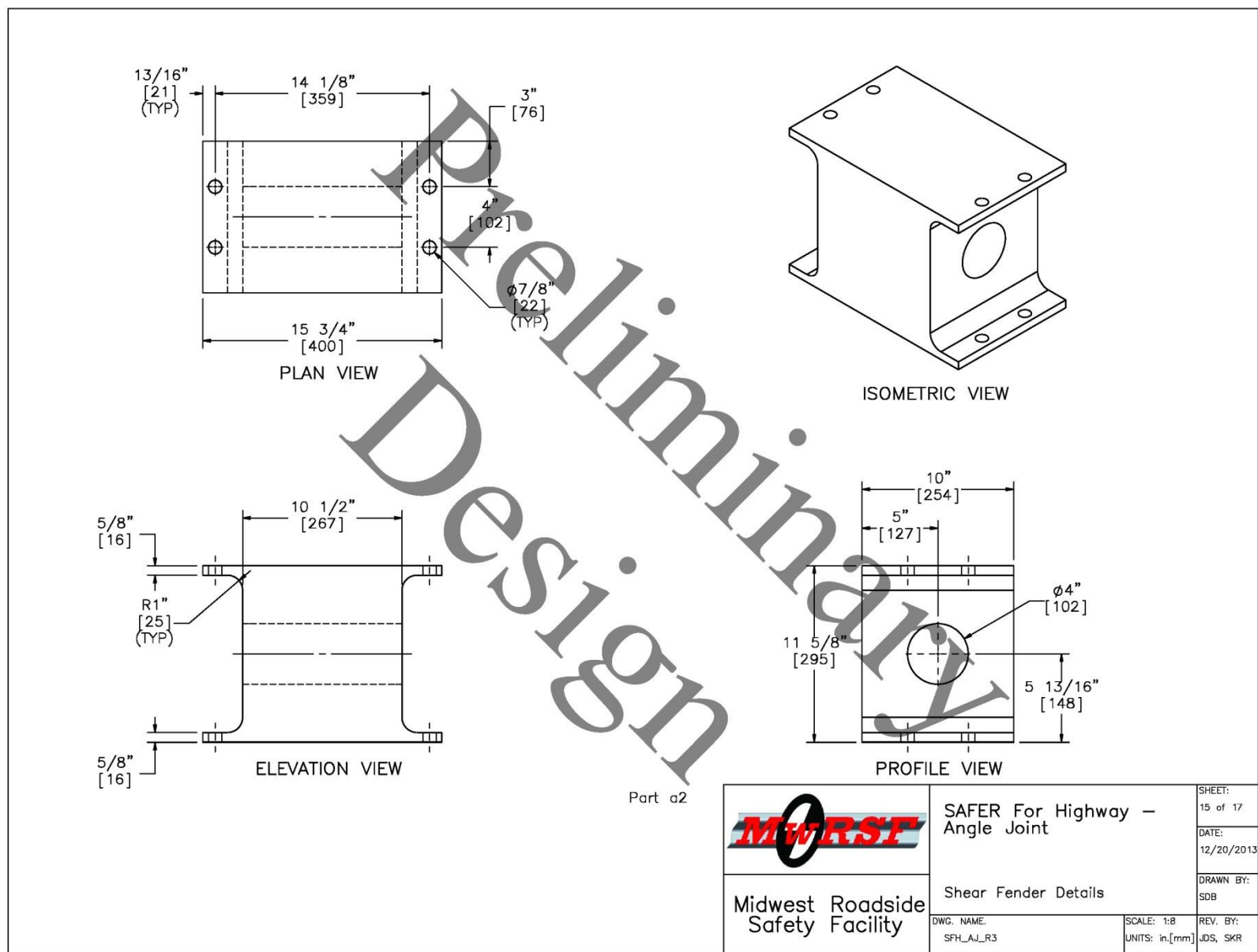


Figure 57. Preliminary Barrier Design, Shear Fender Details

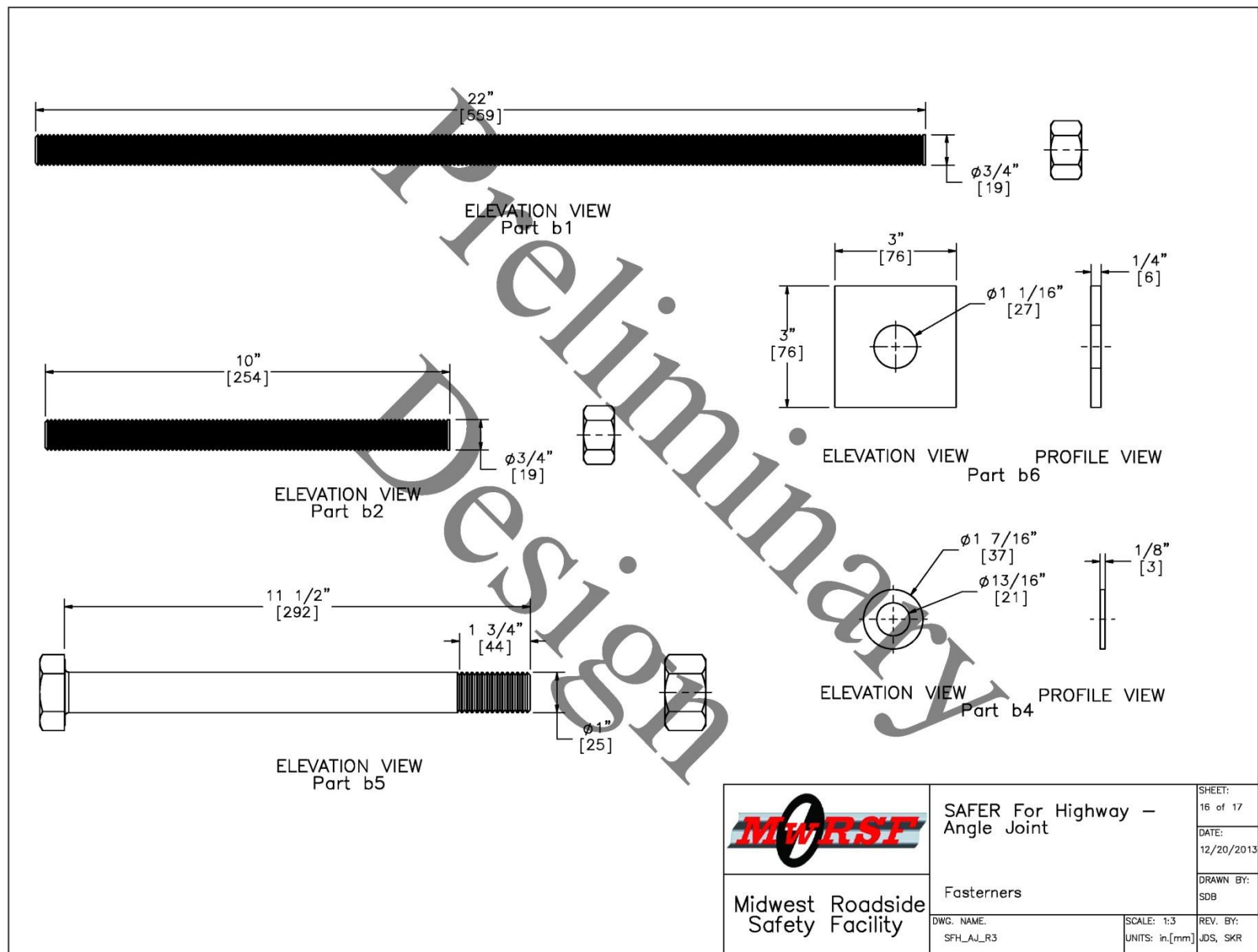


Figure 58. Preliminary Barrier Design, Fasteners


Item No.	QTY.	Description	Material Specification	Hardware Guide
a1	12	Lightweight Concrete Rail	min f'c=5 ksi [34.5 MPa], density=110 pcf	—
a2	48	Morse E46496 Shear Fender	ASTM D2000	—
a3	22	6"x6"x1/2" [152x152x13], 17" [432] Long L-Bracket	A992 Galvanized	—
a4	88	5"x5"x3/8" [127x127x10] Gusset Plate	A572 Grade 50 Galvanized	—
b1	192	3/4" [19] Dia., 22" [559] Long Threaded Rod	A193 Grade B7 Galvanized	—
b2	192	3/4" [19] Dia., 10" [254] Long Threaded Rod	A193 Grade B7 Galvanized	—
b3	576	3/4" [19] Dia. UNC Heavy Hex Nut	ASTM A194 Grade 2H Galv.	—
b4	576	3/4" [19] Dia. Flat Washer	ASTM F436 Galv.	—
b5	88	1" [25] Dia. UNC, 11 1/2" [292] Long Hex Head Bolt and Nut	Bolt ASTM A325 Galv., Nut ASTM A563 A Galv.	FBX24b
b6	176	3"x3"x1/4" [76x76x6] Square Washer	A572 Grade 50 Galvanized	—
c1	336	1/2" [13] Dia., 64" [1626] Long Bent Rebar	A615 Grade 60	—
c2	48	1/2" [13] Dia., 36" [914] Long Bent Rebar	A615 Grade 60	—
c3	96	3/4" [19] Dia., 230 1/2" [5855] Long Rebar	A615 Grade 60	—
c4	48	3/4" [19] Dia., 213 1/2" [5423] Long Rebar	A615 Grade 60	—
c5	96	3/4" [19] Dia., 57" [1448] Long Bent Rebar	A615 Grade 60	—
c6	72	3/4" [19] Dia., 68" [1727] Long Bent Rebar	A615 Grade 60	—
d1	48	17"x8"x1/2" [431x203x13] Anchor Plate	ASTM A572 Grade 50 Galvanized	—
d2	48	4"x4"x1/4" [102x102x6], 4" [102] Long Tube	A500 Grade B Galvanized	—
d3	11	8"x4"x1/4" [203x102x6], 239 1/2" [6083] Long Tube	A500 Grade B Galvanized	—
d4	2	8"x4"x1/4" [203x102x6], 119 1/2" [3035] Long End Tube	A500 Grade B Galvanized	—
d5	12	12 3/4"x6 1/2"x3/16" [324x165x5] Bent Plate	ASTM A572 Grade 50 Galvanized	—
d6	24	1/2" [13] Dia., 5 1/2" [140] Long Dome (Round) Head Bolt and Nut	Bolt ASTM A307 Grade A Galvanized, Nut A563A Galvanized	—
d7	24	1/2" [13] Dia. Flat Washer	ASTM F844 Galvanized	—
d8	—	Epoxy	HILTI HIT-RE500	—
<div style="display: flex; justify-content: space-between; align-items: flex-end;"> <div style="text-align: center;">  <p>Midwest Roadside Safety Facility</p> </div> <div style="text-align: center;"> <p>SAFER For Highway – Angle Joint</p> <p>Bill of Materials</p> </div> <div style="text-align: right;"> <p>SHEET: 17 of 17</p> <p>DATE: 12/20/2013</p> <p>DRAWN BY: SDB</p> </div> </div> <div style="display: flex; justify-content: space-between; margin-top: 10px;"> <div>DWG. NAME: SFH_AJ_R3</div> <div>SCALE: 1:8 UNITS: in.[mm]</div> <div>REV. BY: JDS, SKR</div> </div>				

Figure 59. Preliminary Barrier Design, Bill of Materials

5 COMPUTER SIMULATION

The barrier model used during beam splice development was 160 ft (49 m) long and pinned at each end. As the RESTORE barrier was impacted during those simulations with the 2270P pickup truck model, the barrier deflected and rotated backward, and the pinned end constraints prevented some of that motion. Real-world installations may be significantly longer, and the end constraints would have a negligible effect on the system performance for impact events near the center of the system. Therefore, it was more critical to evaluate the system deflection and rotation without end constraints, so a 240 ft (73 m) long RESTORE model was created without end constraints. The preliminary design for the simulation and for the full-scale crash test was shown previously in Figures 43 through 59.

Further computer simulation on the 240-ft (73-m) long RESTORE barrier was desired prior to crash testing to examine overall barrier performance, vehicle accelerations and velocities, and stresses in the splice parts when impacted by the 1100C Neon passenger car, 2270P Silverado pickup truck, and 10000S single-unit truck vehicle models.

5.1 Baseline Simulations with Rigid Concrete Barriers

Baseline simulations were previously conducted to compare the performance of the RESTORE barrier with that obtained for a rigid, concrete barrier [1]. Several vehicle models were used, including the 1100C Dodge Neon model developed by the National Crash Analysis Center (NCAC) [10] and modified by MwRSF, the 2270P Chevrolet Silverado model developed by NCAC [11-12] and modified by MwRSF, and the 10000S single-unit truck model originally developed by NCAC and calibrated by TTI against available full-scale crash test data [13].

Three simulations were created, then validated and calibrated against full-scale crash tests with rigid concrete barriers. The 1100C Dodge Neon model impacted a 32-in. (813-mm) tall New Jersey barrier in an LS-DYNA simulation at a speed of 62 mph (27.8 m/s) and an angle of

25 degrees. The 2270P Chevrolet Silverado pickup truck model impacted a 36-in. (914-mm) tall single-slope barrier at a speed of 62 mph (27.8 m/s) and an angle of 25 degrees. The 10000S single-unit truck model impacted a 36-in. (914-mm) tall single-slope barrier at 57.2 mph (25.6 m/s) and an angle of 15 degrees. Full simulation results and validation with crash tests can be found in Schmidt, et al. [1].

5.2 RESTORE Barrier Model

The RESTORE barrier model used during the splice development was extended to a 240-ft (73-m) length, and the pinned end constraints were released. The barrier model parts are shown in Figure 60, and the parts, element types, and material models are shown in Table 6. The corresponding part reference numbers in the drawing set are also shown in Table 6. Reference numbers b1-b4 and d6-d7 (bolted connections), c1-c6 (rebar), and d8 (epoxy) were not modeled as discrete parts.

The post rubber model was taken from a previously developed model found in Schmidt, et al. [1]. Significant damage to the concrete beams was not anticipated, so the beams were modeled with rigid shell elements that were free to move in all translational and rotational directions. Each concrete beam was assigned a separate part number from 4999 to 5010, and the translational mass, center of gravity location, and inertia properties were assigned for each beam as calculated in a 3D-CAD model.

The ACJ angle, ACJ gussets, splice bolt heads/nuts, splice bolt washers, and splice bolt shafts (part nos. 4001, 4002, 5020, 5021, and 5022) used fully-integrated, selectively-reduced solid element formulations to control the hourglass energy. The post base plates (part no. 6002) had hourglass control type 3 to control the hourglass energy. The ACJ angle, ACJ gussets, and splice bolt washers (part nos. 4001, 4002, and 5021) were relatively thin and were originally modeled with shell elements. However, it was difficult to properly prestress the splice bolts, as

some contact thickness penetration occurred when those parts were modeled with shell elements. Therefore, they were modeled with solid elements.

The pins (part no. 2028) and loops (part nos. 2125 and 2126) were utilized in previous models to study the effects of end conditions. For this simulation effort, no constraints were applied to the rigid pins, so no fixity existed at the ends. However, the parts remained in the model for ease of comparing pinned ends versus free ends.

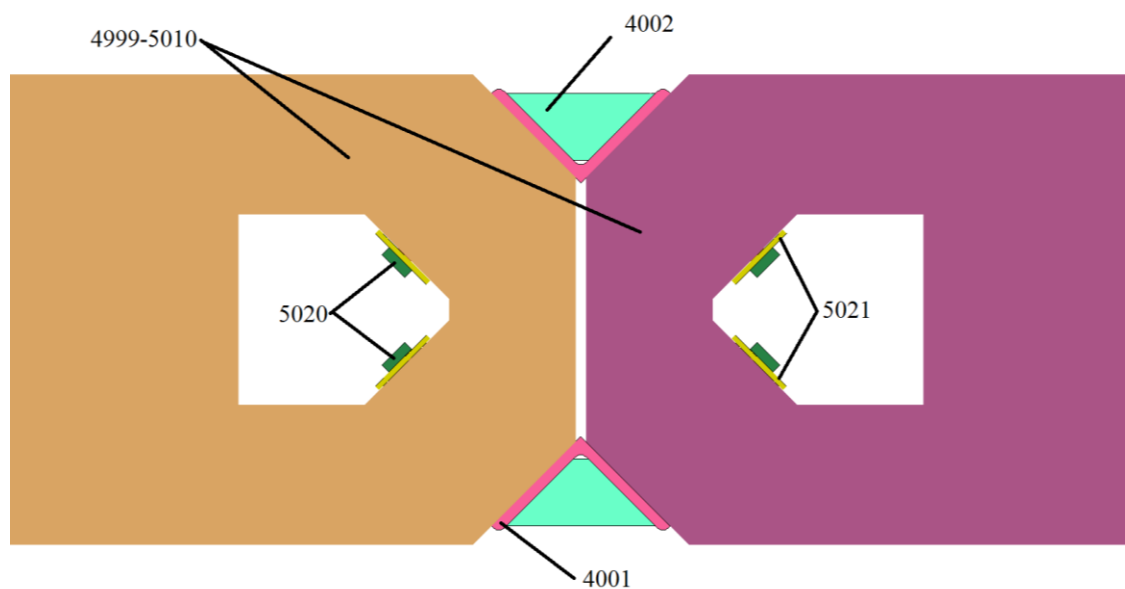
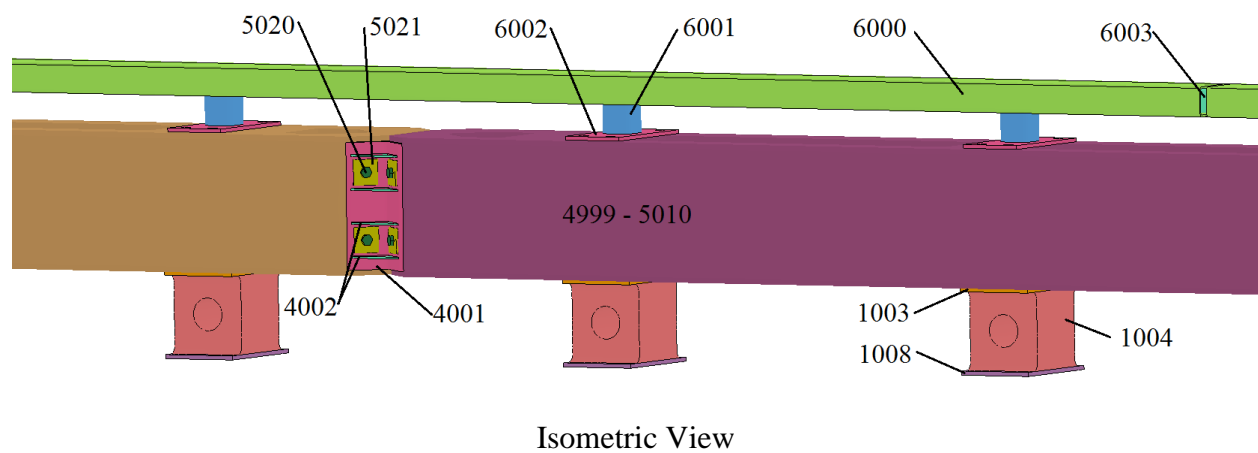


Figure 60. Simulation Part Numbers

Table 6. Barrier Model Parts, Elements, and Materials

Part Description	Drawing Reference No.	Simulation Part No.	Element Type	Material
Post - Top Steel	a2	1003	Type 1 Solid	*MAT_PIECEWISE_LINEAR_PLASTICITY
Post - Rubber	a2	1004	Type 13 Solid	*MAT_SIMPLIFIED_RUBBER/FOAM
Post - Bottom Steel	a2	1008	Type 1 Solid	*MAT_RIGID
Pins	NA	2028	Type 1 Solid	*MAT_RIGID
Loops - Right	NA	2125	Type 1 Solid	*MAT_PIECEWISE_LINEAR_PLASTICITY
Loops - Left	NA	2126	Type 1 Solid	*MAT_PIECEWISE_LINEAR_PLASTICITY
ACJ Angle	a3	4001	Type 2 Solid	*MAT_PIECEWISE_LINEAR_PLASTICITY
ACJ Gussets	a4	4002	Type 2 Solid	*MAT_PIECEWISE_LINEAR_PLASTICITY
Concrete Beam	a1	4999-5010	Type 2 Shell	*MAT_RIGID
Splice Bolt Heads/Nuts	b5	5020	Type 2 Solid	*MAT_PIECEWISE_LINEAR_PLASTICITY
Splice Bolt Washers	b6	5021	Type 2 Solid	*MAT_PIECEWISE_LINEAR_PLASTICITY
Splice Bolt Shafts	b5	5022	Type 2 Solid	*MAT_PIECEWISE_LINEAR_PLASTICITY
Top Tubes	d3, d4	6000	Type 2 Shell	*MAT_PIECEWISE_LINEAR_PLASTICITY
Tube Posts	d2	6001	Type 2 Shell	*MAT_PIECEWISE_LINEAR_PLASTICITY
Post Base Plates	d1	6002	Type 1 Solid	*MAT_PIECEWISE_LINEAR_PLASTICITY
Tube Splices	d5	6003	Type 2 Shell	*MAT_PIECEWISE_LINEAR_PLASTICITY

Several parts were connected with merged nodes:

- 1) Top and bottom steel in the rubber posts (part nos. 1003 and 1008) and the rubber in the post (part no. 1004) to make the post a continuous part;
- 2) Splice bolt heads/nuts (part no. 5020) and the splice bolt shaft (part no. 5022) to make continuous bolts;
- 3) ACJ angle (part no. 4001) and the ACJ gussets (part no. 4002), which is similar to welded parts with no failure; and
- 4) Tube posts (part no. 6001) and the post base plates and top tubes (part nos. 6002 and 6000), which is similar to welded parts with no failure.

Tied contacts were used between the concrete beams (part nos. 4999-5010) and the top steel in the rubber posts (part no. 1003) as well as the post base plates (part no. 6002) to simulate the through-bolts. The bottom steel in the posts (part no. 1008) was constrained from all motion to simulate anchorage via threaded rods epoxied into concrete.

The static and dynamic coefficients of friction defined in the contacts between the vehicles' bodies/tires and the barrier were:

- 1) 0.1 for the 1100C Neon body and 0.3 for its tires;
- 2) 0.1 for the 2270P Silverado body and 0.1 for its tires; and
- 3) 0.1 for the 10000S Ford Single-Unit Truck body and 0.1 for its tires.

The static and dynamic coefficients of friction defined as surface-to-surface contacts between the ACJ, washers, and bolt heads were 0.3.

5.2.1 1100C Dodge Neon

The 1100C Neon model impacted the RESTORE barrier at a speed of 62 mph (27.8 m/s) and an angle of 25 degrees approximately 59 in. (1,500 mm) upstream from the splice between beam segments 5 and 6. The vehicle was successfully contained and redirected, and the vehicle trajectory is shown in Figure 61. The small car was parallel to the system 190 ms after impact and exited the system 290 ms after impact. The vehicle roll and pitch motions were minimal.

Moderate damage occurred to the front and left sides of the car. The left-front tire slightly contacted the first two posts downstream from the splice between beam segments 5 and 6. The tire then appeared as if it was trying to disengage. The body of the car only contacts the front face of the concrete beams, and no part of the car contacted the upper tube assembly. There system did not appear to have any permanent damage. The system did restore fully; however, the rubber material unloading curve had not been validated, and damping was not enabled in the material.

The top upstream end of concrete beam no. 6 laterally deflected a maximum of 7.4 in. (189 mm) and vertically deflected a maximum of 2.9 in. (74 mm). The vertical deflection was due to gravity and a slight rotation of the barrier. Other impact points were simulated but did not demonstrate an increased potential for vehicle snag or significantly change the results.

Accelerations, velocities, and displacements were found at the center of gravity of the 1100C model at every 0.01 ms and filtered using a customized Excel spreadsheet that is used for filtering full-scale crash test data. The lateral and longitudinal occupant impact velocity (OIV) and occupant ridedown acceleration (ORA) for the RESTORE barrier simulation and the baseline simulation are shown in Table 7. The CFC 180 10-ms average lateral acceleration trace is shown in Figure 62, and the peak acceleration is shown in Table 7. The initial peak lateral acceleration was reduced by 17.3 percent in the RESTORE barrier simulation as compared to the baseline simulation into a rigid New Jersey-shaped concrete barrier at the same impact conditions. The lateral OIV was reduced by 20 percent. The longitudinal OIV, lateral ORA, and longitudinal ORA were almost unchanged when compared to the baseline simulation. Note, all of the occupant risk values were below the MASH threshold limits for both the rigid concrete barrier and the RESTORE barrier simulations.

Other parameters (i.e., parallel time and exit time, velocity, and angle) that give an indication of the RESTORE barrier performance were compared to those obtained under simulated impacts with rigid barriers. A comparison of these parameters is shown in Table 8. Parallel and exit times were determined by visual inspection of the simulation. Exit velocity and angle were determined from the nodal output at the center of gravity local node at the exit time. The parallel and exit times were greater and the exit velocity was lower with the RESTORE barrier, which was anticipated since the system deflected and absorbed some of the vehicle's kinetic energy. The vehicle also exited the RESTORE barrier at a lower angle than the rigid barrier.

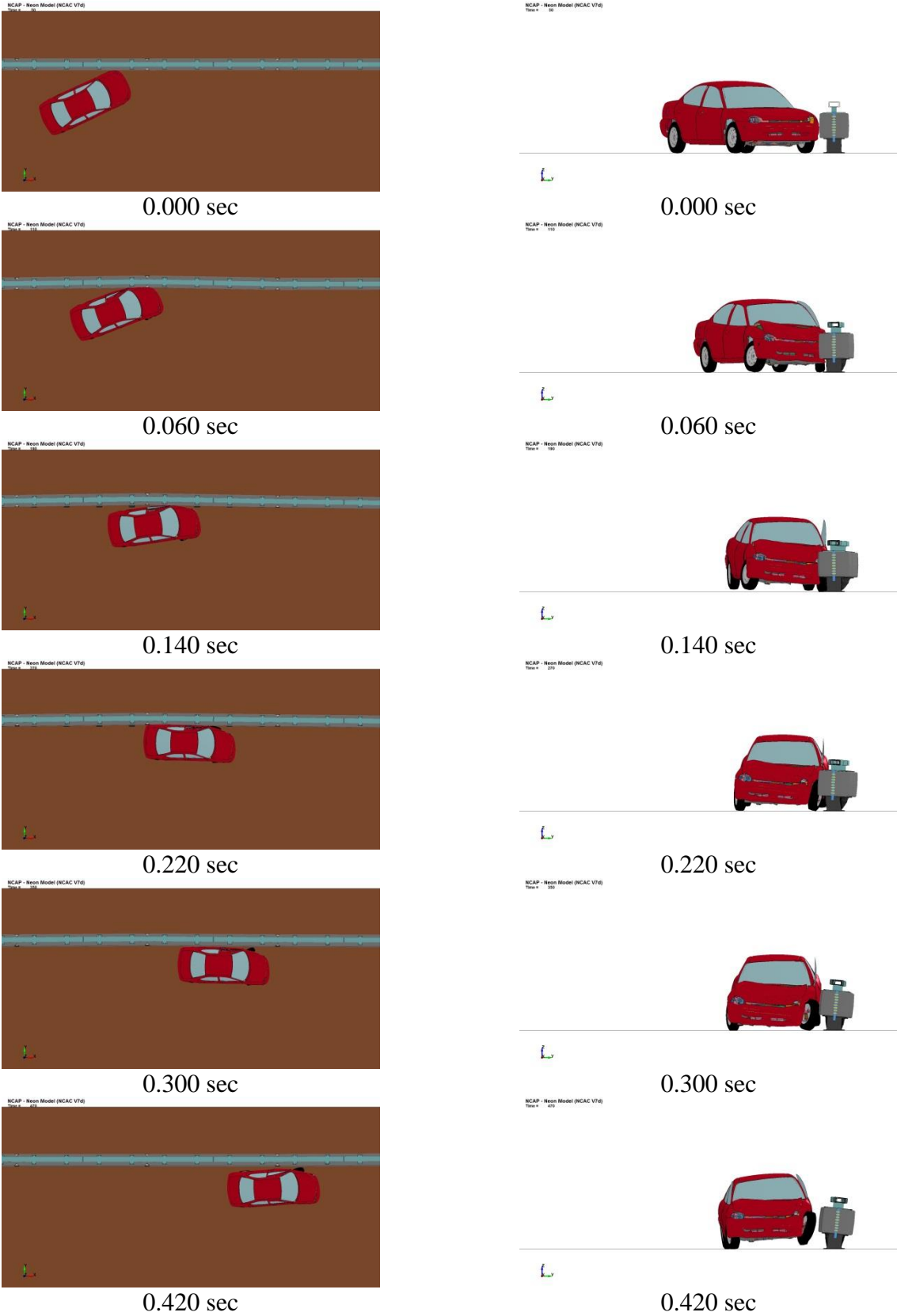


Figure 61. RESTORE Barrier Simulation with MASH Test Designation 4-10 Impact (1100C)

Table 7. Simulation Occupant Risk Data – MASH Test Designation 4-10

Occupant Risk Parameter	New Jersey Baseline Simulation	RESTORE Barrier Simulation	MASH Maximum Limit
Lateral OIV ft/s (m/s)	33.8 (10.3)	27.2 (8.3)	40 (12.2)
Longitudinal OIV ft/s (m/s)	20.7 (6.3)	20.7 (6.3)	40 (12.2)
Lateral ORA g's	9.6	9.7	20.49
Longitudinal ORA g's	6.3	6.7	20.49
Initial Peak CFC 180 10-ms Lateral Acceleration g's	33.6	27.8	NA

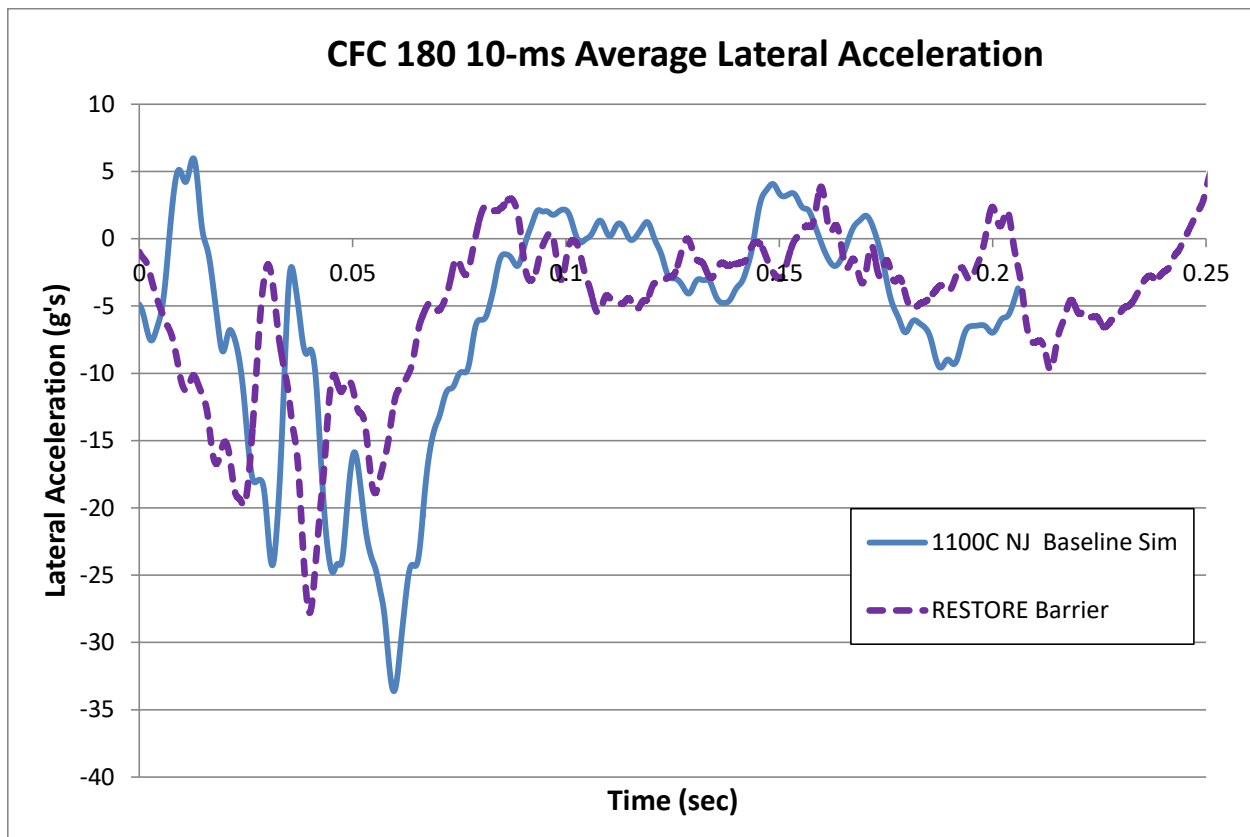


Figure 62. Simulated Lateral Acceleration – MASH Test Designation 4-10

Table 8. Simulation Parallel and Exit Conditions – MASH Test Designation 4-10

Simulation Parameter	New Jersey Baseline Simulation	RESTORE Barrier Simulation
Parallel Time ms	170	190
Exit Time ms	260	290
Exit Velocity mph (km/h)	20.8 (33.5)	17.8 (28.6)
Exit Angle deg	5.3	2.7

5.2.2 2270P Chevrolet Silverado

The 2270P Silverado model impacted the RESTORE barrier at a speed of 62 mph (27.8 m/s) and an angle of 25 degrees approximately 64 in. (1,626 mm) upstream from the splice between beam segments 5 and 6. The vehicle was successfully contained and redirected, and the vehicle trajectory is shown in Figure 63. The pickup truck was parallel to the system 180 ms after impact and exited the system 270 ms after impact. The vehicle had some moderate roll and pitch motions once it exited the system.

Moderate damage occurred to the front and left sides of the truck. The left-front and left-rear tires both slightly contacted the first post upstream from the splice between beam segments 5 and 6 and the first post downstream from the splice between beam segments 5 and 6. The left-front fender contacted the upper tube assembly upon initial impact and the left-rear quarter panel contacted the upper tube assembly upon the rear-end impact, which caused some slight permanent damage to the upper tube assembly. The rest of the system did not appear to have any permanent damage. The system did restore fully; however, the rubber material unloading curve had not been validated, and damping was not enabled in the material.

The top upstream end of concrete beam no. 6 deflected a maximum of 9.9 in. (251 mm) laterally and 5.2 in. (132 mm) vertically during the impact event. The vertical deflection was due to gravity and rotation of the barrier backward. After the pickup truck had exited the system, the inertial mass of the concrete beams continued to rotate backward until the end of the simulation, which was 720 ms after impact. The upstream end of concrete barrier no. 6 deflected over 14 in. (356 mm) laterally and over 10 in. (254 mm) vertically due to this rotation. Other impact points were simulated, but this investigation did not demonstrate an increase in the potential for vehicle snag or significantly change the results.

Accelerations, velocities, and displacements were found at the center of gravity of the 2270P model at every 0.1 ms and filtered using a customized Excel spreadsheet that is used for filtering full-scale crash test data. The lateral and longitudinal OIV and ORA for the RESTORE barrier simulation and the baseline simulation are shown in Table 9. The CFC 180 10-ms average lateral acceleration trace is shown in Figure 64, and the peak is shown in Table 9. The initial peak lateral acceleration was reduced by 28 percent with the RESTORE barrier simulation as compared to the baseline simulation into a rigid single-slope concrete barrier at the same impact conditions. Lateral OIV was reduced by 26 percent, and lateral ORA was reduced by 12 percent. Longitudinal ORA increased compared to the baseline simulation, but it was still below the MASH safety limit. As shown in previous simulations, the rear of the Silverado vehicle model is overly stiff, which causes tailslap to be overestimated in simulations. Thus, the lateral and longitudinal ORA would be expected to be lower in a full-scale crash test than in the simulation. This behavior may also have contributed to the greater pitch and roll motions of the pickup truck after it exited the system.

Other parameters (i.e., parallel time and exit time, velocity, and angle) that give an indication of the RESTORE barrier performance were compared to those obtained under simulated impacts with rigid barriers. A comparison of these parameters is shown in Table 10. Parallel and exit times were determined by visual inspection of the simulation. Exit velocity and angle were determined from the nodal output at the center of gravity local node at the exit time. The parallel and exit times were greater and the exit velocity was slightly lower with the RESTORE barrier, which was anticipated since the system deflected and absorbed some of the vehicle's kinetic energy. The vehicle also exited the RESTORE barrier at a lower angle than the rigid barrier.

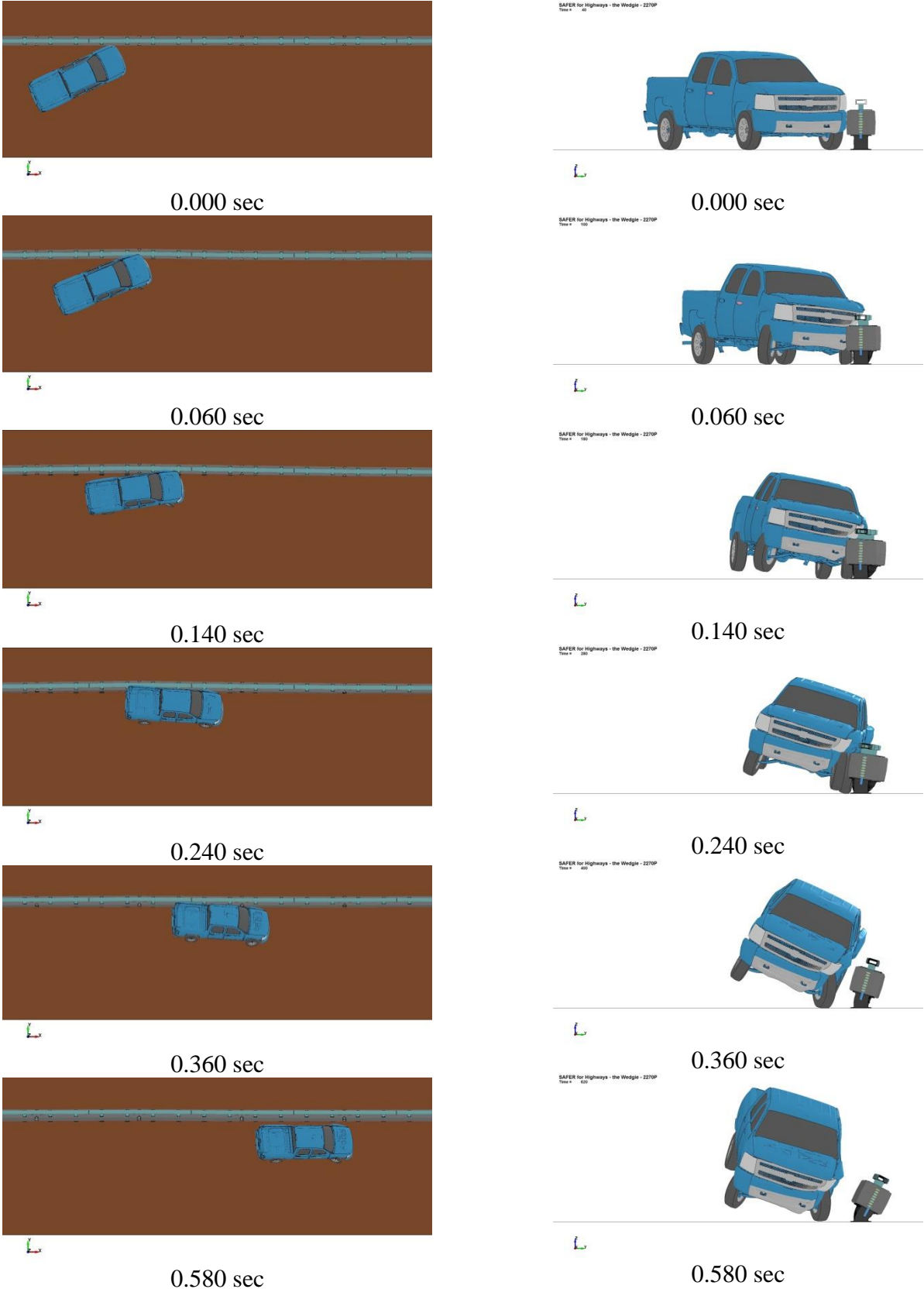


Figure 63. RESTORE Barrier Simulation with MASH Test Designation 4-11 (2270P) Impact

Table 9. Simulation Occupant Risk Data – MASH Test Designation 4-11

Occupant Risk Parameter	Single-Slope Baseline Simulation	RESTORE Barrier Simulation	MASH Maximum Limit
Lateral OIV ft/s (m/s)	25.9 (7.9)	19.2 (5.9)	40 (12.2)
Longitudinal OIV ft/s (m/s)	18.7 (5.7)	14.5 (4.4)	40 (12.2)
Lateral ORA g's	19.0	16.8	20.49
Longitudinal ORA g's	6.8	11.3	20.49
Initial Peak CFC 180 10-ms Lateral Acceleration g's	22.0	15.8	NA

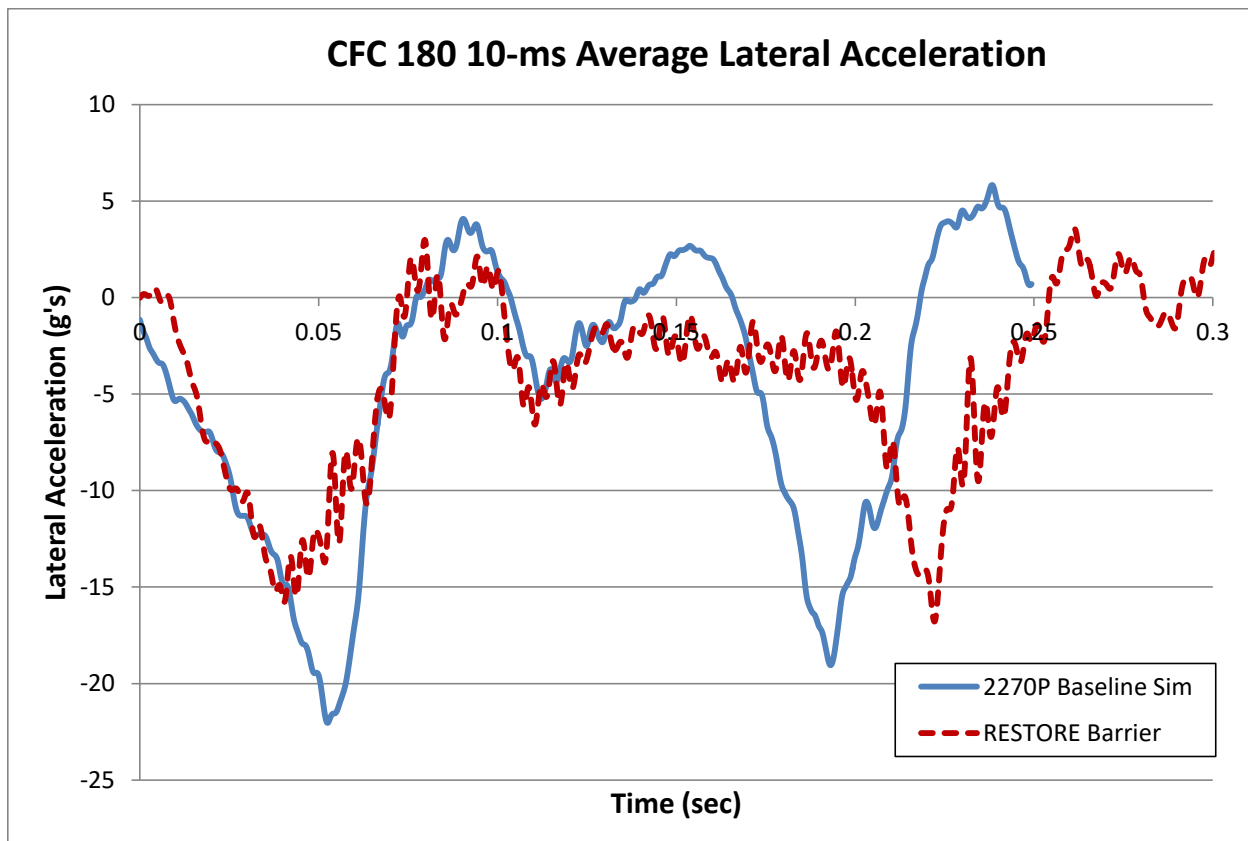


Figure 64. Simulated Lateral Acceleration – MASH Test Designation 4-11

Table 10. Simulation Parallel and Exit Condition – MASH Test Designation 4-11

Simulation Parameter	Single Slope Baseline Simulation	RESTORE Barrier Simulation
Parallel Time ms	160	190
Exit Time ms	260	300
Exit Velocity mph (km/h)	23.1 (37.2)	22.9 (36.9)
Exit Angle deg	5.9	1.9

5.2.1 10000S Single-Unit Truck

The 10000S single-unit truck model impacted the RESTORE barrier at a speed of 56 mph (25 m/s) and an angle of 15 degrees approximately 78 in. (1,981 mm) upstream from the splice between concrete beam nos. 5 and 6. The vehicle appeared to be captured by the barrier, but the simulation had unresolvable errors before the vehicle fully redirected. The vehicle trajectory is shown in Figure 65. After the single-unit truck was being redirected away from the system, the system started to restore to its original position but then deflected farther when the back of the cargo box contacted the rail. The cargo box floor support I-beams snagged on the steel rail base plates, which accentuated pitch and roll motions late in the impact event.

Moderate damage occurred to the front and left sides of the truck. The left-front tire slightly contacted the second, third, and fourth posts downstream from the splice between beam segments 5 and 6. The left-rear tire became airborne after the initial impact and only contacted the front face of the concrete beams. The left-front fender and the box contacted the upper tube assembly, which caused some slight permanent damage to the upper tube assembly. The rest of the system did not appear to have any permanent damage. The posts bent significantly backward during the impact event, and the concrete beams contacted the ground. The system did not restore as the simulation ended in error before the vehicle exited the system.

The system laterally deflected a maximum of 13.5 in. (342 mm) at the top upstream end of concrete beam no. 6. The top of concrete beam no. 6 also vertically deflected a maximum of 7.4 in. (188 mm) due to the cargo box leaning on the top of the barrier and the barrier rotating backward.

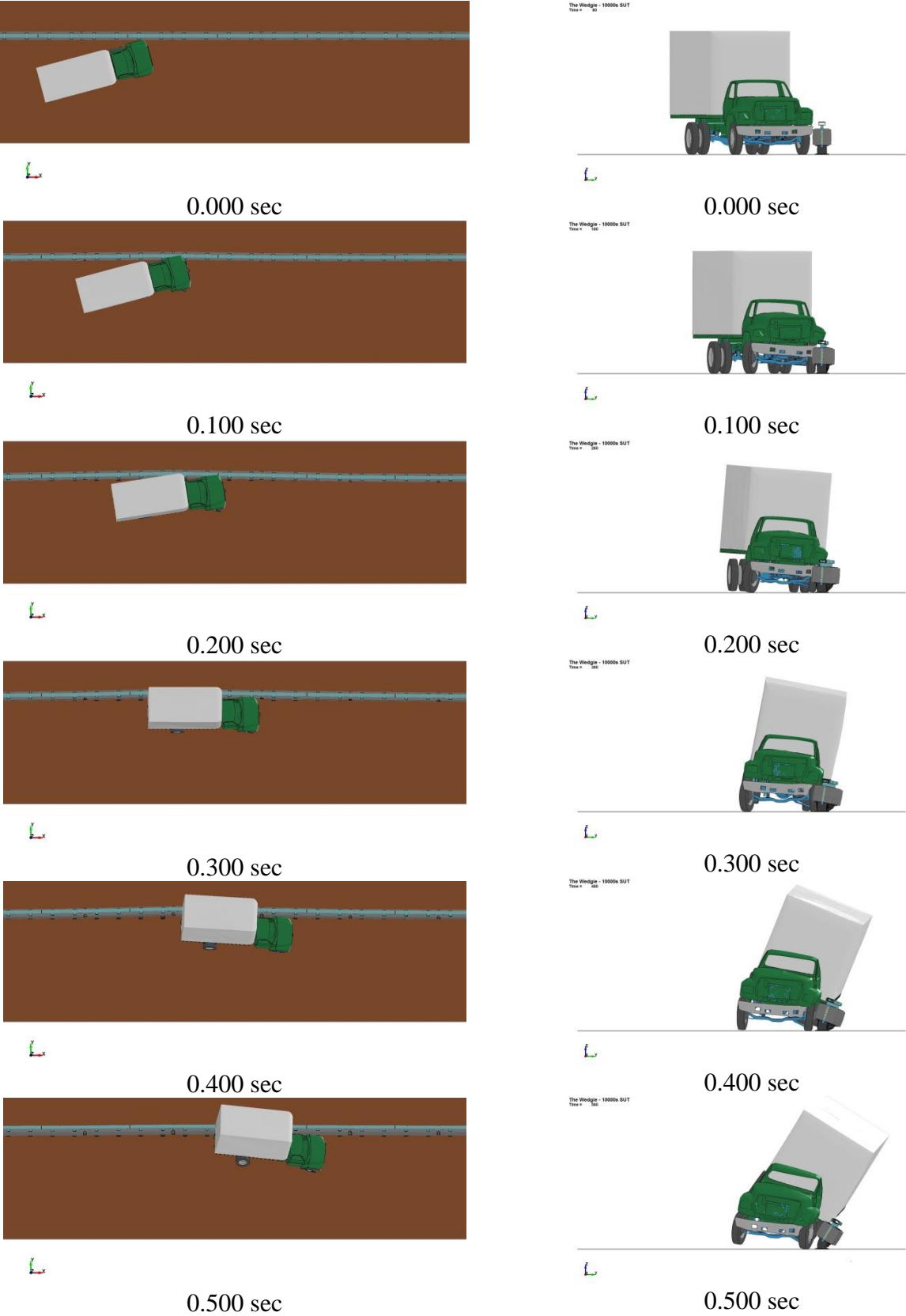


Figure 65. RESTORE Barrier Simulation with MASH Test Designation 4-12 (10000S) Impact

5.3 Simulation Summary

Overall, LS-DYNA computer simulation results indicated that RESTORE barrier has the potential to be a successful MASH TL-4 barrier that reduces the lateral acceleration imparted to passenger vehicle occupants. Passenger vehicle accelerations and occupant risk values were reduced for impacts into the RESTORE barrier as compared to similar impacts into rigid concrete barriers. However, the values were not reduced 30 percent, which was the desired design goal. The initial lateral peak acceleration and the lateral OIV values were reduced up to 17 and 20 percent, respectively, during the 1100C car simulation when compared to a similar impact into a New Jersey shaped concrete barrier. The initial lateral peak acceleration, the lateral OIV, and lateral ORA values were reduced up to 28, 26, and 12 percent, respectively, during the 2270P pickup truck simulation when compared to a similar impact into a single-slope concrete barrier. The initial baseline simulations into rigid concrete barriers provided similar accelerations as the full-scale crash tests, but there were notable differences in the peak values, especially during tailslap. Large accelerations occur during tailslap in the simulations, especially with the 2270P pickup truck model. The pickup truck rear-end model may be stiffer than the pickup trucks used during full-scale crash testing, so the simulation may be exaggerating the tailslap event.

The dynamic barrier deflections during the passenger vehicle impacts were in the desired range. However, the barrier rotation backward in the 2270P pickup truck and 10000S single-unit truck simulations was concerning. However, as noted previously, the restoring force of the rubber material had not been validated and damping was enabled in the material. If the barrier rotates excessively in full-scale crash tests and the barrier could not restore, then additional investigation may be needed.

The barrier also experienced over 7 in. (178 mm) of vertical deflection during the single-unit truck simulation. Much of this movement was caused by barrier rotation, but the box leaning on the rail also pushed the barrier lower. This loss in barrier height could lead to an unsuccessful test if the single-unit truck rolls over top of the barrier. This behavior will be explored through full-scale crash testing.

6 INSTALLATION AND STABILITY EVALUATION

The system shown in Figures 43 through 59 was fabricated and then installed at the MwRSF Outdoor Testing Facility. Since the RESTORE barrier is a completely new system, an installation procedure needed to be established. Initially, the threaded foundation rods were epoxied into the foundation, and then the posts were fastened to the ground. However, it was difficult to align all 16 post bolts with the 16 through-bolt holes in the concrete beams. This difficulty was partly due to variation in the post bolt hole locations in the concrete beams, and that it was difficult to slide the beam into the correct position on top of the rubber posts. Therefore, a new procedure was established for the test installation.

First, the posts were attached to a concrete beam with the through bolts and then set as a unit on the concrete tarmac. Then, the threaded foundation rods were epoxied to the ground, which secured the entire system to the ground. After two adjacent segments were anchored to the ground, the Adjustable Continuity Joint (ACJ) with splice bolts were installed to connect segments. The through bolts were then loosened, and the top steel tube and splices were installed. The process was repeated for the 240-ft (73-m) installation.

The ACJ was easy to install, and adjacent barrier segment joints were aligned to form a continuous barrier face. The gap between barrier segments was a nominal ½ in. (13 mm), but the actual installation joint gaps varied, as shown in Figure 66. Due to the ACJ's ability accommodate joint gaps between ¼ and ¾ in. (6 and 19 mm), these gaps were not an issue. The ACJ also accommodated small variations in gap width on the front and back faces at a joint.

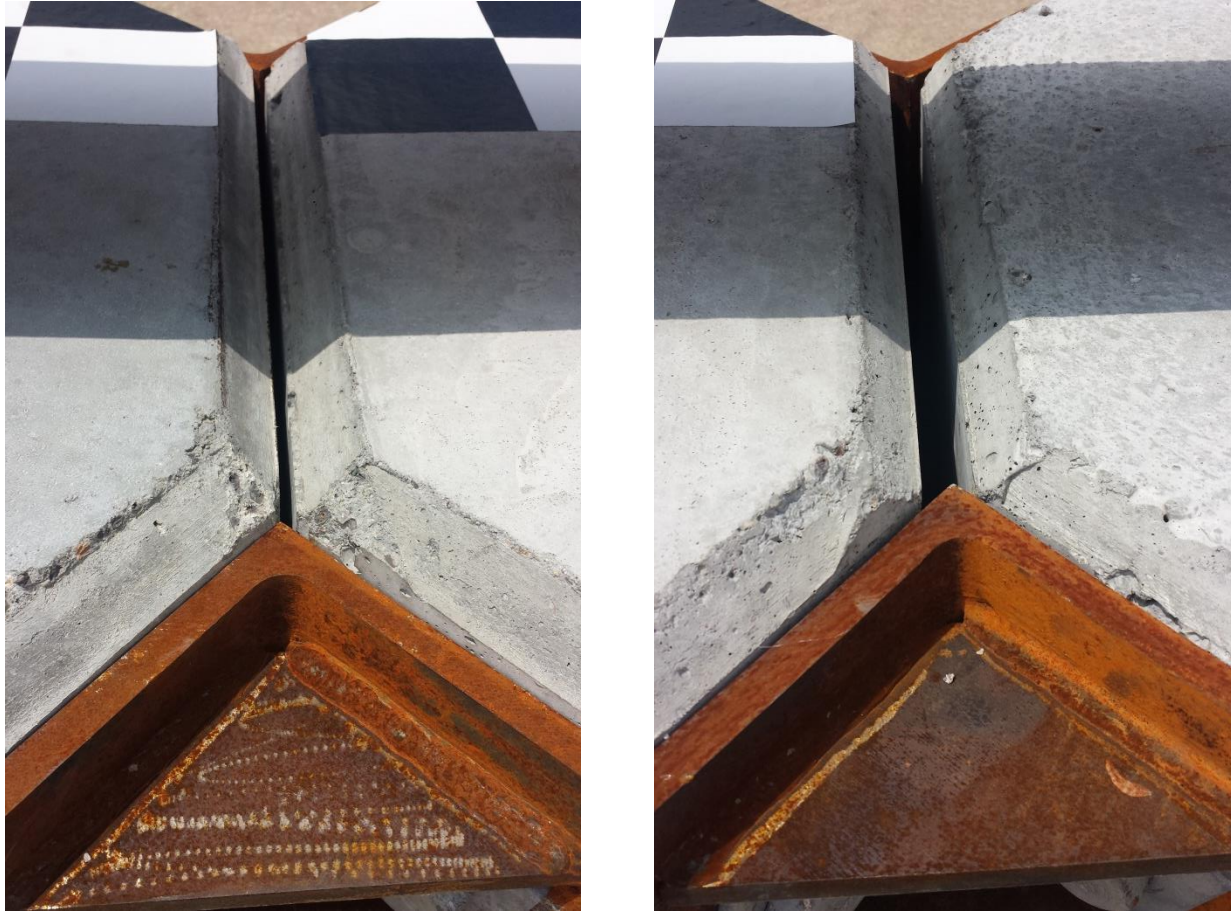


Figure 66. ACJ Variable Gap Width

During installation, the posts appeared unstable and wanted to bend toward one side with the presence of the dead load, so additional supports were utilized while the system was under construction. Once the system was constructed, the additional supports were removed, and the system tended to lean towards one side and posts would compress around the post hole on that side. Several possible reasons for this were discussed:

- 1) concrete tarmac foundation is slightly sloped;
- 2) variations in the post bolt holes in the concrete beam caused the posts to be loaded non-uniformly; and
- 3) posts cannot support the same weight that was observed in an indoor, controlled environment.

All of the possible reasons could occur in real-world installations, so adjustments were needed to increase the stability of the system. For the purpose of evaluating the stability of the system, one barrier segment (4 posts) was disconnected from the rest of the system and evaluated for stability under the static dead load and with lateral pull tests. Two solutions were considered:

- 1) inserting a steel pipe in the post hole to prevent one side from collapsing and
- 2) adding support skids to help support the weight of the system.

6.1 Additional Steel Pipe in Post

A 3½-in. (89-mm) diameter standard steel pipe with a 4-in. (102-mm) outer diameter and a 0.226-in. (5.7-mm) thickness was inserted into the 4-in. (102-mm) diameter hole in each of the four posts. The system was stable and remained upright, as shown in Figure 67. The posts with the steel pipe inserts were dynamically impacted in test nos. SF10P-1 and SF10P-2, as described previously. The steel pipe inserts did not affect the energy absorption of the posts.

A strap was placed around the concrete beam and pulled slowly. When only a single segment was pulled, the posts did not deform in shear but rather rotated backward. When pulled for approximately 6 in. (152 mm) and then released, the barrier restored to within 0.8 in. (20 mm) of its original position. The barrier was pulled for approximately 12 in. (305 mm) and then released, and the barrier restored to within 3.75 in. (95 mm) of its original position. When pulled for approximately 18 in. (457 mm) and then released, the lower corner of the concrete barrier nearly contacted the ground, and the barrier did not restore, as shown in Figure 68. After the steel pipes were removed from the posts, the barrier could not stand upright due to deformation that occurred from the overloading in the pull tests. The pull tests on the posts with the additional steel pipe in the holes resulted in a barrier system that did not fully restore, so alternative support systems were examined.



Figure 67. Barrier Stability with Steel Pipe Inserts



Figure 68. Barrier Deflection with Steel Pipe Inserts

6.2 Development and Installation of Steel Skids

A support skid was designed to provide stability and prevent concrete beams from excessive rotation but still allow the barrier system to deflect and freely restore. Two versions of the skid were designed, as shown in Figure 69. The upper structure of the support skid was a round steel tube with a 6.5-in. (165-mm) outer diameter that fit snugly into the lower portion of 6⁵/₈-in. (168-mm) diameter vertical holes in the concrete beams. Version 1 of the skids did not support any weight of the beams and only provided resistance to rotation. When two Version 1 skids were placed under one barrier segment, the system was stable. However, the beam still leaned slightly to one side as the skids tilted with the beam. The beam was removed from the posts, and the posts had some slight permanent set from the extreme overloading in the prior pull tests which did not allow the barrier to remain completely upright.

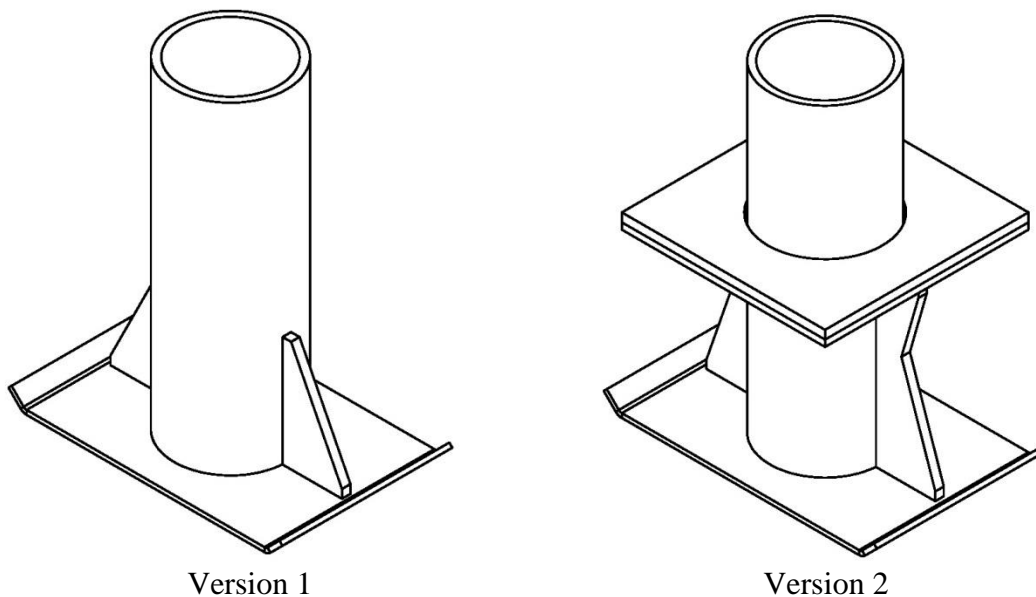


Figure 69. Steel Support Skids

A top steel plate was welded 10⁵/₈ in. (270 mm) above the ground in Version 2 of the skids. Then, steel shims were added on top of the steel plate, until the gap between the bottom of

the concrete beams and the top skid plate was closed. The weight of the rail was taken off of the rubber posts, and the Version 2 skids supported most of the weight of the rail. Since the site terrain was not completely level, a $\frac{3}{8}$ -in. (9.5-mm) shim was installed for one skid and a $\frac{3}{4}$ -in. (19-mm) shim was installed for the second skid. The resulting barrier segment was completely stable and did not lean, as shown in Figure 70. The beam was pulled from the opposite side as the previous pull tests to prevent further permanent set from occurring. The segment was pulled for approximately 18 in. (457 mm), as shown in Figure 71, and then released. The barrier restored completely and no deformation occurred to the skids.

The steel plate shims were removed, and the barrier was stable and not leaning. The permanent set that had been noted previously was no longer present, and it was believed to be eliminated by overloading the posts from the opposite direction. The top skid plate was not supporting any weight of the beam as the heights to the bottom of the beam varied from 11 $\frac{1}{8}$ in. (283 mm) to 11 $\frac{1}{4}$ in. (286 mm). Thus, with only the posts supporting the beam, the system had a vertical deflection of $\frac{3}{8}$ to $\frac{1}{2}$ in. (9.5 to 12.7 mm) at approximately 70 degrees F (21 degrees C). The system also remained completely upright with only the rubber posts supporting the weight of the rail. However, the barrier did begin to lean after several hours. The steel shims were once again inserted in the gap between the bottom of the concrete beams and the top skid plate, and the system continued to remain completely upright and stable. In lieu of having varying thickness steel shims to stabilize the system on varying terrain, thick rubber sheet shims would allow adjustability more easily without multiple parts. Implementing the skids into the barrier system increased the stability and was further pursued.



Figure 70. Barrier Stability with Two Support Skids with Shims



Figure 71. Maximum Barrier Deflection with Two Support Skids with Shims

6.3 Simulations with Skids

Impacts with all three vehicles were simulated on the RESTORE barrier with skids. Simulations with both one and two skids were conducted to determine if the skids changed the barrier performance when impacted.

The skid and part numbers are shown in Figure 72, and a summary of the parts, elements, and materials are shown in Table 11. Since the model was created on level ground and the parts had no real-world variability, shims were not modeled. The skid parts were all connected with merged nodes. The skid top plate was tied to the bottom of each beam rather than modeling the cylinder extending into the holes in the concrete beam. The coefficient of friction between the skids and the ground was 0.30.

In simulations with all three vehicles, barrier variations with one support skid and two support skids under each concrete beam performed very similarly. In both cases, the rotation of the barrier system that occurred previously was almost entirely mitigated.

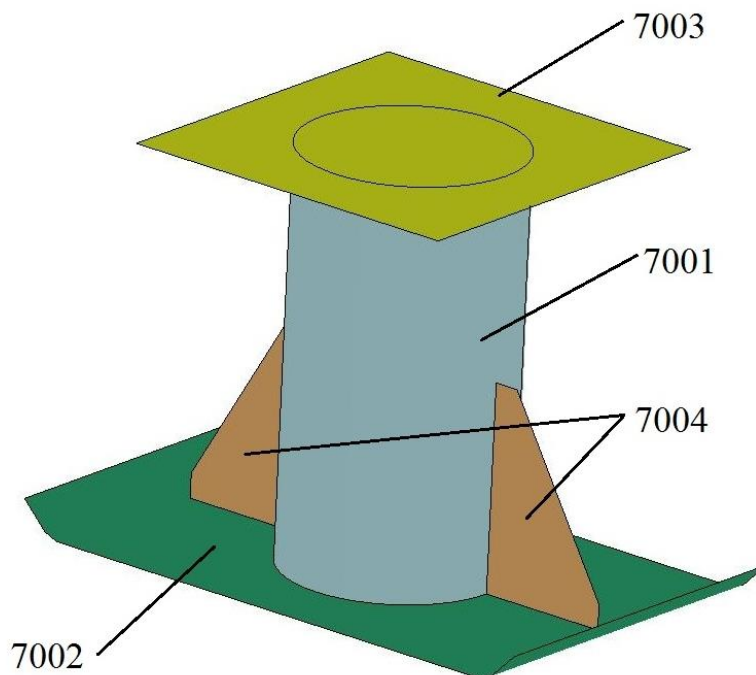


Figure 72. Skid Model

Table 11. Skid Model Parts, Elements, and Materials

Part Description	Simulation Part No.	Element Type	Material
Skid Cylinder	7001	Type 2 Shell	*MAT_PIECEWISE_LINEAR_PLASTICITY
Skid Baseplate	7002	Type 2 Shell	*MAT_PIECEWISE_LINEAR_PLASTICITY
Skid Top Plate	7003	Type 2 Shell	*MAT_PIECEWISE_LINEAR_PLASTICITY
Skid Gussets	7004	Type 2 Shell	*MAT_PIECEWISE_LINEAR_PLASTICITY

The vehicle trajectories and angular motions for both the small car and pickup truck were nearly identical when impacting the systems with and without skids, as shown in Figures 73 and 74, respectively. The barrier performance when subjected small car impacts was very similar to the system without skids, only the dynamic deflections as measured at the top upstream end of beam no. 6 decreased slightly, as shown in Figure 75. The barrier performance under pickup truck impacts was significantly different, as the skids limited the roll motion of the barrier that occurred without skids. This finding was evident when comparing the dynamic deflection measured at the top upstream end of beam no. 6, as shown in Figure 75. The lateral deflection of the barrier with no skids continued to increase after impact with the 2270P pickup truck, whereas the lateral deflection of the barrier with skids returned to zero after impact with the 2270P vehicle. This feature would hopefully allow the barrier to easily restore to its original position.

Other parameters (i.e., parallel time and exit time, velocity, and angle) that give an indication of the RESTORE barrier performance were compared to those obtained under impacts with rigid barriers. A comparison of these parameters is shown in Table 12 for the 1100C small car impacts and Table 13 for the 2270P pickup truck impacts. The parameters were calculated the same as those used during previous simulations, and overall, the results did not change much between prior RESTORE barrier simulations. The simulation with skids had longer exit times and slightly lower exit velocities and angles.

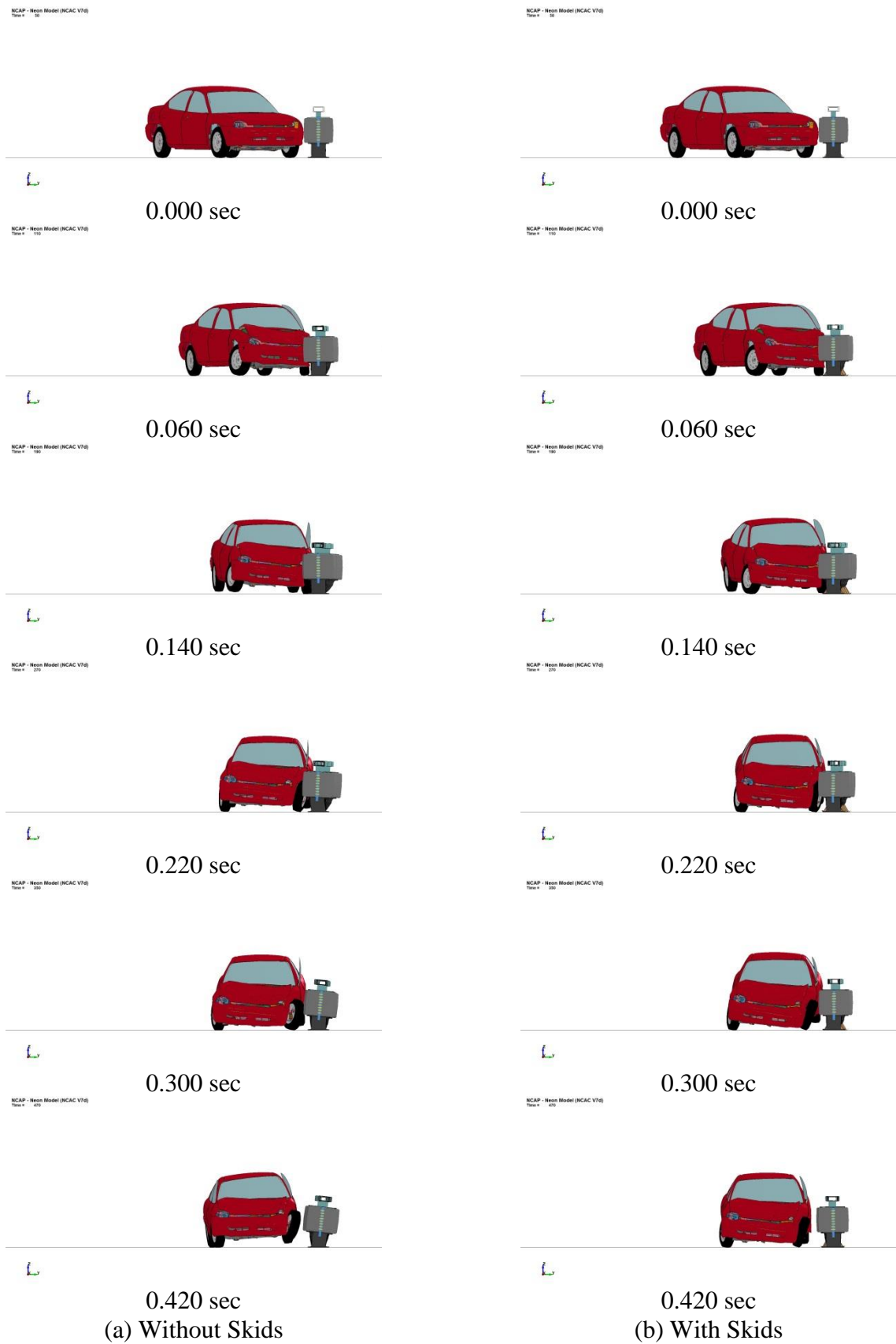


Figure 73. RESTORE Barrier Simulation with Test Designation 4-10 Impacts

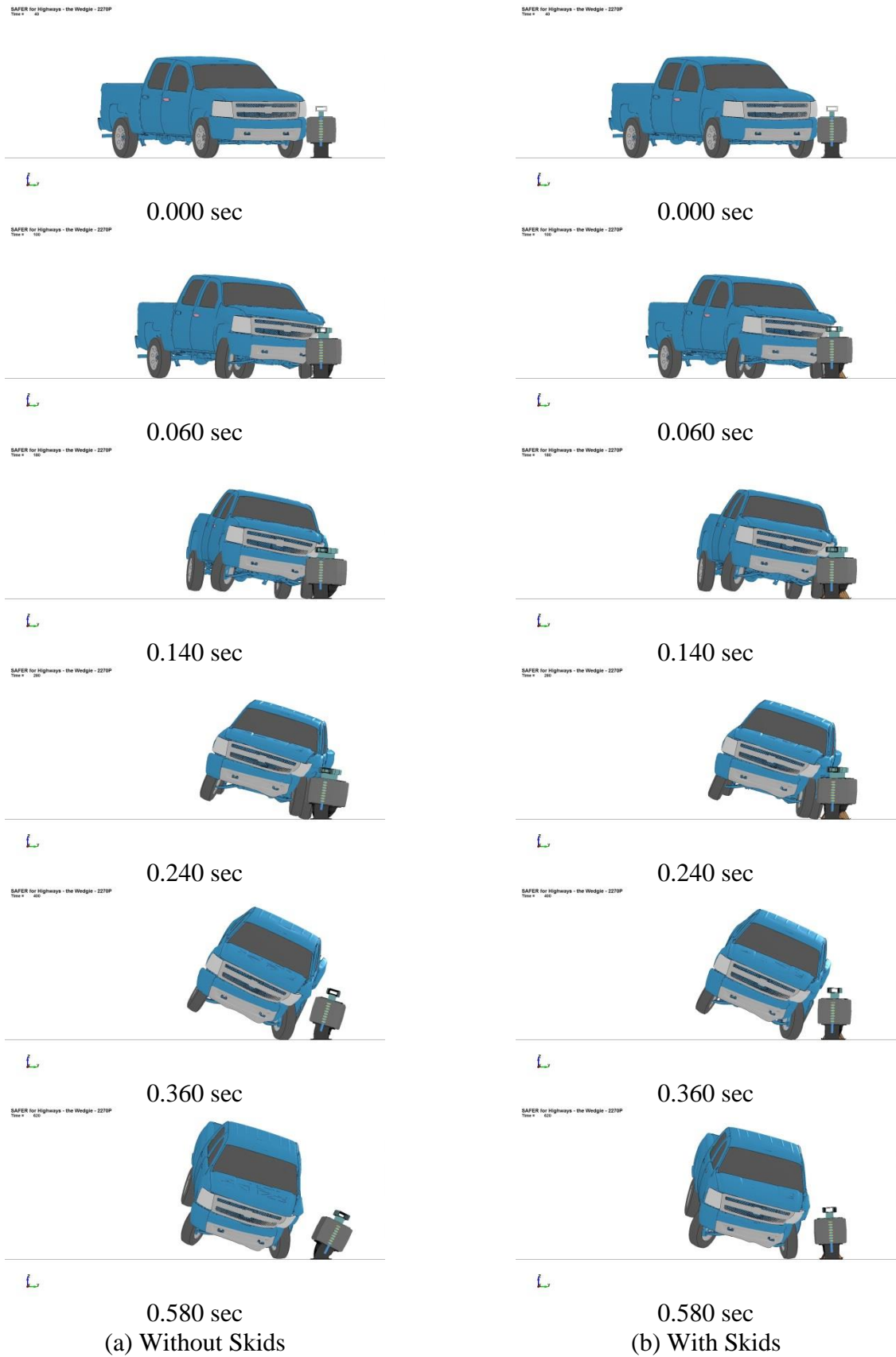


Figure 74. RESTORE Barrier Simulation with Test Designation 4-11 Impacts

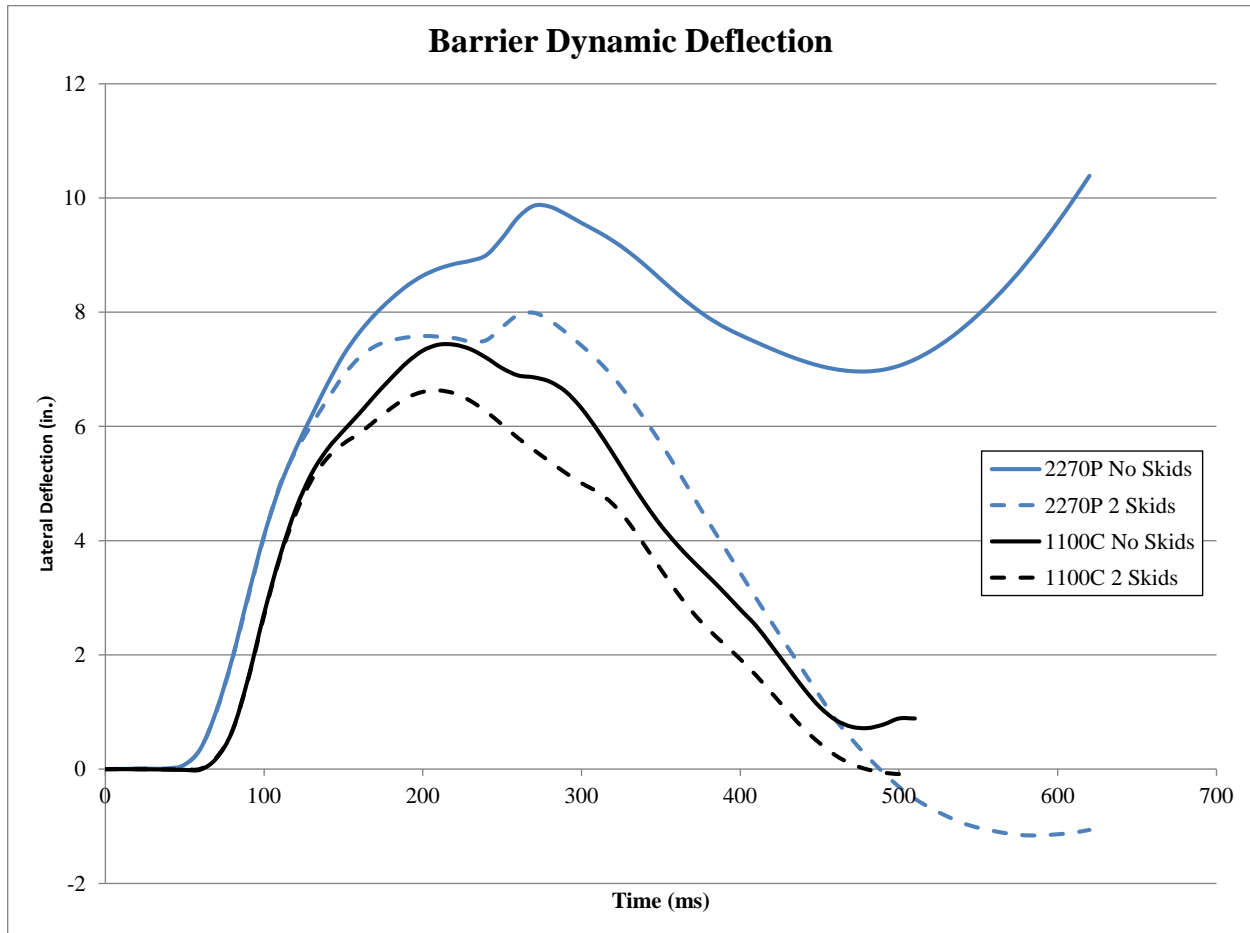


Figure 75. Dynamic Barrier Deflection with and without Skids

Table 12. Simulation Parallel and Exit Conditions – MASH Test Designation 4-10

Simulation Parameter	New Jersey Baseline Simulation	RESTORE Barrier Simulation No Skids	RESTORE Barrier Simulation Two Skids
Parallel Time ms	170	190	210
Exit Time ms	260	290	320
Exit Velocity Mph (km/h)	20.8 (33.5)	17.8 (28.6)	17.2 (27.7)
Exit Angle deg	5.3	2.7	1.5

Table 13. Simulation Parallel and Exit Conditions – MASH Test Designation 4-11

Simulation Parameter	Single Slope Baseline Simulation	RESTORE Barrier Simulation No Skids	RESTORE Barrier Simulation Two Skids
Parallel Time ms	160	190	190
Exit Time ms	260	300	320
Exit Velocity Mph (km/h)	23.1 (37.2)	22.9 (36.9)	22.6 (36.4)
Exit Angle deg	5.9	1.9	1.5

The 10000S vehicle had a very similar trajectory and angular motions in the simulations of the barrier system with and without skids, as shown in Figure 76. In the simulation with skids, the tire interacted with the rubber posts much more than in the simulation without skids. This rubber-rubber contact led to model instabilities. The front axle has disengaged in previous full-scale crash tests [14-15], so the tire trajectory is subjective, as front axle failure was not enabled in the model.

The barrier performance is slightly different between the two simulations, but the barrier still has a significant roll motion, which could lead to the barrier not restoring or to potential vehicle rollover. Since there are many parts of the model that have yet to be validated, it is hard to make predictive conclusions as to the performance of the vehicle and barrier. While it is still somewhat subjective if the 10000S impact into the RESTORE barrier will perform acceptably according to MASH TL-4 safety performance criteria, the skids do not appear to be detrimental to the barrier system. Throughout the duration of the project, several simulation issues occurred and are discussed in Appendix C.

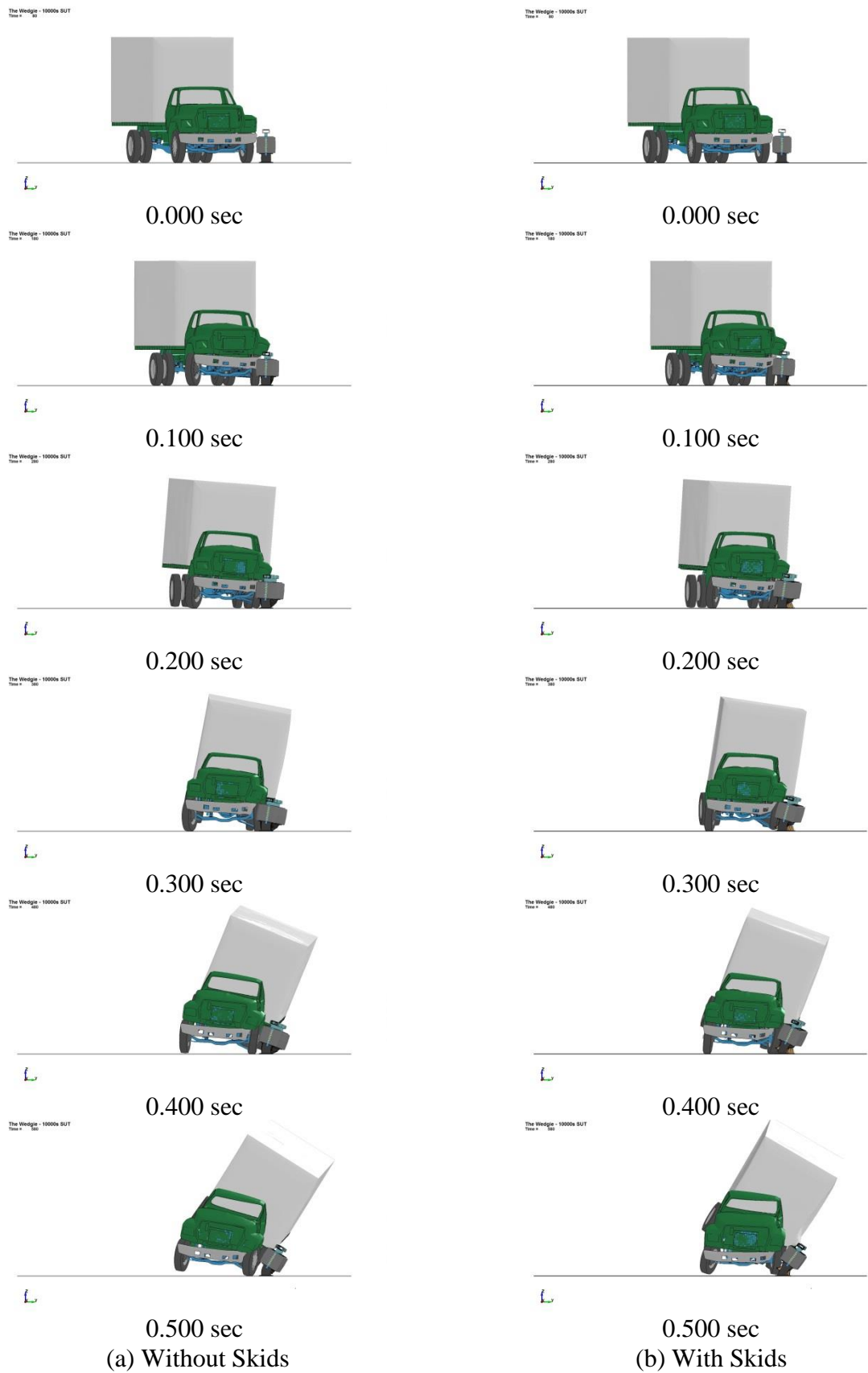


Figure 76. RESTORE Barrier Simulation with Test Designation 4-12 Impacts

7 SUMMARY, CONCLUSIONS, AND RECOMMENDATIONS

Further design and evaluation were conducted on an energy-absorbing, restorable and reusable roadside/median barrier, now designated as the RESTORE barrier, which was previously developed by Schmidt, et al. [1]. A series of dynamic component tests were conducted on 11 $\frac{5}{8}$ -in. (295-mm) tall x 10-in. (254-mm) wide x 15 $\frac{3}{4}$ -in. (400-mm) long rubber posts to characterize their energy-absorption properties. Similar rubber posts measuring 16 in. (406 mm) tall x 14 in. (356 mm) wide x 22 in. (559 mm) long were previously tested [2] and absorbed 1.5 to 1.9 times as much energy as the 11 $\frac{5}{8}$ -in. (295-mm) tall posts. However, the 11 $\frac{5}{8}$ -in. (295-mm) tall posts were desired to reduce the potential for vehicles snagging on the posts by lowering the bottom rail height. To ensure the system would absorb approximately the same amount of energy as the 16-in. (406-mm) tall posts spaced at 10 ft (3.0 m), the post spacing was decreased to 5-ft (1.5-m) increments.

To enhance system stability with the 11 $\frac{5}{8}$ -in. (295-mm) tall rubber posts supporting the static dead weight of the rail, the rail cross section was optimized to weigh under 320 lb/ft (476 kg/m) [2]. This modification was achieved with an 18 $\frac{1}{2}$ -in. (470-mm) tall x 21 $\frac{1}{2}$ -in. (546-mm) wide x 20-ft (6.1-m) long precast lightweight concrete beam with an 8-in. (203-mm) wide x 4-in. (102-mm) tall steel tube mounted on top, for a total height of approximately 38 $\frac{1}{2}$ in. (978 mm) above ground.

Several splices were evaluated to add continuity to adjacent concrete beam segments, including:

- 1) top and bottom splice plates;
- 2) splice tubes at the center of the top and bottom beam faces;
- 3) cross-bolted connection that was originally developed at TTI; and

- 4) the Adjustable Continuity Joint (ACJ), which is an adjustable steel angle on the front and back faces.

Each joint was evaluated using LS-DYNA computer simulation. The cross-bolted connection and the ACJ provided the most continuity and desired barrier deflections during 2270P vehicle impacts. However, the ACJ hardware was easier to implement with the concrete beam internal reinforcement and could accommodate better construction tolerance than the cross-bolted connection. Thus, the ACJ was selected for further evaluation.

A 240-ft (73-m) barrier model was created, and the barrier performance was evaluated with TL-4 impacts with the 1100C, 2270P, and 10000S vehicle models. The 1100C and 2270P vehicle models were successfully captured and redirected. The occupant impact velocity and occupant ridedown acceleration values for the 1100C small car impact were up to 20 percent lower than those observed in simulated impacts into a rigid concrete barrier. Similarly, 2270P pickup truck impacts into the RESTORE barrier resulted in up to 28 percent reductions to the peak lateral acceleration and occupant risk values compared against simulated rigid barrier impacts. The 10000S single-unit truck impact appeared to be captured by the barrier, but the simulation ended before the vehicle fully redirected. The barrier rolled backward during the impact, and it is unknown if the barrier would have restored to its original position.

During the full-scale installation of the system, some system stability concerns arose as the system leaned towards one side. The lateral stability of the system under the static dead load and with lateral pull tests was further evaluated when two solutions were considered:

- 1) inserting a steel pipe in the post hole to prevent one side from collapsing and
- 2) adding support skids to help support the weight of the system.

Adding two support skids under each concrete beam significantly improved the stability of the system. The skids were added to the 240-ft (73-m) LS-DYNA barrier model, and the barrier

performance was evaluated with all three TL-4 impacts. The skids did not negatively affect the performance for any of the impacts. The skids significantly decreased the rotation of the barrier during impacts with the passenger vehicles, so the skids appeared to be an improvement to the system.

Having a rigid support plate at the top of the skid was impractical, as site terrain could vary between all the skids. Thus, the skid design was changed so that the top skid plate was welded at 11 in. (279 mm) above ground, and then a ½-in. (13-mm) thick EPDM rubber pad was placed on top of the top skid plate. This combination allows the beam to compress the rubber pad as needed to adjust for non-level terrain as well as provide some height tolerance.

Details of the final longitudinal barrier hereby recommended for full-scale crash testing according to MASH TL-4 safety performance criteria are shown in Figures 77 through 99.

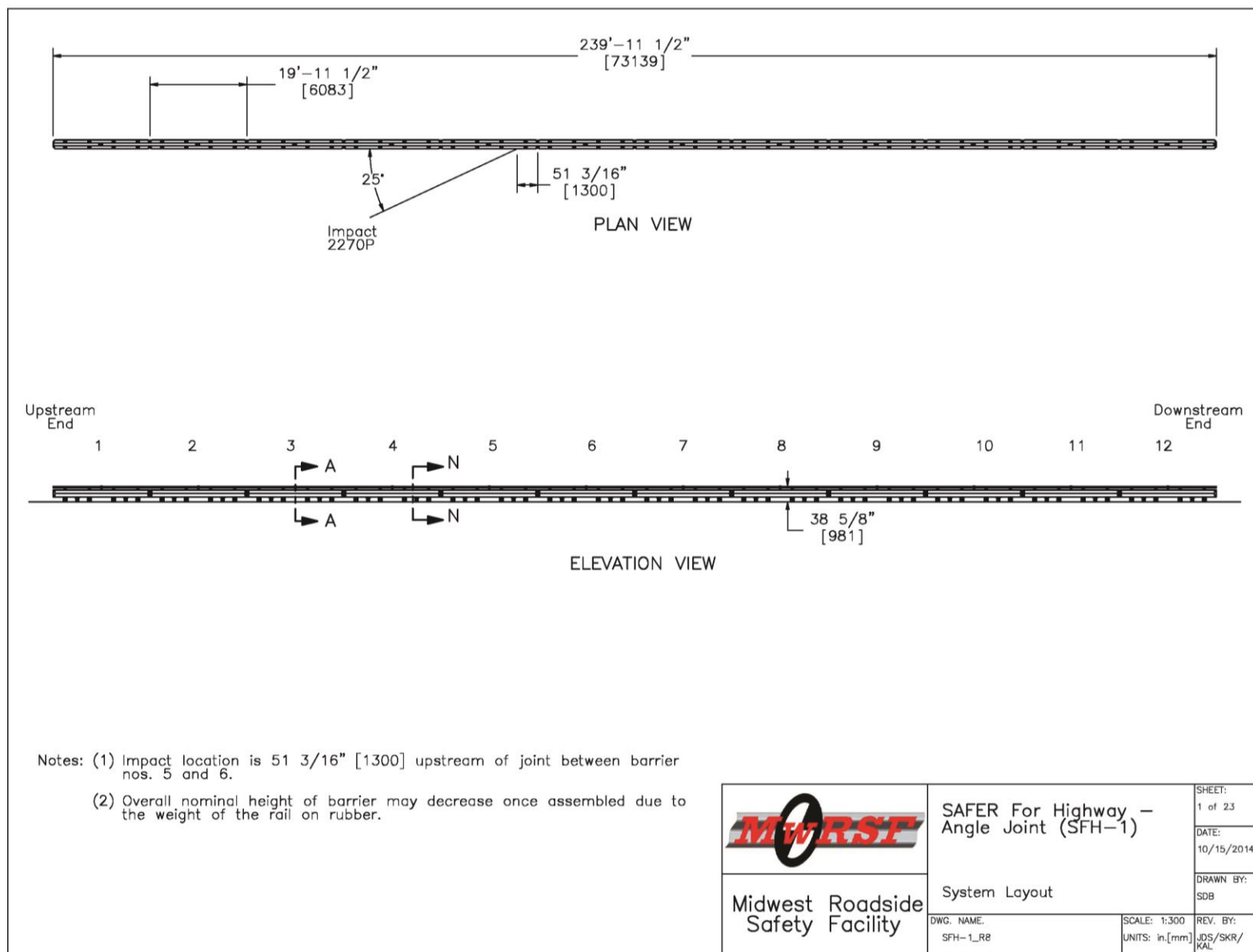


Figure 77. Recommended Barrier Design for Full-Scale Crash Testing, System Layout

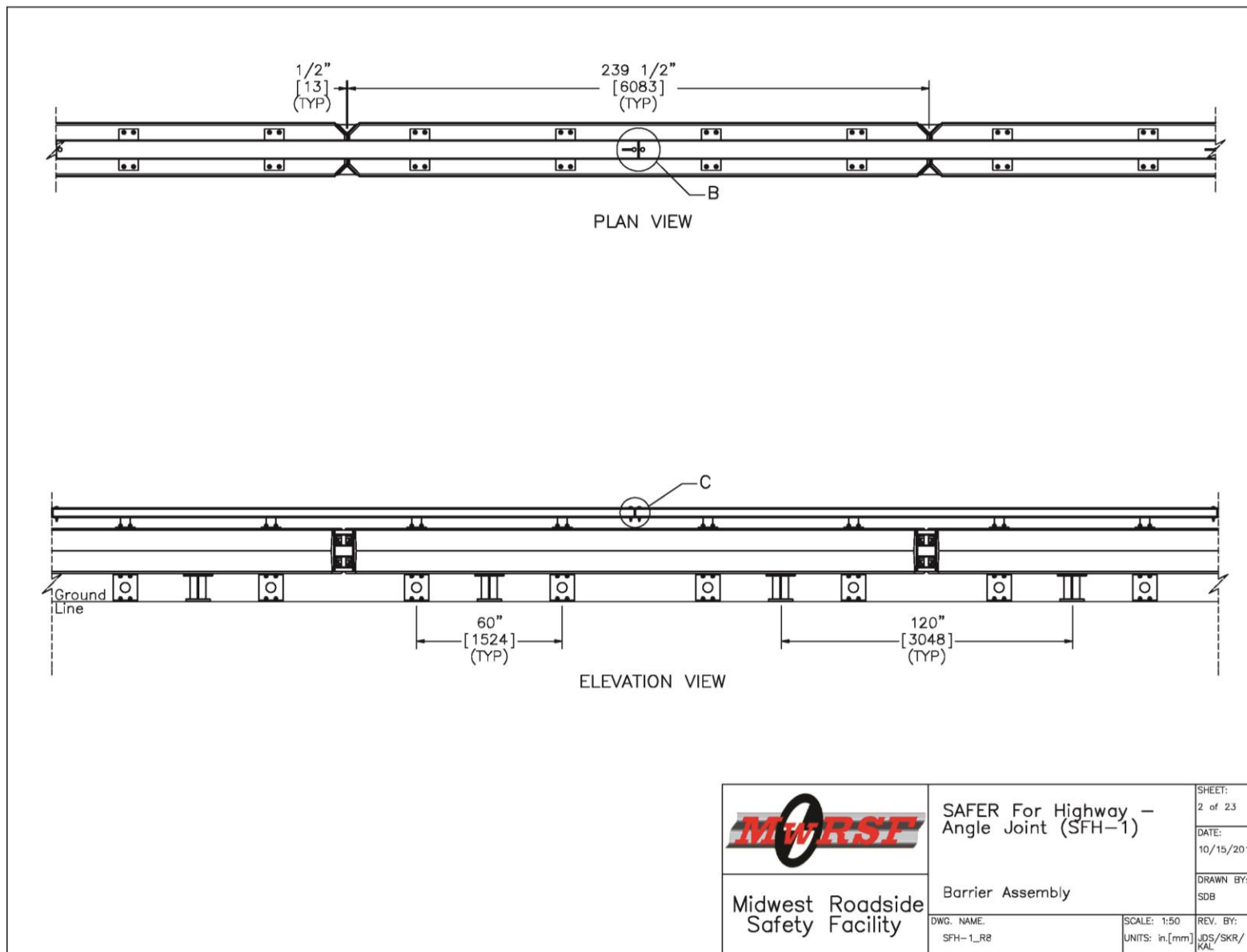


Figure 78. Recommended Barrier Design for Full-Scale Crash Testing, Barrier Assembly

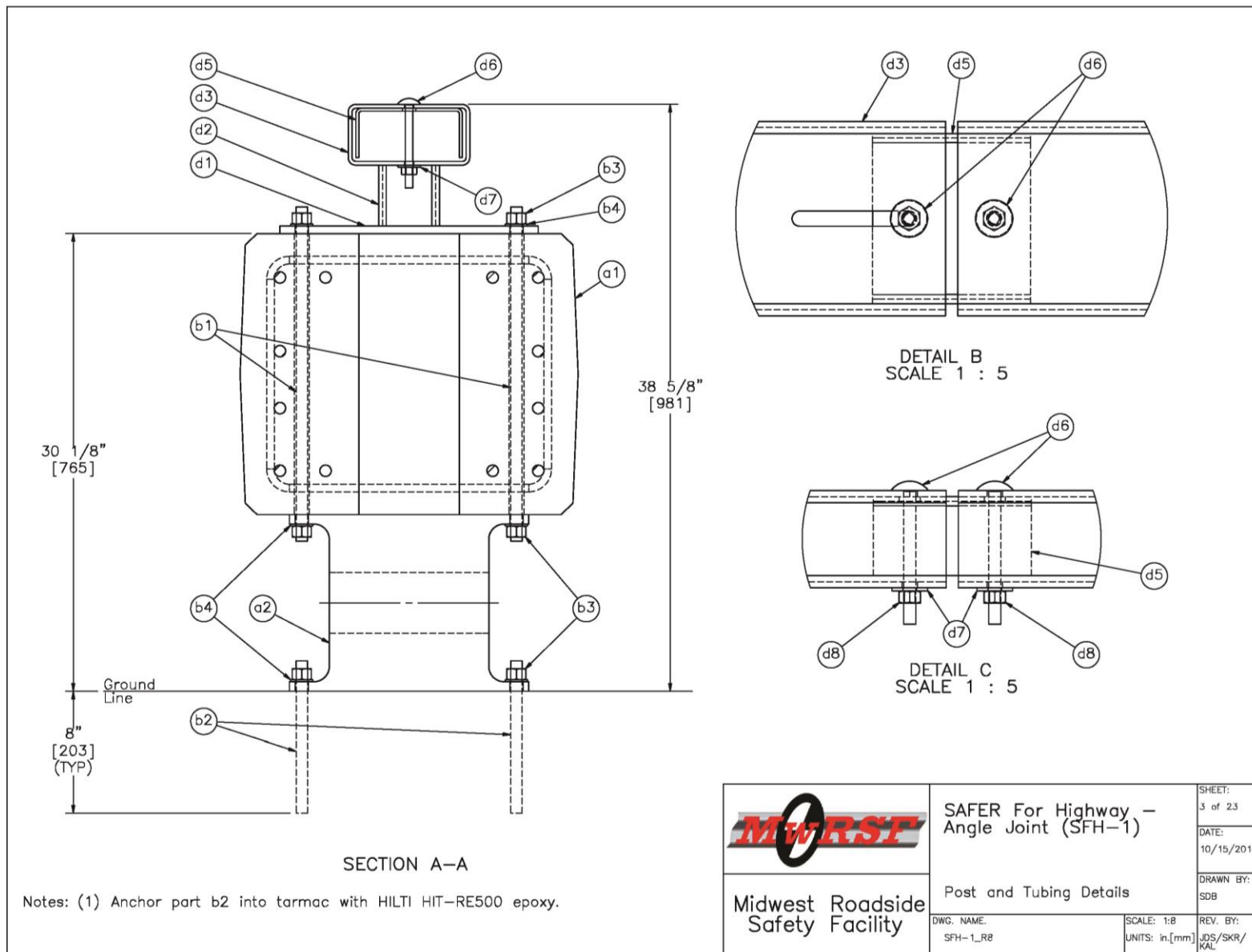


Figure 79. Recommended Barrier Design for Full-Scale Crash Testing, Post and Tubing Details

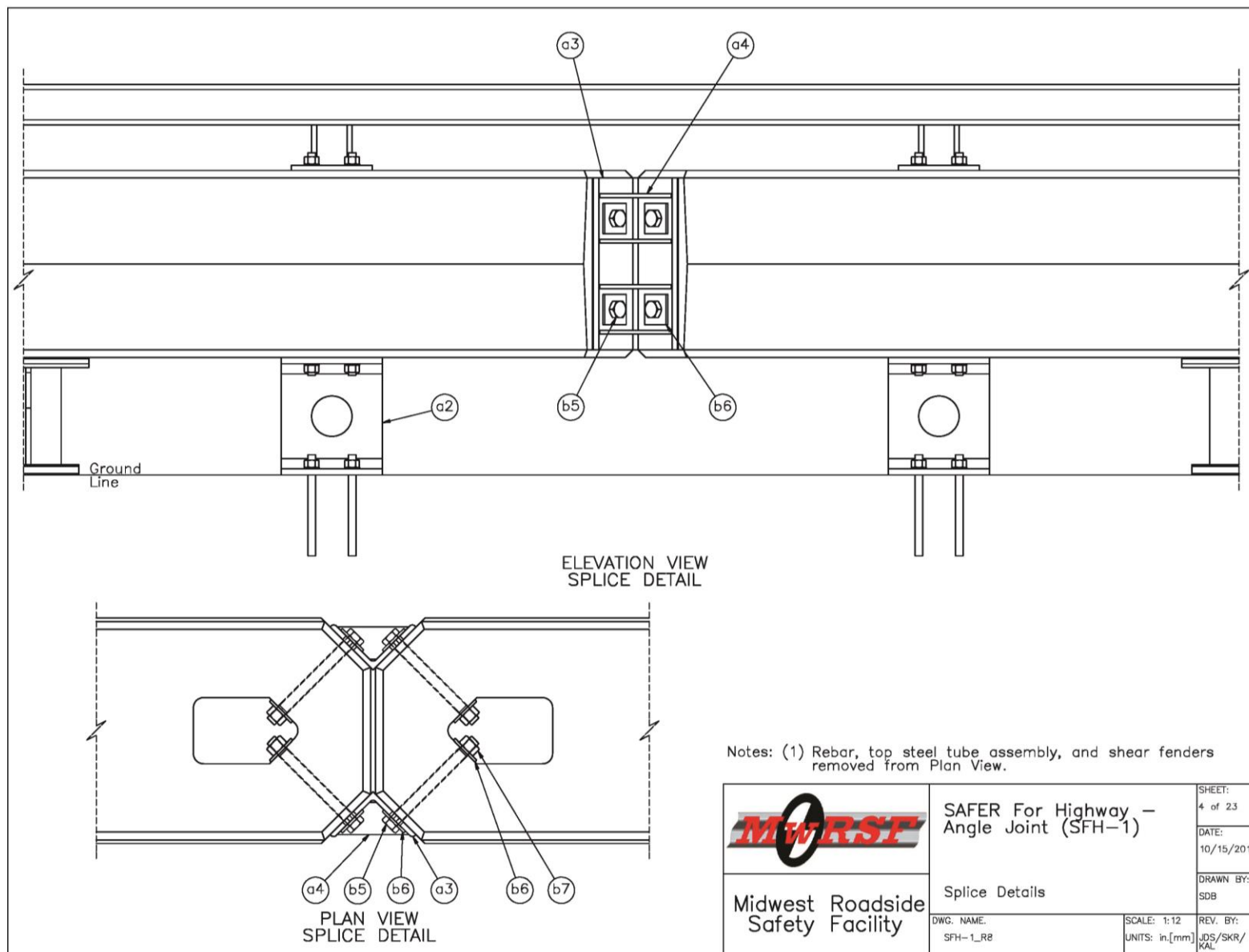


Figure 80. Recommended Barrier Design for Full-Scale Crash Testing, Splice Details

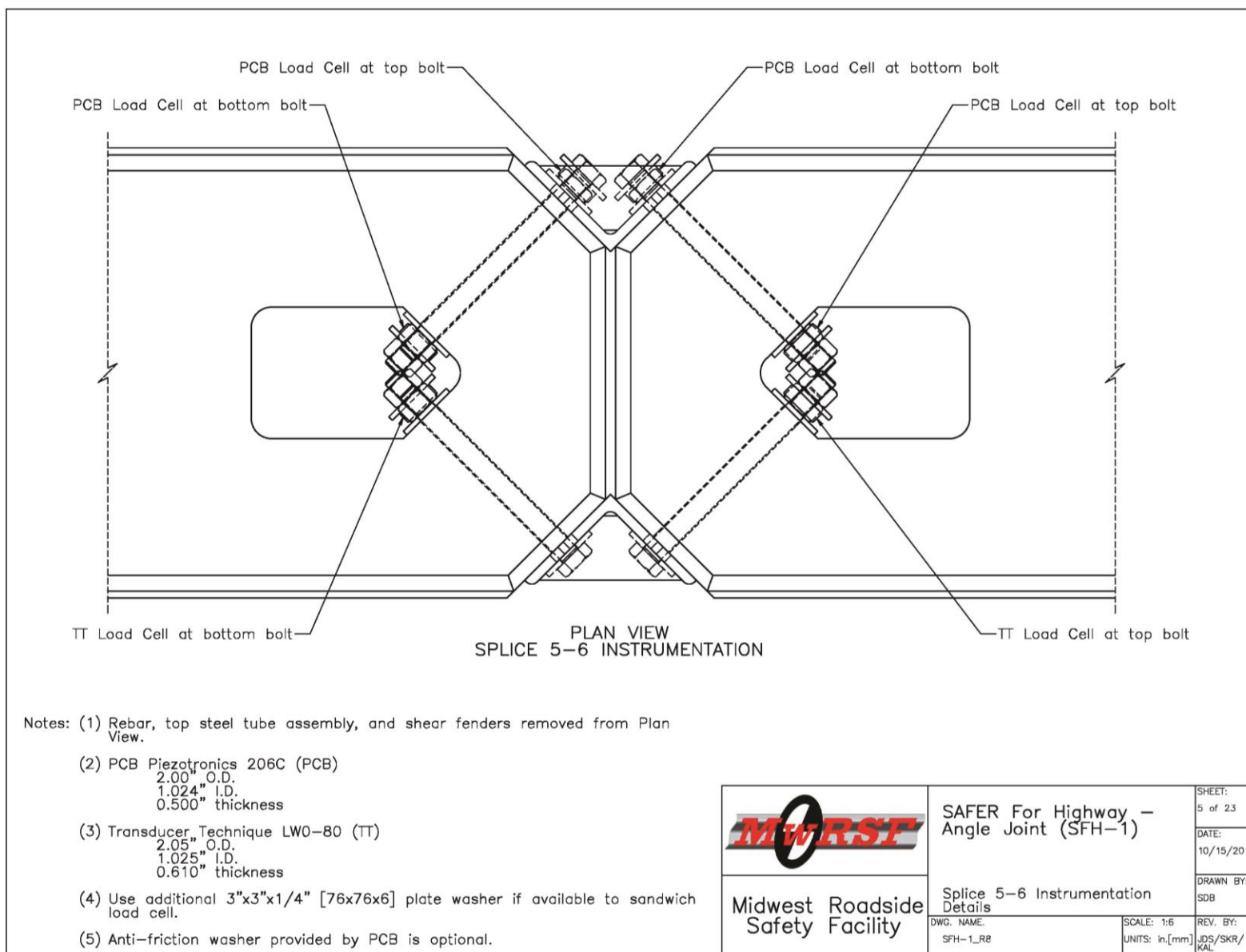


Figure 81. Recommended Barrier Design for Full-Scale Crash Testing, Instrumentation

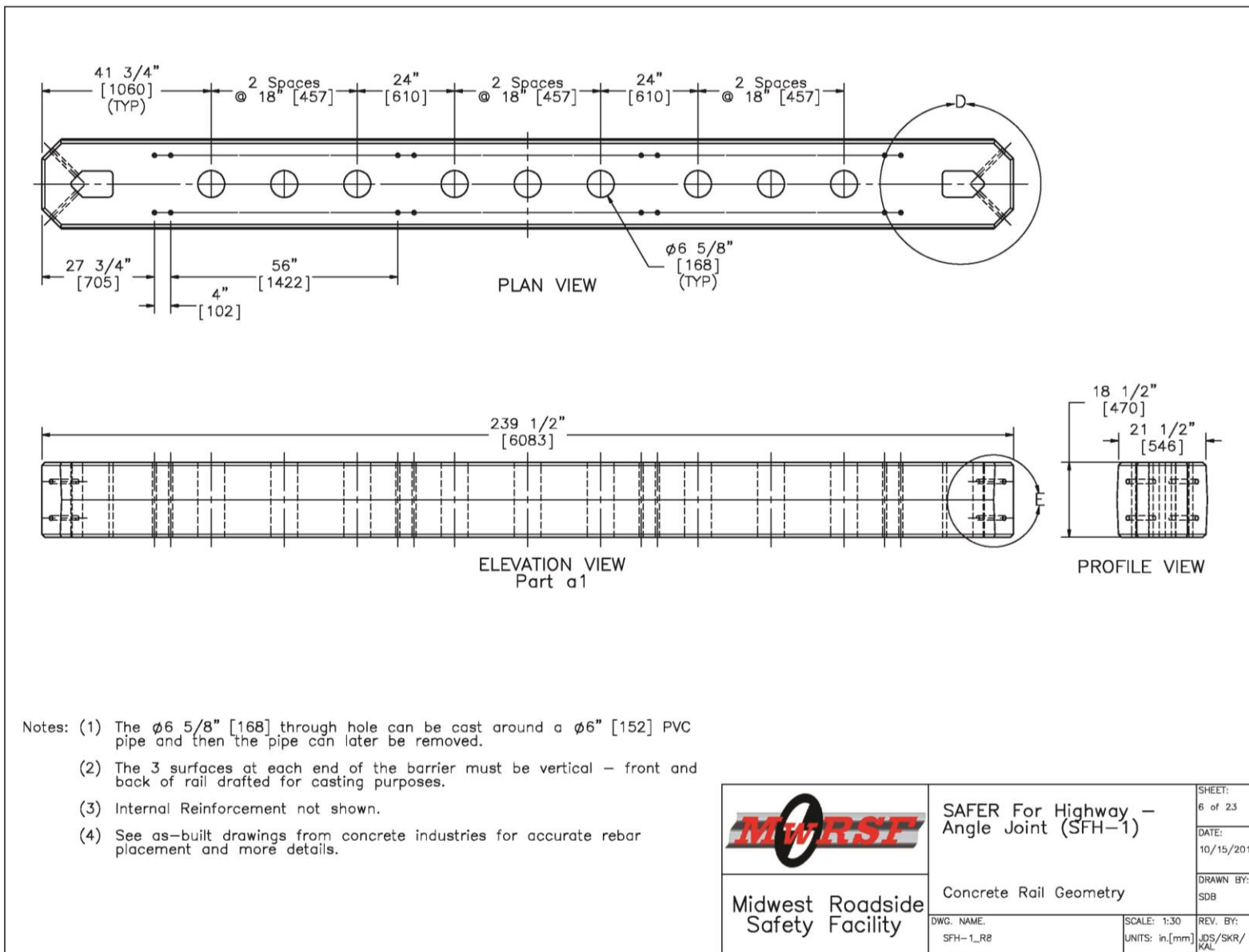


Figure 82. Recommended Barrier Design for Full-Scale Crash Testing, Concrete Rail Geometry

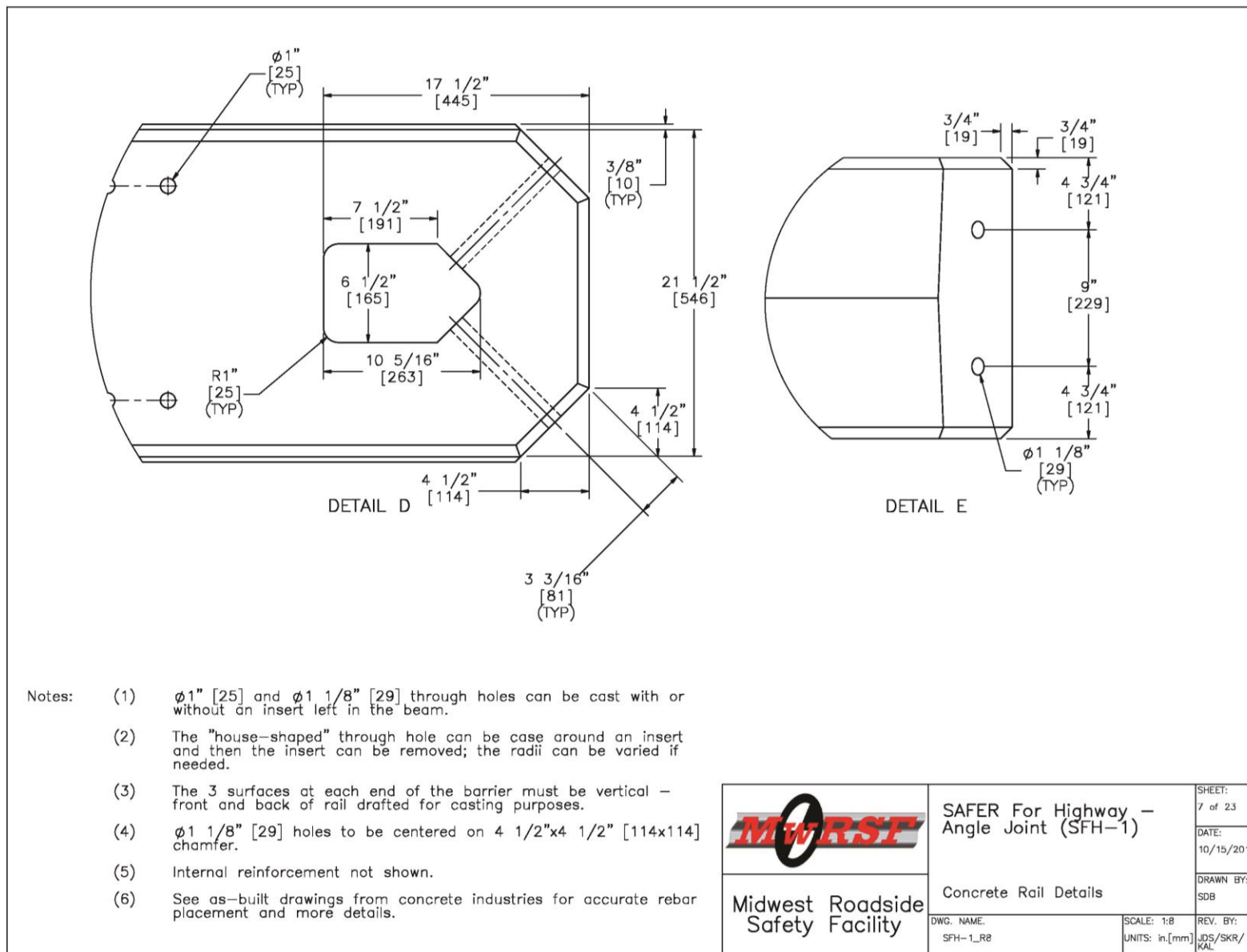


Figure 83. Recommended Barrier Design for Full-Scale Crash Testing, Concrete Rail Details

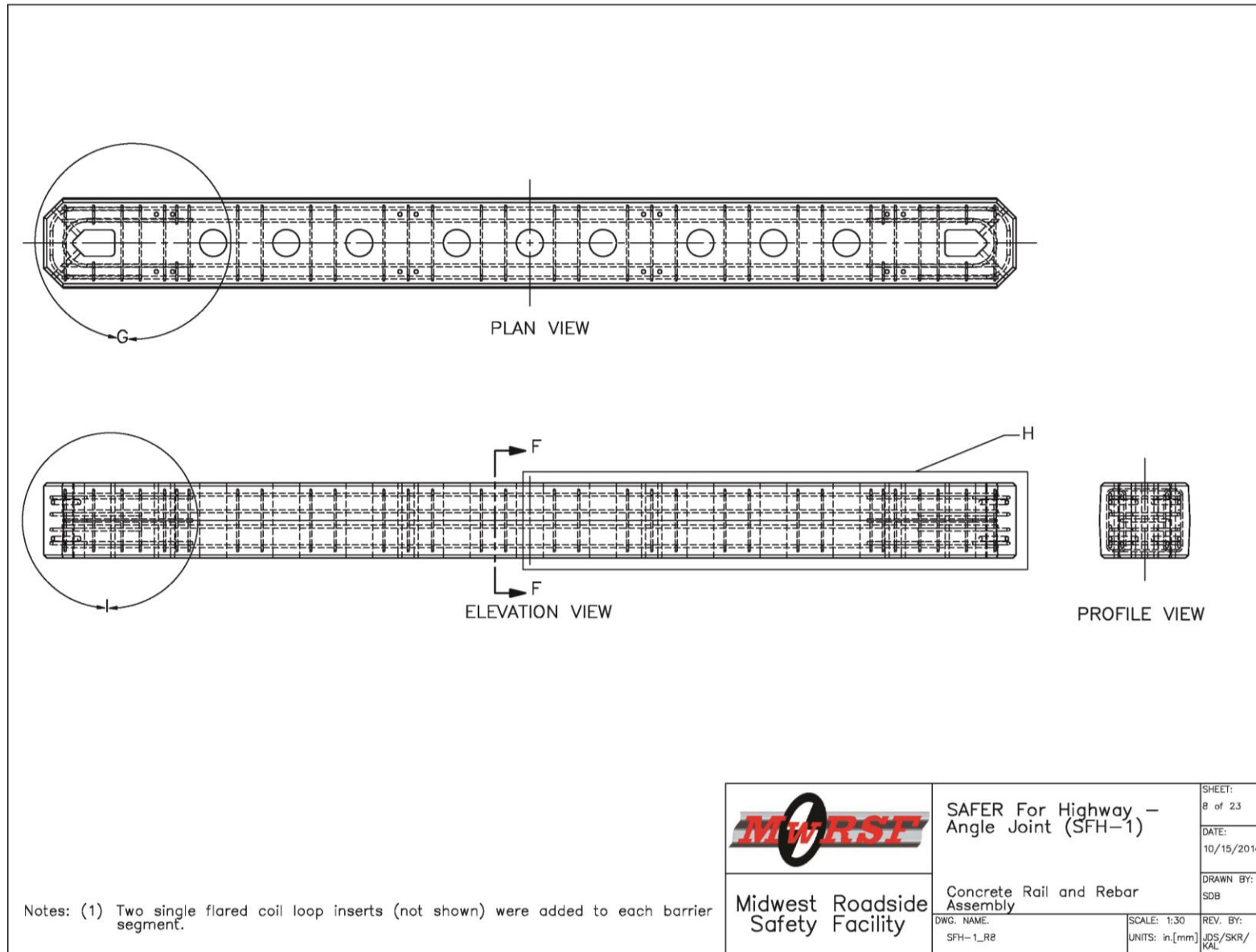


Figure 84. Recommended Barrier Design for Full-Scale Crash Testing, Concrete Rail Details

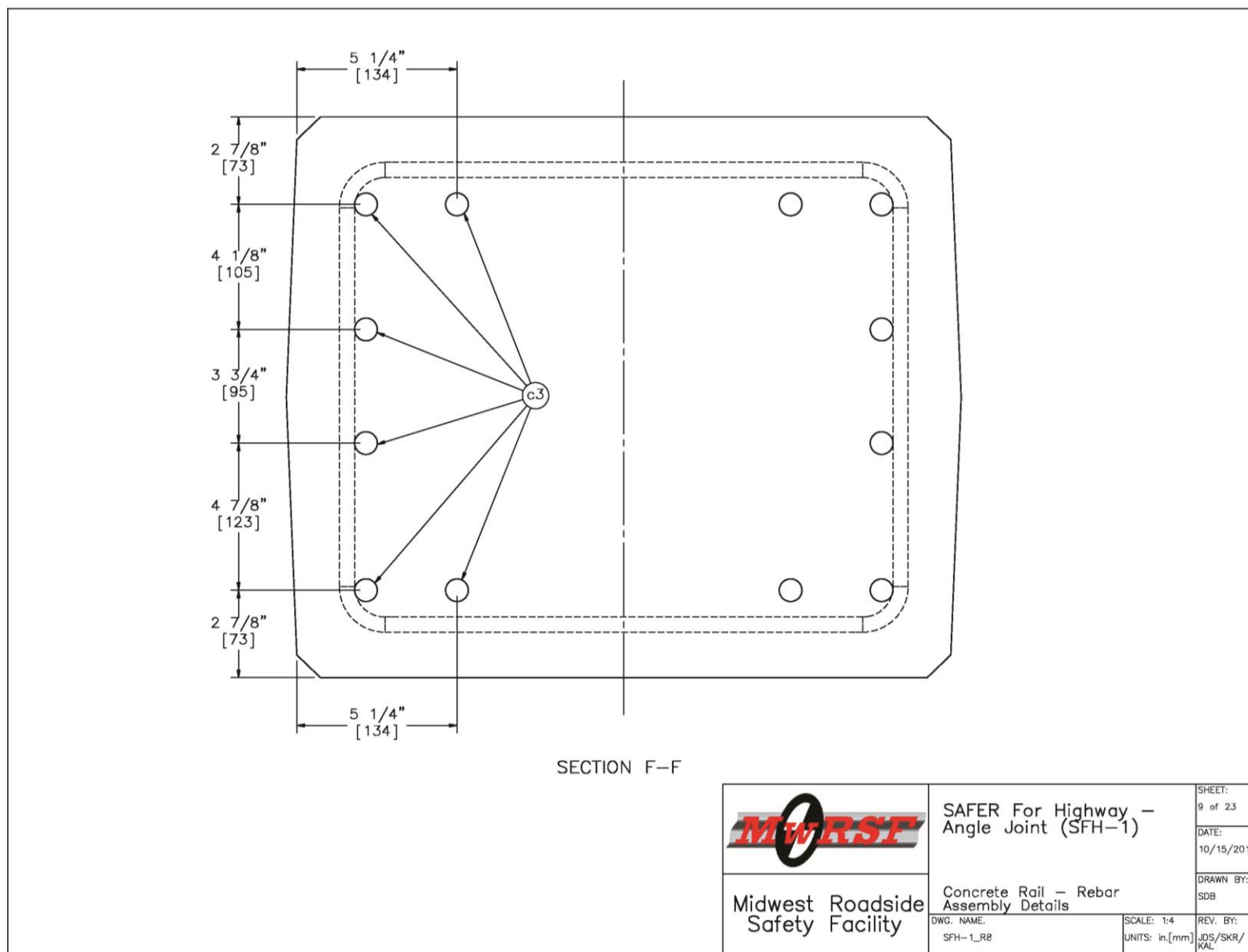


Figure 85. Recommended Barrier Design for Full-Scale Crash Testing, Concrete Rail Details

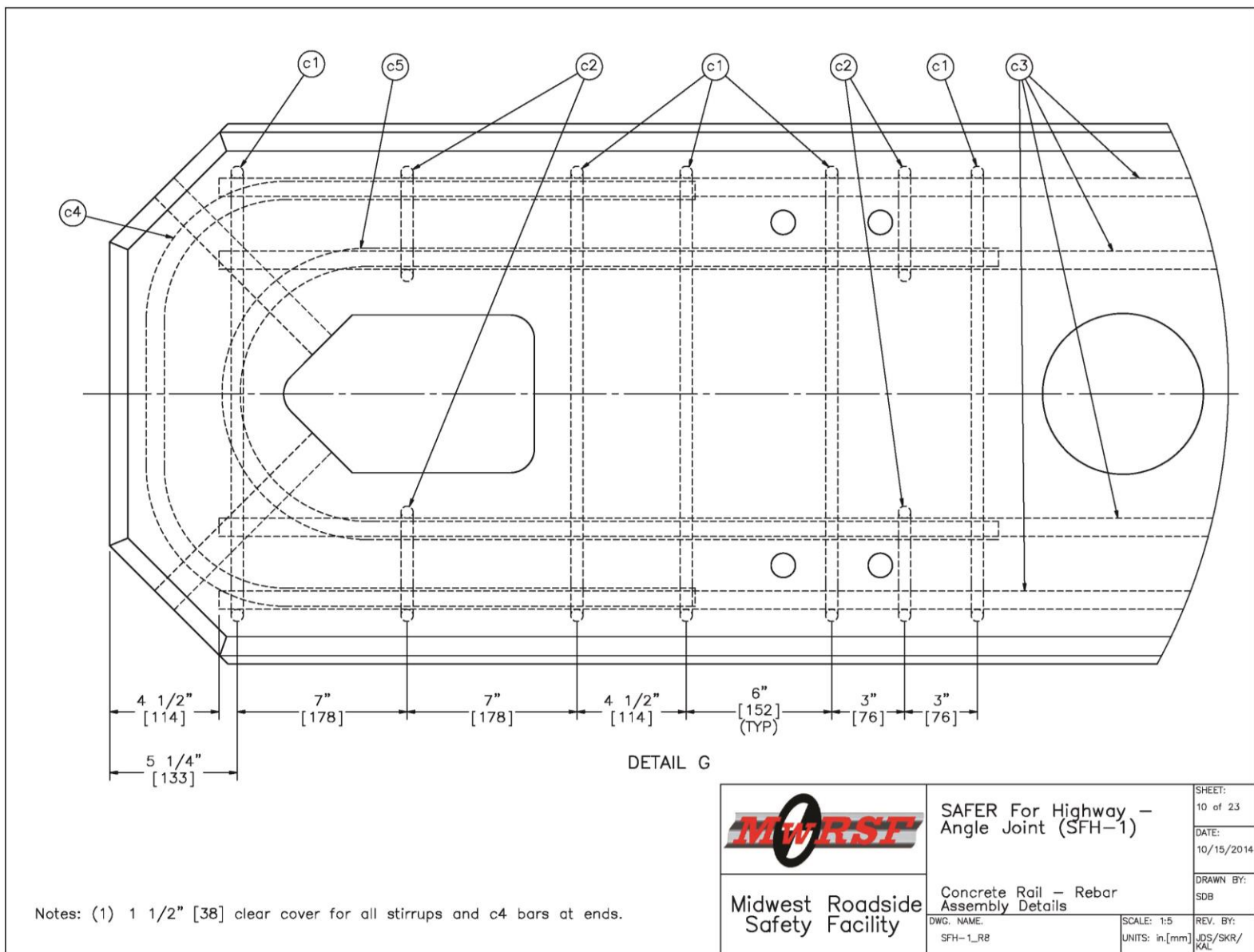


Figure 86. Recommended Barrier Design for Full-Scale Crash Testing, Concrete Rail Details

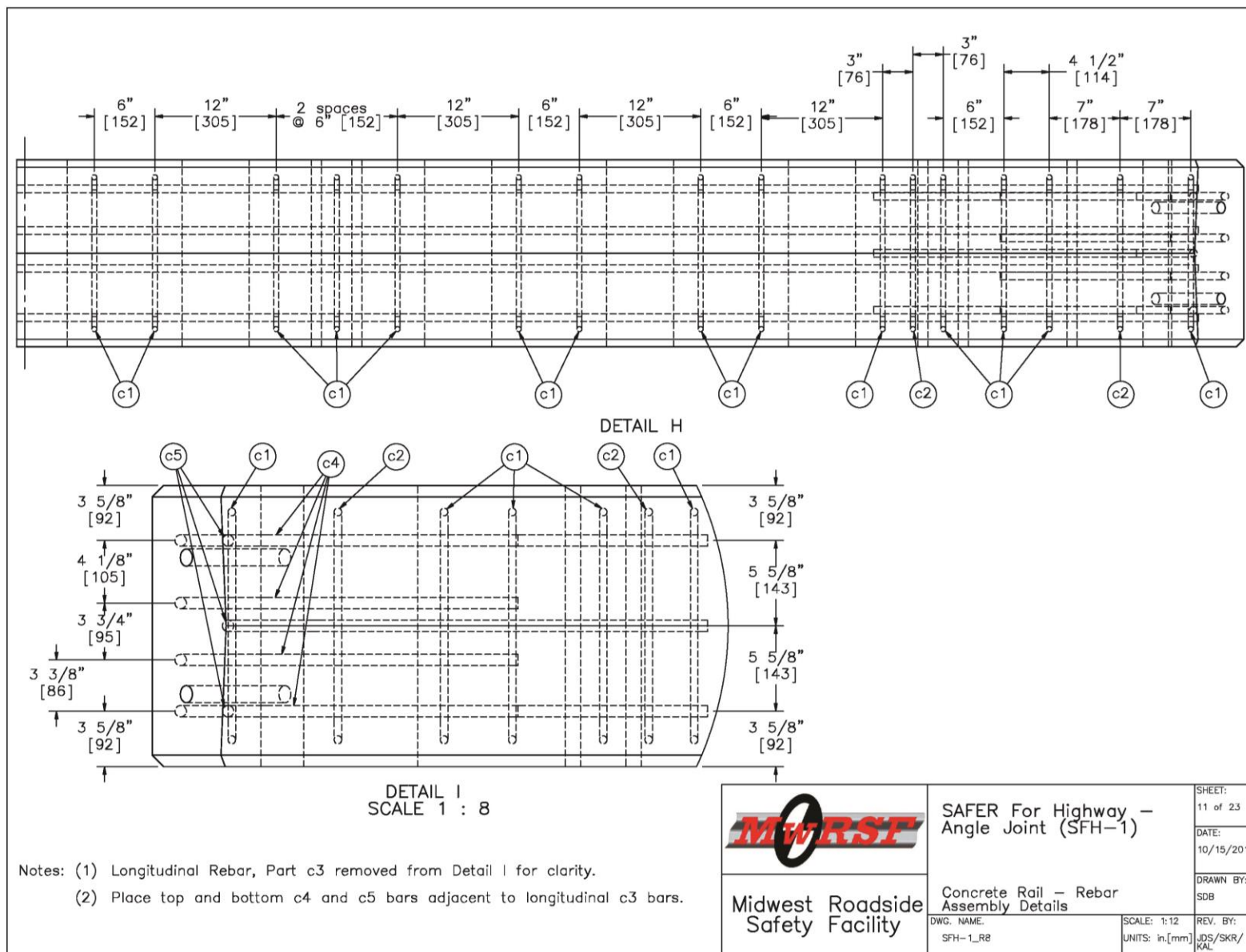


Figure 87. Recommended Barrier Design for Full-Scale Crash Testing, Concrete Rail Details

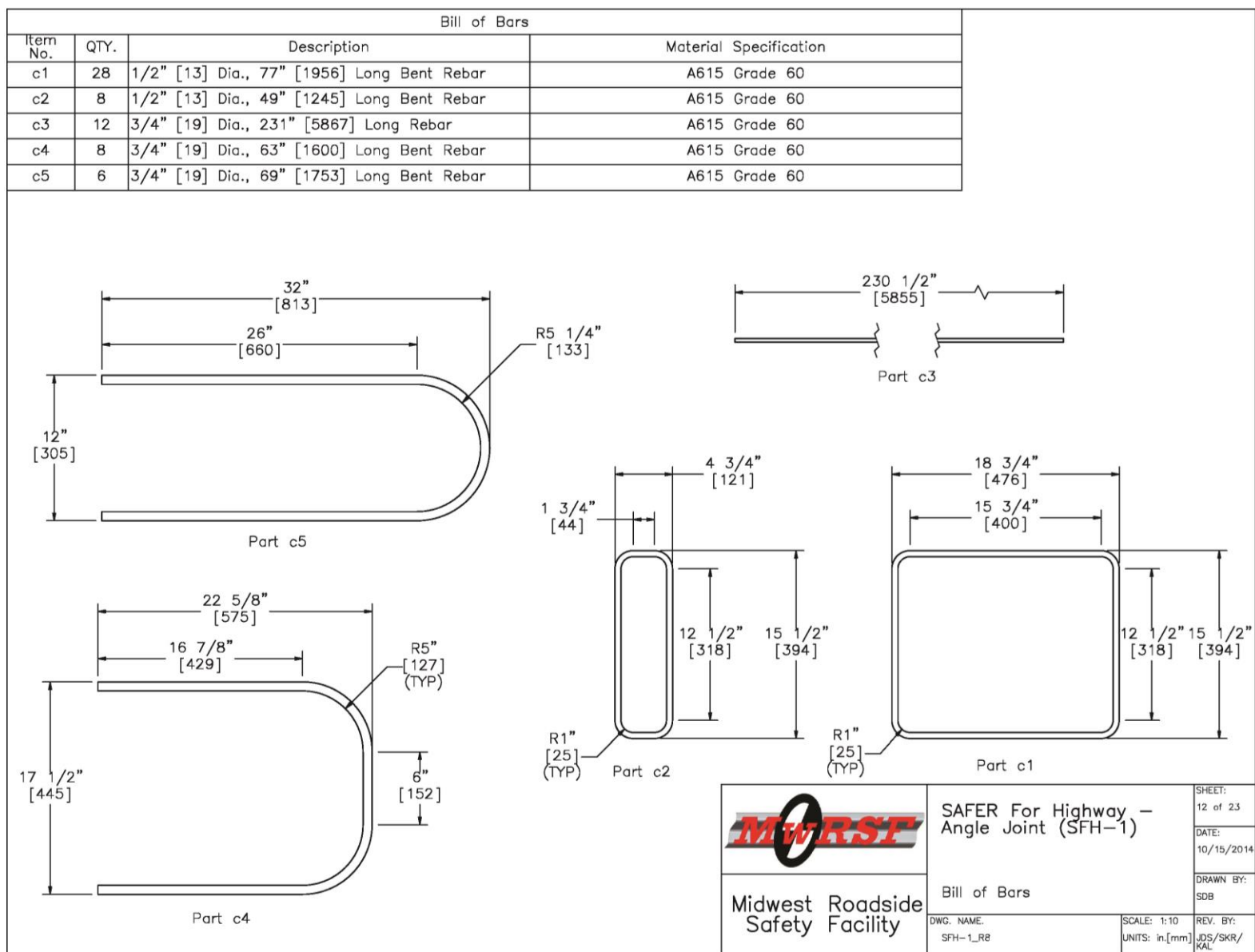


Figure 88. Recommended Barrier Design for Full-Scale Crash Testing, Bill of Bars

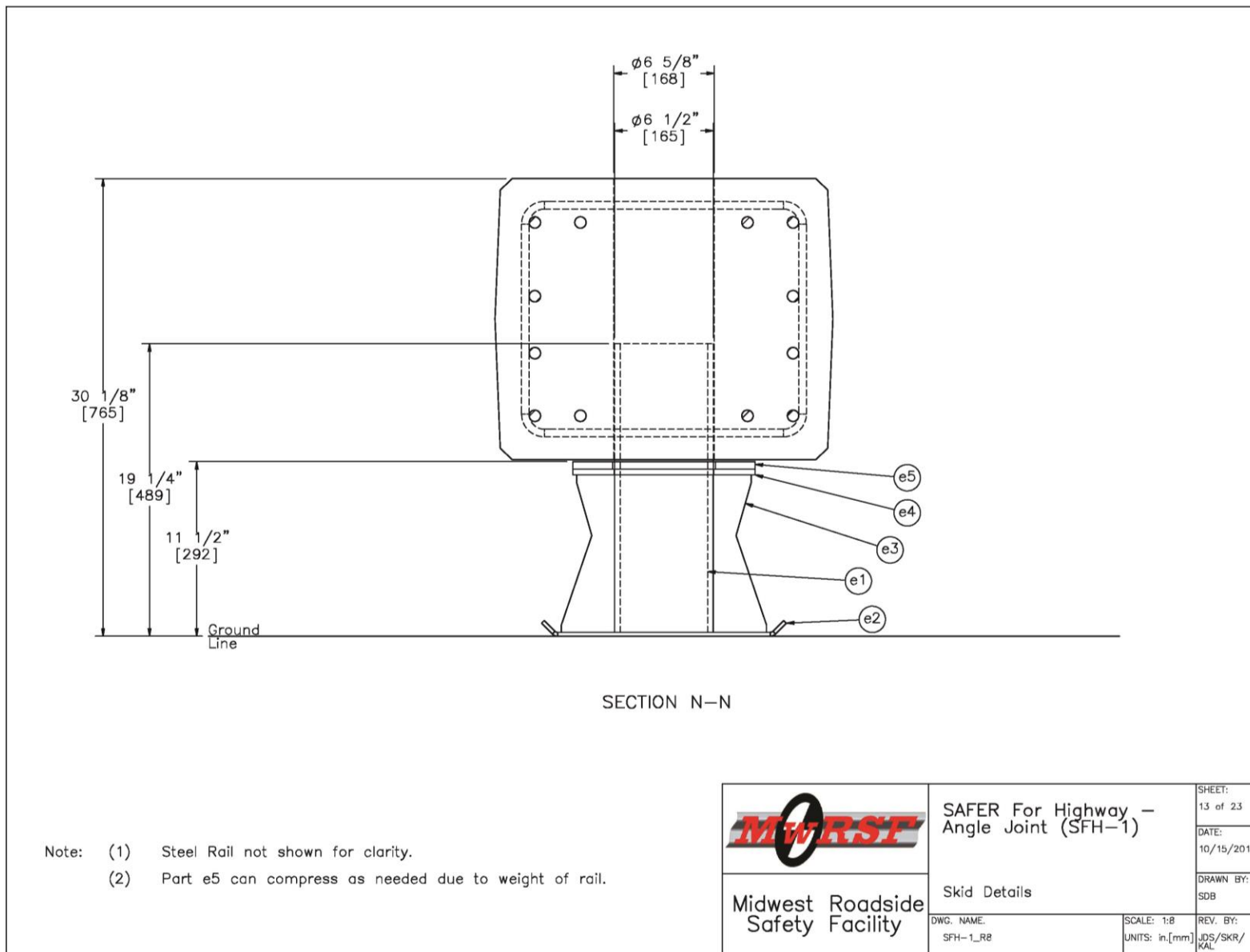


Figure 89. Recommended Barrier Design for Full-Scale Crash Testing, Skid Details

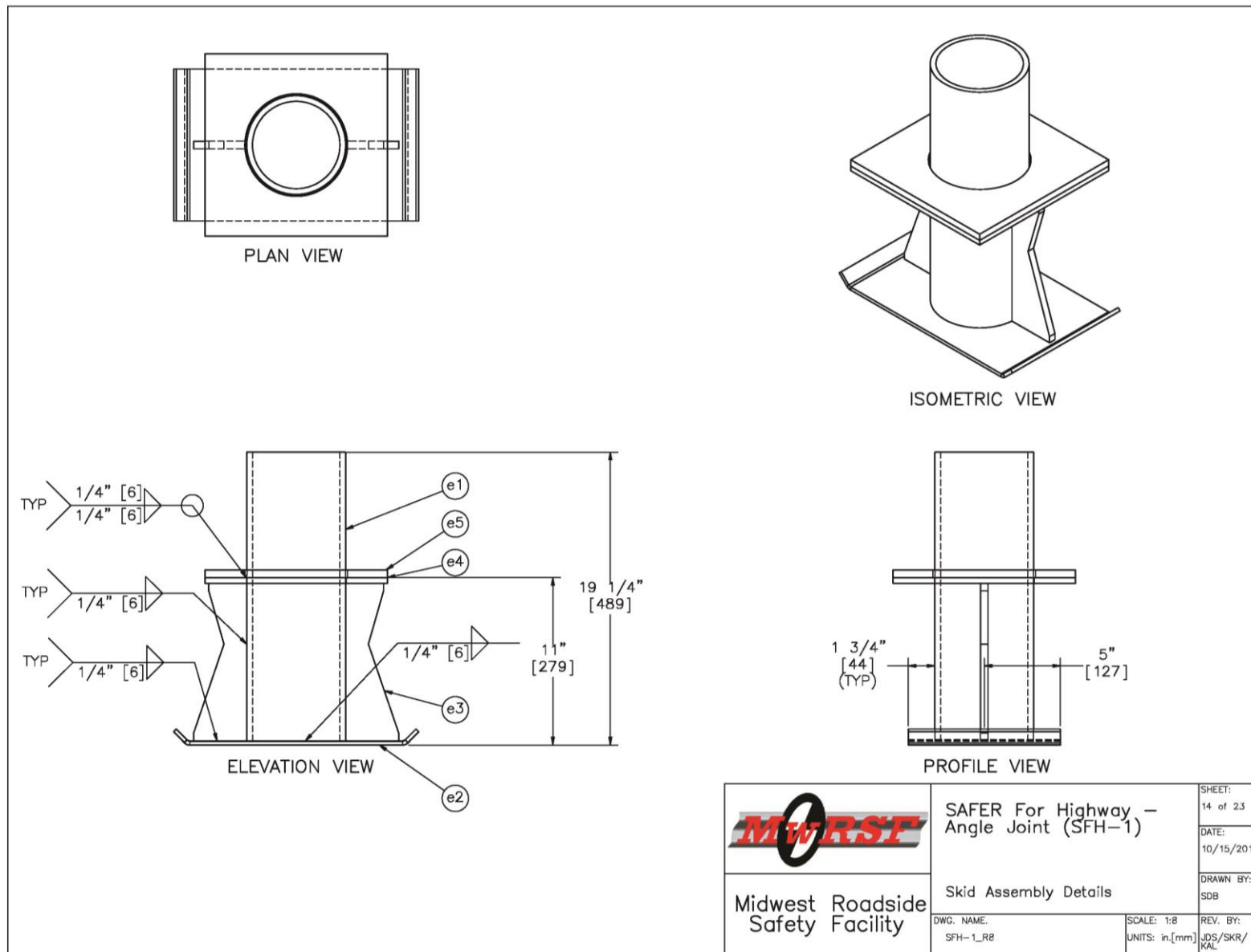


Figure 90. Recommended Barrier Design for Full-Scale Crash Testing, Skid Assembly Details

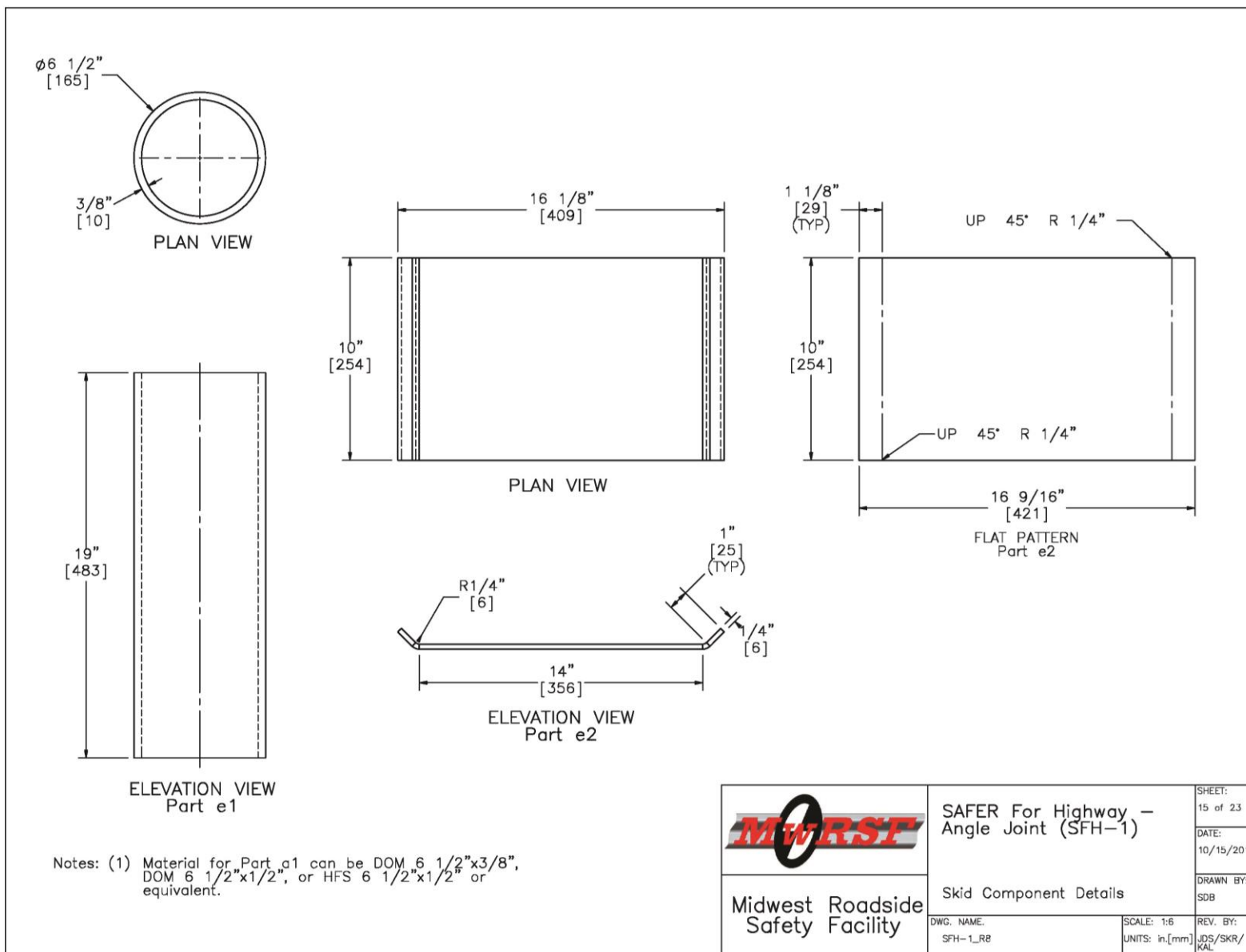


Figure 91. Recommended Barrier Design for Full-Scale Crash Testing, Skid Component Details

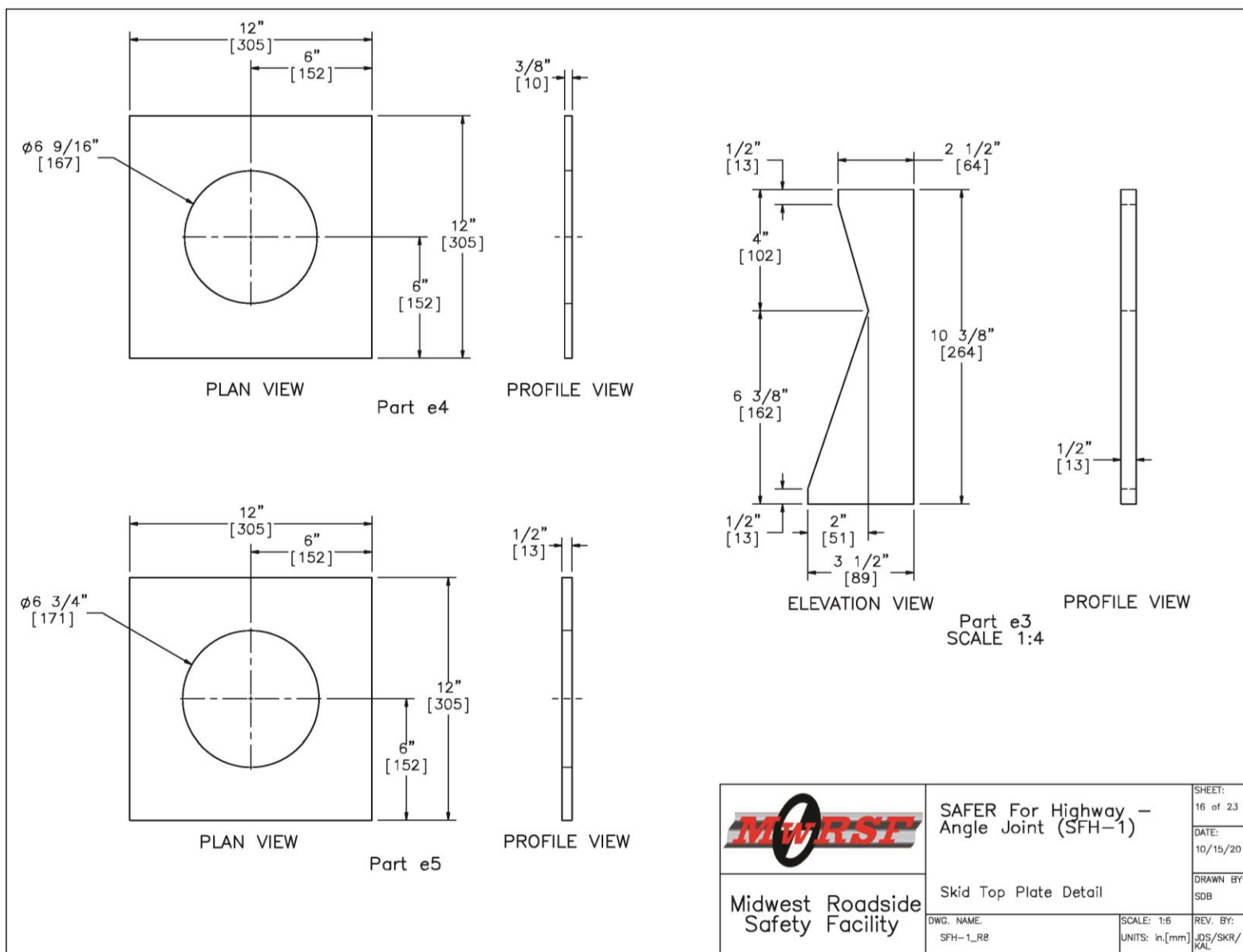


Figure 92. Recommended Barrier Design for Full-Scale Crash Testing, Skid Top Plate Detail

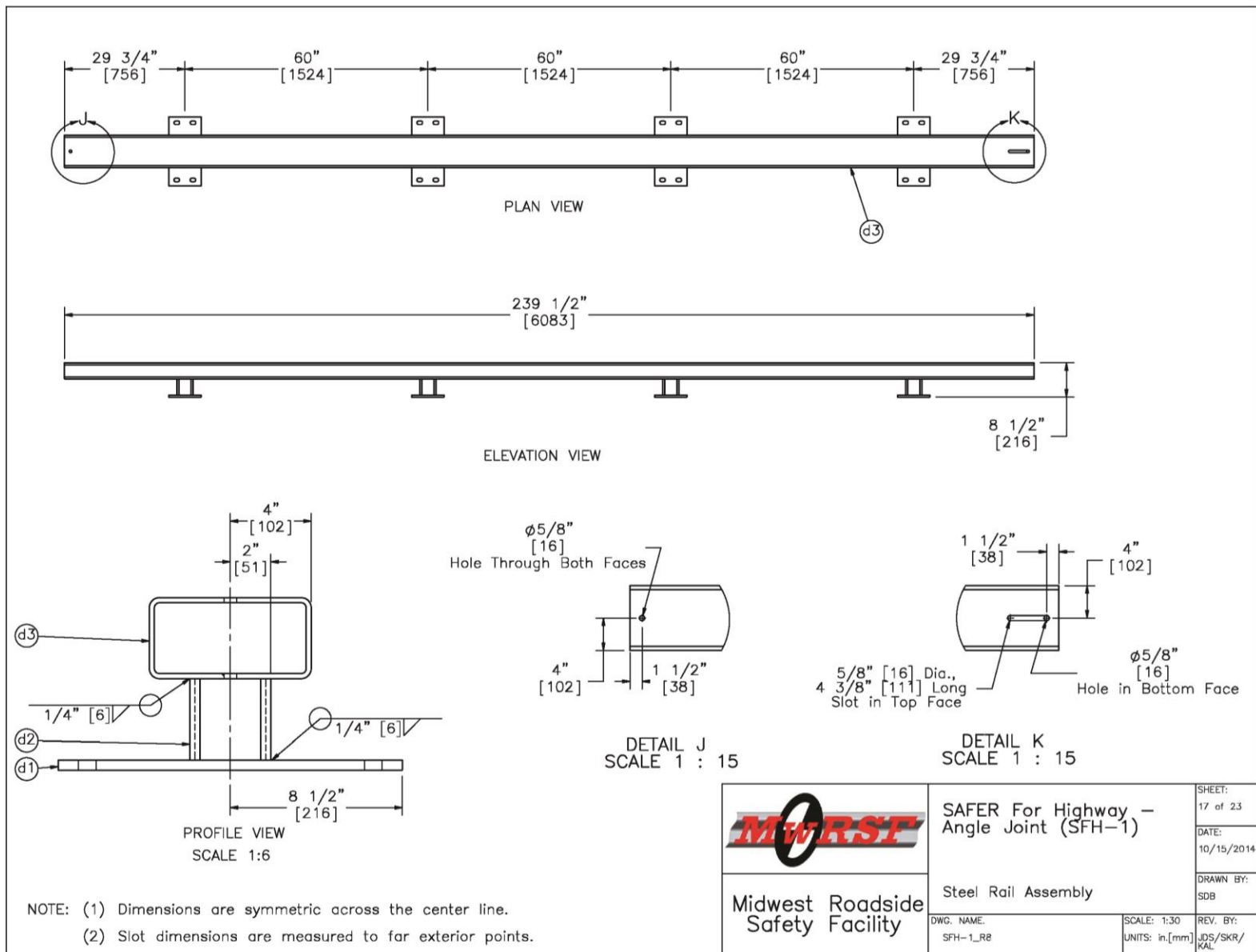


Figure 93. Recommended Barrier Design for Full-Scale Crash Testing, Steel Rail Assembly

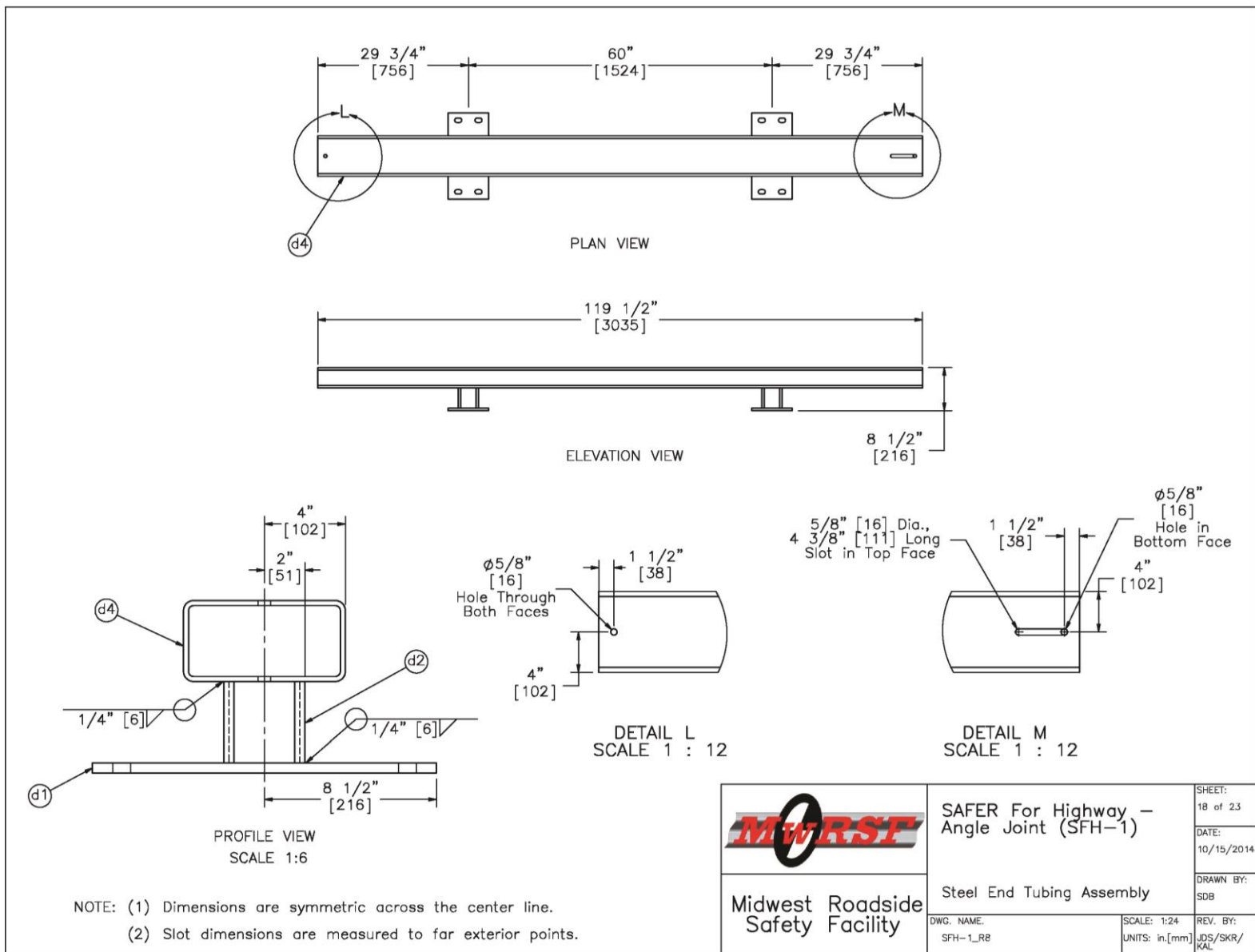


Figure 94. Recommended Barrier Design for Full-Scale Crash Testing, Steel End Tubing Assembly

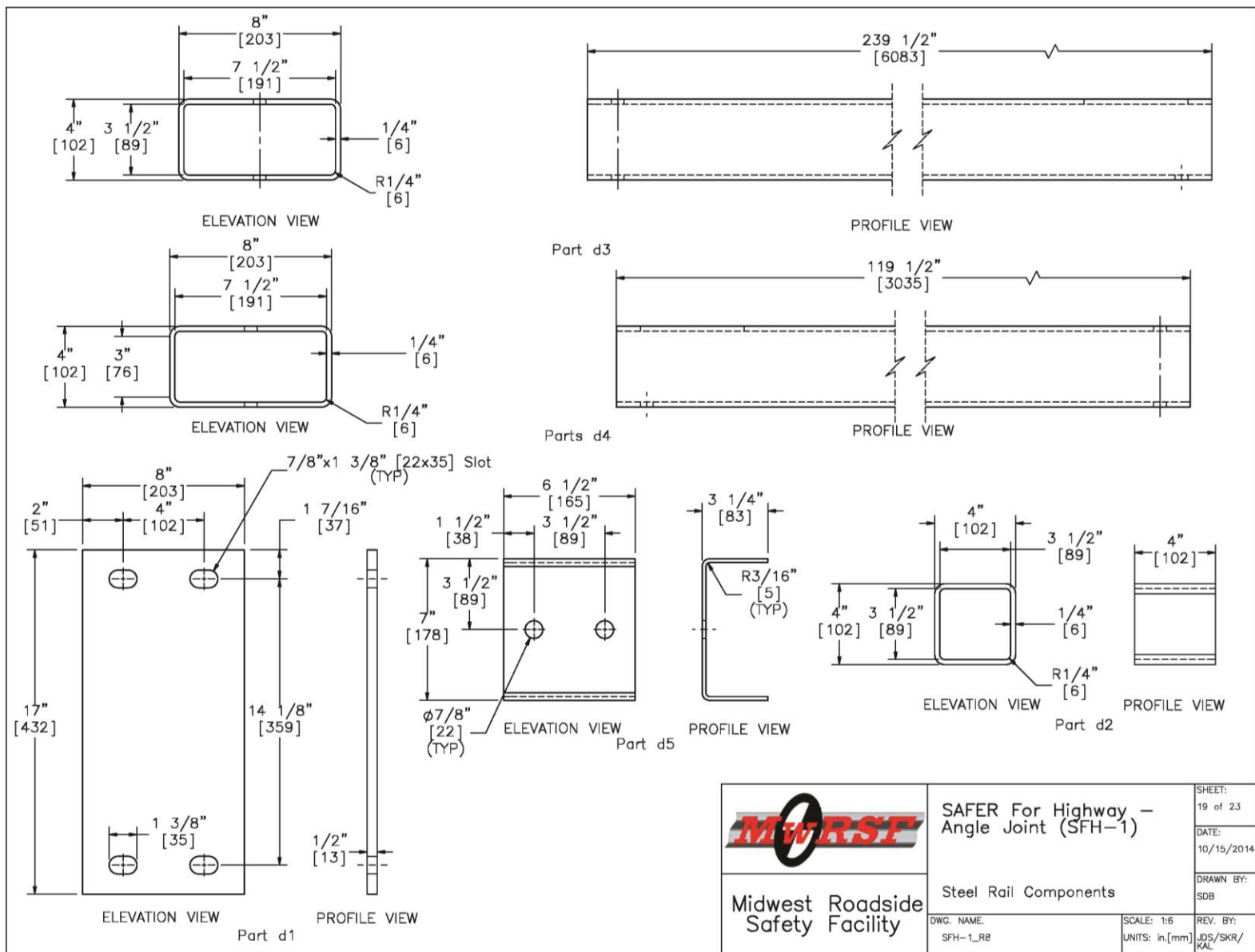


Figure 95. Recommended Barrier Design for Full-Scale Crash Testing, Steel Rail Components

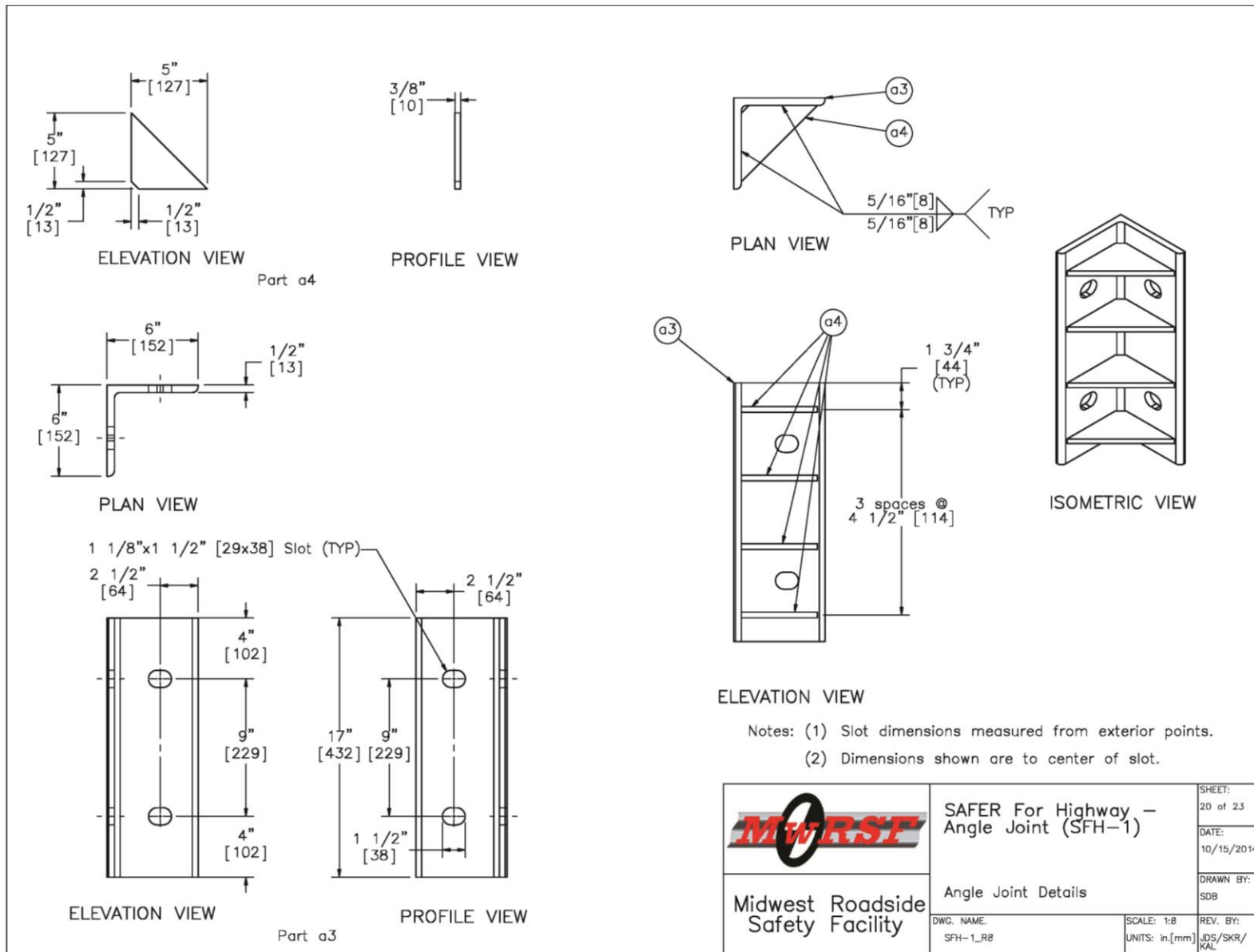


Figure 96. Recommended Barrier Design for Full-Scale Crash Testing, Adjustable Continuity Joint Details

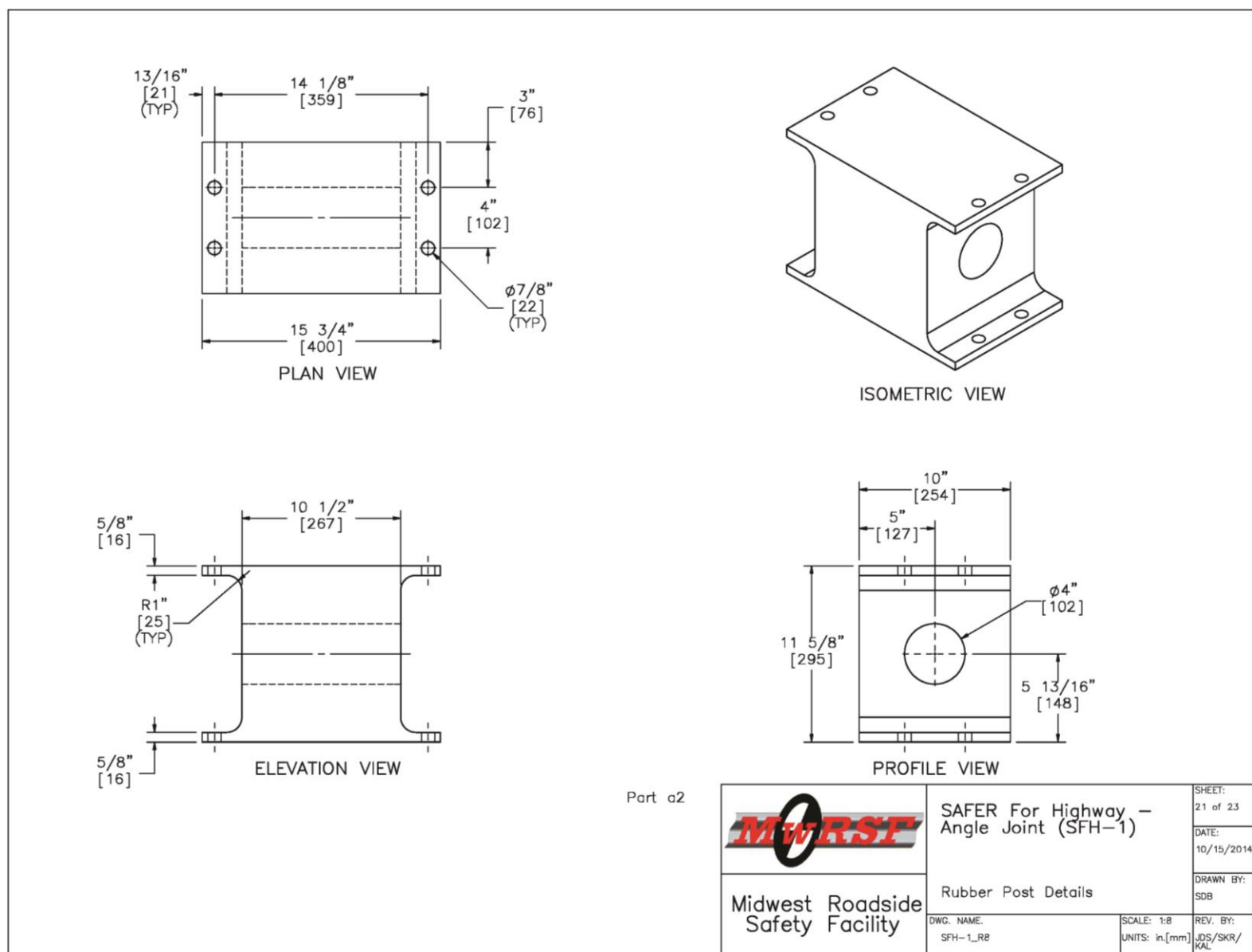


Figure 97. Recommended Barrier Design for Full-Scale Crash Testing, Rubber Post Details

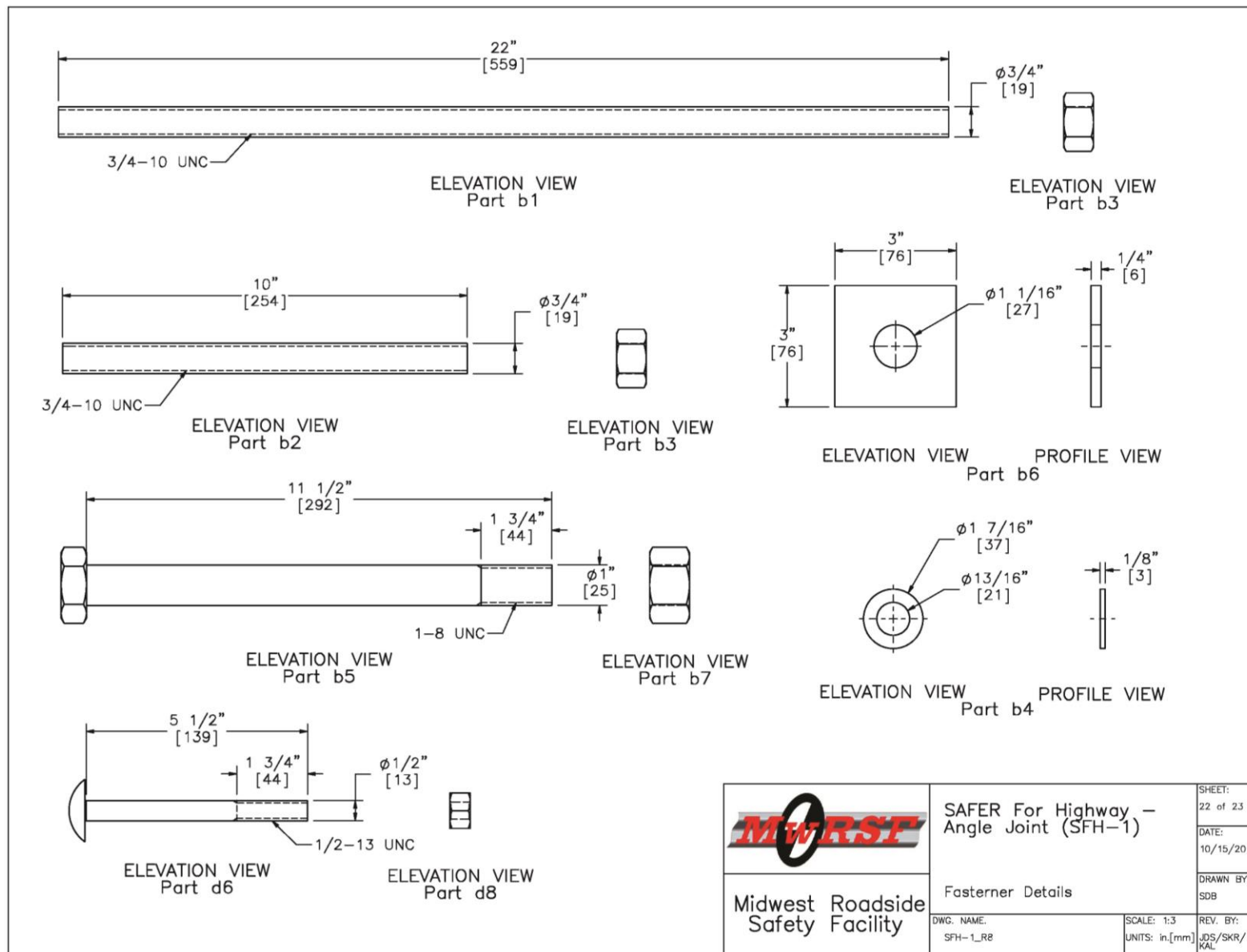


Figure 98. Recommended Barrier Design for Full-Scale Crash Testing, Fastener Details

Item No.	QTY.	Description	Material Specification	Hardware Guide
a1	12	Lightweight Concrete Rail	min f'c=5 ksi [34.5 MPa], density=110 pcf	—
a2	48	Morse E46496 Shear Fender	ASTM D2000	—
a3	22	6"x6"x1/2" [152x152x13], 17" [432] Long L-Bracket	A992 Galvanized	—
a4	88	5"x5"x3/8" [127x127x10] Gusset Plate	A572 Grade 50 Galvanized	—
b1	192	3/4" [19] Dia. UNC, 22" [559] Long Threaded Rod	ASTM A193 Grade B7 Galvanized	—
b2	192	3/4" [19] Dia. UNC, 10" [254] Long Threaded Rod	ASTM A193 Grade B7 Galvanized	—
b3	576	3/4" [19] Dia. UNC Heavy Hex Nut	ASTM A194 Grade 2H Galv.	—
b4	576	3/4" [19] Dia. Flat Washer	ASTM F436 Galv.	FWC20b
b5	88	1" [25] Dia. UNC, 11 1/2" [292] Long Hex Head Bolt	ASTM A325 Galv.	FBX24b
b6	176	3"x3"x1/4" [76x76x6] Square Washer	A572 Grade 50 Galvanized	—
b7	88	1" [25] Dia. UNC Heavy Hex Nut	ASTM A563 DH Galv.	FNX24b
c1	336	1/2" [13] Dia., 77" [1956] Long Bent Rebar	A615 Grade 60	—
c2	96	1/2" [13] Dia., 49" [1245] Long Bent Rebar	A615 Grade 60	—
c3	144	3/4" [19] Dia., 231" [5867] Long Rebar	A615 Grade 60	—
c4	96	3/4" [19] Dia., 63" [1600] Long Bent Rebar	A615 Grade 60	—
c5	72	3/4" [19] Dia., 69" [1753] Long Bent Rebar	A615 Grade 60	—
d1	48	17"x8"x1/2" [431x203x13] Anchor Plate	ASTM A572 Grade 50 Galvanized	—
d2	48	4"x4"x1/4" [102x102x6], 4" [102] Long Tube	A500 Grade B Galvanized	—
d3	11	8"x4"x1/4" [203x102x6], 239 1/2" [6083] Long Tube	A500 Grade B Galvanized	—
d4	2	8"x4"x1/4" [203x102x6], 119 1/2" [3035] Long End Tube	A500 Grade B Galvanized	—
d5	12	12 3/4"x6 1/2"x3/16" [324x165x5] Bent Plate	ASTM A572 Grade 50 Galvanized	—
d6	24	1/2" [13] Dia. UNC, 5 1/2" [140] Long Dome (Round) Head Bolt	ASTM A307 Grade A Galvanized	—
d7	24	1/2" [13] Dia. Flat Washer	ASTM F844 Galvanized	FWC12a
d8	24	1/2" [13] Dia. UNC Heavy Hex Nut	A563A Galvanized	FNX12b
d9	—	Epoxy	HILTI HIT-RE500	—
e1	24	6 1/2" [165] Dia., 3/8" [10] Thick, 19" [483] Long Steel Pipe	AISI 1026	—
e2	24	16 9/16"x10"x1/4" [421x254x6] Base Plate	ASTM A572 Grade 50 Steel	—
e3	48	3 1/2"x10 3/8"x1/2" [89x264x13] Plate Gusset	ASTM A572 Grade 50 Steel	—
e4	24	12"x12"x3/8" [305x305x10] Top Plate	ASTM A572 Grade 50 Steel	—
e5	24	12"x12"x1/2" [305x305x13] EPDM Rubber Sheet	Minimum 50 durometer	—

 Midwest Roadside Safety Facility	SAFER For Highway – Angle Joint (SFH-1)	SHEET: 23 of 23 DATE: 10/15/2014 DRAWN BY: SDB
	Bill of Materials	DWG. NAME: SFH-1_R8 SCALE: 1:8 UNITS: in./mm REV. BY: JDS/SKR/ KAL

Figure 99. Recommended Barrier Design for Full-Scale Crash Testing, Bill of Materials

8 REFERENCES

1. Schmidt, J.D., Faller, R.K., Sicking, D.L., Reid, J.D., Lechtenberg, K.A., Bielenberg, R.W., Rosenbaugh, S.K., and Holloway, J.C., *Development of a New Energy-Absorbing Roadside/Median Barrier System with Restorable Elastomer Cartridges*, Final Report to the Nebraska Department of Roads and the Federal Highway Administration – Nebraska Division, MwRSF Report No. TRP-03-281-13, Midwest Roadside Safety Facility, University of Nebraska-Lincoln, Lincoln, Nebraska, July 16, 2013.
2. Schmidt, J.D., Schmidt, T.L., Faller, R.K., Sicking, D.L., Reid, J.D., Lechtenberg, K.A., Bielenberg, R.W., Rosenbaugh, S.K., and Holloway, J.C., *Evaluation of Energy Absorbers for Use in a Roadside/Median Barrier*, Final Report to the Nebraska Department of Roads and the Federal Highway Administration – Nebraska Division, MwRSF Report No. TRP-03-280-14, Midwest Roadside Safety Facility, University of Nebraska-Lincoln, Lincoln, Nebraska, February 6, 2014.
3. *Manual for Assessing Safety Hardware (MASH)*, American Association of State Highway and Transportation Officials (AASHTO), Washington, D.C., 2009.
4. Holloway, J.C., Faller, R.K., Wolford, D.F., Dye, D.L., and Sicking, D.L., *Performance Level 2 Tests on a 29-in. Open Concrete Bridge Rail*, Final Report to the Nebraska Department of Roads, MwRSF Report No. TRP-03-51-95, Midwest Roadside Safety Facility, University of Nebraska-Lincoln, Lincoln, Nebraska, June 1996.
5. Holloway, J.C., Sicking, D.L., and Faller, R.K., *A Reduced Height Performance Level 2 Bridge Rail*, Transportation Research Record No. 1528, Transportation Research Board, National Research Council, Washington, D.C., 1996.
6. Polivka, K.A., Faller, R.K., Rohde, J.R., Reid, J.D., Sicking, D.L., and Holloway, J.C., *Safety Performance Evaluation of the Nebraska Open Bridge Rail on an Inverted Tee Bridge Deck*, Final Report to the Nebraska Department of Roads, MwRSF Report No. TRP-03-133-04, Midwest Roadside Safety Facility, University of Nebraska-Lincoln, Lincoln, Nebraska, January 21, 2004.
7. Society of Automotive Engineers (SAE), *Instrumentation for Impact Test – Part 1 – Electronic Instrumentation*, SAE J211/1 MAR95, New York City, NY, July, 2007.
8. Morse Rubber Products Co., *Morse Dock Fenders*, MRP 001-84, July 1, 1984.
9. Bligh, R.P., Sheikh, N.M., Menges, W.L., and Heck, R.R., *Development of Low-Deflection Precast Concrete Barrier*, Final Report to the Texas Department of Transportation, Report FHWA/TX-05/0-4162-3, Texas A&M Transportation Institute, Texas A&M University, College Station, Texas, January 2005.
10. FHWA/NHTSA National Crash Analysis Center, *Finite Element Model of Dodge Neon*, Model Year 1996, Version 7, Posted July 3, 2006.

11. FHWA/NHTSA National Crash Analysis Center, *Finite Element Model of Chevy Silverado*, Model Year 2007, Version 2, Posted February 27, 2009.
12. Mohan, P., Marzougui, D., Arispe, E., and Story, C., *Component and Full-Scale Tests of the 2007 Chevrolet Silverado Suspension System*, National Crash Analysis Center, Contract No. DTFH61-02-X-00076, July 2009.
13. Bullard, D.L., Bligh, R.P., and Menges, W.L., *Appendix A: MASH-08 TL-4 Testing and Evaluation of the New Jersey Safety Shape Bridge Rail*, NCHRP Project 22-14, Texas Transportation Institute, College Station, Texas, 2008.
14. Wiebelhaus, M.J., Polivka, K.A., Faller, R.K., Rohde, J.R., Sicking, D.L., Holloway, J.C., Reid, J.D., and Bielenberg, R.W., *Evaluation of Rigid Hazards Placed in the Zone of Intrusion*, Final Report to the Midwest States Regional Pooled Fund Program, MwRSF Report No. TRP-03-141-08, Midwest Roadside Safety Facility, University of Nebraska-Lincoln, Lincoln, Nebraska, January 2008.
15. Polivka, K.A., Faller, R.K., Sicking, D.L., Rohde, J.R., Bielenberg, R.W., Reid, J.D., and Coon, B.A., *Performance Evaluation of the Permanent New Jersey Safety Shape Barrier – Update to NCHRP 350 Test No. 4-12 (2214NJ-2)*, Final Report to the National Cooperative Highway Research Program 22-14(2), MwRSF Report No. TRP-03-178-06, Midwest Roadside Safety Facility, University of Nebraska-Lincoln, Lincoln, Nebraska, October 2006.

9 APPENDICES

Appendix A. Material Specifications

Morse Rubber

CERTIFICATE OF CONFORMANCE

<u>University of Nebraska-Lincoln</u>	<u>10/16/13</u>	<u>EF6496</u>
Company	Date	Part Number

We hereby certify that all items shipped on our Order No. 54803 &
Shipper No. 61145, against your Purchase Order No. 4500265407
comply with all published requirements and specifications.



John E. Rector
Name

Vice President
Title

Morse Rubber L.L.C.
3588 Main Street, Keokuk, IA 52632
Telephone (319) 524-8430 Telefax (319) 524-7290

Figure A-1. Rubber Post Certificate of Conformance

Appendix B. Bogie Test Results

The results of the recorded data from each accelerometer for every dynamic bogie test are provided in the summary sheets found in this appendix. Summary sheets include acceleration, velocity, and deflection vs. time plots as well, as force vs. deflection and energy vs. deflection plots.

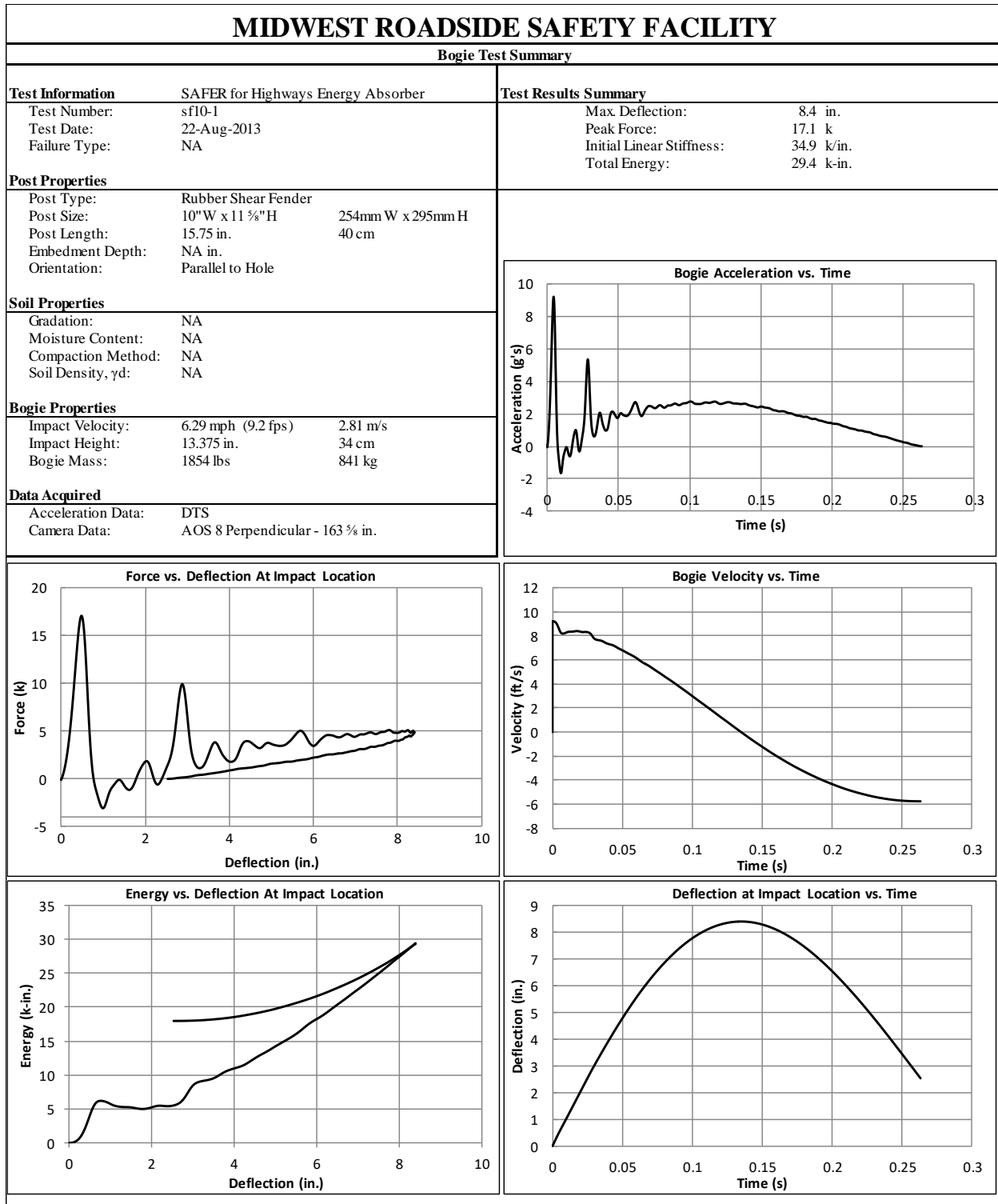


Figure B-1. Test No. SF10-1 Results (DTS)

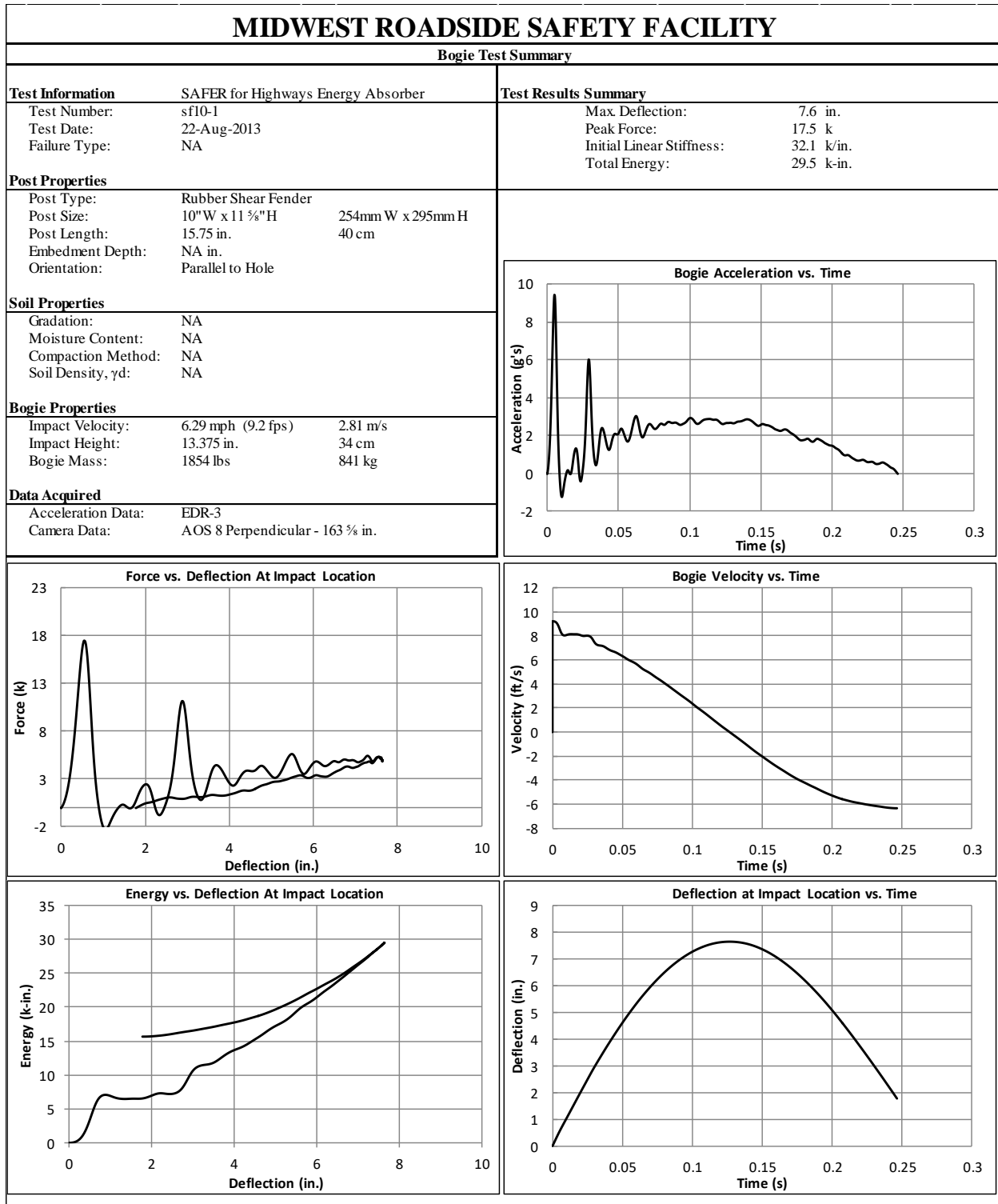


Figure B-2. Test No. SF10-1 Results (EDR-3)

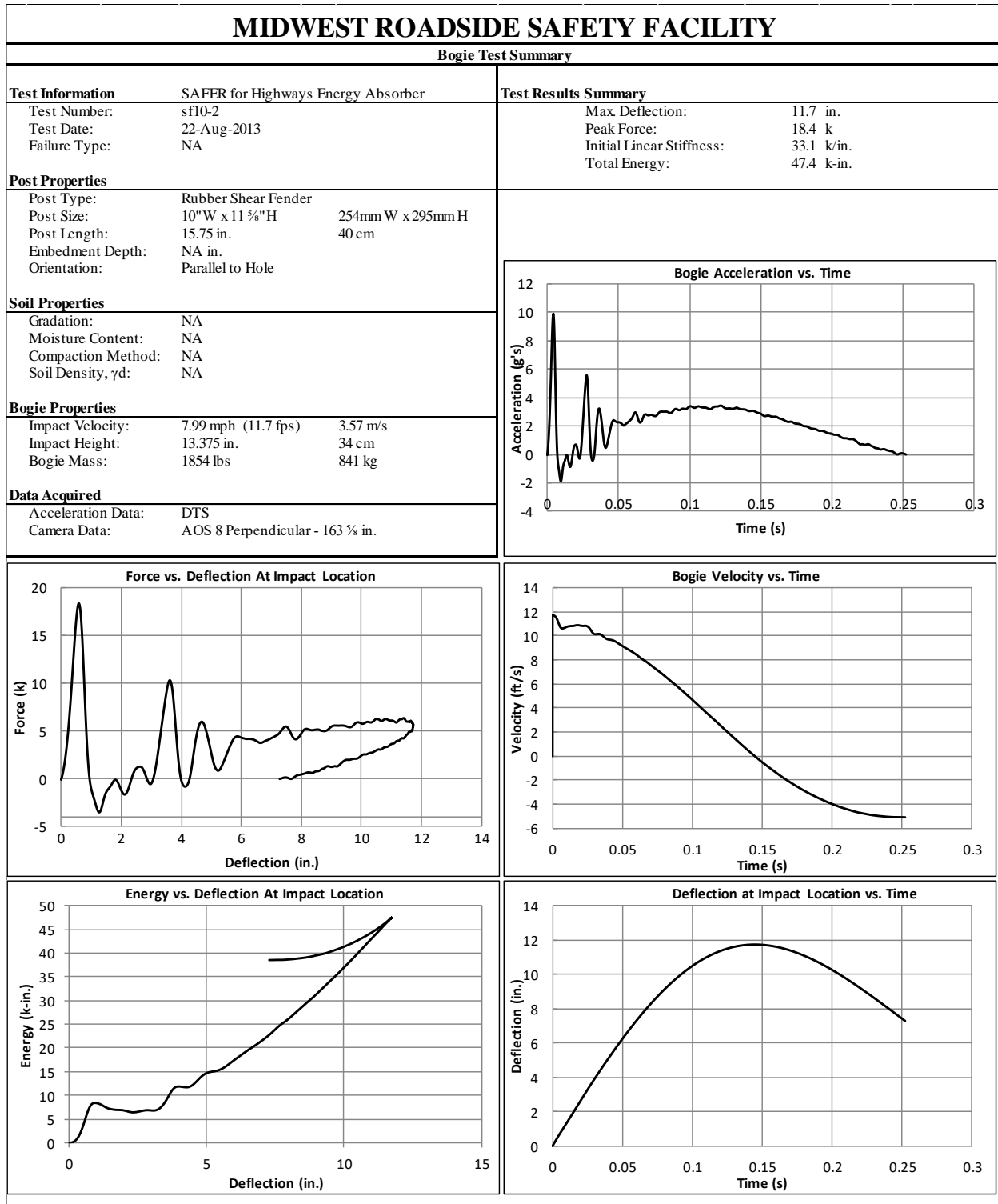


Figure B-3. Test No. SF10-2 Results (DTS)

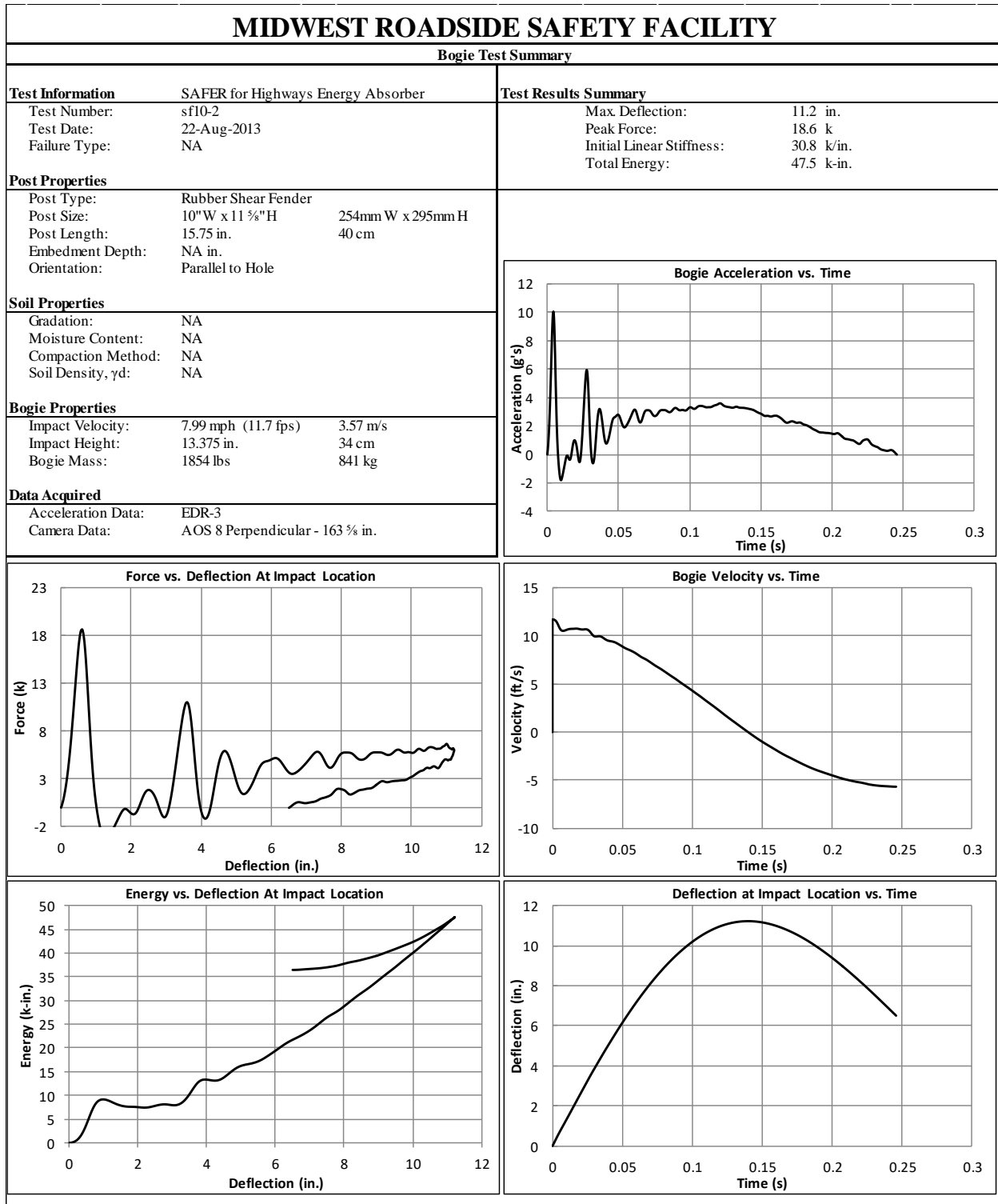


Figure B-4. Test No. SF10-2 Results (EDR-3)

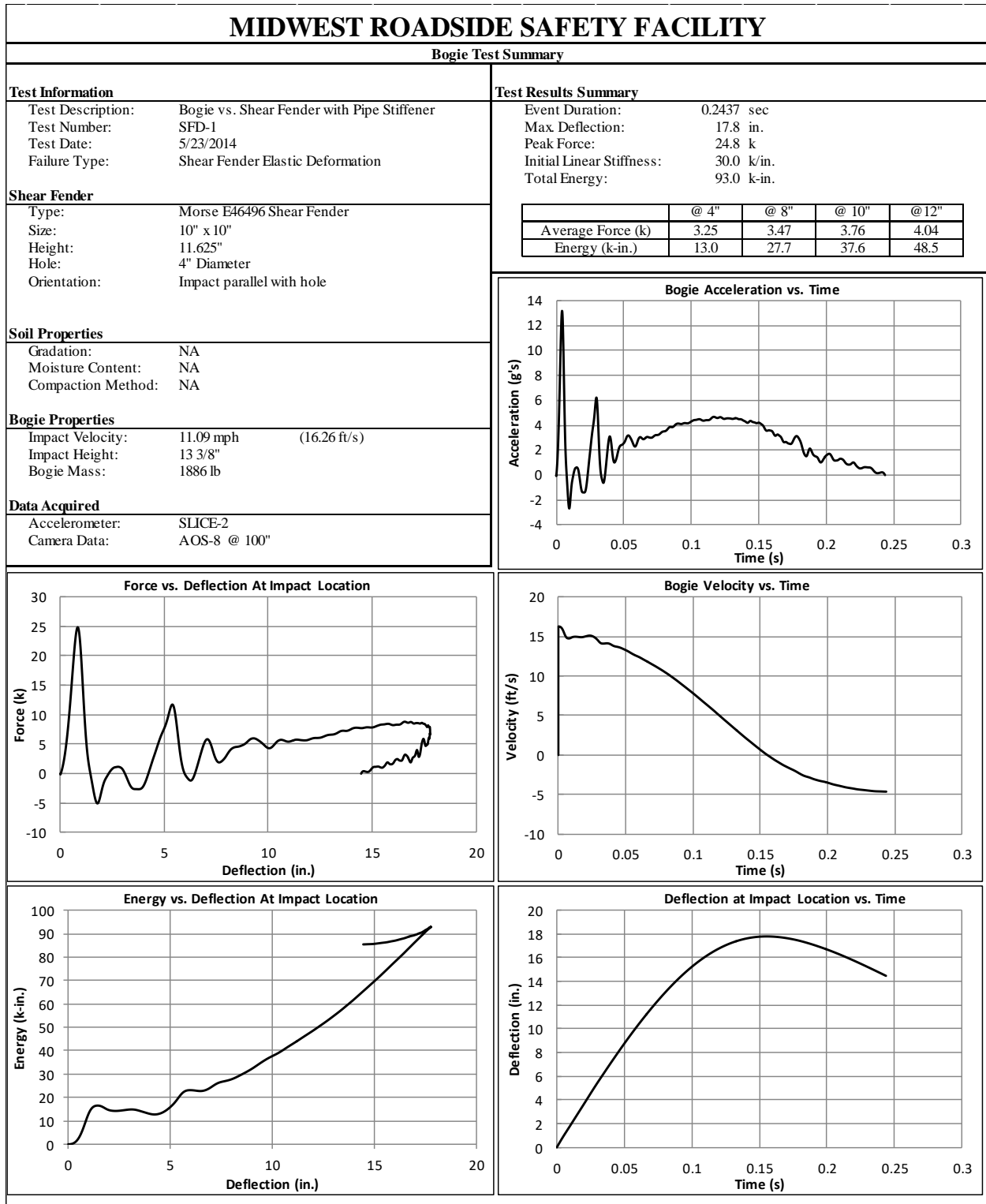


Figure B-5. Test No. SFD-1 Results (SLICE-2)

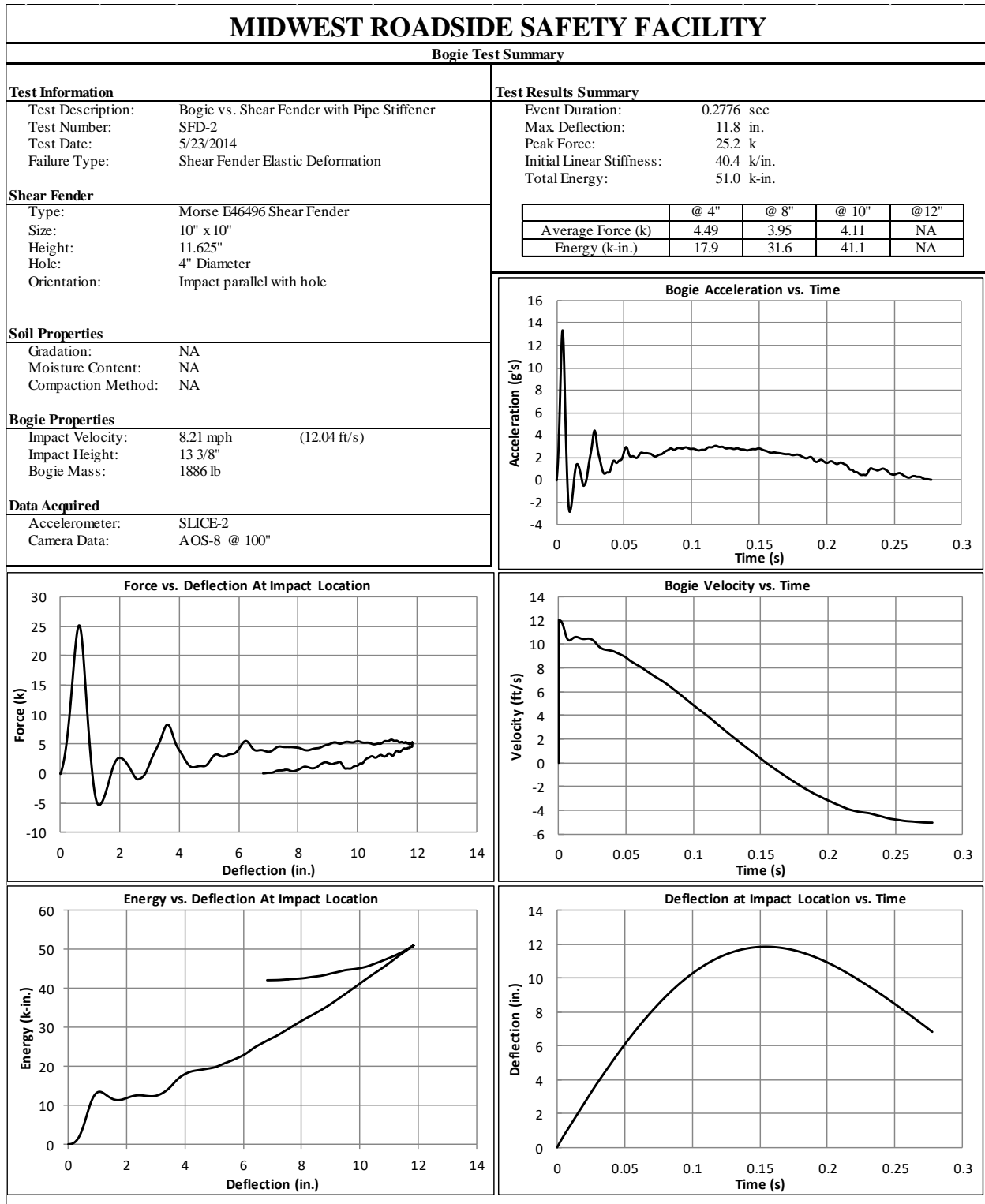


Figure B-6. Test No. SFD-2 Results (SLICE-2)

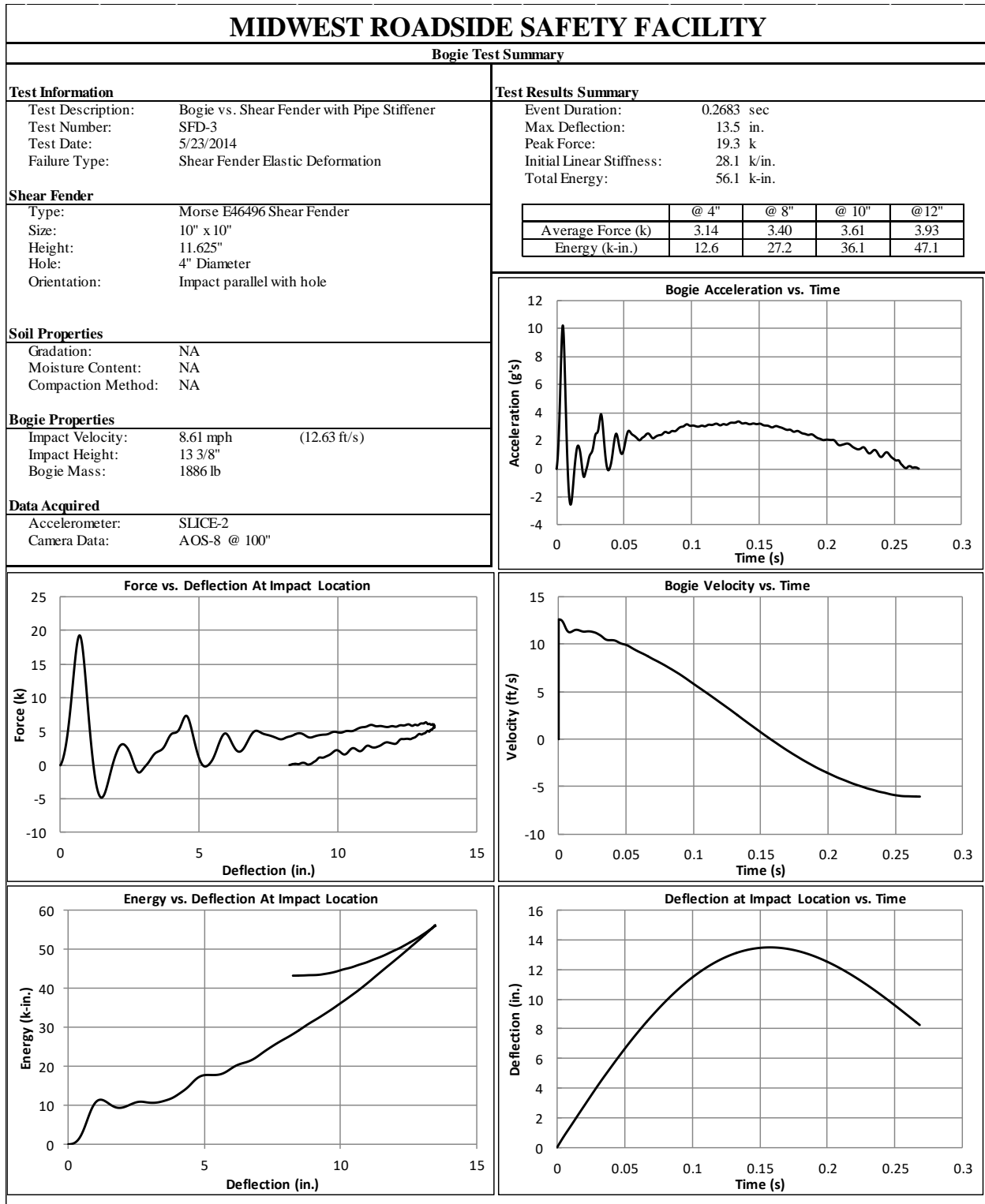


Figure B-7. Test No. SFD-3 Results (SLICE-2)

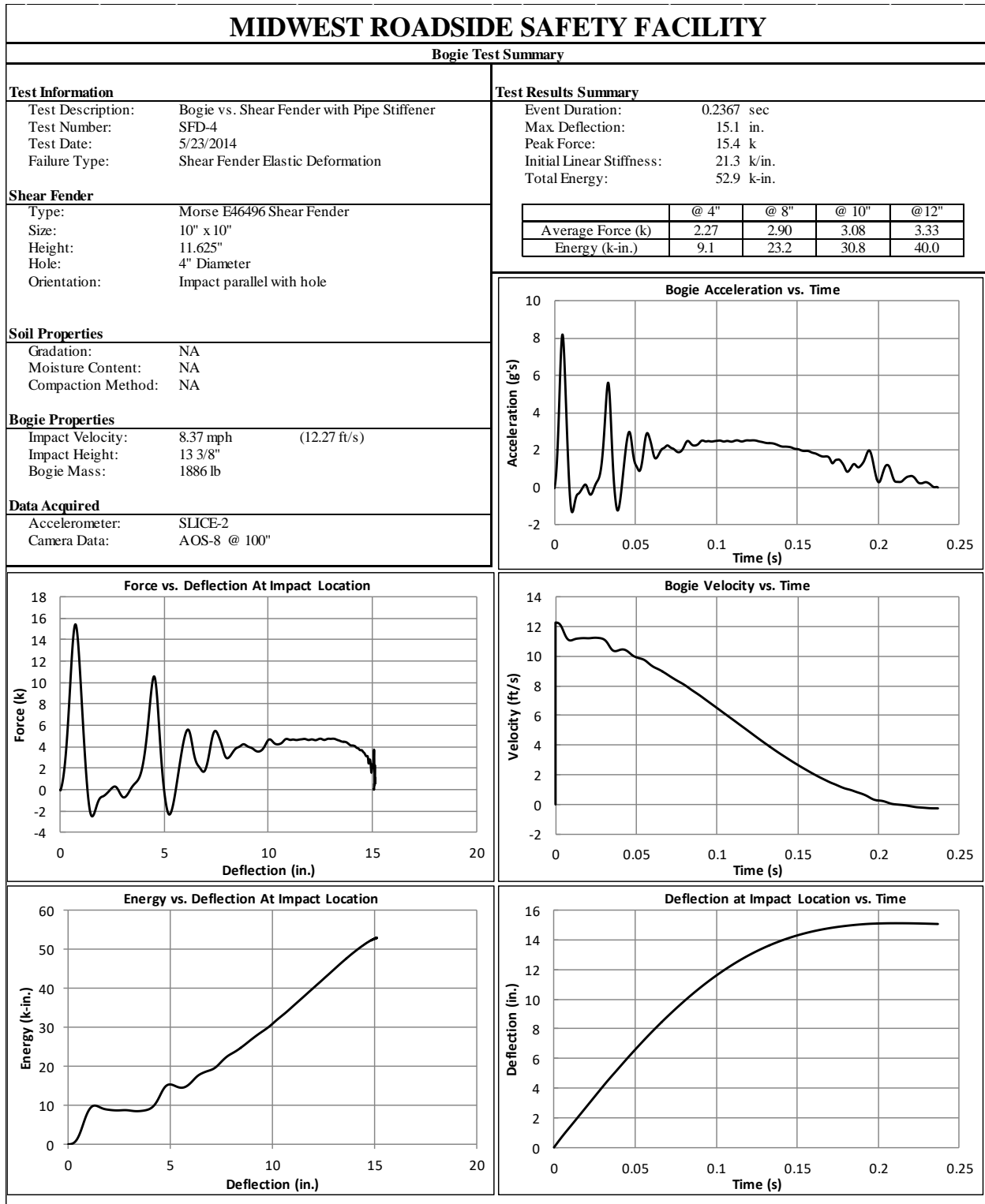


Figure B-8. Test No. SFD-4 Results (SLICE-2)

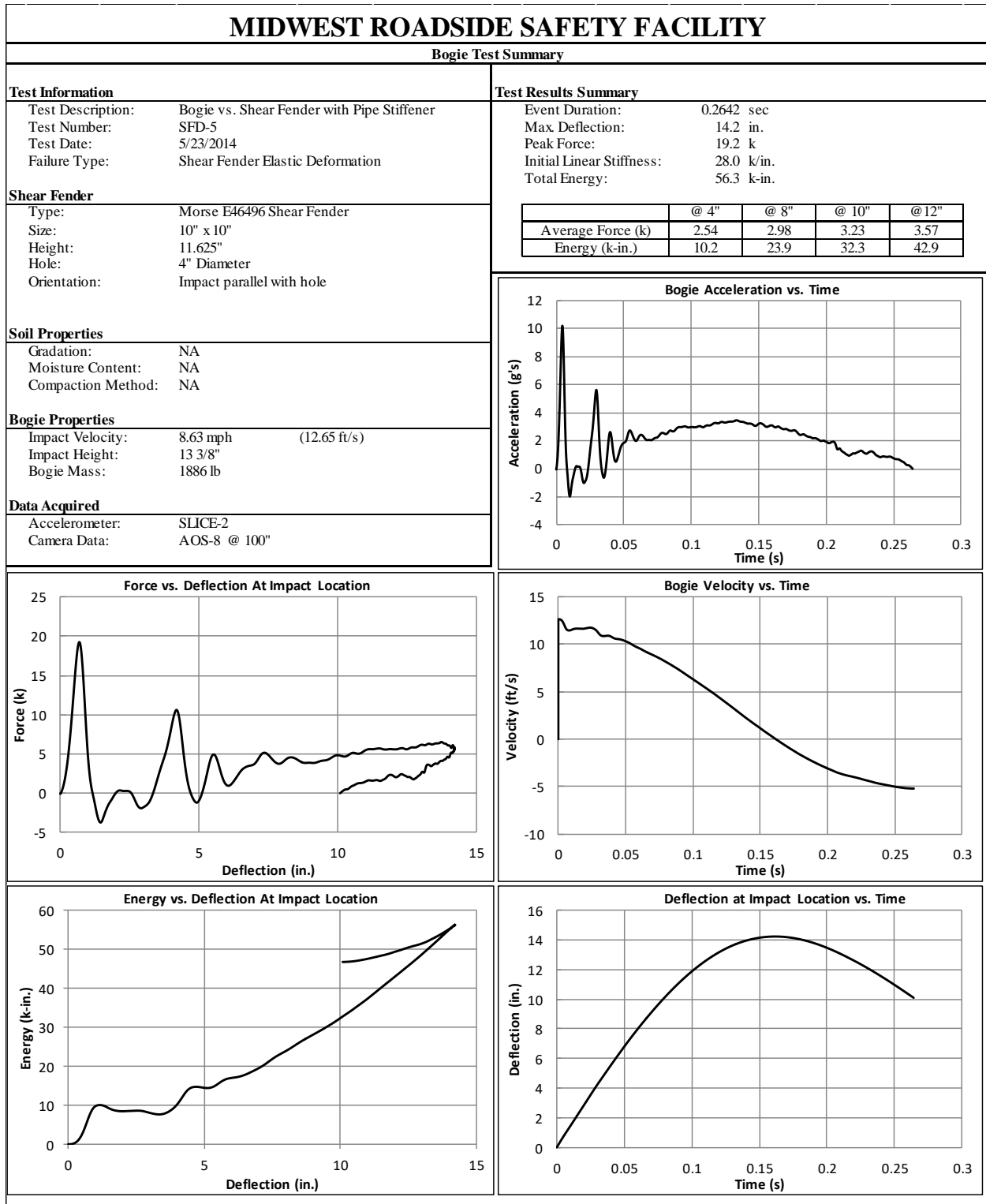


Figure B-9. Test No. SFD-5 Results (SLICE-2)

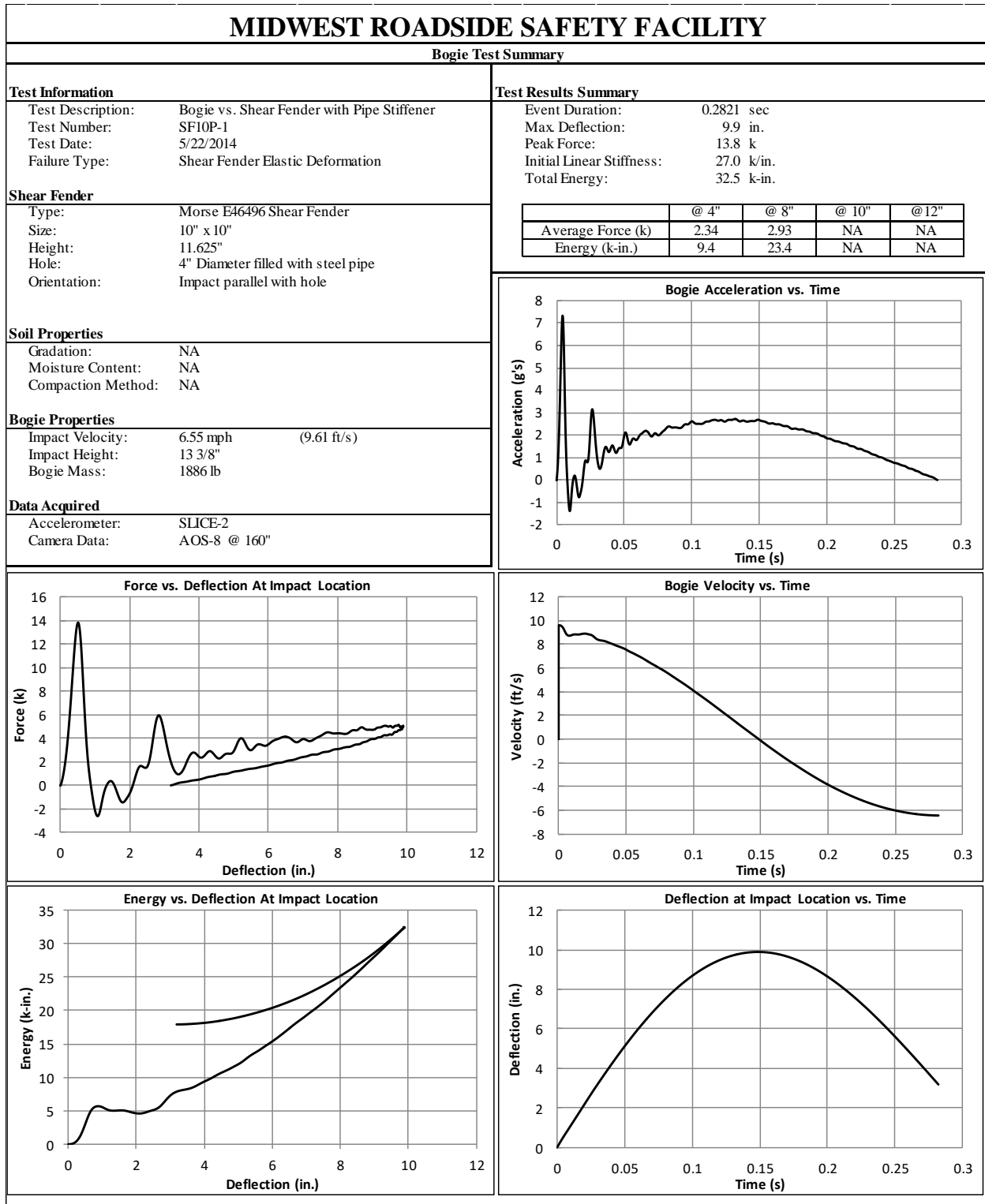


Figure B-10. Test No. SF10P-1 Results (SLICE-2)

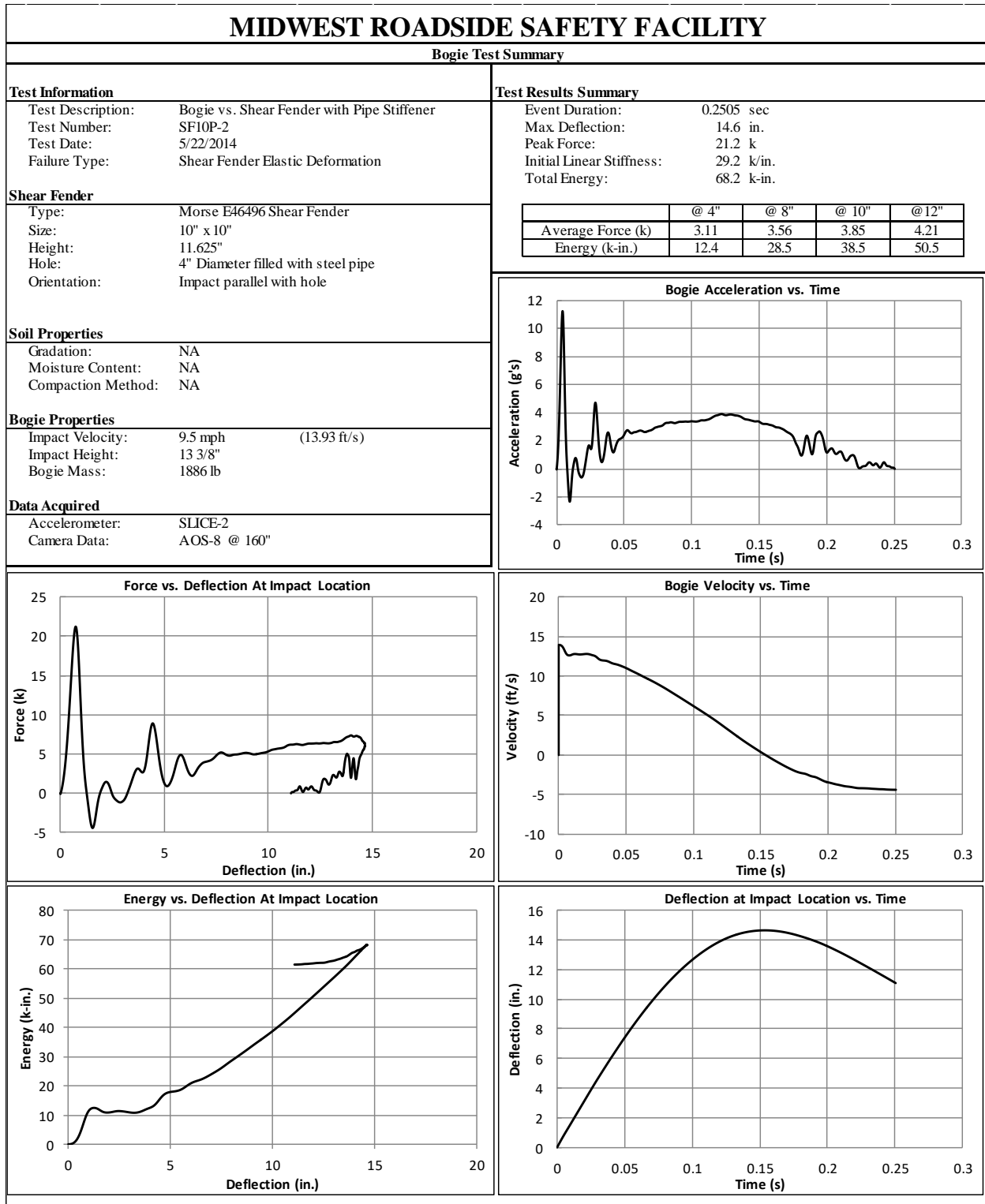


Figure B-11. Test No. SF10P-2 Results (SLICE-2)

Appendix C. Simulation Issues

This project has developed over several years and changes have occurred with simulations, including:

- 1) computing hardware;
- 2) LS-DYNA software (Version 5.0 to 7.1.1); and
- 3) vehicle models.

Consistent vehicle models were used throughout the project whenever possible. However, initial rigid barrier baseline simulations and initial barrier development models [1] were conducted with Version 2 of the Chevrolet Silverado. More recent simulations utilized Version 3 of the Chevrolet Silverado, as the model was more stable on newer versions of LS-DYNA.

With each change in hardware, software, and models, simulations were not re-run to explore the effects, even though these changes can affect the results. For example, the vehicle tires contacting rubber posts led to model instabilities in newer versions of hardware and software that previously did not happen.

END OF DOCUMENT